



This report has been reproduced directly from the best available copy.

Available to DOE and DOE contractors from the Office Of Scientific and Technical Information, P.O. Box 62, Oak Ridge, TN 37831; prices available from (615)576-8401, FTS 626-8401.

Available to the public from the National Technical Information Service, U.S. Department of Commerce, 5285 Port Royal Rd., Springfield, VA 22161

Price: Printed     A09      
Microfiche A01

SUPRI HEAVY OIL RESEARCH PROGRAM  
TWELFTH ANNUAL REPORT  
OCTOBER 1, 1987 - SEPTEMBER 30, 1988

Supri TR 67

By  
William E. Brigham  
Louis M. Castanier

June 1989

Work Performed Under Contract No. DE-FG19-87BC14126

Prepared for  
U. S. Department of Energy  
Assistant Secretary for Fossil Energy

Thomas B. Reid, Project Manager  
Bartlesville Project Office  
P.O. Box 1398  
Bartlesville, OK 74005

Prepared by  
Stanford University  
Petroleum Research Institute  
Stanford, CA 94305-4042



# TABLE OF CONTENTS

	<u>Page</u>
SCOPE OF RESEARCH .....	v
<b>PROJECT 1: FLOW PROPERTIES STUDY</b> .....	<b>1</b>
1.1 Effect of Temperature on Relative Permeability .....	2
(K. Hagedorn)	
1.1.1 Introduction.....	2
1.1.2 Apparatus and Analysis .....	2
1.1.3 Discussion and Results .....	3
1.1.4 Conclusions and Recommendations.....	9
1.1.5 Future Work.....	9
1.1.6 Nomenclature.....	9
1.1.7 References.....	10
1.2 Comparison of Relative Permeability From Centrifuging Versus Coreflooding.....	25
(D. Shimbo)	
1.2.1 Abstract.....	25
1.2.2 Introduction.....	25
1.2.3 Experimental Description.....	26
1.2.4 Relative Permeability From Coreflooding.....	27
1.2.5 Relative Permeability From Centrifuging .....	29
1.2.6 Centrifuge Model Description.....	31
1.2.7 Coreflood Model Description.....	33
1.2.8 Least Squares History Matching.....	33
1.2.9 Results and Discussion .....	35
1.2.10 Conclusions .....	39
1.2.11 Recommendations .....	39
1.2.12 References.....	40
<b>PROJECT 2: IN-SITU COMBUSTION</b> .....	<b>42</b>
2.1 Ignition Devices and Methods for In-Situ Combustion .....	43
(D.C. Shallcross)	
2.1.1 Abstract.....	43
2.1.2 Introduction.....	43
2.1.3 Spontaneous Ignition.....	44
2.1.4 Gas-Fired Burners.....	45
2.1.5 Electric Heaters.....	49
2.1.6 Chemical Methods .....	50
2.1.7 Fuel Pack Methods .....	53
2.1.8 Hot Fluid Injection.....	54
2.1.9 Oxygen Fireflood Ignition.....	54
2.1.10 Concluding Remarks .....	55
2.1.11 Acknowledgements .....	56
2.1.12 References.....	56

2.2 Tube Runs.....	70
(C. Baena)	
2.2.1 Abstract.....	70
2.2.2 Literature Survey .....	70
2.2.3 Problem Statement.....	75
2.2.4 Experimental Apparatus and Procedure.....	76
2.2.5 Experimental Program .....	78
2.2.6 Observations and Results.....	79
2.2.7 Conclusions and Recommendations.....	82
2.2.8 References.....	83
2.3 Multi-Phase, Multi-Component Flow Modeling in Porous Media with Temperature Variations.....	97
(J. Wingard)	
<b>PROJECT 3: STEAM INJECTION WITH ADDITIVES .....</b>	<b>98</b>
3.1 Analysis of Transient Foam Flow in Porous Medium with Catscan.....	99
(D. Liu)	
3.1.1 Introduction.....	99
3.1.2 Equipment.....	99
3.1.3 Progress Report of 1988.....	99
3.1.4 Future Work.....	101
3.2 Characterization of Surfactants as Steamflood Additives .....	110
(D.C. Shallcross, L.M. Castanier, W.E. Brigham)	
3.2.1 Abstract.....	110
3.2.2 Introduction.....	110
3.2.3 Experimental Apparatus and Procedure.....	111
3.2.4 Experimental Observations .....	113
3.2.5 Heat Transfer Mechanisms Within the Sandpack.....	114
3.2.6 Noncondensable Gas .....	116
3.2.7 Conclusions.....	117
3.2.8 Acknowledgements.....	117
3.2.9 References.....	117
<b>PROJECT 4: RESERVOIR DEFINITION .....</b>	<b>133</b>
4.1 Single Well Tracer Studies .....	134
(M. Riley)	
4.1.1 Introduction.....	134
4.1.2 Perturbation.....	134
4.1.3 Change of Variables .....	136
4.1.4 References.....	137
4.2 Thermal Recovery Well Test Design and Interpretation.....	138
(A. Ambastha)	
4.3 Flow Through Perforations.....	139
(G. Ahmed)	
4.3.1 Solution by Green's Function.....	139
4.3.2 Bessel's Function Solution .....	139
4.3.3 Modified Bessel's Function Solution.....	140

4.3.4	Computation.....	142
<b>PROJECT 5: FIELD SUPPORT SERVICES .....</b>		<b>144</b>
5.1	A Comparison of Newton and Quasi-Newton Methods .....	145
	For Parallel Reservoir Simulators	
	(J. Barua)	
5.1.1	Abstract.....	145
5.1.2	Introduction.....	145
5.1.3	Amdahl's Law and Matrix Solution .....	146
5.1.4	Parallel Solution of Nonlinear Equations.....	148
5.1.5	Quasi-Newton Methods .....	149
5.1.6	Quasi-Newton Experiments .....	151
5.1.7	Shared-Memory and Message Passing Architectures .....	152
5.1.8	Programming a Shared-Memory Machine.....	152
5.1.9	Forming the Jacobian and the Function.....	155
5.1.10	Parallelizing Dot-Products.....	155
5.1.11	Parallel Experiments.....	156
5.1.12	Quasi-Newton Experiments.....	157
5.1.13	Newton or Quasi-Newton?.....	158
5.1.14	Conclusions .....	160
5.1.15	Nomenclature .....	161
5.1.16	References .....	161
5.1.17	Appendix.....	162
5.2	Steam Drive Semi-Analytical Model .....	174
	(R. Gajdica)	
5.2.1	Emphasis of this Research.....	174
5.2.2	Major Assumptions.....	175
5.2.3	Initial Conditions .....	175
5.2.4	Boundary Conditions .....	175
5.2.5	Program Structure .....	175
5.2.6	Data Organization.....	176
5.2.7	Fractional Flow Calculations .....	177
5.2.8	Determination of Front Locations.....	178
5.2.9	Pressure Drop Through Injection Well.....	179
5.2.10	Pressure Drop Through Steam Zone.....	179
5.2.11	Pressure Drop Through Water Zone .....	180
5.2.12	Pressure Drop Through Oil Zone.....	180
5.2.13	Pressure Drop Through Production Well.....	180
5.2.14	Calculation of Flow Rates.....	180
5.2.15	Nomenclature .....	180
5.2.16	References .....	183
5.3	Computerized Axial Tomography.....	186
	(L. Castanier)	
5.3.1	Summary.....	186
5.3.2	Objectives .....	186
5.3.3	Choice of a Scanner.....	186
5.3.4	Installation and Maintenance .....	186
5.3.5	Progress to Date.....	187
5.3.6	Future Work .....	188



## **PROJECT 1: FLOW PROPERTIES STUDY**

**This project involves measurement of reservoir parameters such as permeabilities, relative permeabilities, and capillary pressure at conditions of temperature and pressure likely to be encountered in thermal recovery processes.**

## 1.1 EFFECT OF TEMPERATURE ON RELATIVE PERMEABILITY (Karen D. Hagedorn)

### 1.1.1. INTRODUCTION

Numerous laboratory studies have been conducted in an attempt to characterize the effect of temperature on relative permeability. However, the results of these studies have often been contradictory. A number of researchers have reported an increase in oil relative permeability, a decrease in residual oil saturation, and an increase in irreducible water saturation with increasing temperature. The systems used in these experiments differ considerably in the oils, brines, and rock materials used, and the magnitudes of the effects have varied widely. Capillary number and wettability changes have been suggested as the reasons for the observed effects. A study by M.A. Miller (1983) reported no effect of temperature on relative permeability or end point saturations and cited measurement techniques as a possible reason for previously observed changes with temperature. For consolidated sands, however, Miller was only able to produce end point relative permeabilities, and not the curves themselves.

The purpose of this study was to conduct displacement experiments on consolidated sandstone and report the effects of temperature on end point values.

### 1.1.2. APPARATUS AND ANALYSIS

This section describes some aspects of the experimental apparatus used in this study, and the method used to analyze the experimental data. Additional details on these topics may be found in the M.S. Report, "The Effects of Temperature on Relative Permeabilities of Consolidated Sands," by Karen Hagedorn.

The apparatus used in this study was constructed by Sufi (1982) and modified by Jianshe Wang for SUPRI-A (1985-1986). Some additional modifications have been made for this study. An automated data acquisition system allows more frequent and more precise data measurements than on many previous systems. A schematic diagram of the entire apparatus is shown in Fig. 1.1.1.

#### Fluid Collection

The fluid collection and measurement system is shown schematically in Fig. 1.1.2. Fluids produced from the core are cooled in a heat exchanger. They then flow through a back pressure regulator and into the measurement beaker via the production tube, 7. The produced oil is trapped in the confining cup, 4. The momentum dissipator, 3, is designed to prevent impact of the production stream directly on the confining cup. Cumulative oil production is measured by an electronic balance (10) as the change in the buoyant force on the confining cup. An advantage to this design is the ability to record the oil fraction of an emulsion, as long as the emulsion remains trapped under the confining cup. Production of either fluid causes a volume of water to be displaced from the measurement beaker through tube, 2. This amount is recorded by balance, 9. Total fluid production can then be calculated using the data from the two balances and the densities of the two fluids. A thermocouple (8) measures the temperature of the beaker fluids for the density calculations. The most serious problem with this design occurs if air is accidentally produced during a run. There is no way of accounting for the volume of air produced. The additional buoyant force on the confining cup is read as

oil production. Since the density difference between air and water is much greater than between oil and water, a small volume of air produced results in a serious error in the oil/water material balance.

## The Cores

Cylindrical cores with a diameter of one inch and a length of seven inches were used in this study. Mesh screens are placed at both interfaces between the core and end plugs to prevent core material from migrating into the system. The confining sleeve is FEP heat shrinking Teflon and fits over both the core and the end plugs.

## Data Analysis

Relative permeabilities were calculated from the displacement data using the technique presented by Johnson, Bossler, and Naumann (1959).

This technique requires differentiation of the experimental data. Differentiation of displacement data, however, often yields erratic results due to normal experimental fluctuations. For this reason, the data were fitted to smooth, monotonic functions of the following forms:

$$N_p = a_0 + a_1 (\ln W_i) + a_2 (\ln W_i)^2 + a_3 (\ln W_i)^3 + \dots \quad (1.1.1)$$

$$\ln (W_i / I_r) = b_0 + b_1 (\ln W_i) + b_2 (\ln W_i)^2 \quad (1.1.2)$$

These forms were proposed by Miller and Ramey (1983). The second order forms of these equations were used in this study to avoid the problem of change in curvature which sometimes results from the third order form.

Only post-breakthrough data were included in the data match. Very good matches were obtained using these equations. The resulting relative permeability curves were smooth because they were based on smooth functional relationships.

It is important to note that Johnson, Bossler, Naumann relative permeabilities are calculated compared to the oil effective permeability at irreducible water saturation. For this study, all relative permeabilities are reported with respect to the absolute permeability to distilled water. Thus, it is necessary to multiply the Johnson, Bossler, Naumann relative permeabilities by the ratio of the endpoint oil effective permeability to the absolute permeability to distilled water.

### 1.1.3. DISCUSSION AND RESULTS

This section presents the results of the experimental runs and the modifications of the apparatus and analysis procedure that resulted from this study.

## Discussion

Some modifications were made to the apparatus and data analysis procedures used by Sufi and Wang. Several materials were studied to find a confining sleeve material that was both durable and able to operate at sufficiently high temperatures. A new core material was selected because it was said to yield better relative permeability curves than the traditional

Berea cores. The back pressure regulator system was modified to prevent the formation of emulsions. A procedure was established for restoring the cores to their original state after a run. Finally, the procedure for shifting the experimental data was studied to better account for the downstream dead volume.

### Confining Sleeve Material

The FEP heat shrinking Teflon used in this study was selected for its simplicity and its durability. However, this material is limited to an operating temperature of 400°F. For this reason, other materials with higher operating temperatures were also studied.

TEF Teflon has a higher operating temperature than the FEP type, but requires a very high temperature for shrinkage. Lead sheet soldered around the core has an even higher operating temperature, but is prone to failure under confining pressure.

It was therefore decided that the FEP Teflon was the most practical of these materials, and that the maximum operating temperature of this material would be acceptable for this study.

### Core Material

Berea Sandstone is a commonly used experimental core material. However, it often yields a flat production curve after breakthrough. In addition, Berea is very water sensitive, which usually results in problems when measuring absolute permeability with respect to water. The Brown Sandstone was chosen for this study because it yields a more rounded production curve after breakthrough, and does not exhibit this sensitivity to water.

There is a major disadvantage in using the Brown Sandstone, however. It is loosely consolidated at some locations on the cores. This makes it difficult to handle experimentally. The two problems most often encountered with the core material in this study were with the cores breaking and with the ends of the cores becoming rounded. The rounded ends of the core often lead to failure of the confining sleeve at the core/end plug interfaces.

### Core Cleaning

In order to study the effects of temperature on relative permeabilities, it is necessary to make a series of runs at varying temperatures on one core. However, at the end of each run, the core is saturated with water and oil, with the oil near its residual saturation. The core must then be restored to its original state before beginning the next run. There are two basic methods for doing this, both of which will be discussed in this section.

The first method is to flood the core with a series of miscible solvents to remove the oil. Questions have been raised in the past about the effects of these solvents on the wettability of the core. Additionally, it is not known whether the solvents will effectively sweep the entire core. This method was attempted on a Brown Sandstone core. Approximately 15 pore volumes each of mineral spirits, isopropanol, acetone, and water were injected sequentially into the core. The absolute permeability to water after the solvents had been injected was less than one quarter of its original value. It was thus concluded that the solvent injection process would not effectively restore the core to its original state.

The second method of removing the oil from the core is to "cook" it, or burn the oil off. This method involves heating the core slowly to a temperature high enough to allow the oil to undergo combustion. For this study, the cores were heated to 450°C. and held at that temperature for at least 12 hours. This method resulted in good agreement between the "before" and "after" absolute permeabilities and so it was chosen as the best method for restoring the core. A disadvantage to this technique is that the cores tend to become increasingly brittle in the cooking process, thus great care is needed in handling them.

### Back Pressure Regulator

Production of oil/water emulsions has been a problem in many relative permeability studies, especially those at high temperatures. The measurement apparatus used in this project reduces the severity of this problem because it can measure the oil fraction of an emulsion as long as the emulsion remains trapped under the confining cup. The problem remains, however, if the density of the emulsion is close to that of water. When the confining cup is almost full of oil, such as after the oil displacement run, this high density emulsion will fall through the oil phase and strike the oil/water interface with a finite downward velocity. Because the density of the emulsion is so close to that of water, this velocity is often enough to allow the emulsion to flow out from under the full confining cup. It was discovered that when this high density type of emulsion was produced in this study, it was not being formed in the core, but rather in the back pressure regulator.

The design of the regulator was modified to prevent these emulsions from forming, but to still have a minimum of dead volume.

### Curve Shifting

Because the upstream and downstream parts of the system are filled with oil at the beginning of the water displacement run, the measured values for both water injection and oil production will include those volumes throughout the run. It is thus necessary to shift the production and injection data so that they only reflect injection into and production from the core itself.

Shifting the injection data is quite simple. Assuming a piston-like displacement in the upstream tubing, the amount of water actually injected at any time is the measured value minus the volume of the upstream tubing. Thus, a fixed value is subtracted from each measured injection datum. Thus, there will be several data at the beginning of the run that will be negative as a result of this curve shifting calculation. These data correspond to injection of the oil which initially filled the upstream tubing, and are not considered part of the water displacement run.

Shifting the production data is more complicated. Instead of subtracting one fixed value from each datum, every measured value must be shifted individually according to the fractional flow of oil in the downstream part of the system at that time. The curve shifting equations are formulated from mass balances on the overall core and tubing system. This procedure is described by Miller (1983), and was modified only slightly for this study.

## Results

A total of eight runs was made on two different Brown Sandstone cores. A summary of these runs is given in Table 1.

Table 1  
Summary of Run Data

run	core	T(°F)	$S_{wi}$	$S_{or}$	$k_{abs}$
1	1	75	0.164	0.262	2.914
2	1	160	0.251	0.295	1.828
3	1	215	0.268	0.300	1.841
4*	1	285	0.236	0.296	1.916
5	1	75	0.227	0.197	3.229
6	2	75	0.279	0.412	0.838
7	2	160	0.335	0.375	0.700
8	2	215	0.367	0.437	0.671

\* Run was terminated due to confining sleeve failure

### Irreducible Water Saturation

The irreducible water saturations measured for the various runs are included in Table 1. There appears to be an increase in the measured  $S_{wi}$  with temperature for both cores (Fig. 1.1.3). This phenomenon has been observed in many previous studies. However, a plot of water production versus oil injected indicates that the irreducible water saturation had not been reached after 14 pore volumes have been injected. An example of the water production is shown as Fig. 1.1.4. All of the curves in this study exhibited behaviour similar to that seen in Fig. 1.1.4. The data after breakthrough form a straight line of positive slope and do not appear to break over or approach a finite value. Jones and Roszelle (1978) suggested that a plot of saturation versus the reciprocal of injected volume could be extrapolated to the ordinate axis to yield the saturation at infinite injected volume. Presumably, this value would represent the irreducible saturation. Figure 1.1.5 is a graph of water saturation versus the reciprocal of the volume of oil injected. The data appear to extrapolate to the origin rather than to some finite value. This, of course, is not possible. It appears from the data that the oil is "extracting" water from somewhere, possibly due to solubility effects or from an unknown hold-up in the downstream system.

Although it is not known how the water saturation would behave with additional injection, it is obvious that the endpoint saturation recorded in the run is not the true irreducible water saturation. Thus, it cannot be concluded that the irreducible water saturation increases with temperature. It can only be said that the water saturation after 14 pore volumes have been injected increases with an increase in temperature. As suggested by Miller and Ramey (1983), this may be due to the decrease in oil viscosity with temperature, which results in a less favorable displacement.

The fractional flow and pressure drop data needed to calculate the drainage relative permeability curves was collected during the oil displacement runs. However, due to the unusual behaviour of the water production curves, as in Fig. 1.1.4, no attempt was made to calculate these curves in this study. They would have been meaningless.

### Residual Oil Saturation

Residual oil saturations were calculated by extrapolating graphs of oil saturation versus the reciprocal of water injected to the ordinate axis, representing infinite injected volume. The dotted line on Fig. 1.1.6 shows this type of extrapolation. In contrast to the saturation graphs for the oil displacement runs (Fig. 1.1.5), the water displacement curves are quite straightforward to extrapolate. In addition, it can be seen from these graphs that the water saturation in the second core tends to level out much more quickly than the saturation in the first core. The relative permeability curves of the two cores behave differently from each other also, as will be seen later. Also, for both cores, the runs at high temperatures tend to approach residual saturation more quickly. This is probably because the displacement becomes more favorable as the viscosity of the oil decreases.

Figure 1.1.7 shows the extrapolated residual oil saturations versus temperature for the two cores. The data for the first core apparently show a slight increase in  $S_{or}$  with increasing temperature. However, the second core shows no discernible trend in  $S_{or}$  with temperature. Neither of these results supports previous findings of a decrease in  $S_{or}$  with increasing temperature. However, since the  $S_{or}$  values reported in the literature are measured at differing volumes of water injected and are not usually calculated in the similar manner, comparison between any of them is not really practical.

### Relative Permeabilities

The relative permeability curves for Cores 1 and 2 are presented in Figs. 1.1.8 and 1.1.9. Relative permeability compared to the absolute permeability to distilled water is graphed versus reduced water saturation. The reduced water saturation,  $S_{w, red}$ , is defined as:

$$S_{w, red} = \frac{S_w - S_{wi}}{1 - S_{or} - S_{wi}} \quad (1.1.3)$$

The reduced saturation for each run was calculated using the  $S_{or}$  and  $S_{wi}$  for that particular run. The reason for plotting the data in this manner is that the relationships between the curves are seen more clearly on this expanded scale. The shapes of the curves and their relationships to one another are the same as if the relative permeability data had been plotted versus the absolute water saturation,  $S_w$ .

It is obvious from Figs. 1.1.8 and 1.1.9 that the two cores do not behave the same at elevated temperatures. Core 1 shows no increase in either  $k_{ro}$  or  $k_{rw}$  from room temperature to 160°F (Fig. 1.1.8). However, there is a significant increase in both  $k_{ro}$  and  $k_{rw}$  at 215°F. The results of Run 4 (285°F) are subject to some doubt. A confining fluid leak was discovered late in this run and this leak may have begun earlier. The results of this run do not seem to fit with the results of the other three runs. However, Run 4 did show the same qualitative increase in both  $k_{ro}$  and  $k_{rw}$  as Run 3, even if the magnitudes of the increases are different. An increase in relative permeabilities to both water and oil was also reported by Poston, *et al.* (1970).

In contrast to Core 1 the data for Core 2 show a slight decrease in both water and oil relative permeabilities with increasing temperature (Fig. 1.1.9). This phenomenon is not known to have been reported previously in the literature. Relative permeability ratios,  $k_{rw}/k_{ro}$ , for the two cores are shown in Figs. 1.1.10 and 1.1.11. There does not appear to be any discernible trend with temperature. This finding was also reported by Poston, *et al.* (1970).

A possible explanation for the difference in behaviour between the two cores lies in the shapes of the production curves. Core 1 production curves have a much smoother, more rounded shape after breakthrough than do those of Core 2, which tend to resemble the production curves for Berea Sandstone. The functional form for  $N_p$ , given by Eq. 1.1.1 fits the data for Core 1 quite well. However, this form does not reproduce the shape of the original data for Core 2 very well, especially the data immediately after breakthrough. The curve fit is somewhat flatter than the actual data. Since the data immediately after breakthrough determines, to a large extent, the shape of the relative permeability curves, a bad fit to this portion of data yields meaningless curves.

This problem of matching consolidated core production data with a smooth function was also reported by Miller and Ramey (1983). They performed experiments on consolidated Berea cores, but were unable to generate relative permeability curves using either the quadratic or cubic forms of Eq. 1.1.1.

Because of the problem in matching the experimental data, it was concluded that the results of the runs on Core 2 were not representative of the actual physical processes taking place. However, since the curve fit matches were quite good for Core 1, the data were considered to be representative.

A final run (Run 5) was made on Core 1 at room temperature to study the reversibility of the effects observed on endpoint saturations and on relative permeabilities. Figure 1.1.12 shows the relative permeabilities versus reduced water saturation for the first room temperature run (Run 1) compared to the last run at the same temperature (Run 5). Although there is a slight change in oil relative permeability and in  $S_{wi}$  and  $S_{or}$ , it is clear that the effects observed in runs 2 through 4 are, for the most part, reversible. Poston, *et al.* (1970) also reported a slight hysteresis in irreducible water saturation. It was postulated by them that the cores had become increasingly water-wet with temperature.

### Absolute Permeability

The measured absolute permeabilities to distilled water are presented in Table 1. For both cores, there is a decrease in absolute permeability at elevated temperatures. However, the absolute permeability for Run 5 shows that this phenomenon is reversible. Sydansk (1980) reported that absolute permeability to distilled water decreased due to progressive plugging from clay migration. Maini and Batycky (1983) suggested that this phenomenon could be corrected by reversing the flow direction. In this study, successive runs were performed with alternating flow directions. Figure 1.1.13 presents the absolute permeability to distilled water versus temperature for Cores 1 and 2. It is obvious from these data that, if plugging indeed occurred, reversing the flow direction did not correct it, but reducing the temperature did. It seems more likely that the reduction seen in absolute permeability to water is a temperature effect only. However, in Core 2, the data of Fig. 1.1.13 show little temperature effect.

## 1.1.4. CONCLUSIONS AND RECOMMENDATIONS

### Conclusions

Based on the results of this study, the following conclusions have been drawn:

1. The functional relationship used to match the  $N_p$  data is appropriate for cores that yield rounded production curves after breakthrough. However, the production curves with little oil production after breakthrough are not matched well by this form.
2. Both oil and water relative permeabilities increased with increasing temperature to above 215°F. The effect on  $k_{rw}$  was completely reversible when the temperature was subsequently reduced. There was apparently a slight hysteresis observed as oil relative permeability showed a small increase from its original value.
3. Irreducible water saturation was not reached after 14 pore volumes of oil had been injected. The "end point" water saturation after 14 pore volumes of injection increased slightly with increasing temperature.
4. "Practical" residual oil saturation after 14 pore volumes of injected water increased slightly with increasing temperature.

### 1.1.5. FUTURE WORK

Based on the results presented in this study, the following recommendations are made for future work on this topic:

1. Study different functions to find a more appropriate match to use for the production curves resulting from all types of fractional flow curves.
2. Reduce the downstream dead volume, especially in the back pressure regulator, to reduce the effect of fractional flow on the shifted data. Smaller diameter tubing will also decrease the volume slightly.
3. Include the effects of oil/water solubility in the calculations.
4. Determine the effect of flow rate on the stability of relative permeability curves from the criteria presented by Sufi *et al.* (1982).
5. Further investigate confining sleeve alternatives with higher operating temperatures.

### 1.1.6. NOMENCLATURE

$A$	Cross-sectional area
$D$	Downstream dead volume (pore volumes)
$f_o$	fractional flow of oil
$f_{o2}$	fractional flow of oil at the outlet face
$f_w$	fractional flow of water
$f_{w,d}$	fractional flow of water in the downstream dead volume
$I_r$	dimensionless injectivity, $(q/\Delta p)/(q/\Delta p)_{initial}$
$k_{abs}$	absolute permeability to water
$k_{eff}$	effective permeability at end point saturation
$k_{ro}$	relative permeability to oil
$(k_{ro})_2$	relative permeability to oil at the outlet face

- $k_{rw}$  relative permeability to water  
 $(k_{rw})_2$  relative permeability to water at the outlet face  
 $L$  core length  
 $N_p$  dimensionless oil production (in pore volumes)  
 $N_{p, meas}$  experimentally measured oil production (in pore volumes)  
 $\Delta p$  pressure drop  
 $q_{tot}$  total flow rate  
 $S_{or}$  residual oil saturation  
 $\bar{S}_w$  average water saturation  
 $S_{wi}$  irreducible water saturation  
 $S_{w, red}$  reduced water saturation,  $(S_w - S_{wi}) / (1 - S_{or} - S_{wi})$   
 $S_{w2}$  water saturation at outlet face  
 $T$  temperature  
 $U$  upstream dead volume (pore volumes)  
 $W_i$  dimensionless water injection (pore volumes)  
 $W_{i, meas}$  experimentally measured water injection (pore volumes)  
 $\mu_o$  oil viscosity  
 $\mu_w$  water viscosity  
 $\nu$  kinematic viscosity  
 $\rho_o$  oil density  
 $\rho_{ob}$  oil density at beaker conditions  
 $\rho_{oo}$  oil density at oven conditions  
 $\rho_w$  water density  
 $\rho_{wb}$  water density at beaker conditions  
 $\rho_{wo}$  water density at oven conditions

## REFERENCES

1. Casse, F.J. and Ramey Jr., H.J.: "The Effect of Temperature and Confining Pressure on Single-Phase Flow in Consolidated Rocks," *J. Pet. Tech.* (August 1980), p. 1051.
2. Davidson, L.B.: "The Effect of Temperature on the Relative Permeability Ratio of Different Fluid Pairs in Two Phase Systems," *J. Pet. Tech.* (August 1969), p. 1037.
3. Gobran, B.D., Brigham, W.E. and Ramey Jr., H.J.: "Absolute Permeability as a Function of Confining Pressure, Pore Pressure, and Temperatures," SPE #10156. Paper presented at the SPE 56th Annual Fall Technical Conference and Exhibition, San Antonio (October 5-7, 1981).
4. Edmonson, T.A.: "Effect of Temperature on Waterflooding," *J. Can. Pet. Tech.*, (October-December, 1965), p. 236.
5. Johnson, E.F. and Bossler, D.P. and Nauman, V.O.: "Calculation of Relative Permeability from Displacement Experiments", *Trans. AIME*, (1959) No. 370, 216.

6. Lo, H.Y. and Mungan, N., "Effect of Temperature on Water-Oil Relative Permeabilities in Oil-Wet and Water-Wet Systems", *SpePaper 4505*, 48th Annual Meeting, (Sept. 30 - Oct. 3, 1973), Las Vegas,
7. Maini, B.B. and Batycky, J.P., "Effect of Temperature on Heavy-Oil/Water Relative Permeabilities in Horizontally and Vertically Drilled Core Plugs", *SpePaper 12115*, 58th Annual Technical Conference and Exhibition, Oct. 5-8, 1983, San Francisco.
8. Miller, M.A. and Ramey Jr., H.J., "Effect of Temperature on Oil/Water Relative Permeabilities of Unconsolidated and Consolidated Sands", *SpePaper 12116*, 58th Annual Technical Conference and Exhibition, Oct. 5-8, 1983, San Francisco.
9. Poston, S.W. and Ysrael, S. and Hossain, A.K.M.S. and Montgomery III, E.F. and Ramey Jr., H.J., "Effect of Temperature on Irreducible Water Saturation and Relative Permeability of Unconsolidated Sands", *Soc. Pet. Eng. J.*, June, 1970, p. 171.
10. Sinnokrot, A.A. and Ramey Jr., H.J. and Marsden Jr., S.S., "Effect of Temperature Level upon Capillary Pressure Curves", *Soc. Pet. Eng. J.*, March 1971, p. 13
11. Sufi, A.S. and Ramey Jr., H.J. and Brigham, W.E., "Temperature Effects on Relative Permeabilities of Oil-Water Systems", *Spe Paper 11071*, 57th Annual Technical Conference and Exhibition, New Orleans, Sept. 26-29, 1982.
12. Sydansk, R.D., "Discussion of the Effect of Temperature and Confining Pressure on Single-Phase Flow in Consolidated Rocks", *J. Pet. Tech.*, August 1980, p. 1329.
13. Torabzadeh, S.J. and Handy, L.L., "The Effect of Temperature and Interfacial Tension on Water/Oil Relative Permeabilities of Consolidated Sands", *Spe Paper 12689*, SPE/DOE Fourth Symposium on Enhanced Oil Recovery, April 15-18, 1984, Tulsa
14. Weinbrandt, R.M. and Ramey Jr., H.J. and Cass'e, F.J., "The Effect of Temperature on Relative and Absolute Permeability of Sandstones", *Soc. Pet. Eng. J.*, October, 1975, p. 376
15. Sageev, A. and Gobran, B.D. and Brigham, W.E. and Ramey Jr., H.J., "The Effect of Temperature on the Absolute Permeability to Distilled Water of Unconsolidated Sand Cores", *Proceedings, 6th Workshop on Geothermal Reservoir Engineering*, Stanford University, Dec. 16-18, 1980, p. 297.
16. Numere, D. and Brigham, W.E. and Standing, M.B., "Correlations for Physical Properties of Petroleum Reservoir Brines", *Technical Report No. 1*, November, 1977 Stanford University Petroleum Research Institute,
17. Welge, H.J., "A Simplified Method for Computing Oil Recovery by Gas or Water Drive", *Trans. AIME, No. 91*, 195, 1952.
18. Jones, S.C. and Roszelle, W.O., "Graphical Tehniques for Determining Relative Permeability from Displacement Experiments", *J. Pet. Tech.*, May, 1978, p. 807
19. Miller, M.A., "Effect of Temperature on Oil-Water Relative Permeabilities of Unconsolidated and Consolidated Sands", *Technical Report No. 64* Stanford Geothermal Program, June, 1983.

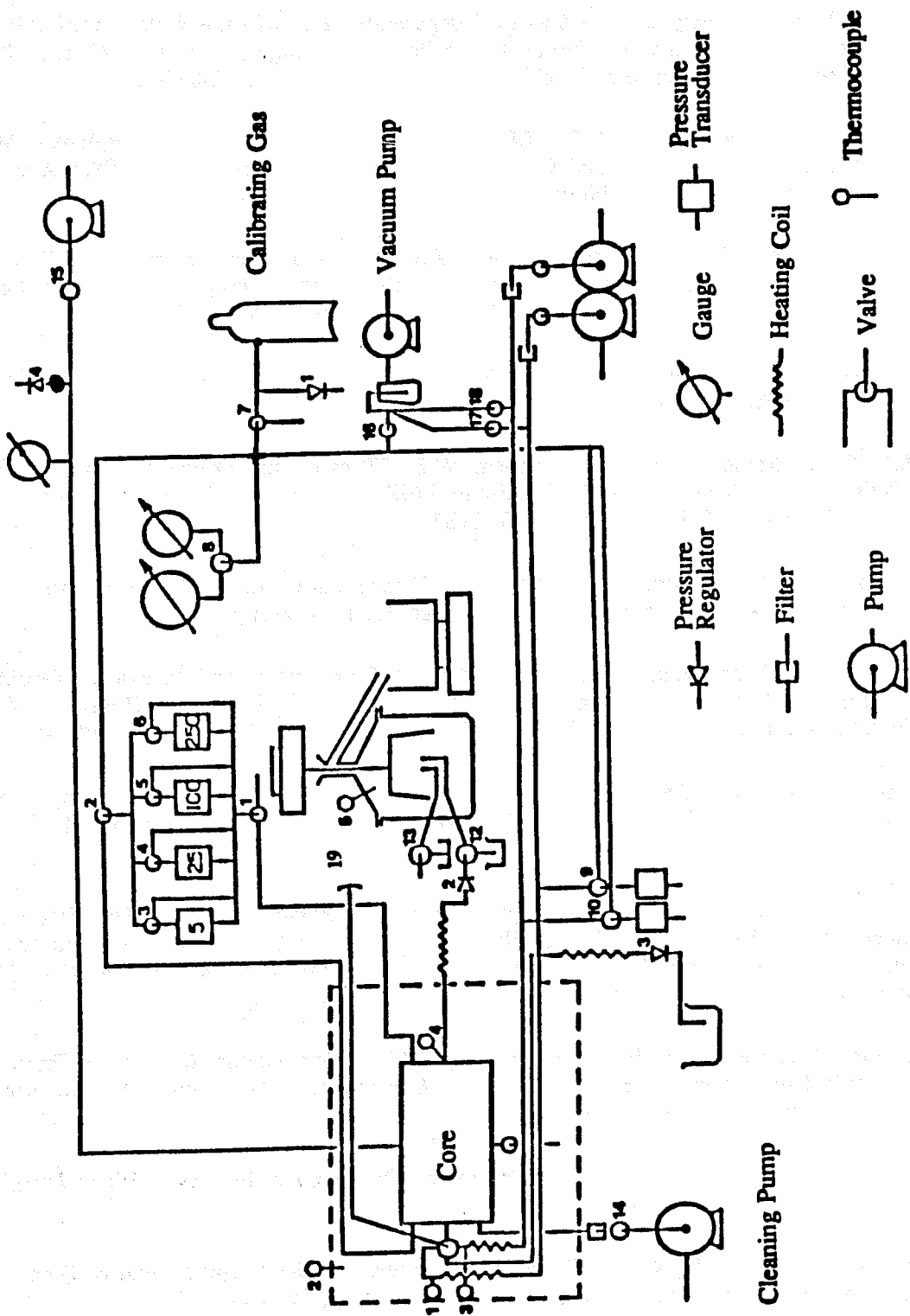


Figure 1.1.1 Experimental apparatus.

1. Neck Diameter Tube
2. Overflow Tube
3. Momentum Dissipator
4. Oil Confining Cup
5. Hanging Wire
6. Oil Drainage Pipe
7. Production Pipe
8. Thermocouple
9. Total Production Balance
10. Oil Fraction Balance

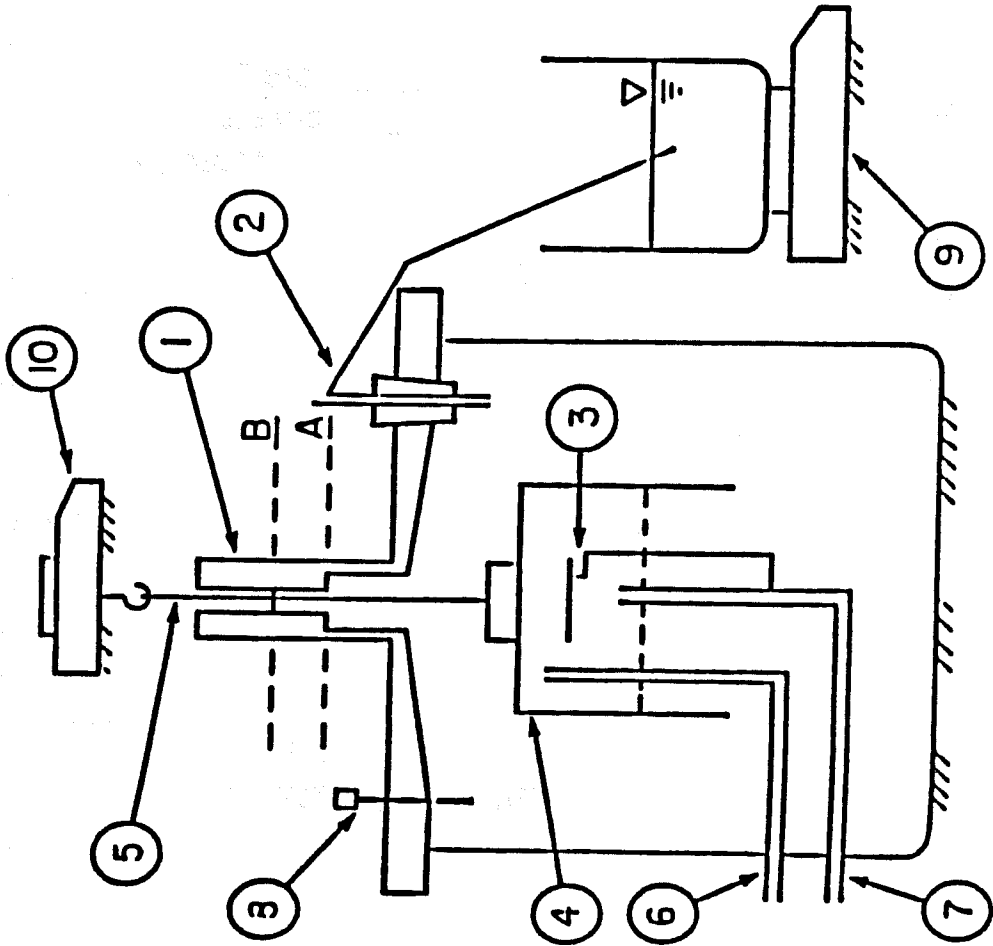


Figure 1.1.2 Measurement apparatus.

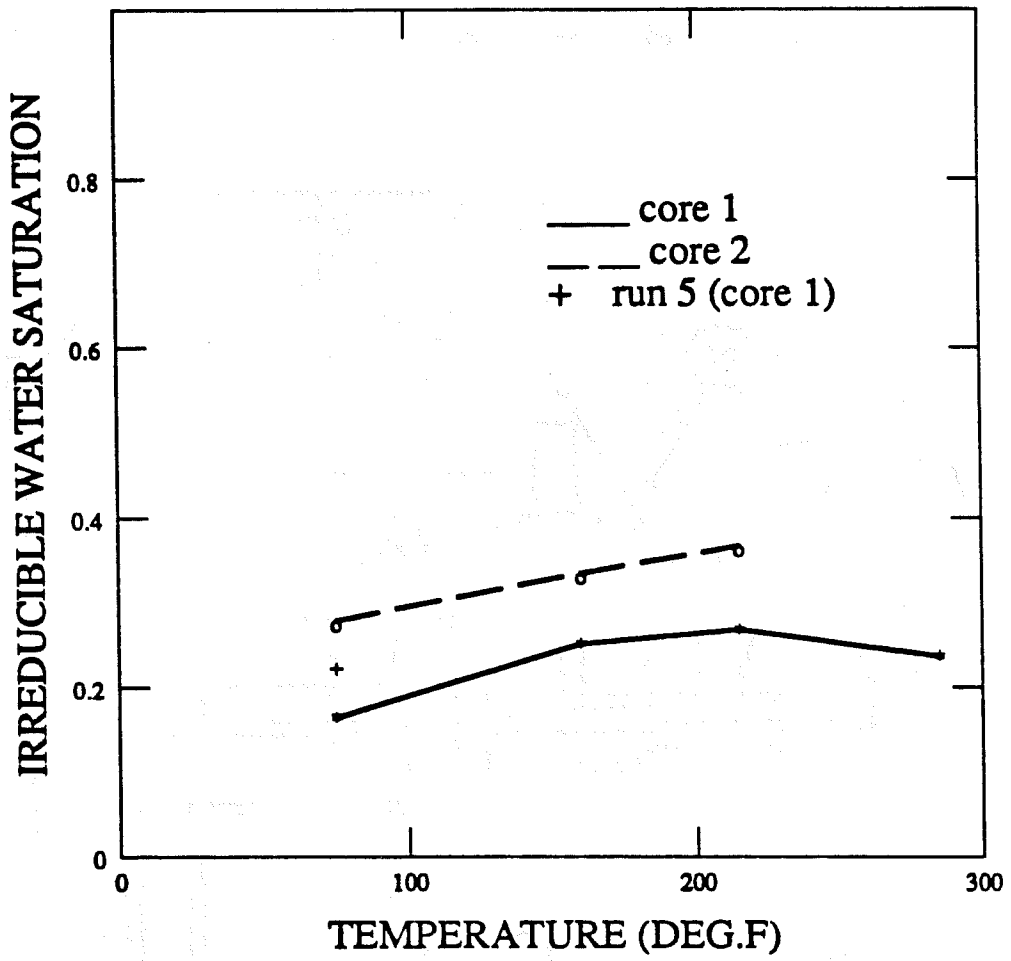


Figure 1.1.3 Irreducible water saturation versus temperature.

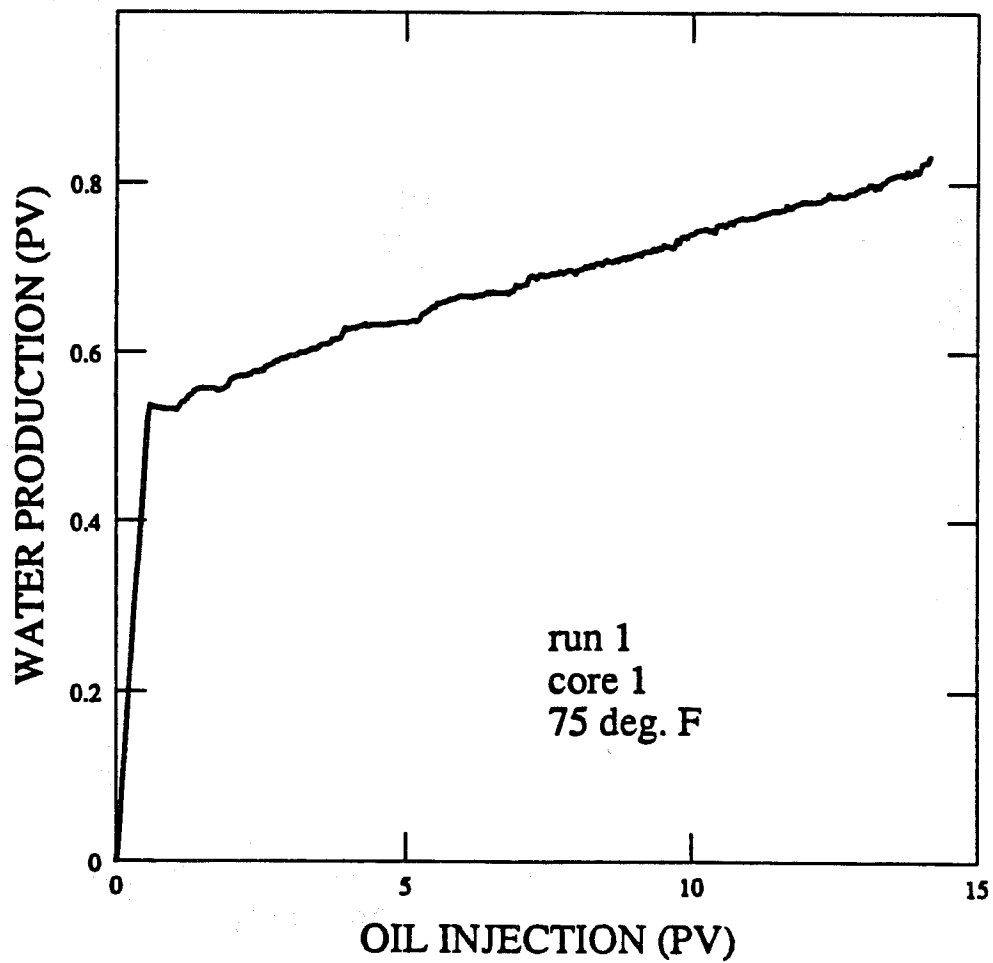


Figure 1.1.4 Production curve for drainage displacement.

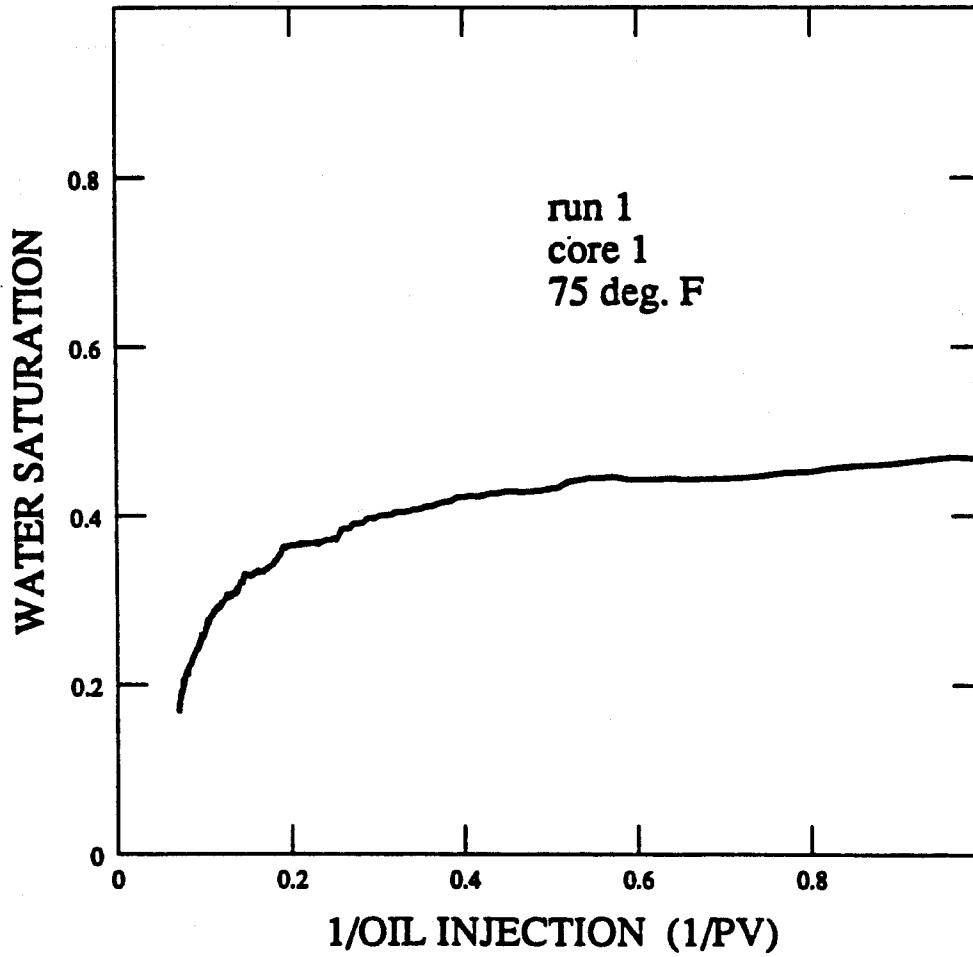


Figure 1.1.5 Water saturation versus reciprocal of oil injection volume, run 1, core 1, 75°F.

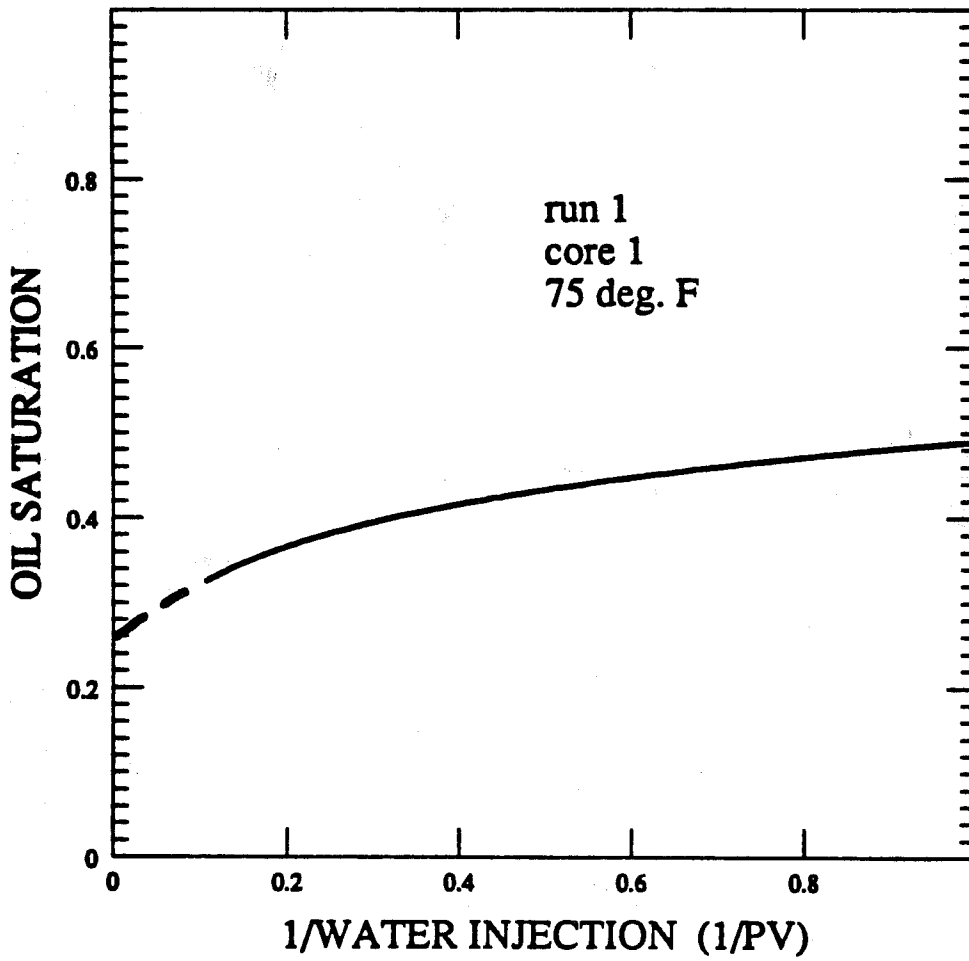


Figure 1.1.6 Oil saturation versus reciprocal of water injection volume, Run 1, Core 1, 75°F.

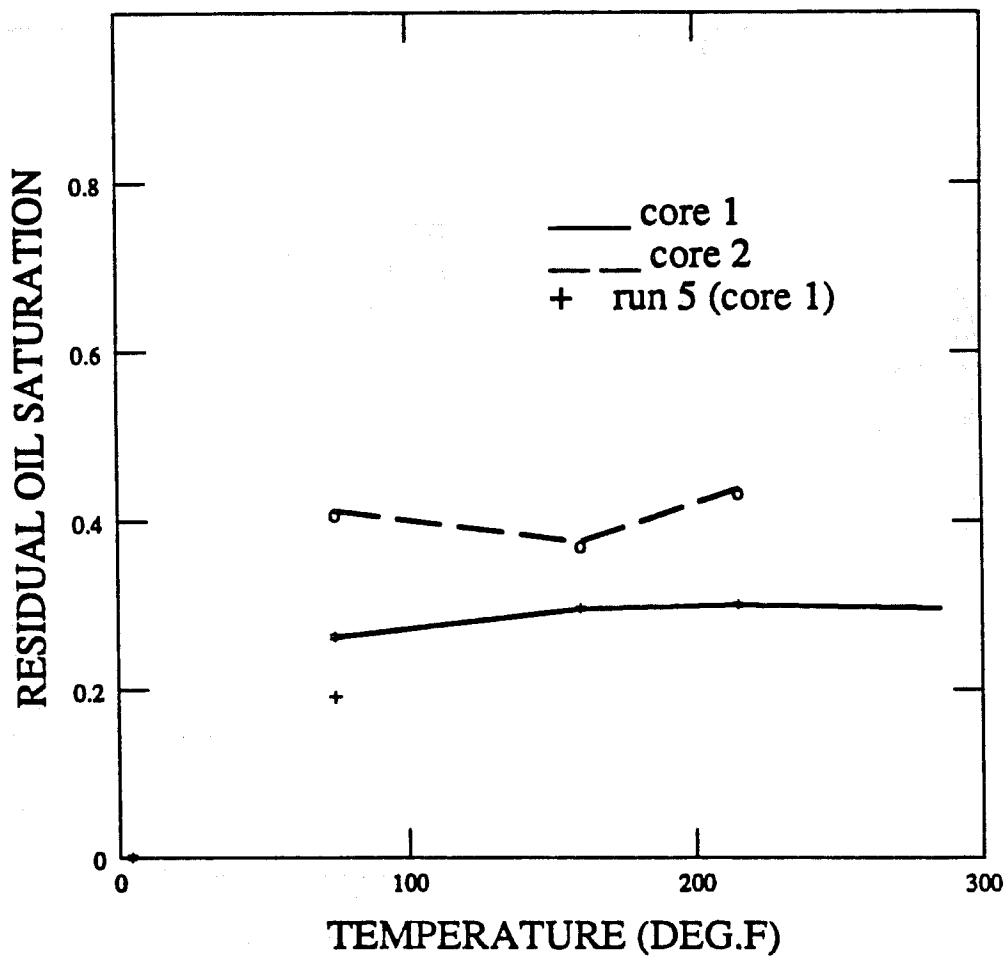


Figure 1.1.7 Residual oil saturation versus temperature, brown sandstone.

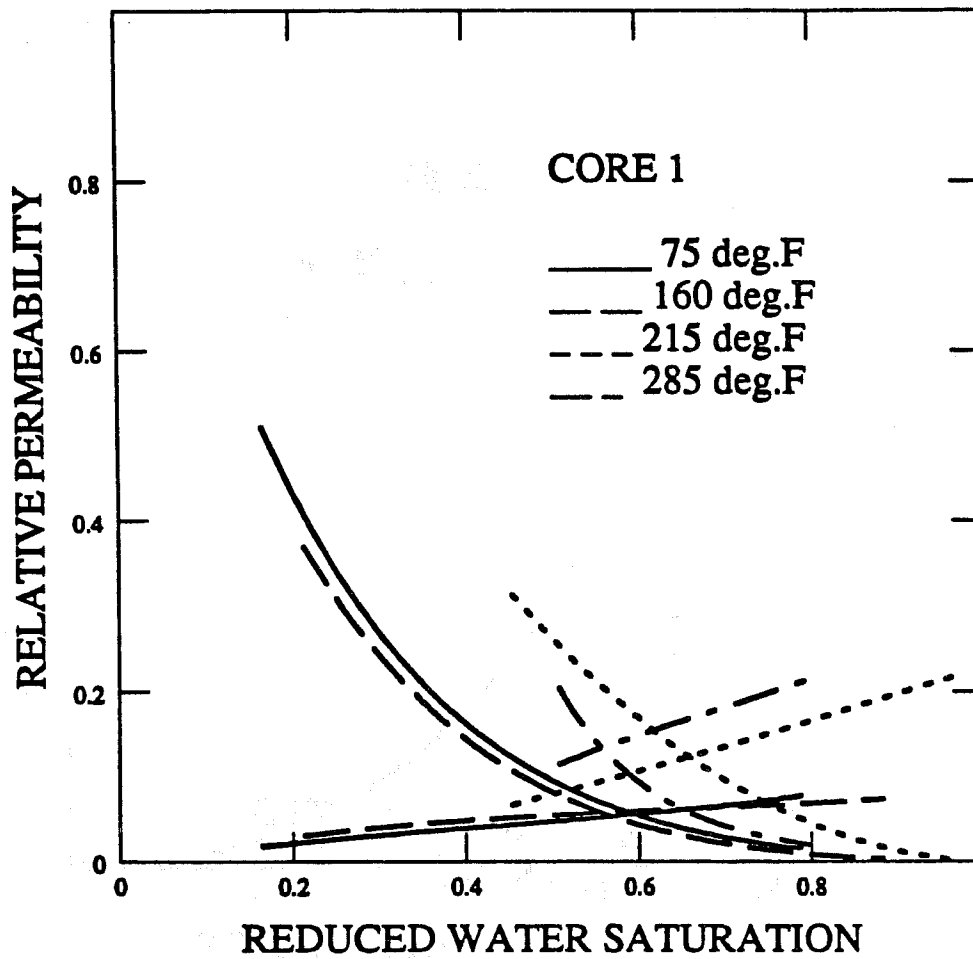


Figure 1.1.8 Relative permeabilities--Core 1.

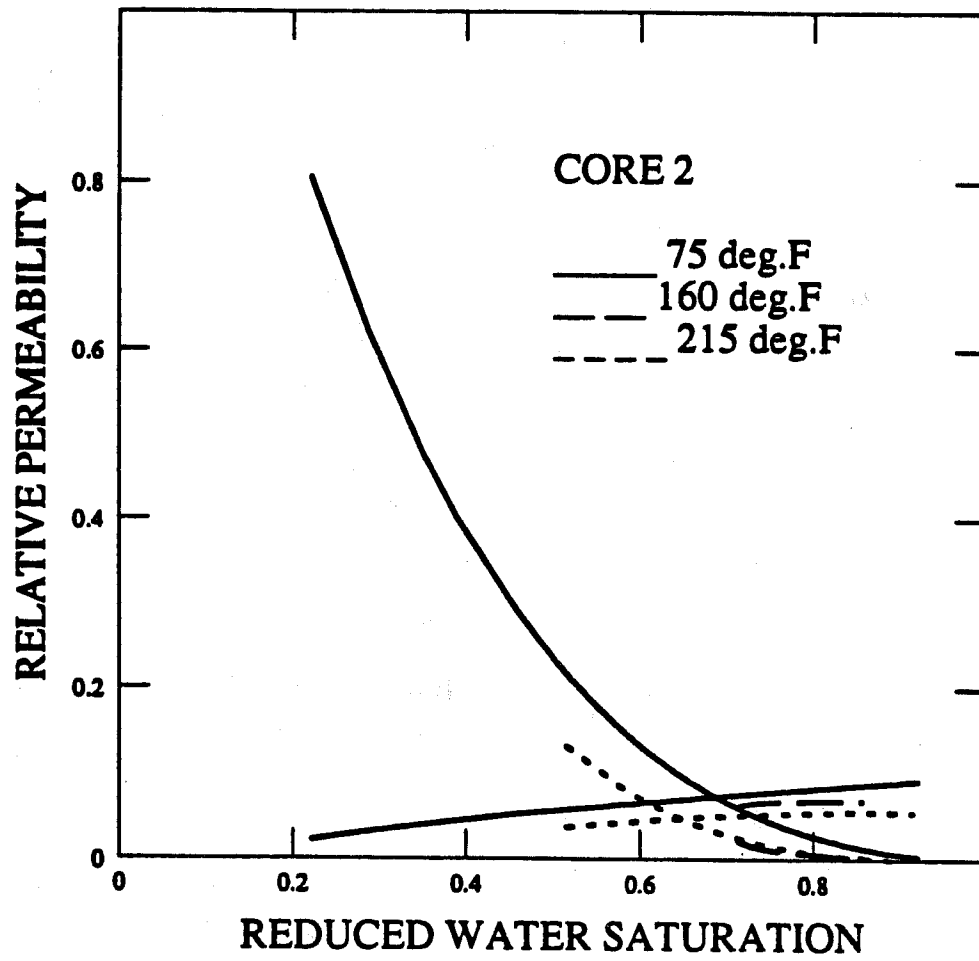


Figure 1.1.9 Relative permeabilities--Core 2.

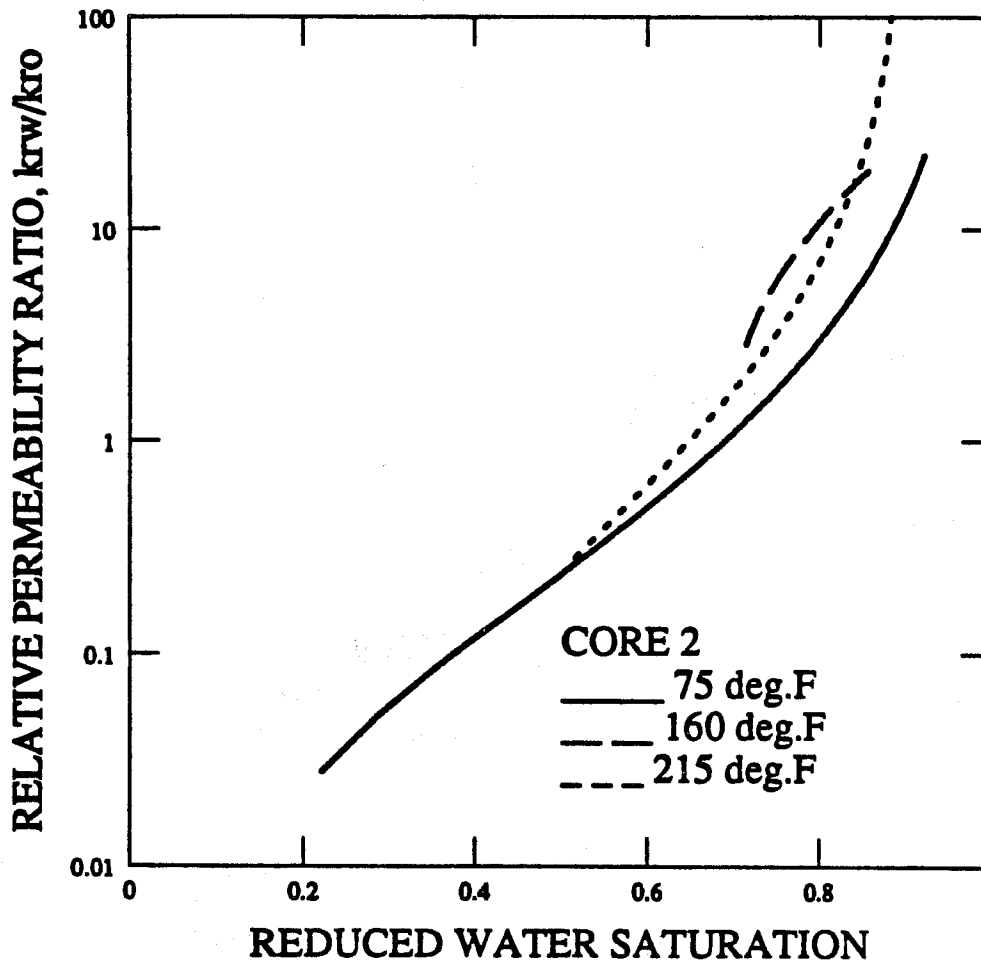


Figure 1.10 Relative permeability ratio--Core 1.

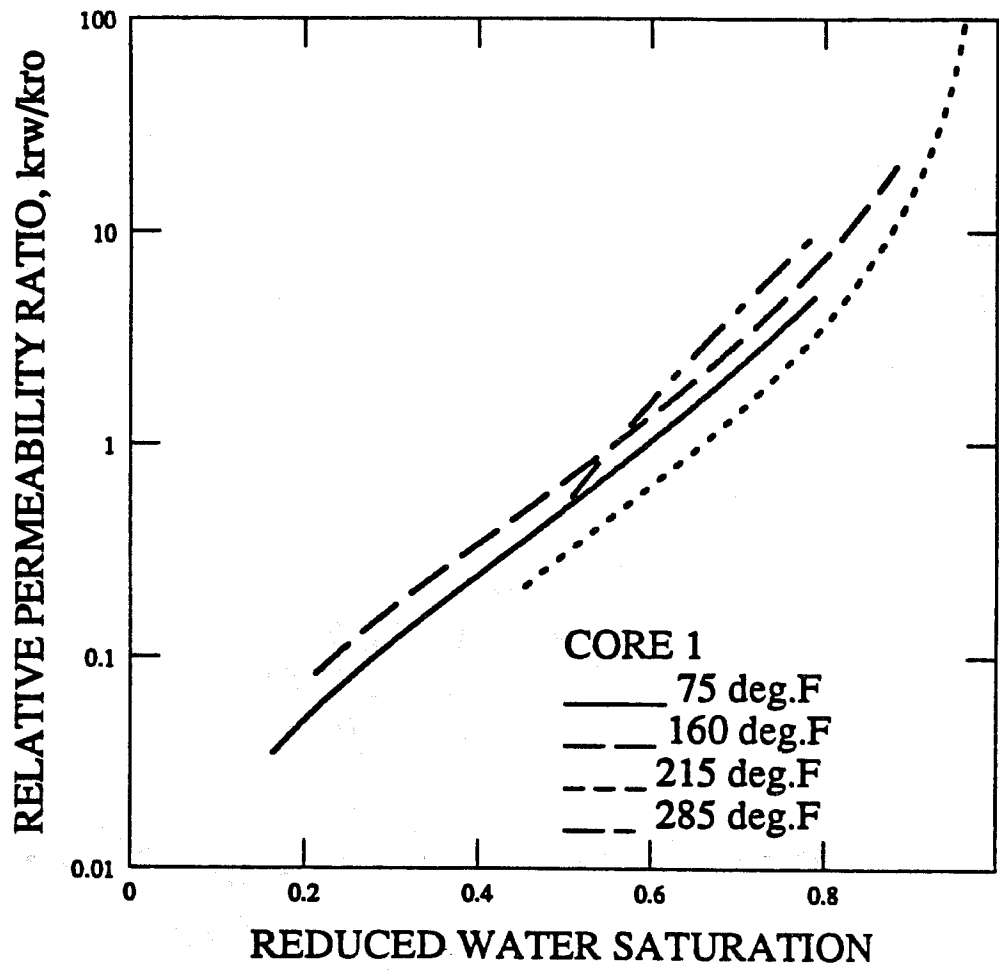


Figure 1.11 Relative permeability ratio--Core 2.

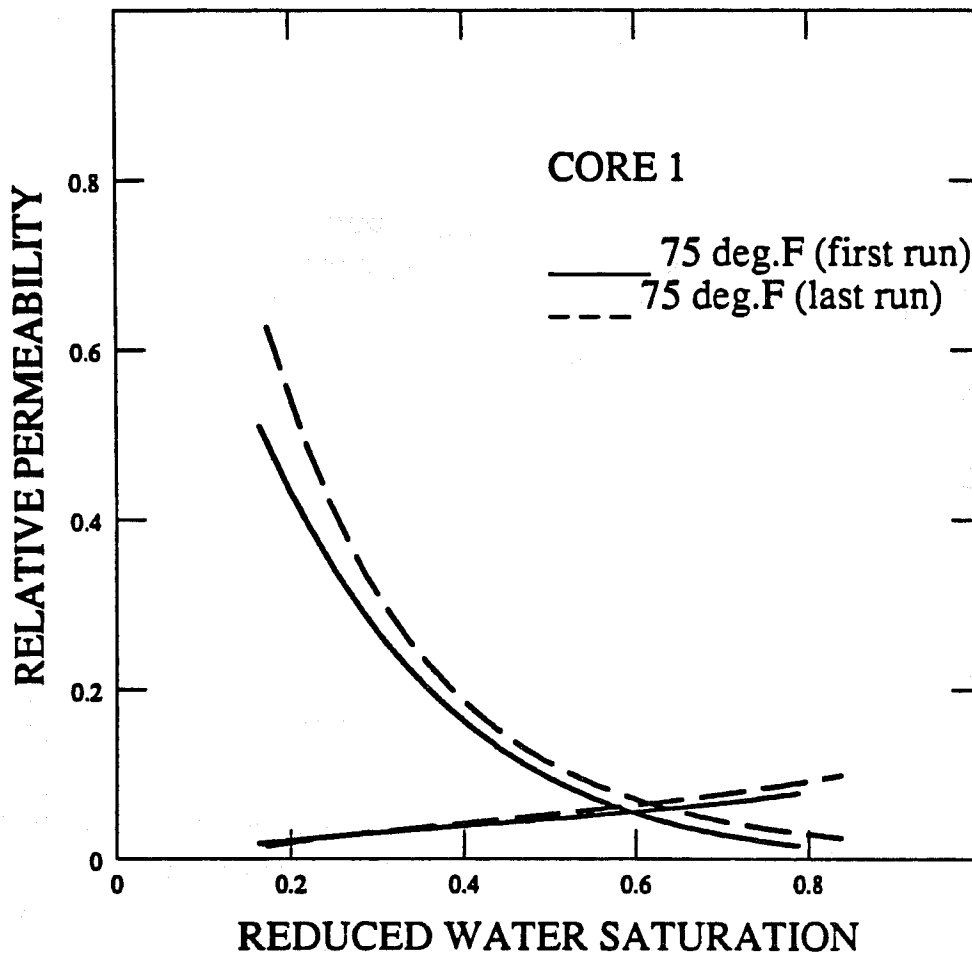


Figure 1.1.12 Room temperature relative permeabilities--Core 1.

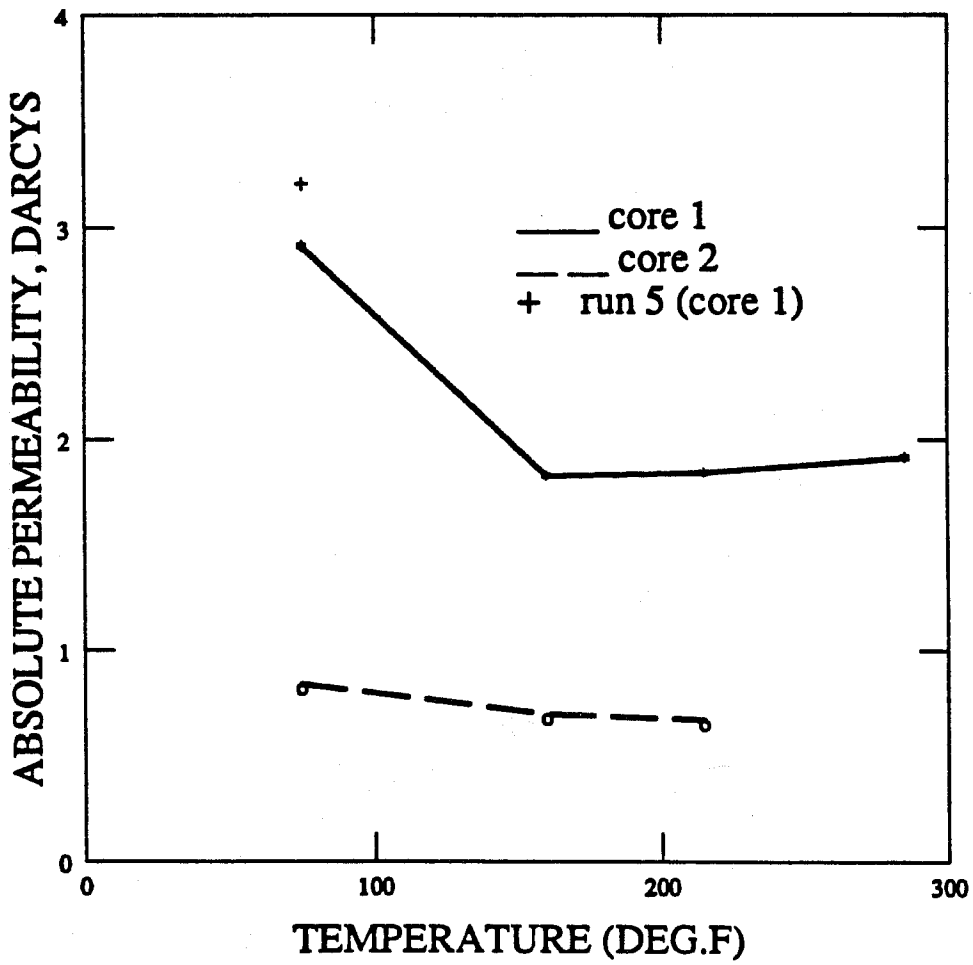


Figure 1.1.13 Absolute water permeability versus temperature.

## 1.2 A COMPARISON OF RELATIVE PERMEABILITY FROM CENTRIFUGING VERSUS COREFLOODING (David Shimbo)

A technical report on this topic is in the draft stage. The following is a summary of this work.

### 1.2.1. ABSTRACT

Laboratory measurement of relative permeability has traditionally taken place using unsteady-state coreflood tests. Procedures also exist for deriving relative permeabilities from centrifuge data, but the shapes of the curves are different than those from coreflooding. This research compared coreflood relative permeabilities versus centrifuge relative permeabilities by obtaining coreflood and centrifuge data from the same piece of Berea sandstone for gas/oil and oil/water systems. A one dimensional coreflood/centrifuge model, a least squares history matching algorithm, and the Corey relationships were used to reproduce the experimental data. Jones-Roszelle and Hagoort relative permeability curves were compared with the Corey curves that were obtained from simulation history matching.

Comparison of the two sets of relative permeability curves from centrifuging versus coreflooding for the oil/water system displayed similar shapes and endpoints for the wetting phase, but showed different shapes and endpoints for the nonwetting phase.

### 1.2.2. INTRODUCTION

Measurement of relative permeability from laboratory data has become an increasingly important subject in reservoir engineering as the need has arisen for more accurate forecasting of production and ultimate recovery. Engineers now recognize that the shape of the relative permeability curve is as important as the endpoint saturation.

Several methods of measuring relative permeability are available, but the Johnson, Bossler, and Naumann (JBN) unsteady state coreflood technique has predominated over other methods because of its simplicity and relatively short experimental time. This method essentially floods a saturated core plug with a nonwetting fluid at a constant rate. Cumulative recoveries of the wetting and nonwetting phases are measured at the outlet face versus time. These recovery versus time relationships are converted to relative permeability curves using a graphical technique developed by Jones and Roszelle.

Relative permeability for the wetting phase can also be measured from centrifuge data using a method developed by Hagoort. An oil-saturated core is placed in a centrifuge with gas introduced at the inlet face. The centrifuge is rotated at a constant speed, and cumulative recovery vs. time is measured at the outlet face. This data is then converted to relative permeabilities using a log-log plot to determine Corey coefficients for the wetting phase.

The relative permeability curves from centrifuging and coreflooding often differ in both shape and endpoint saturations. Centrifuge curves cover a wider range of saturations and have a tendency to exhibit lower residual wetting phase saturations. Coreflood curves require extrapolation to residual saturation endpoints, and measurement error often results from the graphical determination of slope.

The objectives of this research are:

1. Build a generalized coreflood/centrifuge simulation model for determining relative permeability.
2. Compare laboratory relative permeability data from the same rock using the Jones and Roszelle method for coreflooding versus the Hagoort method for centrifuging.
3. Use a simulation model, a least squares algorithm, and laboratory data to history match Corey parameters for both centrifuge relative permeabilities and coreflood relative permeabilities.

This problem was investigated from two different perspectives:

1. Experimental analysis of laboratory data - Coreflood and centrifuge relative permeability experiments on Berea sandstone samples were completed by Chevron. This data was processed using the Jones and Roszelle method for coreflooding and the Hagoort method for centrifuging. Relative permeability results were compared.
2. Simulation models - Linear coreflood and centrifuge simulation models were built that included terms for capillary pressure and centrifugal gravity. A least squares algorithm that adjusted the coefficients in the Corey equations was used to match experimental data with model data. The experimental relative permeability curves from coreflooding and centrifuging were compared with the history match relative permeability curves.

By comparing relative permeability curves from coreflooding versus centrifuging, the key parameters that influence the relative flow of oil, gas, and water through porous media will be identified. This, in turn, may improve the application of raw laboratory relative permeability curves to large scale engineering problems.

### 1.2.3. EXPERIMENTAL DESCRIPTION

Experimental data was supplied by Chevron Oilfield Research Company (COFRC). Coreflooding and centrifuge displacement tests were performed using Berea sandstone cores. All tests were performed in the drainage mode with gas (nitrogen or air) displacing white oil or with depolarized kerosene displacing a glycerol/brine mixture. For each Berea core, the following experimental procedure was followed:

1. Air permeability and helium porosity was measured using the long core (4.5" × 1").
2. The core was saturated with the wetting phase, then an unsteady state drainage relative permeability test was performed.
3. The long core was cleaned and dried, then cut into four equal segments (1" × 1").
4. Air permeability and helium porosity were measured on each of these segments.
5. Each core was saturated with the wetting phase, then placed in a centrifuge for drainage capillary pressure measurement.

6. The coreplugs were cleaned, then air permeability was measured again.
7. The coreplugs were saturated with the wetting phase. Transient wetting phase production was measured at several rotational speeds (1000, 2000, 3000, 4000 R.P.M.)

Centrifuge capillary tests were run on all samples. Graphs of  $P_c$  versus  $S_w$  for the gas/oil system showed residual oil saturations ranging from 0.10 to 0.25. The water/oil system showed more consistent residual saturations of about 0.10. Each of these capillary pressure curves was converted into a simple functional form using the relationship:

$$P_c = A \ln \left( \frac{S_w - S_{wir}}{1 - S_{wir}} \right) + P_{th} \quad (1.2.1)$$

$P_c$  = capillary pressure (atm)

$P_{th}$  = entry pressure (atm)

A = constant obtained from cubic spline fit of experimental data

The gas/oil coreflood test ran for about 80 minutes and displaced 6.0 cc. (0.48 pore volumes) of oil. The production versus pore volume injected graph showed consistent displacement data. Additional early time recovery data would have been useful for history matching.

The water/oil coreflood ran for about 8 hours and displaced 8.0 cc. of the wetting phase (0.666 pore volumes) with a total injection of about 40 pore volumes. Breakthrough took place at about 2.4 minutes. The production versus pore volume injected graph showed slight inconsistencies in early time.

Both gas/oil and oil/water centrifuge data were slightly irregular in early time, probably due to measurement error. Higher RPM runs resulted in residual saturations as low as  $S_{wir} = 0.13$  for the 3000 RPM gas/oil run and  $S_{wir} = 0.16$  for the 4000 RPM water/oil run.

Rotational speed versus time data were supplied for the centrifuge so that history matching could account for acceleration from zero to a stabilized RPM. This data were quite useful for history matching, since the amount of production during this initial acceleration period (50-60 seconds) was significant.

This experimental procedure provided the raw data necessary to calculate unsteady state coreflood relative permeability, centrifuge relative permeability, and capillary pressure from the same rock sample.

#### 1.2.4. RELATIVE PERMEABILITY FROM COREFLOODING (Jones-Roszelle)

The Jones-Roszelle graphical technique for determining relative permeability was a useful way to provide an initial guess for history matching and also to verify the final history match solution using a nonsimulation technique. This technique assumes capillary pressure is negligible. Two graphs were necessary: (1) average nonwetting phase saturation ( $S_{navg}$ ) versus pore

volume injected ( $PV_{inj}$ ), and (2) effective viscosity versus pore volume injected. Average nonwetting saturation was calculated using:

$$S_{navg} = \frac{N_p}{V_p} \quad (1.2.2)$$

$S_{navg}$  = average nonwetting phase saturation

$N_p$  = produced water ( $cm^3$ )

$V_p$  = total pore volume ( $cm^3$ )

$S_{navg}$  was graphed versus pore volume of oil injected on a Cartesian scale. The saturations at the outlet face of the core were determined by drawing a series of tangents to the curve. The intercepts with the ordinate axis were the outlet face saturations. These outlet face saturations were converted to fractional flows, which were then converted to relative permeabilities.

Effective viscosity was determined from:

$$\lambda^{-1} = \mu_b \frac{\Delta p q_b}{\Delta p_b q} \quad (1.2.3)$$

$\lambda^{-1}$  = effective viscosity (cp)

$\mu_b$  = viscosity of fluid used to find absolute permeability (cp)

$\Delta p$  = pressure drop across core (psia)

$\Delta p_b$  = pressure drop when finding absolute permeability (psia)

$q$  = injection rate (cc/sec)

$q_b$  = injection rate used when finding absolute permeability (cc/sec)

A Cartesian graph of effective viscosity versus pore volume injected was prepared. Using the same tangent method as previously described, a series of tangents to the average viscosity curve were extended to the axis. The intercepts with the ordinate axis were the outlet face effective viscosities ( $\lambda_{eff}^{-1}$ ).

Fractional flow for the wetting and nonwetting phases was determined using:

$$f_w = 1 - f_n = \frac{S_{navg} - S_{nint}}{PV_{inj}} \quad (1.2.4)$$

$f_w$  = fractional flow for wetting phase

$f_n$  = fractional flow for nonwetting phase =  $1 - f_w$

$S_{winj}$  = outlet face wetting phase saturation

$PV_{inj}$  = pore volume injected

Point values for relative permeability were calculated from:

$$k_{rw} = \frac{f_w \mu_w}{\lambda_{eff}^{-1}} \quad (1.2.5)$$

$$k_{rn} = \frac{f_n \mu_n}{\lambda_{eff}^{-1}} \quad (1.2.6)$$

$k_{rw}$  = wetting phase relative permeability

$k_{rn}$  = nonwetting phase relative permeability

$\mu_w$  = wetting phase viscosity (cp)

$\mu_n$  = nonwetting phase viscosity (cp)

$\lambda_{eff}^{-1}$  = outlet face effective viscosity

Values for the oil/water coreflood from the Berea sandstone are graphed in the Results and Discussion section.

### 1.2.5. RELATIVE PERMEABILITY FROM CENTRIFUGING (Hagoort's Technique)

Hagoort derived a graphical technique for determining nonwetting phase relative permeability using the Corey relationship. He assumed an insignificant capillary pressure effect and a large mobility difference between gas and liquid phases.

Measurements during centrifuge displacement gave production versus time data. These were converted to dimensionless values:

$$N_p = \frac{\text{cumulative production}}{\phi^* AL} \quad (1.2.7)$$

$$t_d = \frac{\Delta \rho_{og} g k t}{\mu_o \phi^* L} \quad (1.2.8)$$

and

$$\phi^* = \phi (1 - S_{wir} - S_{or}) \quad (1.2.9)$$

$N_p$  = pore volume produced

$t_d$  = dimensionless time

$\phi^*$  = reduced porosity

$S_o$  = oil saturation

$S_{wir}$  = irreducible water saturation

$S_{or}$  = residual oil saturation

$\Delta\rho_{og}$  = density difference between oil and gas phases (g/cc)

$g$  = gravitational factor =  $4\pi^2 f^2 r_m$

$f$  = rotational frequency (cycles/min)

$r_m$  = average length of rotational axis (cm)

$k$  = permeability (Darcys)

$\mu_o$  = viscosity of oil (cp)

$A$  = cross sectional area ( $cm^2$ )

$L$  = length of coreplug (cm)

$t$  = time (sec)

A plot of  $\ln(1 - N_p)$  versus  $\ln(t_d)$  was used to determine coefficients for a modified form of the Corey equation:

$$k_{rw} = k_{r0}^0 \left[ \frac{S_o - S_{or}}{1 - S_{or} - S_{wir}} \right]^n \quad (1.2.10)$$

$k_{r0}^0$  = wetting phase factor

$n$  = wetting phase exponent

The exponential coefficient  $n$  was determined from the slope of the resulting straight line using the relationship:

$$\text{slope} = \frac{d \ln(1 - N_p)}{d \ln(t_d)} = - \frac{1}{n - 1}$$

The factor  $k_{r0}^0$  was obtained from the intercept at  $t_d = 1$ . Hagoort noted that  $k_{r0}^0$  is a dimensionless curve fitting parameter and does not have any significance with respect to the endpoint of the oil relative permeability curve.

Experimental data for the 1000, 2000, and 3000 RPM gas/oil centrifuge systems show that two distinct slopes occur. The first slope represents the acceleration period from startup to constant R.P.M. The second slope represents centrifugal displacement under constant acceleration, and is used to determine the Corey coefficients.

### 1.2.6. CENTRIFUGE MODEL DESCRIPTION

The centrifuge model is a linear one-dimensional multicell model that simulates a nonwetting phase displacing a wetting phase (drainage mechanism) in a coreplug under centrifugal acceleration. A 1" by 1" coreplug initially 100% saturated with the wetting phase is accelerated from 0 to 3000 RPM, then centrifuged at a constant RPM until recovery of the wetting phase is insignificant. Accurate measurements of centrifuge speed, recovery, and time are important throughout the run since the shape and endpoints of the relative permeability curves are quite sensitive to these parameters. High permeability samples are an incompressible rock system quite sensitive to the initial acceleration period because a significant pore volume is displaced before the centrifuge reaches a stabilized rotational speed.

Important assumptions in the derivation of flow equations for the centrifuge include:

1. An incompressible rock system
2. Homogeneous porosity and permeability
3. Incompressible fluids
4. Linear Darcy flow
5. Two phases - wetting and nonwetting

An approach similar to the one described by O'Meara and Crump is used to derive the two phase flow equations.

The centrifuge model consisted of 40 cells with intercell flow controlled by Darcy's law and an additional term for centrifugal acceleration. This modified form of Darcy's law was combined with the continuity equations to solve for saturation. The saturation solution was discretized, then solved explicitly. To maintain model stability, timestep size was automatically reduced if the saturation change in any cell exceeded 5%. A material balance check was also included to monitor solution error.

Flow of the wetting and nonwetting phases takes place according to relative permeability and fractional flow equations using the Corey relationships.

$$k_{rw} = \left[ \frac{S_w - S_{wir}}{1 - S_{wir}} \right]^{C1} \quad (1.2.11)$$

$$k_{rn} = C3 \left[ 1 - \frac{S_w - S_{wir}}{1 - S_{wir}} \right]^{C2} \quad (1.2.12)$$

$k_{rn}$  = nonwetting phase relative permeability

$k_{rw}$  = wetting phase relative permeability

C1, C2, C3 = Corey constants used in history matching experimental data

$S_w$  = water saturation

$S_{wir}$  = irreducible water saturation

Capillary pressure effects were also included in both centrifuging and coreflooding models. Experimental capillary pressure data from the rock samples were curve fit using a nonlinear regression program and defined using the following simple exponential relationship:

$$P_c = A \ln \left[ \frac{S_w - S_{wir}}{1 - S_{wir}} \right] + P_{th} \quad (1.2.13)$$

$P_c$  = Capillary pressure (atm)

$A$  = Capillary pressure factor

$P_{th}$  = Entry/threshold pressure (atm)

### Boundary Conditions for the Centrifuge

Centrifuging is performed under a drainage mode, so the core is initially 100% saturated with the wetting phase, then displaced by the nonwetting phase using centrifugal force. Therefore, since only the nonwetting phase is entering the coreplug, the velocity of the wetting phase at the inlet face is zero.

$$u_{w,inlet} = 0 \quad (1.2.14)$$

At the outlet face, several important assumptions are made. Since no production of the nonwetting phase takes place in centrifuging, it is proposed that the outlet face is 100% saturated with the wetting phase. The nonwetting phase displaces the wetting phase throughout the core except at the outlet face, which remains 100% wetting phase saturated. Within the core, the wetting phase saturation gradually decreases until only the irreducible saturation remains. This leads to the conclusion that capillary pressure is zero at the outlet face

$$S_{w,outlet} = 1.0 \quad (1.2.15)$$

$$P_{c,outlet} = 0.0 \quad (1.2.16)$$

It should be noted that this model is accurate for oil/water displacement, but may not be representative for gas/oil systems because of the assumption of incompressible fluids.

### 1.2.7. COREFLOOD MODEL DESCRIPTION

Coreflood model equations were defined using the same methodology and assumptions as the centrifuge derivation, except that the term for centrifugal acceleration was excluded from Darcy's law.

A 40 cell linear system was used to simulate the 1" by 1" coreplug. To verify the model, saturation profiles at various times were generated and compared with Buckley-Leverett calculations. Breakthrough from the Buckley-Leverett  $f_w$  versus  $S_w$  plot was  $S_{w,breakthrough} = 0.76$  while the model showed initial breakthrough at  $S_{w,breakthrough} = 0.72$ .

Additionally, a commercial simulator (black oil BOAST) was run using similar input data. Although breakthrough times were the same for both models, the saturation profiles were different because the BOAST model is more implicit and automatically adjusts timestep size. Numerical dispersion was much less in the explicit model than it was in the IMPES BOAST model.

#### Boundary Conditions for Coreflooding

Initial conditions for coreflooding under a drainage mode assumed the 100% wetting phase saturated core being displaced by the nonwetting phase at a constant injection rate.

$$S_{w,initial} = 1.0 \quad (1.2.17)$$

$$q_{inj} = \text{constant} \quad (1.2.18)$$

Before breakthrough, assuming an incompressible fluid, the nonwetting phase injection rate at the inlet face equals the wetting phase production rate at the outlet face.

$$u_{nw}(x = 0, t) = u_w(x = L, t) \quad (1.2.19)$$

After breakthrough, the nonwetting phase injection rate at the inlet face equals the wetting phase production rate plus the nonwetting phase production rate at the outlet face.

$$u_{nw}(x = 0, t) = u_{nw}(x = L, t) + u_w(x = l, t) \quad (1.2.20)$$

The outlet face of the coreflood allows production of both the wetting and nonwetting phases according to Corey relative permeability and fractional flow relationships.

### 1.2.8. LEAST SQUARES HISTORY MATCHING

The Corey relative permeability relationships were used to obtain an accurate history match of production data. The functional form consisted of three coefficients and two parameter groups for the wetting and nonwetting phases.

$$k_{rw} = \left[ \frac{S_w - S_{wir}}{1 - S_{wir}} \right]^{C1} \quad (1.2.21)$$

$$k_{rn} = C3 \left[ 1 - \frac{S_w - S_{wir}}{1 - S_{wir}} \right]^{C2} \quad (1.2.22)$$

$k_{rw}$  = wetting phase relative permeability

$k_{rn}$  = nonwetting phase relative permeability

$S_w$  = water saturation

$S_{wir}$  = irreducible water saturation

$C1$  = exponential factor for wetting phase

$C2$  = exponential factor for nonwetting phase

$C3$  = factor for nonwetting phase

A least squares history matching algorithm similar to the Firoozabadi and Aziz methodology was used to identify the optimal Corey coefficients that would best match experimental production data. The solution for the Corey coefficients was obtained by minimizing the least squares error defined by:

$$E = \sum_{j=1}^m w_j \left[ R_j^{obs} - R_j^{calc} \right]^2 \quad (1.2.23)$$

$E$  = sum of the difference between observed and calculated recoveries

$w_j$  = weighting factor at time  $j$

$R_j^{obs}$  = observed recovery at time  $j$

$R_j^{calc}$  = calculated recovery at time  $j$

$C_x$  = Corey coefficients  $C1, C2, C3$

$m$  = number of history match points

The derivative of this error was taken with respect to each Corey coefficient:

$$\frac{\partial E}{\partial C_x} = \frac{\partial}{\partial C_x} \sum_{j=1}^m w_j \left[ R_j^{obs} - R_j^{calc} \right]^2 = 0 \quad x = 1, 2, 3 \quad (1.2.24)$$

A first order expansion of  $R_j^{calc}$  resulted in a 3x3 matrix which was solved using Cramer's rule.

The methodology for history matching consisted of calculating an initial guess for each of the three Corey coefficients using the Jones-Roszelle or Hagoort graphical techniques. The irreducible water saturation ( $S_{wir}$ ) was obtained from capillary pressure curve endpoints from each coreplug. Capillary pressure curves were input into the model using Eq. 1.2.2.

1. Initial base case run for C1, C2, and C3
2. Increment of C1,
3. Increment of C2
4. Increment of C3.

Differences between the initial guess and incremental runs were calculated, and then compared with the difference between the initial guess and actual experimental data. Derivatives were calculated and substituted into the 3x3 matrix. The resultant solution to the matrix provided new incrementing values for the Corey coefficients. If each of the incrementing values was within a given tolerance limit, then the history match run was concluded. If any of the coefficients was greater than the tolerance limit, then a new iteration would begin with updated Corey coefficients.

Another analytical approach for determining the derivative of calculated recoveries ( $\partial R_i / \partial C_x$ ) in Eq. 1.2.24 can be obtained by calculating ( $\partial S_w / \partial C_x$ ) in the explicit numerical model. Using this method, the model only needs to be run once for each iteration, since the derivatives for C1, C2, and C3 can be explicitly calculated.

## 1.2.9. RESULTS AND DISCUSSION

This section is separated into four different parts. First, the graphical analysis of coreflood and centrifuge data will be reviewed. Secondly, simulation model behavior and sensitivities to timestep length, cell size, and capillary pressure will be discussed. Thirdly, relative permeability curves derived from Hagoort's and Jones-Roszelle techniques will be compared with relative permeability curves obtained from history matching. And finally, coreflood relative permeability curves will be compared with centrifuge relative permeability curves.

### Results from Jones-Roszelle and Hagoort Techniques

The Jones-Roszelle graphical technique was used to analyze the oil/water coreflood data. The curves were skewed toward higher water saturations with the nonwetting phase having higher relative permeabilities than the wetting phase. This could be due to the large variation in viscosity between the wetting phase (7.12 cp) and the nonwetting phase (1.5 cp). A graph of average nonwetting phase saturation versus  $1/PV_{inj}$  extrapolated to  $1/PV_{inj} = 0$  indicated a irreducible wetting phase saturation of about 32% which is considerably higher than the capillary pressure measurement  $S_{wir} = 10\%$ . A longer coreflood run or higher injection rates may be necessary to obtain a more accurate  $S_{wir}$ .

Gas/Oil Corey Coefficients from Hagoort's Technique

Sample	Centrifuge Speed (RPM)	$N$	$k_{rw}^0$	$S_{wir}$
BA-1A	1000	10.96	0.80	0.10
BA-1A	2000	6.07	1.2	0.10
BA-1A	3000	5.16	1.3	0.10

Experimental data from the centrifuge for the gas/oil system was processed using Hagoort's graphical technique. This methodology supplies a wetting phase exponent ( $n$ ) similar to the wetting phase Corey exponent ( $C1$ ), and also an additional wetting phase factor ( $k_{rw}^0$ ).

$$k_{rw} = k_{rw}^0 \left[ \frac{S_w - S_{wir}}{1 - S_{wir}} \right]^n \quad (1.2.25)$$

The residual wetting phase saturation ( $S_{wir}$ ) was obtained from capillary pressure measurements and was consistently in the range of 0.09 - 0.13. Centrifuge production data from the gas/oil system was obtained at 1000, 2000, and 3000 RPM. Graphs of  $\ln(1 - N_p)$  versus  $\ln(t_d)$  for 2000 and 3000 RPM runs were consistent and gave similar exponential coefficients and factors. The graph for the 1000 RPM case had a higher exponential coefficient and lower factor. All runs exhibited two distinct slopes - an early time slope associated with acceleration of the centrifuge to a stabilized RPM, and a late time slope associated with stabilized centrifugal displacement. The late time slope was used to calculate coefficients for Hagoort's calculations. The slope and intercept for the 1000 RPM case was more difficult to determine because of a smooth transition from the accelerating phase to the stabilized centrifugal displacement phase.

To verify Hagoort's model, graphs of experimental versus calculated data were made using the equation:

$$N_p = 1 - \left[ 1 - \frac{1}{n} \right] \left[ \frac{1}{k_{ro} n t_d} \right]^{\frac{1}{n-1}} \quad (1.2.26)$$

$N_p$  = cumulative production as a fraction of PV (pore volumes)

$n$  = Hagoort's exponential coefficient

$k_{ro}$  = Hagoort's relative permeability

$t_d$  = dimensionless time

For all cases, the late time history match was adequate, but the early time match was poor because of centrifuge acceleration and the limitations of the functional relationship. This can also be verified by examining the  $\ln(1 - N_p)$  versus  $\ln(t_d)$  graphs and noting that the straight line fit matches late time data but not early time data.

## Coreflood and Centrifuge Model Sensitivities

Sensitivities to timestep length and cell size were tested on both the coreflood and centrifuge models to determine operating limitations. The coreflood model was stable for timesteps up to 5 seconds and showed an increasingly dispersed front as cell size increased. The centrifuge model became unstable for timesteps greater than 0.2 seconds. This instability was due to the explicit nature of the solution and was caused by large changes in saturation, relative permeability, or capillary pressure for individual cells. An internal check was installed to reduce timestep size if the saturation change was greater than 5% in any cell. An increasingly dispersed front was noted for both coreflooding and centrifuging as cell size increased.

Model sensitivities that examined capillary pressure sensitivities showed that capillary pressure has a significant effect on both coreflooding and centrifuging, especially in early time before the advancing front has reached the outlet face. Capillary pressures caused dispersion of the advancing front for coreflooding. Because centrifuging does not allow production of the injected phase, both frontal dispersion and delay of the advancing front was noted when capillary pressures were included.

Sensitivities to variations in each of the Corey coefficients were run using history matched values for the 4000 RPM oil/water system. Each Corey coefficient was incremented by a fixed value while the two other coefficients remained constant. The production seemed most sensitive to the wetting phase coefficient  $C1$  and least sensitive to the nonwetting phase factor  $C3$ .

## History Match vs Graphically-Derived Relative Permeability Curves

### Centrifuge History Match Summary

Sample	System	Centrifuge Speed	$C1$	$C2$	$C3$	$S_{wir}$
BA-2A	water/oil	4000	4.26	12.43	0.10	0.10
BA-2A	water/oil	4000	did not converge			0.32
BA-2C	water/oil	3000	5.0	10.0	1.0	0.10
BA-2C	water/oil	3000	did not converge			0.32
BA-1A	gas/oil	1000	4.99	8.52	0.95	0.10
BA-1A	gas/oil	2000	5.21	11.11	0.95	0.10
BA-1A	gas/oil	3000	5.02	8.64	0.95	0.10

The coreflood and centrifuge models were history matched using initial guesses from the Jones-Roszelle and Hagoort graphical techniques. Tolerances were adjusted and irregular history match points were smoothed to allow the model to converge within a reasonable time limit. Most centrifuge model runs converged within 20-25 iterations or came within a reasonable error limit. Graphs of experimental data versus simulation history match data for both the oil/water systems show good matches in both early time and late time.

An additional set of water/oil centrifuge runs were completed that used the irreducible wetting phase saturation from the Jones-Roszelle coreflood displacement analysis ( $S_{wir} = 0.32$ ). Neither the 3000 or 4000 RPM runs converged because the higher residual saturation did not allow sufficient recovery.

Coreflood History Match Summary

Sample	System	C1	C2	C3	$S_{wir}$
BA-2	Oil/Water	3.66	1.87	1.0	0.10
BA-2	Oil/Water	1.71	0.40	0.30	0.32

Oil/water coreflood runs were more difficult to history match, particularly early time data. Although a good match was obtained for late time data, early time matching was difficult even after curve smoothing the input data. More early time coreflood data and measurement of injection rate, breakthrough time, and production data for both the wetting and nonwetting phases would verify whether the model's assumption of constant injection rate was correct.

The oil/water coreflood run using the Jones-Roszelle  $S_{wir} = 0.32$  gave a worse history match than using the endpoint saturation from capillary pressure tests ( $S_{wir} = 0.10$ ). This implies that the  $S_{wir}$  obtained from the Jones-Roszelle technique is too high.

A comparison of oil/water history matched Corey curves for 3000 and 4000 RPM showed that the lower RPM system had a higher C3 factor on the nonwetting phase term. The wetting phase curves for both RPM's matched adequately. The gas/oil system curves at 1000 and 3000 RPM matched closely for both phases. This close match can be explained by the small variation of the wetting phase coefficient C1, since the simulation model response rate is much more sensitive to this parameter than it is to C2 and C3. The match of the 2000 RPM nonwetting curves is average, probably due to the curve smoothing of irregular data in early time.

A comparison of Jones-Roszelle relative permeability curves versus history match relative permeability curves for the oil/water coreflood showed a good correlation with, both sets of curves skewed toward higher water saturations. The major difference between the two sets of curves was the lower relative permeability of both phases for the Jones-Roszelle analysis. This is probably due to measurement error of tangent point saturations and effective viscosities.

The gas/oil history matched centrifuge curves for 2000 and 3000 RPM compared favorably with the wetting phase curves derived from Hagoort's method. This favorable match is due to the fact that both approaches use the same relative permeability (Corey's formula) and have similar exponential coefficients ( $n = C1 = 5.0$ ). The 1000 RPM curves were a poor match, probably because of the difficulties associated with determining the proper slope and intercept using Hagoort's method.

Comparison of Coreflood versus Centrifuge Relative Permeability Curves

The final comparison between centrifuge relative permeability curves and coreflood relative permeability curves (Fig. 1.2.1) showed a good correlation for the wetting phase curves, but completely different shapes for the nonwetting phase curves. The Jones-Roszelle graphical technique implied a much higher irreducible water saturation for coreflooding than centrifuging ( $S_{wir,coreflood} = 0.32$  versus  $S_{wir,centrifuge} = 0.10$ ). This difference in endpoints has a large effect on the shape of the nonwetting phase curve. It may be necessary to run the centrifuge at an injection rate comparable to the coreflood displacement rate. This could be accomplished by running the centrifuge at a lower RPM (500-1000) and using the centrifuge history match model to determine an average production rate throughout the run. This average production rate could be used as the injection rate for the coreflood experiment.

The most significant difference between coreflooding versus centrifuge relative permeability curves appears to be the irreducible water saturation ( $S_{wir}$ ). Does centrifugal acceleration apply abnormally high force to the pore spaces and reduce  $S_{wir}$  to unrealistically low values? Or does unsteady state coreflooding leave a residual  $S_{wir}$  that is too high because the experiment is not run long enough? It appears that the Jones-Roszelle coreflood  $S_{wir}$  is too high, but this answer is inadequate because we do not have good understanding of the physics of pore-to-pore movement of oil, gas, and water. A model that includes compressible fluid effects would provide a more accurate simulation of both coreflooding and centrifuging for the gas/oil system. Also, CATSCANs of experimental coreflooding and centrifuging at various times throughout the run may give useful insights into saturations profiles before and after breakdown.

### 1.2.10. CONCLUSIONS

1. A coreflood and a centrifuge model was derived from the same initial set of equations using different boundary conditions.
2. Coreflood and centrifuge data was obtained from the same Berea coreplug for gas/oil and oil/water systems under the drainage mode.
3. This experimental data was processed using the Jones-Roszelle graphical technique for coreflooding and Hagoort's graphical technique for centrifuging to obtain relative permeability curves.
4. A least squares history match algorithm was used to derive Corey relative permeability curves from both centrifuging and coreflooding.
5. The graphically derived Hagoort curves compared favorably with the history match curves for centrifuging.
6. The graphically derived Jones-Roszelle curves compared favorably with history match curves for coreflooding. Endpoint irreducible wetting phase saturations ( $S_{wir}$ ) obtained from the Jones-Roszelle extrapolation technique may be too high.
7. The wetting phase curves compared favorably between coreflooding and centrifuging.
8. The nonwetting phase curves were different in both shape and irreducible wetting phase saturation endpoints ( $S_{wir,coreflooding} = 0.32$ ,  $S_{wir,centrifuging} = 0.10$ ) between coreflooding and centrifuging.

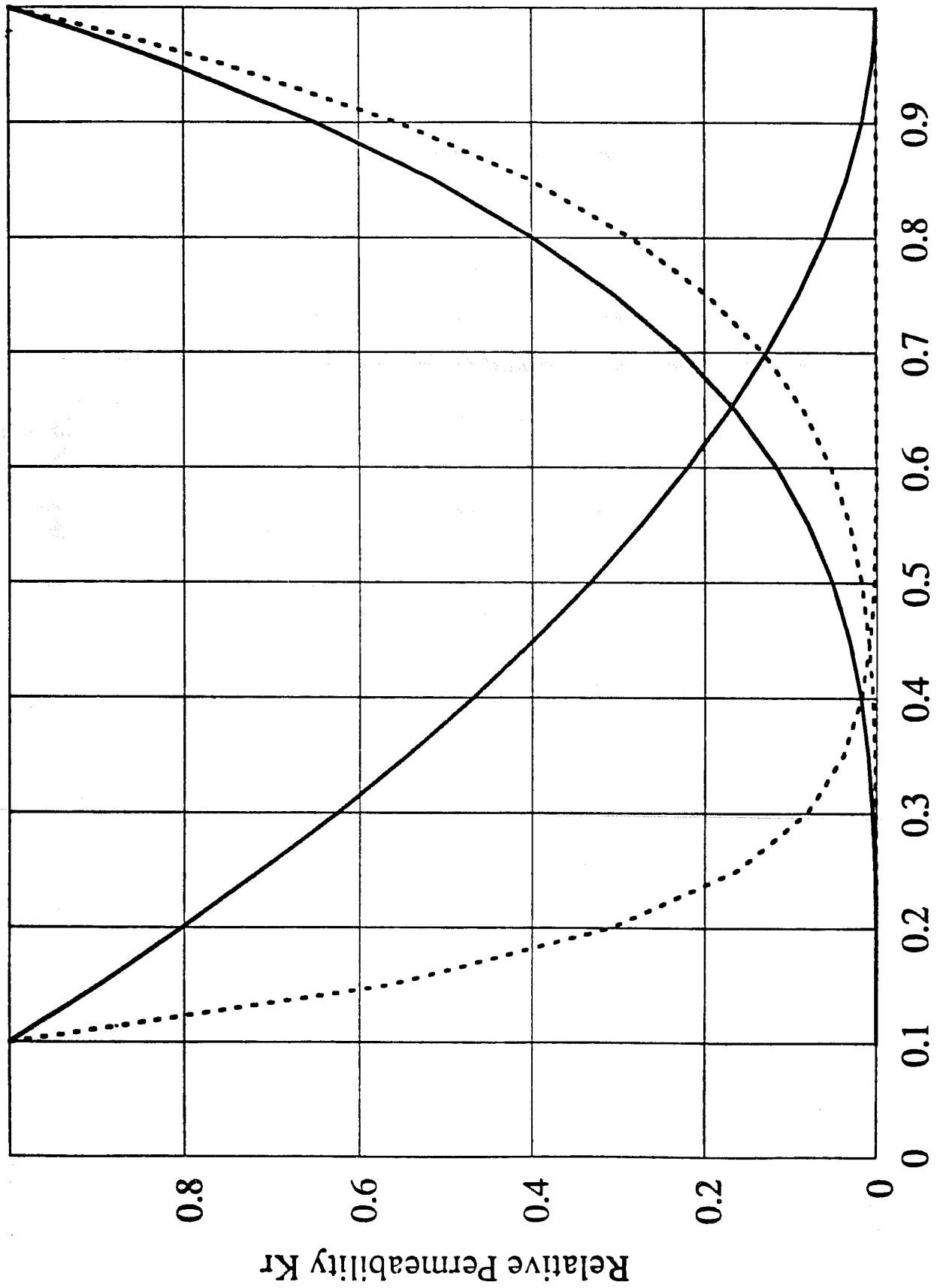
### 1.2.11. RECOMMENDATIONS

1. Modify both coreflood and centrifuge models to include compressible fluids. If larger timesteps are desired to reduce computer time, a more implicit solution is recommended.
2. Analyze data from other types of sandstone coreplugs to see if relative permeability relationships between coreflooding and centrifuging are consistent.

3. Run centrifuge displacement experiments at 500 and 1000 RPM. Accurately measure centrifuge speed, pressure drop across the coreplug, and production rate. Run the coreflood at an injection rate equivalent to the average centrifuge production rate, and continue running until the irreducible water saturation is comparable to the centrifuge run (if possible).
4. CATSCAN coreplugs at various times throughout the centrifuge and coreflood runs to determine saturation profiles.

#### 1.2.12. REFERENCES

1. Aziz, K. and Settari, A.: Petroleum Reservoir Simulation, Applied Science Publishers, Ltd., London (1979).
2. Buckley, S.E. and Leverett, M.C.: "Mechanism of Fluid Displacement in Solids", Trans., AIME (Feb. 1941) 107-116.
3. Chierici, G.L.: "Novel Relations for Drainage and Imbibition Relative Permeabilities", *Soc. Pet. Eng. J.* (June 1984) 275-276.
4. Corey, A.T.: "The Interrelation Between Gas and Oil Relative Permeabilities", *Producer's Monthly* (Nov. 1954) 38-41.
5. Firoozabadi, A. and Aziz, K.: "Relative Permeability from Centrifuge Data," SPE Paper 15059, 56th Cal. Reg. Mtg. SPE, Oakland, Ca. (April 2-4, 1986).
6. Firoozabadi, A., Soroosh, H., and Hasanpour, G.: "Drainage Performance and Capillary Pressure Curves Utilizing A New Centrifuge", SPE Paper 15060.
7. Hagoort, J.: "Oil Recovery by Gravity Drainage," *Soc. Pet. Eng. J.* (June, 1980) 139-150.
8. Johnson, E.F., Bossler, D.P. and Naumann, V.O.: "Calculation of Relative Permeability from Displacement Experiments", Trans., AIME (Dec. 1958) 68-74.
9. Leverett, M.C.: "Capillary Behavior in Porous Solids", *J. Pet. Tech.* (Aug. 1940), pp 152-169.
10. O'Meara, D.J. and Crump, J.G.: "Measuring Capillary Pressure and Relative Permeability in a Single Centrifuge Experiment", SPE Paper 14419, 60th Ann. Tech. Mtg, Las Vegas, Nev. (Sept. 22-25, 1985).
11. Welge, H.J.: "A Simplified Method for Computing Oil Recovery by Gas or Water Drive", Trans., AIME, 195, (1952), pp 91-98.



Coreflood Coefficients  
 C1=3.66  
 C2=1.87  
 C3=1.0  
 $S_{wir} = 0.10$

Centrifuge Coefficients  
 C1=5.0  
 C2=10.0  
 C3=1.0  
 $S_{wir} = 0.10$

Figure 2.1.1 Coreflood vs centrifuge curves for water/oil system.

## **PROJECT 2: IN-SITU COMBUSTION**

SUPRI's work on in-situ combustion has focused on studies of the effect of metallic additives on the combustion kinetics and an analytical description of the flow system in a CO<sub>2</sub>-steam oil system such as can be found ahead of an oxygen enriched combustion front. In addition, tube runs have been started to verify the results obtained in the kinetics experiments. A detailed survey has been made of ignition techniques used in combustion projects.

## **2.1 IGNITION DEVICES AND METHODS FOR IN-SITU COMBUSTION (D. C. Shallcross)**

### **2.1.1. ABSTRACT**

One of the most important tasks during a fireflood is to ensure the ignition of the oil-bearing stratum efficiently and safely. Many different devices have been developed and employed to achieve this aim. The target zone may ignite spontaneously upon injection of an oxygen-containing gas without the aid of special equipment. Alternatively, ignition may be hastened or enhanced by the use of gas-fired downhole burners, electric downhole heaters, or other, chemical means. Other methods involve increasing the reactivity of the formation contents by doping the stratum with compounds that ignite and burn more readily than the reservoir oil. This report surveys the range of ignition methods and devices that have been developed and applied in the field. Not only are successful ignition systems discussed, but also those designs that failed to ignite a formation. In discussing the various techniques, factors considered include reliability, specialized equipment and materials requirements, and safety. Another consideration is whether a system or device may be easily reused if ignition is not successful on the first attempt. The use of oxidizing gases other than air is also discussed.

### **2.1.2. INTRODUCTION**

Ignition is one of the most critical phases of a fireflood. It is important to ensure that the formation is ignited on the first attempt, and that it subsequently remains alight. Depending upon the circumstances it may be difficult, if not impossible, to reignite a fireflood that has died. A failed first ignition attempt might consume all the oil in the immediate vicinity of the ignition well, leaving too little oil to allow a second successful ignition attempt.

In some formations spontaneous ignition occurs when air is injected into the ignition well. Spontaneous ignition is not always desirable as there is little control over where ignition occurs. For this reason, it is usually desirable to ignite a fireflood using some artificial means. Fuel packs that are introduced into the ignition well, when burnt generate heat that raises the temperature of the oil-bearing strata to the oil's ignition point. Gas-fired downhole burners and downhole electric heaters similarly introduce heat into the formations, but in a more controlled fashion. Hot fluids such as steam may be injected into the reservoirs to raise the reservoir temperature to a point at which ignition will occur in a shorter amount of time once air injection begins. By injecting chemical compounds into the formations, the reactivity between the oxygen and the reservoir fluids may be greatly enhanced. By doping the reservoir with self-igniting fluids such as linseed oil, ignition is assured when injection of the oxygen-containing gas begins.

This report surveys the various ignition techniques and equipment that have been developed and applied both successfully and unsuccessfully in the field. Many of the techniques and much of the equipment discussed is drawn from the vast body of patent literature available. Field data are also presented from more than fifty ignition attempts using the full range of techniques.

### 2.1.3. SPONTANEOUS IGNITION

Three conditions should be met for spontaneous ignition to occur in a reasonable period of time: the oil must be at least moderately reactive; the zone to be ignited must not be too thin; and, the initial reservoir temperature must not be too low. When oil is contacted by oxygen at reservoir temperatures, exothermic low temperature oxidation reactions will yield a range of oxygenated hydrocarbons such as aldehydes, ketones and esters. Being exothermic, the reactions that generate these compounds also liberate heat to the environment. The oils that are more reactive generate greater quantities of heat and thus heat their surroundings more rapidly. In thick reservoirs nearly all of the heat generated by the oxidation reactions goes to heat the reservoir; little is lost to the surroundings. In thinner reservoirs a much higher proportion of the heat generated will be lost to the overlying and underlying strata. If the rate of heat lost to these zones increases until it matches the rate of heat generated by the reactions, then the temperature of the reservoir will stop increasing, and spontaneous ignition will be prevented. Even in relatively thick zones, if the initial reservoir temperature is particularly low, spontaneous ignition will not occur within a reasonable length of time. This is because the time required for spontaneous ignition increases with decreasing temperature. Therefore, for the reservoir to ignite spontaneously the oil must be at least moderately reactive at the initial reservoir temperature and the reservoir must not be too thin.

The time required for spontaneous ignition to occur within an oil reservoir may be estimated using an equation developed by Tadema and Weijdema (1970):

$$t_{ign} = \frac{(\rho C)^* T_o \left[ 1 + 2T_o \frac{R}{E} \right]}{\phi S_o \rho_o H A_o P_{O_2}^n \frac{E}{RT_o}} e^{\frac{E}{RT_o}}$$

where

- $t_{ign}$  ignition delay time
- $(\rho C)^*$  equivalent heat capacity per unit volume of the porous medium,
- $T_o$  initial reservoir temperature
- $R$  ideal gas constant
- $E$  activation energy of the oil's low temperature oxidation reactions
- $\phi$  is the porosity
- $S_o$  oil saturation
- $\rho_o$  oil density
- $H$  heat of the oil's low temperature oxidation reaction
- $A_o$  pre-Arrhenius factor of the oil's low temperature oxidation reactions
- $P_{O_2}$  partial pressure of oxygen
- $n$  is the reaction order with respect to oxygen

The equation was developed assuming that all the heat generated by the oxidation reactions is used to heat the formation locally, and that no heat is lost to the surrounding strata. Also, in evaluating an integral in the derivation of the above equation, certain other approximations were made which result in the expression for the ignition time being independent of the ignition temperature.

The spontaneous ignition model of Burger (1976) improves upon the earlier model by accounting for the heat transfer by conduction and convection into the formation. The one-dimensional model does not consider however heat loss to either the overlying nor underlying strata. Burger's model permits the estimation of the ignition time and the location of the ignition point. The ignition delay time used in the model is defined as the time required after air injection begins for the temperature anywhere near the ignition well to exceed 250°C.

Spontaneous ignition has been employed to ignite firefloods in several fields (Table 2.1.1). In one Venezuelan field, Bowman (1965) reported that ignition occurred in as little as two days, whereas in the Gloriana field ignition had not occurred after three months of air injection (Buchwald *et al*, 1973). The Heidelberg field is typical of a deep reservoir in which the high initial reservoir temperature aids spontaneous ignition in a reasonable period (Mace, 1975). At the other extreme, the SE Pauls Valley field, having an initial temperature of just 18°C, did not ignite spontaneously (Elkins *et al*, 1972). A gas-fired downhole burner had to be employed to achieve ignition.

#### 2.1.4. GAS-FIRED BURNERS

Historically, the use of gas-fired downhole burners has been one of the most popular methods for igniting firefloods. The heat required for ignition is generated downhole by the burning of a mixture of fuel gas and an oxygen-containing gas. Typically, the burner is lowered down the hole to a point just above the top of the target formation. For safety, the fuel gas and the oxygen-containing gas, usually air, are supplied to the burner from the surface through separate conduits. The two gas streams mix within a combustion chamber which is used to shield the other downhole equipment from the high flame temperatures. The gases are ignited within the chamber by some means, such as by the use of a spark plug, electrical element or chemical compound. The heat generated by the burner is imparted to the surrounding formation either indirectly or directly.

A typical gas-fired downhole burner is shown in Fig. 2.1.1. To use the burner, a tubing string with a pump seat at the bottom is first lowered into the cased ignition well. The seat is positioned above the top of the oil-bearing stratum so that it is away from the heat generated within the stratum by the fireflood. The burner is then lowered inside the tubing string on a second, smaller tubing, until it rests on the seat. O-rings or other devices are used to ensure a seal between the burner and the outer tubing string. The fuel gas is then supplied down the inner tubing, while the primary oxidizing gas, in most cases air, is injected into the annulus between the two tubing strings. A number of small conduits in the burner just above the combustion chamber allow the air to flow into the chamber and mix with the fuel gas. In this example the gases are ignited using a spark plug which is connected by an armoured electrical cable to the surface. The cable is attached to the inner tubing string. The secondary air that is injected down the casing annulus serves a number of useful roles. Firstly, the gas cools the burner unit as it flows around it and helps to control the temperature within the well. More importantly, it is this supply of air that is used to oxidize the oil within the target formation. Finally, a constant flow of air into the casing annulus prevents the hot combustion gases from flowing back up the well instead of into the formation. A feature of this design is that the burner may easily be pulled from the well and run down another, at any time. Many early gas-fired burners could only be used once, as the high temperatures generated downhole destroyed the units. Most burners in use today incorporate thermocouples into the design to monitor the temperatures in the well, in the combustion chamber, and around the ignition system. These thermocouples are not shown in the diagram.

The above design may be modified in many ways. Many early workers suggested supplying the gases to the burner using parallel instead of concentric tubing strings. Many operators were concerned that if the gases did not burn cleanly, then the particulate matter generated by the flame could lodge in the surrounding formation resulting in a decrease in the reservoir permeability immediately adjacent to the well and a loss in injectivity. To prevent this from occurring, some engineers suggested that the combustion product gases be returned to the surface, instead of being injected into the well (MacSporran, 1963). The primary air and fuel gas are injected into the closed combustion chamber. Some of the heat generated by the combustion is transferred to the secondary air flowing around the outside of the chamber. The heat contained in the combustion gases is lost, however, as those gases are withdrawn to the surface. Also, the system requires three parallel tubing strings to be run into the well.

Oil-bearing strata do not always ignite on the first attempt. Also, when they do ignite, the combustion front sometimes dies early in the process for a variety of reasons. It is therefore important that the downhole burner be designed so that it may be used more than once without having to be pulled from the hole. A reusable gas ignition system is therefore vital.

The gases may be ignited within the combustion chamber by electrical or chemical means. One of the simplest methods involves the use of a spark plug (Piros, 1954; Palm 1965), wherein the gases are ignited by the spark that flashes between the plug's electrodes. Most such designs that utilize spark plugs suffer from two main problems, however. Firstly, the plug is often so badly damaged when it ignites the gases that it cannot be used again, and secondly, the gas flowrates must be very carefully controlled, or ignition will not occur. An alternative electrical method uses resistance heating elements (Campion *et al*, 1961; Rees, 1967; McDonald, 1968; Todd, 1969). Howard *et al* (1978, 1979, 1980) recommend the use of three nichrome wire elements connected in delta. Resistance heaters are usually more robust than spark plugs, and so are preferred by most workers.

Chemical methods have also been used to ignite the burner gases. An early method suggested, was to inject slugs of calcium phosphide and water down a tubing string into the combustion chamber (Kaasa, 1960). During the passage down the tubing, the phosphide and water would react to form a mixture of mono- and di-phosphides. Upon contact with the air within the combustion chamber, the phosphide spontaneously ignites, so igniting the injected fuel gas. Linseed oil containing a catalyst such as cobalt naphthenate and dimethyl aniline may be injected in place of the phosphide (Rees, 1967).

A chemical method used to ignite the burner gases, similar to that of Kaasa, was patented by Emery (1960) and used in an attempt to ignite a formation in Venango County, Pennsylvania. Campbell *et al* (1966) reported that although the burner was successfully ignited, the surrounding formation did not ignite. The workers concluded that the in-situ combustion process was not successful because the concentration of fuel near the ignition well was not sufficient to sustain combustion. The phosphides recommended for use by Kaasa and Emery are examples of pyrophoric materials; those that spontaneously ignite in the presence of oxygen under ambient conditions. Pyrophoric materials other than phosphides that have been suggested for gas ignition include silane and disilane (Bousaid, 1973). The pyrophoric material may be introduced in either a substantially pure form, or diluted in an inert carrier gas such as nitrogen, argon or helium.

The pyrophoric material used to ignite the gas-fired burner of Hujsak (1967) is not injected into the ignition well, but is instead lowered down within a sealed container. The main components of Hujsak's downhole equipment are illustrated in Fig. 2.1.2. Figure 2.1.3 presents a more detailed diagram of the pyrophoric chamber. An intermediate size tubing string is run into the cased injection well. Attached to the string's lower end by means of a

number of spacer bars is a larger diameter heat shield. This shield extends a distance below the string and forms the combustion chamber. Fuel gas is injected down the tubing string while air is supplied down the casing annulus.

The chemical igniter assembly is lowered through the tubing string on a cable until it rests on a seating nipple. At the base of the assembly is a closed chamber containing the pyrophoric material used for ignition of the gases (Fig. 2.1.2). The upper end of the assembly is closed by a plunger connected to a rod that runs up through the igniter housing and spring to a weighted bar suspended from the cable. When the assembly is landed on the nipple, the cable is kept in tension so that the rod and plunger keep the pyrophoric chamber closed. Air and fuel gas are then injected into the well. The fuel gas flows down around the bar and spring, and passes through a series of holes around the top of the housing, into an open mixing chamber. To ignite the combustible mixture, the cable tension is eased, and the weight of the bar is allowed to depress the plunger, releasing the housed chemical. Release of the chemical ignites the gases. Hujsak suggests that compounds such as alkyl boranes (e.g. triethylborane) be used as the pyrophoric material. Once the fuel gas is ignited, the chemical igniter assembly is withdrawn, up away from the combustion chamber a distance of about 6 m. This protects the assembly from the high combustion temperatures of the combustion chamber.

Hujsak's burner is reported to have been used successfully in a number of fields to initiate firefloods. The author himself reports that it was used to ignite a formation at a depth of 1525 m. Hardy *et al* (1972) report that the burner was deployed in a 13.97 cm casing to ignite the May-Libby reservoir at a depth of 1040 m. The burner was also used in the Glen Hummel field in Wilson County, Texas (Buchwald *et al*, 1973).

A major disadvantage of such chemical methods for burner ignition is that the use of pyrophoric materials poses a hazard to the operators. Any contact between the pyrophoric material and air above the combustion chamber could lead to serious damage to the tubing and well casing.

The likelihood of the electrical igniter being burnt out is reduced in the gas burner design proposed by Hazard *et al* (1965). A modified version of their design is presented in Fig. 2.1.4. The shape of the combustion chamber and the location of the combustible gas entry ports are designed to limit the amount of gas that reaches the electrical igniter. The fuel gas and primary air supply are delivered to the burner down concentric tubing strings in a manner similar to that described earlier. The gases mix to form a combustible gas in a mixing chamber above the combustion chamber. The lower chamber is tapered with an upwardly-pointed apex. The combustible gas is introduced into the combustion chamber through at least two ports that are positioned and angled such that a swirling motion is imparted to the gases. A downward vortex flow is therefore established within the chamber. An electrical igniter is housed in a small cylindrical cavity at the chamber's apex, away from the direct flow lines of the combustible gases. As the gas enters the chamber most flows downwards, but a small amount will diffuse upward to the igniter. It is this small amount that is ignited and in turn ignites the main gas streams. Flashback preventers are installed in the conduits connecting the two chambers to prevent ignition of the gases in the upper chamber. It should be noted that the aspect ratio of Fig. 2.1.4 has been reduced for clarity. In practice the electrical igniter would be located away from the entry ports a distance of between 2½ and 4 times the diameter of the combustion chamber.

Modifications to the basic burner design have been suggested to overcome particular conditions that may exist within the ignition well. One of these modifications evolved as an attempt to counter the problem in using a downhole burner within a well that contains standing liquid at a point where the heating is desired (Rees, 1967). Columns of water and oil are

common in many wells. Most gas-fired burners are designed with the combustion chamber open at its lower end. When such burners are lowered into a liquid-filled well, the liquid can flow into the combustion chamber to the ignition system. Depending upon the type of method used to ignite the gases in the chamber, the ignition system can be rendered inoperable. In order to prevent the well liquids from entering the combustion chamber, Rees suggests closing the lower end of the combustion chamber with a plug, before the burner is lowered into the hole (Fig. 2.1.5). The plug remains in place until the burner is ready for use. Fuel gas and air are then injected into the chamber and the plug is blown away from the chamber when a predetermined pressure is attained. The burner is then ignited normally. Preferably the plug is made from a material such as plastic that burns and is destroyed by the burner flame. An obvious disadvantage of this design is that the method to keep the liquid from the chamber may only be used once. Any liquid that has entered the combustion chamber after an unsuccessful ignition attempt may be difficult to remove, and may prevent a second ignition of the feed gases.

One of the features of the burner design presented in Fig. 2.1.4 is that it may be used repeatedly in liquid-filled wells. The location of the gas ignitor in a cavity closed at its upper end protects the igniter from any liquid that might invade the combustion chamber. The igniter would be protected within a pocket of gas. Any liquid that had invaded the chamber could be blown out by the injection of the fuel gas and air.

One problem often encountered in using a gas-fired burner to ignite a fireflood is that the well casing and other downhole equipment may be damaged by the excessive temperatures generated by the burner. In most cases the flow of the secondary air past the burner will cool the unit and the combustion gases sufficiently, however, some workers have designed burners that further reduce the temperature of the exhaust gases. The dual chamber burner of Palm (1965) is illustrated in Fig. 2.1.6. Before being exhausted into the well, the hot combustion gases flow into an upper chamber where they preheat the air and fuel gas mixture. The combustion gases, cooled by the exchange of heat with the feed gas, exit the burner through a series of ports in the wall of the upper chamber.

A problem common to all types of gas-fired burners is that they may be severely damaged by the excessive temperatures generated within the burning stratum. To prevent overheating, the burners are usually located within the ignition well above the top of the stratum to be ignited. There they are shielded from the high fireflood temperatures by the overlaying, non-combustible stratum. The disadvantage of having to position the burner above the formation is that if the formation is particularly thick, ignition will commence only in the upper sections of the formation. It is more desirable to ignite the formation uniformly across its entire interval.

A simple method to heat and ignite the lower portions of a thick formation is to attach an extended heat shield to any of the burners described above (Hujsak, 1966). The heat shield is precut so that its lower, open end hangs level with the bottom of the target stratum. Thus, the hot gases produced within the burner emerge at the base of the formation. In this way, the heat generated by the burner may be applied to the base of a thick reservoir while the burner remains above the formation.

Data from twenty different firefloods in which downhole burners were used is presented in Table 2.1.2. As may be seen, the burners have been used to ignite formations at depths ranging from 30 m to 1890 m. Of the twenty projects reported, only the one in the Charco-Redondo field failed to ignite using a gas-fired burner (Widmyer *et al.*, 1977). In this field, when the air injection rate was increased from 3700  $m^3/d$  to 25500  $m^3/d$  one week after the first ignition attempt, spontaneous ignition occurred within three days.

### 2.1.5. ELECTRIC HEATERS

The use of electrical igniters is often favoured over gas-fired burners due to their relatively simple operation. No dangerous chemicals or gases are required on site. The sole requirement at the wellhead is a source of electricity which may be supplied by a mobile generator.

There are two basic concepts for downhole electric heater design. In the simpler and more common design an electric heater is lowered into the well on an armoured cable. The cable not only bears the weight of the heater, but also supplies the electric power and may carry signals from any thermocouples present. Air is injected down the well and heat is imparted to the air as it passes around and along the electric elements. In the second design, the heater is lowered on the end of a tubing string (Gadelle *et al*, 1982). The helical electric elements are wound around the last metre of the string providing a heated section through which the injected air must pass. The end of the string incorporates baffles and jackets such that the air must pass over the heated section several times before passing into the well.

The electric heaters described by Alexander and Martin (1968) and Joseph (1977) have designs of the first type. In their patent, Alexander and Martin describe a heater consisting of three elements that are run parallel with the well's axis. Each element is located at the vertice of an equilateral triangle using insulated spacers and are constructed of Nichrome wire wound helically within a metallic sheath. Each element has a length of approximately 5.38 m of which the central 4.55 m is active and is capable of delivering 13 kW of heat. Power is supplied to the upper ends of the elements via an electrical conduit run down within the armoured cable. The electrical connections between the conduit and the elements are made within an enclosed space protected from the well environment. Similarly, the lower ends of the elements are protected by being enclosed. One thermocouple located below the heaters is used to monitor the air temperature within the well, whilst a second is used to measure the element temperature. This heater was used to successfully ignite a formation in the North Tisdale Field in Wyoming. The heater was operated at a depth of 258 m.

Another electric heater was used to ignite five patterns in the Bodcau Field of Louisiana (Joseph, 1977). The 30 kW, 440V heater consisted of six elements, each rated to  $194 \text{ W/cm}^2$  of surface area. Each element had an active heating length of 2.18 m. The unit was designed to operate within a 17.8 cm casing. Power was supplied to the heater through an insulated and armoured three-conductor cable having an outside diameter of 2.0 cm. A thermocouple was run down a 2.54 cm thermowell within the casing to monitor the downhole temperature.

Prior to ignition, the injection wells were cleaned by air to remove any water or oil from the well. Air was then injected at a rate of  $5700 \text{ m}^3/\text{d}$  until the offset producing wells began to vent the injected air. After pressure falloff tests, the heater was run into the well and positioned some distance above the perforated interval. Air was injected past the heater at  $5700 \text{ m}^3/\text{d}$  and heated to about  $150^\circ\text{C}$ . After the target interval had been heated at this temperature for several hours, the power to the heater was increased and the injected air heated to  $316^\circ\text{C}$ . This electrical output was maintained until ignition was confirmed by an analysis of the gases produced by the offset wells.

In describing the operation of the electric heater, Joseph discusses a number of operational problems that arose. A twenty minute shutdown of the air compressor allowed very hot air to move up the hole. The air was sufficiently hot to melt the insulation in the cable and short out the heater. On another occasion while the heater was being pulled from the well its cable coiled around the one-inch thermowell and became wedged. After the thermowell was cut free, the heater could be pulled from the well.

A limitation of the depth at which downhole electric heaters may be used is imposed by the electric power losses along the length of the supply cable. Like all electrical conductors, the cable used to supply the electric power to the heater downhole has a small electric resistance. As a result a significant proportion of the power supplied at the wellhead can be dissipated as heat within the cable. The amount of electrical power lost depends upon the cable material chosen, the cable diameter, the depth of operation, the line voltage, and whether the power is supplied by single- or three-phase transmission. Moss (1965) showed that at 610 m using a No. 8 electrical cable and a 20 kW, 400 V single phase power source, 7 kW will be dissipated within the cable. As Moss noted, line losses can be reduced by using larger diameter cable, increasing the voltage and by using three-phase, instead of single phase power.

Table 2.1.3 presents data from a dozen firefloods in which electric heaters were used for ignition. The deepest reservoir ignited was at a depth of 707 m, less than half as deep as the deepest formation ignited by a gas-burner (Table 2.1.2). As with the burners, electric heaters have been used to successfully ignite reservoirs having initial temperatures less than 20°C.

### 2.1.6. CHEMICAL METHODS

Ignition of an oil-bearing stratum may be enhanced by injecting directly into the stratum compounds that react exothermically. Often these compounds are autoignitable fluids that liberate more heat than the native oil when oxidized. The range of compounds that may be used to enhance ignition is not limited to those that undergo oxidation reactions. The heat from virtually any exothermic reaction can be harnessed to heat the formation to ignition, if the required reactants can be delivered safely down the wellbore and into the formation.

A typical chemical ignition method is described by Klein and Dean (1968). A quantity of an autoignitable fluid such as tung oil is injected into the formation around the ignition well. This fluid is then pushed away from the immediate vicinity of the well by a slug of another fluid such as diesel oil. An oxygen-containing gas is then injected into the formation and the tung oil ignites. The heat generated within the formation is sufficient to ignite the native oil. The workers conducted a series of laboratory experiments to study the possible use of a range of autoignitable fluids. Found suitable for use as the autoignitable fluid were linseed oil, red oil, castor oil, turpentine and tall oil. They also noted that a small amount of an oxidation catalyst such as cobalt naphthenate enhanced ignition.

The purpose of the injection of the second fluid is to push away from the wellbore the highly reactive, autoignitable fluid so that the well is not subjected to the severe temperatures. To accomplish this, the second fluid should be less reactive than, and miscible with, the autoignitable fluid. Light crude oil, diesel oil and kerosene can all be used as the displacing fluid. It is important though that the autoignitable fluid not be injected too far into the formation, otherwise the combustion front established could burn back toward the ignition well.

Using the above procedure and compounds, reservoirs with initial temperatures above 66°C may be ignited. The workers report the results from another series of experiments conducted to investigate those chemicals that may be used to ignite cooler reservoirs (Dean and Klein, 1970). From a series of laboratory experiments they found that a mixture of tung oil and tall oil, containing between 70 and 90 percent by weight tung oil can be used to ignite a system with an initial temperature of 27°C. As before, the addition of a small amount of an oxidation catalyst was found to be beneficial.

Based upon the results of a series of laboratory experiments, Bednarski *et al* (1965) suggest using unsaturated aliphatic compounds or unsaturated non-hydrocarbon oils as the injected

autoignitable fluid. They recommend that the aliphatic compounds contain at least sixteen carbon atoms per molecule. Examples of suitable compounds are linoleyl alcohol, eleostearic acid and clupadonic acid. They suggest that the unsaturated non-hydrocarbon oils have iodine numbers between 100 and 130. (The iodine number of a unsaturated oil is the mass in grams of iodine that can be absorbed by 100 grams of oil.) Examples of suitable oils include fish oil, corn oil and poppyseed oil. It should be noted however, that some of these oils may contain natural oxidation inhibitors which could suppress the desired oxidation reactions. Oxidation catalysts such as cobalt naphthenate, cobalt tallate and cobalt octoate may be added to the injected solution to enhance the desired reactions. The compounds may be diluted using suitable solvents such as a light hydrocarbon naphtha. The authors also note that ignition is significantly enhanced by adding a small amount of magnesium powder. The recommended maximum dose is ten percent by weight. The powder must be sized so that it will not clog the formation and reduce permeability when injected.

Prior to the injection of the autoignitable fluid, the reservoir in the immediate vicinity of the ignition well may be heated to enhance ignition (Holmes, 1968; Cornelius and Klein, 1969). Steam would be suitable as the heating fluid. Injecting steam into the well purges the well of oxygen, and heats and cleans the target formation around the wellbore.

In the process described by Holmes, steam is injected until the temperature of the formation near the well has reached 150°C. A volume of linseed oil is then introduced into the well. The amount of linseed oil injected must be sufficient to wet the exposed face of the formation. An excessive amount of oil could reduce the formation permeability by clogging the region around the well. Once injection of the oil is complete, the conduit down which the oil was injected is steam cleaned to remove any traces of the oil. Only a limited quantity of steam is used for cleaning so that the linseed oil is not pushed too far into the formation. Air is then injected into the well down a conduit, other than the one down which the linseed oil was injected. The linseed oil, heated by the pre-injection of the steam ignites upon being contacted by the injected air.

Holmes reports that the above process was successfully used to ignite a formation at a depth of 349 m. The gross interval of the target formation was 23 m but the gravity of the oil is not specified. Eighty percent quality steam was injected at a rate of 3.5 m<sup>3</sup>/hr cold water equivalent over a three hour period. At the injection pressure of 7.2 MPa, the steam had a temperature of 288°C. The injected steam released 32 GJ into the formation. A mixture of 0.21 m<sup>3</sup> of boiled linseed oil and 0.62 m<sup>3</sup> of raw linseed oil was then injected into the tubing and displaced with steam. While steam injection continued, air was injected down the casing annulus at a rate of about 28000 m<sup>3</sup>/d. The linseed oil spontaneously ignited and ignition of the formation was detected shortly later by the production of combustion gases from a nearby well.

A patent issued to Jones and Williams (1971) suggests using polymers derived from hydrocarbon processing which have iodine numbers greater than 130. Examples of autoignitable materials which are suggested as suitable are conjunct polymers formed by the following reactions: acid catalyzed polymerization of hydrocarbons; acid catalyzed alkylation of hydrocarbons; and, acid catalyzed isomerization of hydrocarbons. A lower limit of 130 for the iodine number is recommended to ensure that the oxidation rates are high enough to achieve ignition.

Another chemical ignition method is described in the patent issued to Pusch *et al* (1977). They recommend injecting slugs of diesel oil and an autoignitable fluid such as linseed oil into

the formation around the ignition well. During injection of these slugs, nitrogen is simultaneously injected at a low rate to prevent the igniter fluids from circulating back toward the injection well. A slug of water is then injected. Finally, the oxygen-containing gas is injected at a typical rate of  $30 \text{ m}^3/\text{hr}$  per  $\text{m}^2$  of rock surface.

Not all chemical ignition methods require oxygen to be one of the reactants in the exothermic reaction. Meier (1973) describes a method in which hydrogen peroxide is introduced into a formation which had previously been injected with a compound that reacts exothermically with the peroxide. A number of different solid or liquid compounds may be used to react with the hydrogen peroxide. These include catalytically active substances and other compounds that either oxidize or reduce the peroxide. Permanganates are examples of suitable oxidizing substances while hydrazine, hydroxylamine and their derivatives are examples of suitable hydrogen peroxide reducing substances. The compound is injected into the formation first. An 80 to 90 percent aqueous solution of the peroxide is then injected into the wellbore and contacted with the other reactant. It is important to ensure that the first compound is introduced into the wellbore in such a way that no traces of it are left within the well to be prematurely contacted with the peroxide. Flushing the tubing with an agent such as paraffin oil could prevent ignition within the wellbore. This particular chemical ignition method is potentially hazardous and requires the operators to handle dangerous chemicals.

A process patented by Garthoffner (1986) could be applied to ignite an oil reservoir. Metallic magnesium in the form of an aqueous colloidal suspension is injected into the formation. There it reacts with the connate water to produce magnesium hydroxide and hydrogen gas. As this reaction is strongly exothermic, it is accompanied by an increase in the formation temperature around the wellbore. Garthoffner suggests that candidate reservoirs for this process contain oils of densities between  $934 \text{ kg/m}^3$  and  $1000 \text{ kg/m}^3$ .

Often the problem in igniting an oil-bearing formation is not that the oil is not reactive enough for spontaneous ignition to occur, but rather that the oil saturation is too low. The chemical ignition method suggested by Bandyopadhyay (1972) increases the fuel concentration around the ignition well by injecting a water emulsion of a carbon black material into the formation. The slug will preferentially displace the connate water rather than the more viscous oil, thus increasing the fuel content of the stratum. Once the emulsion has been injected, some form of wellbore heater is lowered into the well and used to heat the air that is injected into the well. The author suggests that the water emulsion contains less than 30 weight percent of carbon black. The carbon black should be sized between 0.1 and  $300 \mu\text{m}$  so that the emulsion will be smaller than the smallest pore size likely to be encountered. The injected emulsion can also contain additives that improve the emulsion's injectivity and displacement properties. These additives might include surfactants and wetting agents. One advantage of this ignition method is that the compounds and emulsion may be easily and safely prepared and handled by field personnel.

Parrish *et al* (1974) helped induce ignition in the Sloss field, Nebraska, by injecting  $24 \text{ m}^3$  of a more reactive crude into the target formation. After the injection of the crude, water and solvents were injected to clean the crude from the tubular goods. Air was then injected at a rate of between  $1400$  and  $2800 \text{ m}^3/\text{d}$  for several days. Six 32 hectare five-spot patterns were ignited in this manner. The target zone had a net pay thickness of  $4.4 \text{ m}$  and was at an average depth of  $1890 \text{ m}$ . The original oil gravity was  $831 \text{ kg/m}^3$ . Crude oil was not used to induce ignition in the next four patterns to be lit, as the workers found that the injected oil caused some wellbore plugging. In a similar manner  $76.3 \text{ m}^3$  of a  $922 \text{ kg/m}^3$  crude were injected into an ignition well in the North Ward-Estes Field of Ward County, Texas (Anthony *et al*, 1981).

### 2.1.7. FUEL PACK METHODS

One of the earliest methods used to ignite oil-bearing formations was to pack the ignition borehole in the vicinity of the target formation with a highly combustible fuel pack. While air was injected, the pack was ignited and the released heat raised the temperature of the surrounding formation to ignition. Typically, the fuel packs consisted of charcoal briquettes, adsorbent ceramic pieces soaked with heavy oil, or mixtures of the two. Usually the fuel was packed into the well past the top of the target formation. This was done to allow for the subsidence of the pack as it burnt. Often the packs were ignited by simply dropping a red hot charcoal, a railroad flare or fuse on them (Trantham and Marx, 1966).

The disadvantages of using such methods are many, however. Firstly, burning the fuel pack within the well can cause severe damage to the well casing and downhole equipment. Secondly, once the packs are ignited the only method to control the process is by regulating the injection rate of the air. This does not afford great control over the process. Thirdly, if the fuel pack does not burn cleanly then the combustion gases and the air may carry particulate material into the formation. This material could clog the reservoir surrounding the well, and thus reduce its permeability. Also, because of its very nature, the method can only be used to ignite a formation near the bottom of the well. Finally, when applied to thicker formations, most of the injected air will be consumed in the upper section of the pack. As a consequence, ignition will occur first at the top of the formation, resulting in a combustion front that does not conform vertically.

To overcome the last of these fuel pack problems, Reichle (1963) proposed igniting the fuel pack throughout its depth, and not just at its top. During its preparation, igniters of one form or another are dispersed throughout the pack at intervals of between 0.7 m and 3.0 m. The igniters are then simultaneously ignited after air injection has begun. The igniters could be incendiary elements such as railroad fuses or small charges of unpacked or loose gun powder.

If the fuel pack is left in the well for a long time before being ignited then it may be invaded by connate water that seeps in from the surrounding reservoir. This water will hamper, and in some cases prevent, the ignition of the pack. In his patent, Harvey (1967) suggests preparing the fuel pack mixture with a small but effective concentration of an oil soluble surfactant. The surfactant renders the fuel pack oil-wettable and hydrophobic.

Gilchrist (1965) describes the preparation of an ignition fuel pack consisting of a mixture of a liquid hydrocarbon, a polymer and charcoal briquettes. The liquid hydrocarbon and the polymer are blended together at a temperature above the polymer's melting point. The blended mixture is then allowed to solidify in molds of regular shapes to form pellets. Gilchrist recommends the use of 1-olefin polymers including polyethylene, polypropylene and poly-1-butene while suitable trans-diene polymers include high trans-polybutadiene and high trans-polyisoprene. To enhance combustion small amounts of the oxides of aluminium, silicon, titanium and zirconium may be added to the blend. The shape of the pellets is chosen so that the pack remains permeable to air during combustion.

Land *et al* (1977) report that a fuel pack was successfully used to ignite a tar sand at Northwest Asphalt Ridge in Utah. The tar sand used in the field experiment was 3.0 m thick and located at a depth of 91 m. Charcoal briquettes were placed into the open hole up to the casing shoe. Nineteen litres of diesel fuel was then pumped into the ignition well to soak the briquettes. Attempts at igniting the fuel pack by dropping lighted fuses down the well failed, probably because they went out during the fall. An expendable 660 W electric heater was then lowered to the pack on a 2.54 cm tubing string and the pack was ignited. During the initial

stages of the ignition, air was injected at a rate of  $2.8 \text{ m}^3/\text{hr}$ . Two hours after ignition, the workers report that one percent by volume of propane was injected with the air. This continued for two days until the fireflood was established.

A second in-situ combustion field test was conducted in Utah tar sands, this time at a depth of 107 m and across a zone thickness of 4 m (Johnson *et al*, 1980). The first attempt at igniting the formation by injecting steam failed. The workers then packed the ignition well with diesel-soaked charcoal briquettes. An 800 W electric heater was lowered into the well, but the ignition attempt failed when a pressure buildup in the wellbore blew the fuel pack and the burnt out heater from the well. The third attempt to ignite the well proved successful. The ignition well was packed with alternating layers of diesel-soaked charcoal and burning charcoal. Upon ignition, the rate of air injection was  $17500 \text{ m}^3/\text{d}$ .

### 2.1.8. HOT FLUID INJECTION

Hot fluids may be injected into the reservoir in order to raise the temperature in the region around the wellbore. Preheating the reservoir in this way prior to air injection significantly decreases the time required for ignition. This method is particularly suitable for those reservoirs having a relatively low initial temperature. However, heat losses from the wellbore above the pay interval limit the depth at which the technique may be applied. Ramey (1962), Willhite (1967) and Prats (1982) discuss how such heat losses may be evaluated.

Because of its high heat content, steam is the preferred heating fluid in most cases. Black and Nichols (1968) show that not only will the injected steam heat the oil-bearing formation, but it will also reduce the injector's skin. For ignition purposes steam is usually generated at the surface, and mobile generators of the type described by Sowa and Munding (1980) may be used. In recent years however downhole steam generators have been developed that allow steam to be injected into wells that were previously considered to be too deep for steam injection (Hamrick and Rose 1976; Fox 1983). At the time of writing there are no reports of downhole steam generators having been used to provide the steam for in-situ combustion ignition.

Alexander *et al* (1965) patented the process of injecting a heating gas into a formation to enhance ignition. Their patent suggested injecting a hot gas such as air or nitrogen. Due to its low heat content the use of a gas as the heating fluid usually is not favoured, however.

### 2.1.9. OXYGEN FIREFLOOD IGNITION

The performance of an in-situ combustion process can be improved by injecting substantially pure oxygen rather than air into the formation. The main advantage of the process is that the inert nitrogen is not injected into the formation. As a result, for a given flowrate of oxygen, the required compressor capacity is reduced. Also, the concentration of the beneficial gas, carbon dioxide, is much higher ahead of the combustion front. In their survey Garon *et al* (1986) show that oxygen firefloods have already been used to recover oil.

Lacking the inert nitrogen that is present in air, substantially pure oxygen is a potentially hazardous gas that must be handled with extreme care. In an oxygen-rich environment, even normally safe steel can burn. As a consequence, the ignition phase of an oxygen fireflood can be very dangerous and must be undertaken with great caution.

To help overcome the potential hazards associated with handling oxygen, these firefloods are usually ignited using air as the oxidizing gas. Any of the ignition methods described in the previous sections may be employed to achieve ignition. Once the fireflood has become established and the combustion front has moved at least 10 m from the ignition well, then the concentration of oxygen in the oxidizing gas is gradually increased.

In two patents Shu (1983, 1984) suggests that during the ignition phase a  $\text{CO}_2/\text{O}_2$  mixture be used as the oxidizing gas, rather than air. As before, once the fireflood has been established the oxygen concentration is increased. Shu suggests that the nitrogen in the air will reduce the effective permeability for oil in the reservoir, while the  $\text{CO}_2$  will lower the oil's viscosity. In the second patent Shu describes how his concept may be used with a gas-fired burner to ignite a formation. Using nearly any type of gas-fired burner that operates with a secondary oxidizing gas supply (such as that illustrated in Fig. 2.1.2) a combustible gas mixture is burnt in the combustion chamber to generate heat downhole. This heat is carried into the formation by the combustion product gases and a  $\text{CO}_2/\text{O}_2$  mixture that is injected down the casing annulus as the secondary oxidant. During ignition Shu recommends that the mixture should contain between 55 and 80 percent by volume of carbon dioxide. Once ignition has been confirmed, the burner is pulled from the hole and the carbon dioxide content in the injected gases is decreased.

The chemical ignition method of Pusch *et al* (1977) described in an earlier section, was devised especially for oxygen firefloods. The method entails injecting into the slugs of diesel oil and an autoignitable fluid into the formation through perforations. Initially air is used as the oxidizing gas until the fireflood is established, at which time the oxygen concentration is increased up to 96 percent. In an effort to prevent the perforated casing from burning in the oxygen-rich environment, the authors suggest that the number and size of the perforations be carefully chosen so that the injected oxygen passes through them under critical flow conditions. Critical flow conditions are defined as those under which at the appropriate temperature the gas is expelled at the velocity of sound. Under such conditions heat is drawn from the surrounding area, including the steel casing, to such an extent that rapid cooling occurs. This cooling prevents the steel's ignition temperature (about  $1100^\circ\text{C}$ ) from ever being reached. The authors also note that adequate cooling effects can also be achieved in the borehole region under sub-critical flow conditions.

#### 2.1.10. CONCLUDING REMARKS

If spontaneous ignition does not occur or is not desired then the most appropriate artificial ignition method to use will depend upon the characteristics of the reservoirs and the oil, and on the services and utilities available on site. Advantages, disadvantages and limitations are associated with each of the artificial methods discussed in this report.

- Downhole gas-fired burners provide good control over the temperature of the oxidizing gas as it is injected into the formation. They may also be operated at depths below the reach of electric heaters. Their disadvantages include the requirements of burning dangerous gases, and of running multiple tubing strings into the wells. Also, if the gases do not burn cleanly, particulate material may be carried into the formation, possibly resulting in a reduction in the formation permeability.
- Excellent control of the oxidizing gas injection temperature is provided by the use of electric heaters. They are relatively easy to use and they may be deployed into the well on a single cable. Their operation requires no dangerous materials and the heaters may be used repeatedly. However, due to electrical power losses in the cable, they suffer from a practical depth limitation.

- Chemical ignition methods may be used on their own, or may be used together with electric heaters and downhole burners. Many chemical methods do require the handling and storage of dangerous materials.
- Fuel packs are simple to prepare but their use suffers from many problems associated with poor control over the ignition process, damage to the wellbore caused by excessive temperatures and clogging. The two applications reported in recent years were in wells less than 110 m deep.
- Steam is the most suitable hot fluid to inject into a well prior to the injection of the oxidizing gas. Care must be taken however to ensure that the steam does not displace the oil too far away from the ignition well. Also, due to the wellbore heat losses, hot fluid injection as a method to enhance ignition is not practical in deep wells.

### 2.1.11. ACKNOWLEDGEMENTS

The author gratefully acknowledges the support of the Commonwealth Scientific and Industrial Research Organization, Australia. This work was performed at the Stanford University Petroleum Research Institute under U.S. DOE contract DE-FG19-87BC14126.

### 2.1.12. REFERENCES

1. Alderman J.H., Fox R.L., and Antonation R.G.: "In Situ Combustion Pilot Operations in the Wabasca Heavy Oil Sands Deposit of North Central Alberta, Canada," SPE Paper No. 11953.
2. Alexander J.D., Dew J.N., and Martin W.L.: "Low Temperature In-Situ Combustion," U.S. Patent No. 3,209,825 (October 5, 1965).
3. Alexander J.D. and Martin W.L.: "Oil Well Ignition Device," U.S. Patent No. 3,379,256 (April 23, 1968).
4. Anthony M.J., Taylor T.D., and Gallagher B.J.: "Fireflooding a High Gravity Crude in a Watered-Out West Texas Sandstone," Proceedings 1981 SPE/DOE Second Joint Symposium on Enhanced Oil Recovery, SPE/DOE Paper No. 9711 (1981) 7-19.
5. Bandyopadhyay P.: "Method for In Situ Combustion Ignition," U.S. Patent No. 3,672,450 (June 27, 1972).
6. Bednarski V.N., Kunetka R.E., and Allen J.C.: "Initiation of In Situ Combustion in a Secondary Recovery Operation for Petroleum Production," U.S. Patent No. 3,180,412 (April 27, 1965).
7. Black W.M. and Nichols J.H.: "Steam Stimulation In-situ Combustion Backflow Process," U.S. Patent No. 3,369,604 (February 20, 1968).
8. Bousaid I.S., Fontaine M.F., and Korstad R.J.: "Method for Initiating In-Situ Combustion," U.S. Patent No. 3,774,682 (November 27, 1973).
9. Bowman C.H.: "A Two-Spot Combustion Recovery Project," *Journal of Petroleum Technology*, 17 (1965) 994-998.
10. Buchwald R.W., Hardy W.C., and Neinast G.S.: Case Histories of Three In-Situ Combustion Projects," *Journal of Petroleum Technology*, 25 (1973) 784-792.
11. Burger J.G.: "Spontaneous Ignition in Oil Reservoirs", *Society of Petroleum Engineers Journal*, 16 (1976) 73-81.
12. Cady G.V., Hoffman S.J., and Scarborough R.M.: "Silverdale Combination Thermal Drive Project," SPE Paper No. 8904 (1980).

13. Campbell G.G., Burwell E.L., Sterner T.E., and Core L.L.: "Why a Fire Flood Project Failed," *World Oil*, 162(2), 46-50.
14. Campion F.E., Glass E.D., Kirkpatrick J.W., and Vaughn J.C.: "Burner Apparatus," U.S. Patent No. 2,997,105 (August 22, 1961).
15. Casey T.J.: "A Field test of the In-Situ Combustion Process in a Near-Depleted Water Drive Reservoir," *Journal of Petroleum Technology*, 23, 153-160.
16. Cato R.W. and Frnka W.A.: "Getty Oil Reports Fireflood Pilot is Successful Project," *Oil and Gas Journal*, 66(7), (1968) 93-97.
17. Clark G.A., Jones R.G., Kinney W.L., Schilson R.E., Surkalo H., and Wilson R.S.: "The Fry In-Situ Combustion Test - Field Operations," *Journal of Petroleum Technology*, 17, (1965a) 343-347.
18. Clark G.A., Jones R.G., Kinney W.L., Schilson R.E., Surkalo H., and Wilson R.S.: "The Fry In-Situ Combustion Test - Performance," *Journal of Petroleum Technology*, 17 (1965b) 348-353.
19. Cornelius A.J. and Klein F.A.: "Igniting an Underground Formation," U.S. Patent No. 3,457,995 (July 29, 1969)
20. Dean M.R. and Klein F.A.: "Initiating In Situ Combustion using an Autoignitable Composition," U.S. Patent No. 3,490,530 (January 20, 1970).
21. Densmore W.: 1975, ' "Bellevue Field Cities Service Oil Co.," *Improved Oil Recovery Field Reports*, 1(3), 471-480.
22. Densmore W.: "Bellevue Field Cirties Service Oil Co. - ERDA," *Improved Oil Recovery Field Reports*, 2(3), (1976) 415-424.
23. Elkins L.F., Morton D., and Blackwell W.A.: "Experimental Fireflood in a Very Viscous Oil-Unconsolidated Sand Reservoir, S.E. Pauls Valley Field," SPE Paper No. 4086, Oklahoma (1972)
24. Emery L.W.: "Ignition of Fuel for Lighting a Well," U.S. Patent No. 2,941,595 (June 21, 1960).
25. Fairfield W.H. and White P.D.: "Lloydminster Fireflood Performance, Modifications Promise Good Recoveries," *Oil and Gas Journal*, 80(6) (1982) 101-112.
26. Fox, R.L.: "Downhole Steam Generator Having a Downhole Oxidant Compressor," U.S. Patent No. 4, 380,267 (April 19, 1983).
27. Frnka W.A.: "Bellevue Field Getty Oil Co.," *Improved Oil Recovery Field Reports*, 2(2), (1976) 275-284.
28. Fuchida T.: "Laboratory and Field Experiments on Fire-Flood Recovery Method," *Producers Monthly*, 23(9) (1959) 30-35.
29. Gadelle C.P., Lessi J., and Sarda J.P.: "La gazeification souterraine profonde du charbon en France. l'experience de Bruay-en-Artois," *Revue Institut Francais du Petrole*, 37 (1982) 157-181.
30. Garon A.M., Kumar M., and Cala G.C.: "The State of the Art of Oxygen Fireflooding," *In Situ*, 10(1) 1-26.
31. Garthoffner E.H.: "In-Situ Combustion in Hydrocarbon-Bearing Formations," U.S. Patent No. 4,615,391 (October 7, 1986).
32. Gates C.F. and Sklar I.: "Combustion as a Primary Recovery Process - Midway Sunset Field," *Journal of Petroleum Technology*, 23 (1971) 981-986.
33. Gates C.F., Jung K.D., and Surface R.A.: "In-Situ Combustion in the Tulare Formation, South Belridge Field, Kern County, California," *Journal of Petroleum Technology*, 30 798-806.

34. Gilchrist R.E.: "In Situ Combustion Initiation," U.S. Patent No. 3,208,520 (September 28, 1965).
35. Green K.B.: "The Fireflood: Cox Penn Sand," *Oil and Gas Journal*, **65(29)** (1967) 66-69.
36. Hamrick J.T. and Rose L.C.: "Downhole Recovery System," U.S. Patent No. 3,982,591 (September 28, 1976).
37. Hardy W.C., Fletcher P.B., Shepard J.C., Dittman E.W., and Zadow D.W.: "In-situ Combustion in a Thin Reservoir Containing High-Gravity Oil," *Journal of Petroleum Technology*, **24** (1972) 199-208.
38. Harvey R.R.: "Hydrophobic Fuel Pack and Well Ignition Therewith," U.S. Patent No. 3,323,591 (June 6, 1967).
39. Hazard H.R., Hummell J.D., and Schulz E.J.: "Method and Apparatus for Burning a Combustible Mixture in a Well," U.S. Patent No. 3,180,417 (April 27, 1965).
40. Holmes B.G.: "Method for Initiating In Situ Combustion within a Subterranean Formation," U.S. Patent No. 3,379,254 (April 23, 1968).
41. Howard C.E., Calvin D.G., and Pitts R.W.: "Method for In Situ Combustion for Enhanced Thermal Recovery of Hydrocarbons from a Well and Ignition System Therefor," U.S. Patent No. 4,079,784 (March 21, 1978).
42. Howard C.E., Calvin D.G., Pitts R.W.: "Ignition System for an Automatic Burner for In Situ Combustion for Enhanced Thermal Recovery of Hydrocarbons from a Well," U.S. Patent No. 4,137,968 (February 6, 1979).
43. Howard C.E., Calvin D.G., and Pitts R.W.: "Method for Forming an Automatic Burner for In Situ Combustion for Enhanced Thermal Recovery of Hydrocarbons from a Well," U.S. Patent No. 4,205,725 (June 3, 1980).
44. Hujsak K.L.: "Ignition of Thick Pay Formations," U.S. Patent No. 3,272,262 (September 13, 1966).
45. Hujsak K.L.: "Bottom-Hole Igniter Tube," U.S. Patent No. 3,307,609, (March 7, 1967).
46. Ireton E.T.: "Little Tom Field Hanover Petroleum Corp. - ERDA," *Improved Oil Recovery Field Reports*, **1(1)** (1975) 93-101.
47. Ireton E.T.: "Little Tom Thermal Recovery Demonstration Project, Zavala County, Texas," Proceedings Second ERDA Symposium on Enhanced Oil and Gas Recovery, **1**, Paper No. F-7 (1976).
48. Jenkins G.R. and Kirkpatrick J.W.: "Twenty Year's Operation of an In-situ Combustion Project," *Journal of Canadian Petroleum Technology*, **18(1)** (1979) 60-66.
49. Johnson L.A., Fahy L.J., Romanowski L.J., Barbour R.V., and Thomas K.P.: "An Echoing In-Situ Combustion Oil Recovery Project in a Utah Tar Sand," *Journal of Petroleum Technology*, **32(2)** (1980) 295-305.
50. Jones F.B. and Williams R.P.: "Process for Igniting Hydrocarbon Materials within a Subterranean Formation," U.S. Patent No. 3,583,484 (June 8, 1971).
51. Joseph C.: "Bodcau In-situ Combustion Project-Ignition," U.S. DOE Report SAN/1189-3 (1977).
52. Kaasa O.G., 1960, "Ignition of Fuel for Lighting a Well," U.S. Patent No. 2,941,596 (June 21, 1960).
53. Kelley A.: 1975, "Talco Field Paluxy (Carr Sand) Unit Exxon Co. U.S.A.," *Improve Oil Recovery Field Reports*, **1(2)**, 317-328.
54. Klein F.A. and Dean M.R.: "Igniting a Carbonaceous Stratum for In-situ Combustion," U.S. Patent No. 3,400,763 (September 10, 1968).
55. Koch R.L.: "Practical Use of Combustion Drive at West Newport Field," *Petroleum Engineer*, **37(1)** (1965) 72-81.

56. Kuhn C.S. and Koch R.L.:  
1953, "In-Situ Combustion - Newest method of Increasing Oil Recovery," *Oil and Gas Journal*, 52(14), 92-114.
57. Land C.S., Cupps C.Q., Marchant L.C., and Carlson F.M. : "Field test of Reverse - Combustion Oil Recovery from a Utah Tar Sand," *Journal of Canadian Petroleum Technology*, 16(2) (1977) 34-38.
58. Little T.P.: "Successful Fireflooding of the Bellevue Field," *Petroleum Engineer*, 47(11) (1975) 57-66.
59. Little T.P.: "Bodcau In Situ Combustion Project: Pre-Contract Work and Plan for Project Development," U.S. DOE Report SAN-1189-77-1 (1977).
60. Mace, C.: "Deepest Combustion Project Proceeding Successfully," *Oil and Gas Journal*, 73(46) (1975) 74-81.
61. MacLean A.M.: "Brea Olinda Field Union Oil Company of California," *Improved Oil Recovery Field Reports*, 1(1) (1975) 15-28.
62. MacSporran C.: "Process and Apparatus for In Situ Combustion," U.S. Patent No. 3,072,189 (January 8, 1963).
63. Marberry J.E. and Bhatia S.K.: "Fosterton Northwest - A Tertiary Combustion Case History," SPE Paper No. 4764 (1974).
64. Marrs H.G. and Hughes P.T.: "Kirby's Fireflooding Pilot Looks Good," *Oil and Gas Journal*, 68(48), (1970) 74-81.
65. McDonald E.E.: "Well Assembly for Heating a Subterranean Formation," U.S. Patent 3,372,754 (March 12, 1968).
66. Meier A.: "Method for the Ignition of In-Situ Combustion for the Recovery of Petroleum," U.S. Patent No. 3,777,816 (December 11, 1973).
67. Moss J.T.: "Practical Notes on Ignition in Fire Flooding', *Petroleum Engineer*, 37(5) (1965) 72-77.
68. Parrish D.R., Rausch R.W., Beaver K.W. and Wood H.W.: "Underground Combustion in the Shannon Pool, Wyoming," *Journal of Petroleum Technology*, 14 (1962) 197-205.
69. Parrish D.R., Pollock C.B., Ness N.L., and Craig F.F.: (1974) "A Tertiary COFCAW Pilot test in the Sloss Field, Nebraska," *Journal of Petroleum Technology*, 26, 667-675.
70. Pebdani F.N., Longoria R., Wilkerson D.N., and Venkatesan V.N.: (1988) "Enhanced Oil Recovery by Wet In-Situ Combustion: Esperson Dome Field, Liberty County, Texas," Proceedings 1988 SPE Annual Technical Conference and Exhibition, EOR/General Petroleum Engineering Volume, pp 157-166, SPE Paper No. 18072.
71. Prats M.: "Thermal Recovery," SPE Monograph Volume 7, SPE Dallas (1982) 128-132.
72. Pusch G., Klatt H.J., and Frohlich W.: "Method for Initiating an In-Situ Recovery Process by the Introduction of Oxygen," U.S. Patent No. 4,042,026 (August 16, 1977).
73. Ramey H.J. Jr.: "Wellbore Heat Transmission," *Journal of Petroleum Technology*, 14 (1962) 427-440.
74. Rees W.A.: "Bottom Nole Burner," U.S. Patent No. 3,315,745 (April 25, 1967).
75. Reichle, A.D., 1963 "Ignition for In Situ Combustions, U.S. Patent No. 3,072,190 (January 8, 1963).
76. Saxon J.: "In-Situ Combustion Method for Oil Recovery," *Producer's Monthly*, 18(5) (1954) 18-20.
77. Shu, W.R.: "In-situ Combustion Method for Recovery of Heavy Oil Utilizing Oxygen and Carbon Dioxide as Initial Oxidant," U.S. Patent No. 4,410,042 (October 18, 1983).
78. Shu W.R.: "Method for Initiating an Oxygen Driven In-situ Combustion Process," U.S. Patent No. 4,474,237 (October 2, 1984).

79. Smith, M.W.: "Simultaneous Underground Combustion and Water Injection in the Carlyle Pool, Iola Field, Kansas," *Journal of Petroleum Technology*, **18** (1966) 11-18.
80. Sowa A. and Munding G.: "Method and Apparatus for Extracting Crude Oil from Previously Tapped Deposits," U.S. Patent No. 4,224,991 (September 30, 1980).
81. Tadema H.J., Wei and Dema J.: "Spontaneous Ignition of Oil Sands," *Oil and Gas Journal*, **68(50)** (1970) 77-80.
82. Terwilliger P.L., Clay R.R., Wilson L.A., and Ginzalez-Gerth E.: "Fireflood of the P2-3 Sand Reservoir in the Miga Field of Eastern Venezuela," *Journal of Petroleum Technology*, **27** (1975) 9-14.
83. Terwilliger P.L.: "Fireflooding Shallow Tar Sands - A Case History," *Journal of Canadian Petroleum Technology*, **15(4)** (1976) 41-48.
84. Todd J.C.: "Estimating the Combustion Drive Air Requirement by Backflowing an Injection Well in the Delaware-Childers Field," *Society of Petroleum Engineers Journal*, **9** (1969) 351-356.
85. Trantham J.C. and Marx J.W.: "Bellamy Field Tests: Oil from Tar by Counterflow Underground Burning," *Journal of Petroleum Technology*, **18** (1966) 109-115.
86. Widmyer R.H., Howard C.E., Fontaine M.F., and Haynes S.: (1977) "The Charco Redondo Thermal Recovery Pilot," *Journal of Petroleum Technology*, **29** (1977) 1522-1532.
87. Willhite G.P., 196: "Over-All Heat Transfer Coefficients in Steam and Hot Water Injection Wells," *Journal of Petroleum Technology*, **19** (1967) 607-615.
88. Wright D.E. and Binsley R.L.: "Feasibility Evaluation of a Downhole Steam Generator," SPE Paper No. 9775 (1981).

TABLE 1  
COMBUSTION FIELD OPERATIONS IN WHICH SPONTANEOUS  
IGNITION WAS ATTEMPTED

Field	Location	Ignition Year	Depth (m)	Net Pay (m)	Porosity (%)	Oil Sat (%)	Res Temp (°C)	Oil Density (kg/m <sup>3</sup> )	Injection Pres (MPa <sub>g</sub> )	Air Injection Rate (m <sup>3</sup> /d)	Ignition Delay Time (days)	Reference
South Bridge	California	1956	213	9.1	36	60	31	980	--	--	--	Cetes <i>et al</i> (1978)
Midway Sunset	California	1960	640	39.3	36	75	52	969	6.55	29000	18	Cetes and Stür (1971)
--	Venezuela	1960	1372	7.0	35	94	66	1004	11.72	--	2	Bowman (1965)
Miga	Venezuela	1964	1234	18.2	22.6	78	63	979	17.24	227000	--	Terwilliger <i>et al</i> (1975)
Chanco-Badondo	Texas	1966	61	3.0	30-35	15-45	22	946	0.41	25500	3	Widmyer <i>et al</i> (1977)
Tois Liz	Texas	1968	1113	4.9	28	65	59	910	3.45	1700	--	Buchwald <i>et al</i> (1973)
Charlana †	Texas	1969	511	1.8	35	58	44	929	6.55	--	>90	Buchwald <i>et al</i> (1973)
Glen Hommel	Texas	1969	741	3.4	36	70	45	922	8.27	--	--	Buchwald <i>et al</i> (1973)
Fountain Northwest †	Saskatchewan	1970	945	8.4	--	--	52	912	5.10	14000	--	Murberry and Bhowia (1974)
SE Pook Valley †	Oklahoma	1970	1311	--	39	39	18	1000	13.10	60000	--	Elkins <i>et al</i> (1972)
Headberg	Mississippi	1971	3402	--	16.4	85	105	904-959	17.24	29000	--	Mico (1975)
Bron Olinde	California	1972	1067	38.1	29	50	57	922	4.83	71000	--	Maclean (1975)
Talco Texas	Texas	1972	1295	5.5	26	--	64	922	3.31	10000	--	Kelley (1975)

† Ignition attempt failed

TABLE 2  
COMBUSTION FIELD OPERATIONS THAT USED GAS-FIRED  
DOWNHOLE BURNERS FOR IGNITION

Field	Location	Ignition Year	Depth (m)	Net Pay (m)	Porosity (%)	Oil Sat (%)	Res Temp (°C)	Oil Density (kg/m <sup>3</sup> )	Injection Pres (MPa <sub>a</sub> )	Air Injection Rate (m <sup>3</sup> /d)	Heat Injected (MJ)	Reference
SE Kansas	Kansas	1956	253	2.7	20.3	77	26	916	6.65	10000	--	Emery (1962)
Niitsu	Japan	1957	187	10.1	--	--	24	945	--	9000	7900	Fuchida (1959)
KYROCK	Kentucky	1959	30	6.2	22	64	13	997	0.93	14000	--	Terwilliger(1976)
Shannon Pool	Wyoming	1959	290	10.1	23.3	60	20	904	--	11400	16000	Perrish <i>et al</i> (1962)
Reno Pool	Pennsylvania	1963	158	7.9	--	--	--	--	5.48	3840	104000	Campbell <i>et al</i> (1966)
Sloss	Nebreska	1963	1890	3.4	20	30	93	831	--	--	32000	Perrish <i>et al</i> (1974)
Charce-Rodendo †	Texas	1966	61	3.0	30-35	15-45	22	946	0.41	3700	59000	Widmyer <i>et al</i> (1977)
May Libby	Louisiana	1966	1022	0.6-3.7	31.24	70	57	825	--	5600	--	Hardy <i>et al</i> (1972)
Glen Hommed	Texas	1968	741	4.6	36	70	45	922	8.38	16500	--	Bochwald <i>et al</i> (1973)
Pipe Island	Louisiana	1969	314	--	35.2	52	27	927	--	2800-8600	--	Merris and Hughes (1970)
Golden Lake	Alberta	1969	488	7.0	35	82	21	979-986	10.44	11000	--	Fairfield and White (1982)
SE Prude Valley	Oklahoma	1970	1311	30.5	39	39	43	1000	13.20	13000	27000	Elkins <i>et al</i> (1972)
Bellevue (A)	Louisiana	1971	107	18.3	34.9	63.3	24	940	0.48	6390	--	Denmore (1975), Linds (1975)
Bellevue (B)	Louisiana	1974	107	18.3	33.9	73.6	24	940	0.20-1.23	2900-10000	--	Denmore (1976)
Little Tom	Texas	1976	853	4.3	22.3	57.1	52	946	11.06	8600	--	Leson (1975, 1976)
Silverdale	Alberta	1977	79	5.8	31	86	21	962	--	8600	--	Cady <i>et al</i> (1980)
North-Ward-Boss	Texas	1978	820	11.0	20	31-37	27	860	10.17	27000	--	Anthony <i>et al</i> (1981)
Athabasca	Alberta	1970's	259	45.7	--	--	--	--	--	--	10000	Jenkins and Kluteptrick (1979)
Joli Fox	Alberta	1981	363	3.7	---	--	--	953-983	--	--	33350	Aldeman <i>et al</i> (1983)
Esperon Dome	Texas	1984	820	6.4-13.7	31	36	52	928	--	7790	14000	Pebden <i>et al</i> (1988)

† Ignition attempt failed

TABLE 3  
COMBUSTION FIELD OPERATIONS THAT USED ELECTRIC HEATERS FOR IGNITION

Field	Location	Ignition Year	Depth (m)	Net Pay (m)	Porosity (%)	Oil Sat (%)	Res Temp (°C)	Oil Density (kg/m <sup>3</sup> )	Injection Pres (MPa <sub>a</sub> )	Air Injection Rate (m <sup>3</sup> /d)	Heat Injected (MJ)	Power (kW)	Voltage (V)	Reference
-	Oklahoma	1952	55	4.5	29	60	16	943	-	1190	34000	--	--	Rubin and Koch (1953), Saxon (1954)
West Newport	California	1958	427	51.8	37	-	41	965	-	--	22000	25	--	Koch (1965)
Fry	Illinois	1961	268	17.1	19.7	68	18	883	-	2800	24000	40	--	Clark et al (1965a, 1965b),
Ed Cox	Oklahoma	1962	457	7.9-23.5	-	-	--	887-966	-	--	--	--	--	Green (1967)
North Government Wells	Texas	1962	707	5.5	32	59	49	922	2.58	5700	7600	--	--	Casey (1971)
Bellview	Louisiana	1963	101	22.6	38.3	56.6	27	940	1.20	5700	--	20	440	Cato and Fritts (1968), Fritts (1976)
Jola	Kansas	1963	262	10.7	25.3	68	23	937	1.89	5900	31000	20	--	Smith (1966)
Bookee (A)	Louisiana	1976	114	4.9	33.9	72.6	24	940	-	5700	3700	30	440	Joseph (1977), Little (1977)
Bookee (B)	Louisiana	1976	117	3.0	33.9	72.6	24	940	-	5100	600	30	440	Joseph (1977), Little (1977)
Bookee (C)	Louisiana	1976	118	3.0	33.9	72.6	24	940	-	5700	4170	30	440	Joseph (1977), Little (1977)
Bookee (D)	Louisiana	1976	119	3.0	33.9	72.6	24	940	-	5700	1400	30	440	Joseph (1977), Little (1977)
Bookee (E)	Louisiana	1976	124	3.0	33.9	72.6	24	940	-	4670	3800	30	440	Joseph (1977), Little (1977)

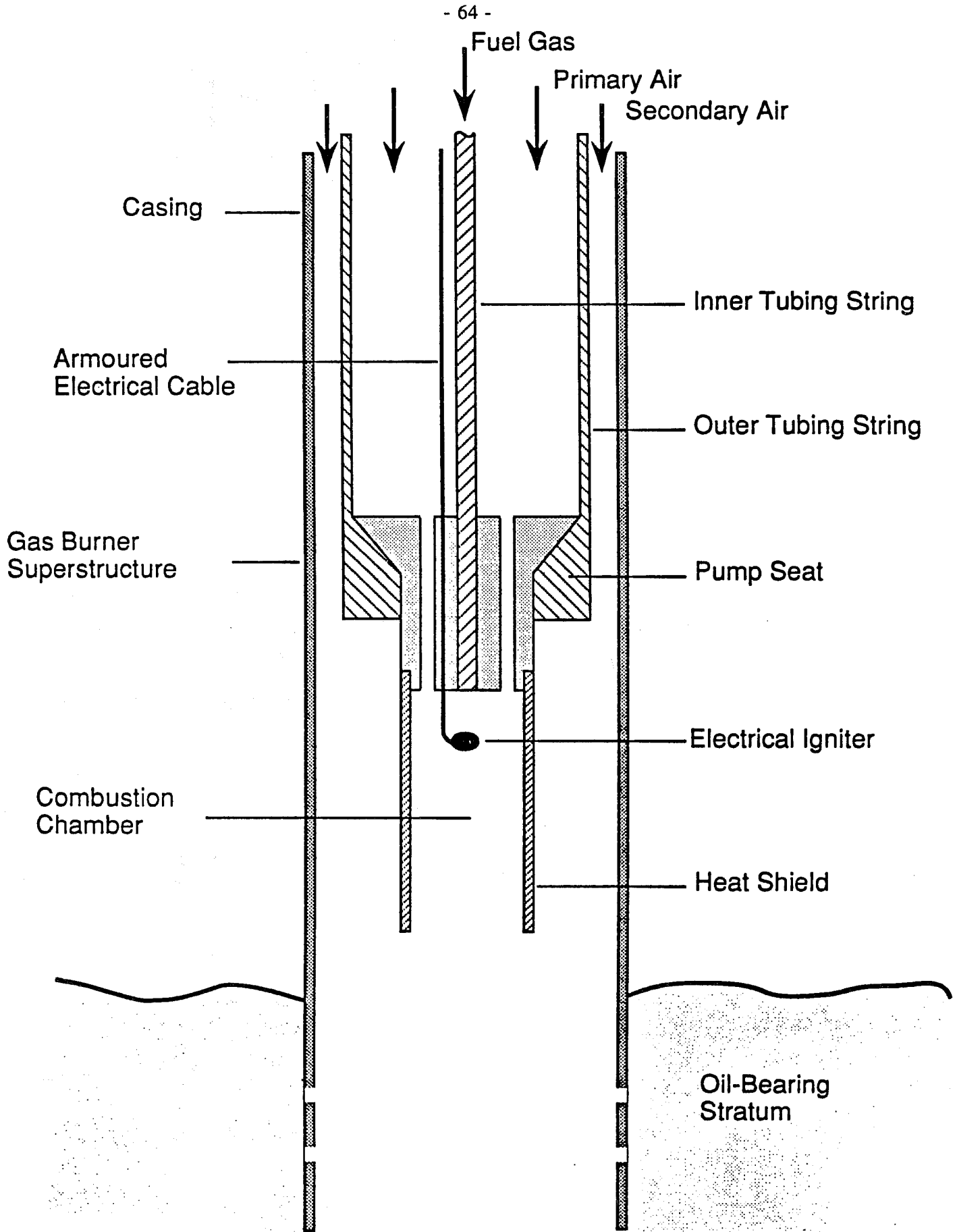


Figure 2.1.1 A typical gas-fired downhole burner modeled after designs of Howard *et al.* (1978, 1979, 1980).

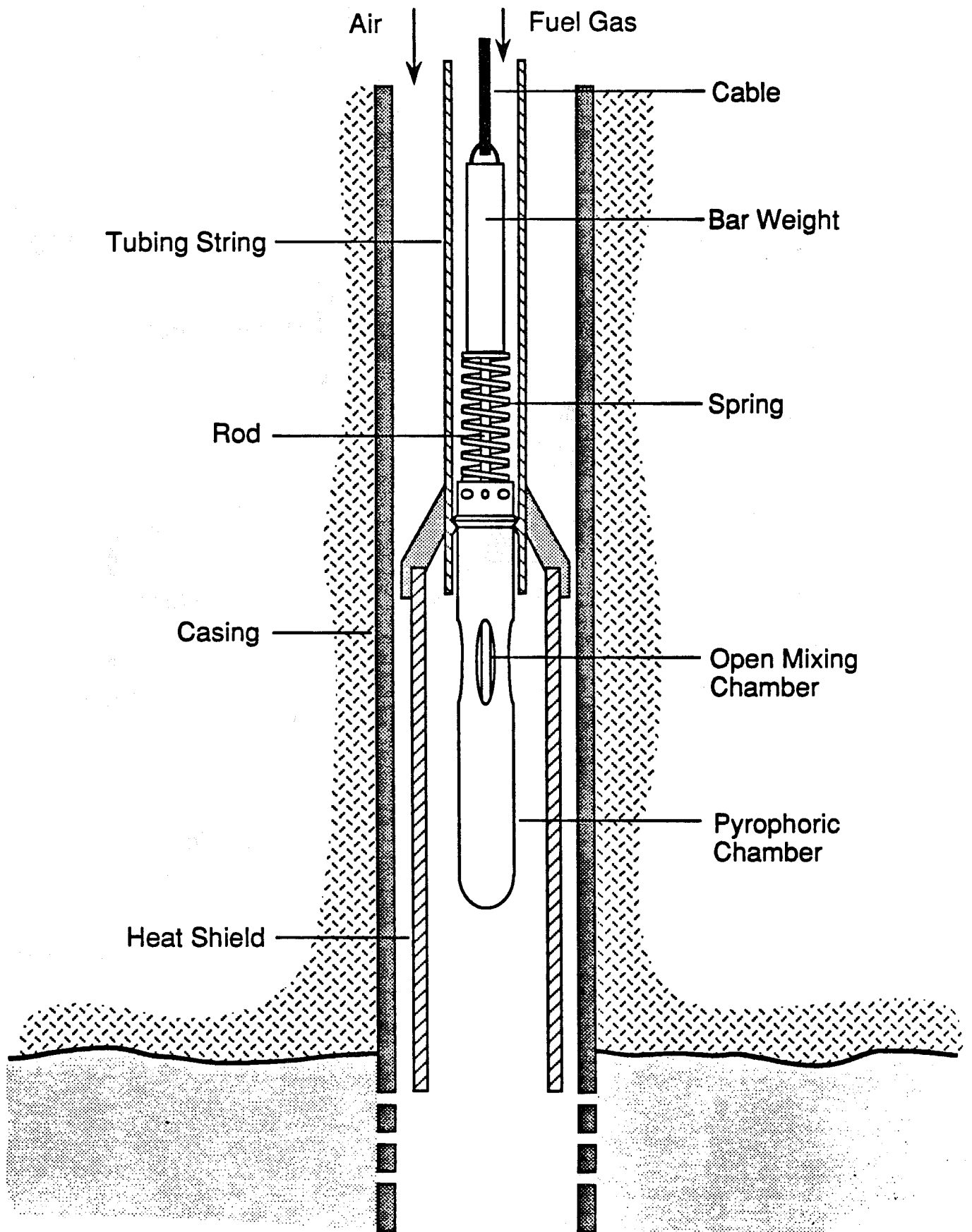


Figure 2.1.2 Hujsak's (1967) chemically-ignited gas-fired burner.

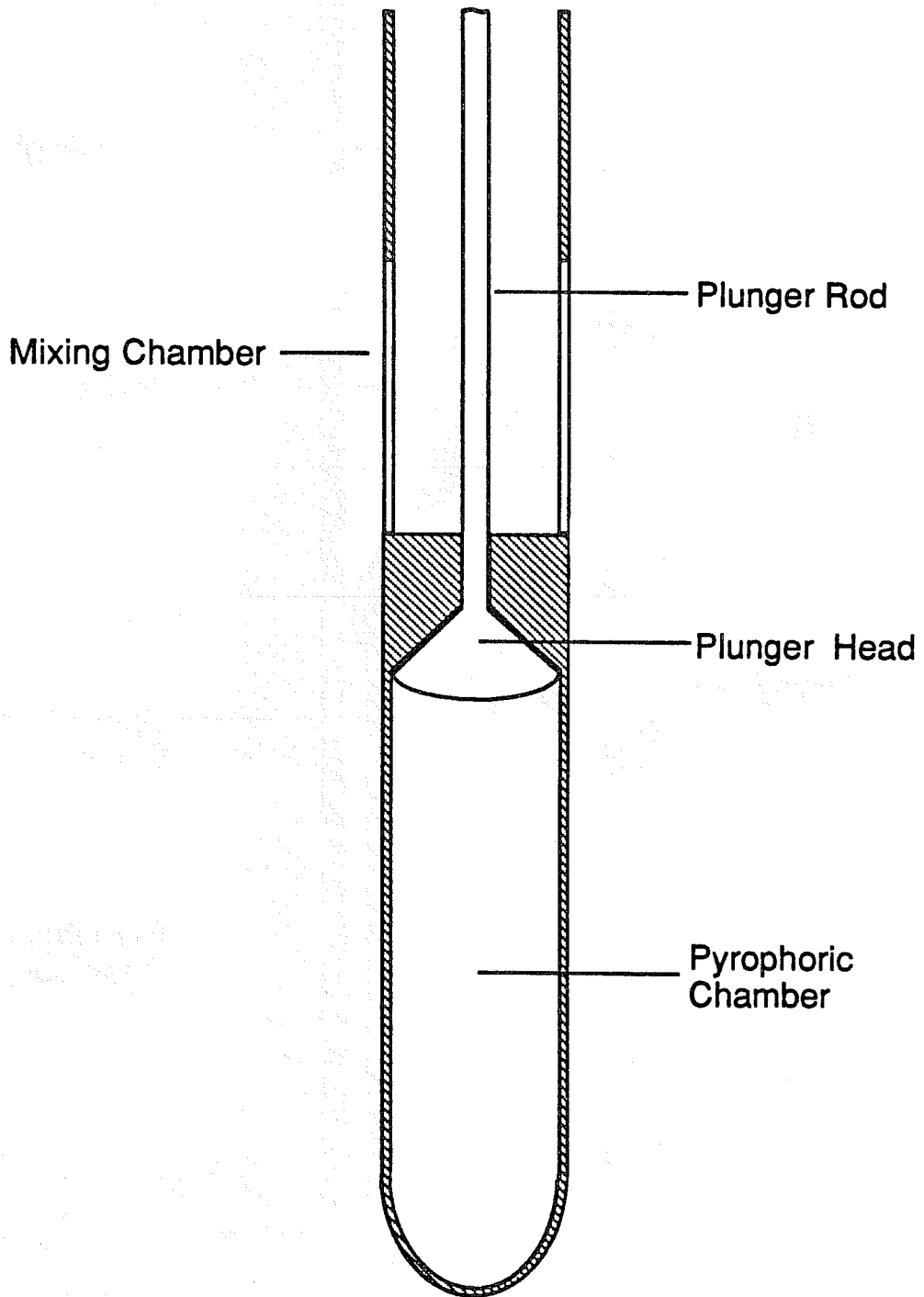


Figure 2.1.3 Detail of the pyrophoric chamber of Hujsak's (1967) burner.

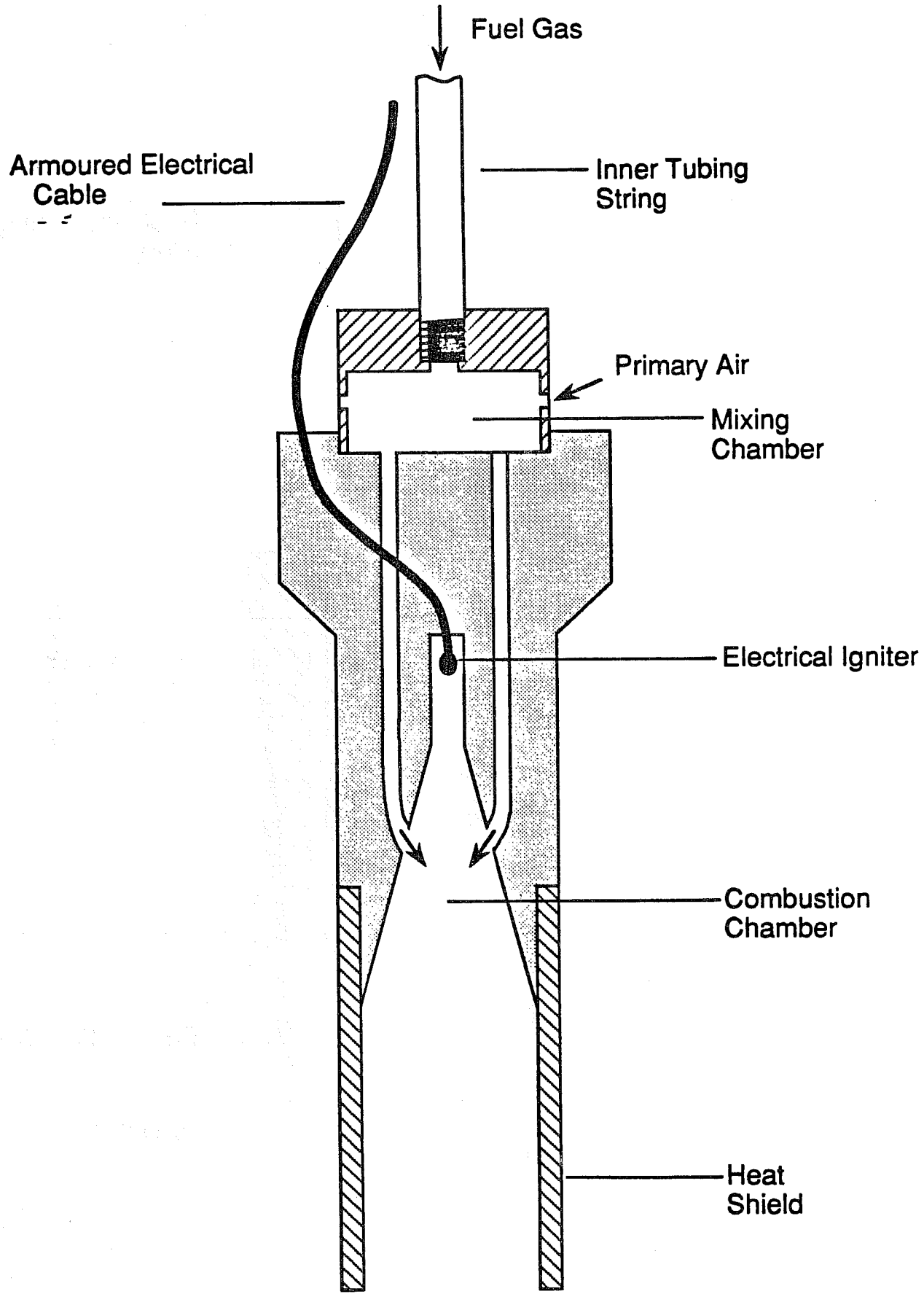


Figure 2.1.4 Modified design of Burner of Hazard *et al.* (1965).

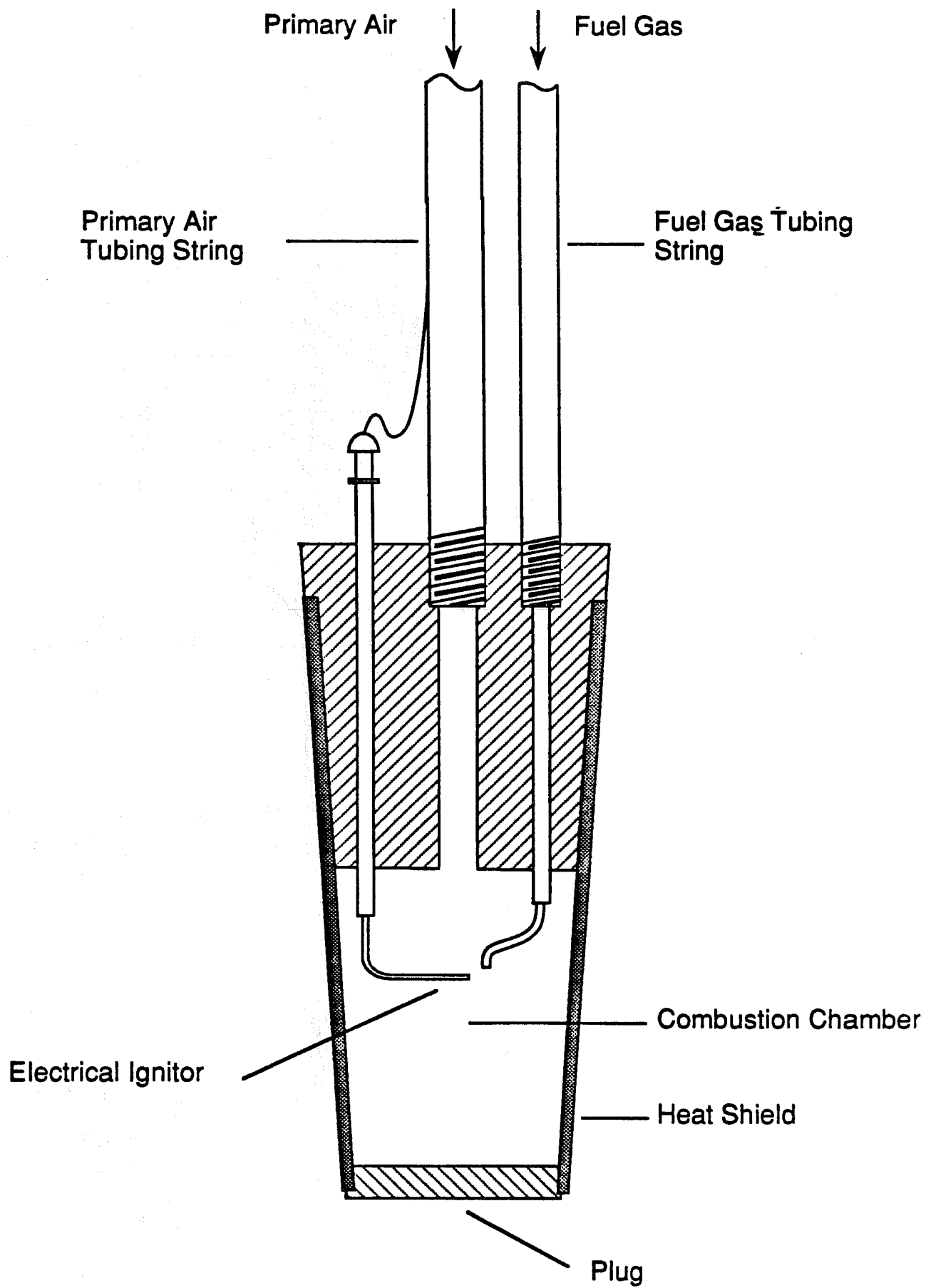


Figure 2.1.5 Burner with plug designed by Rees (1967) to prevent well fluids from entering combustion chamber.

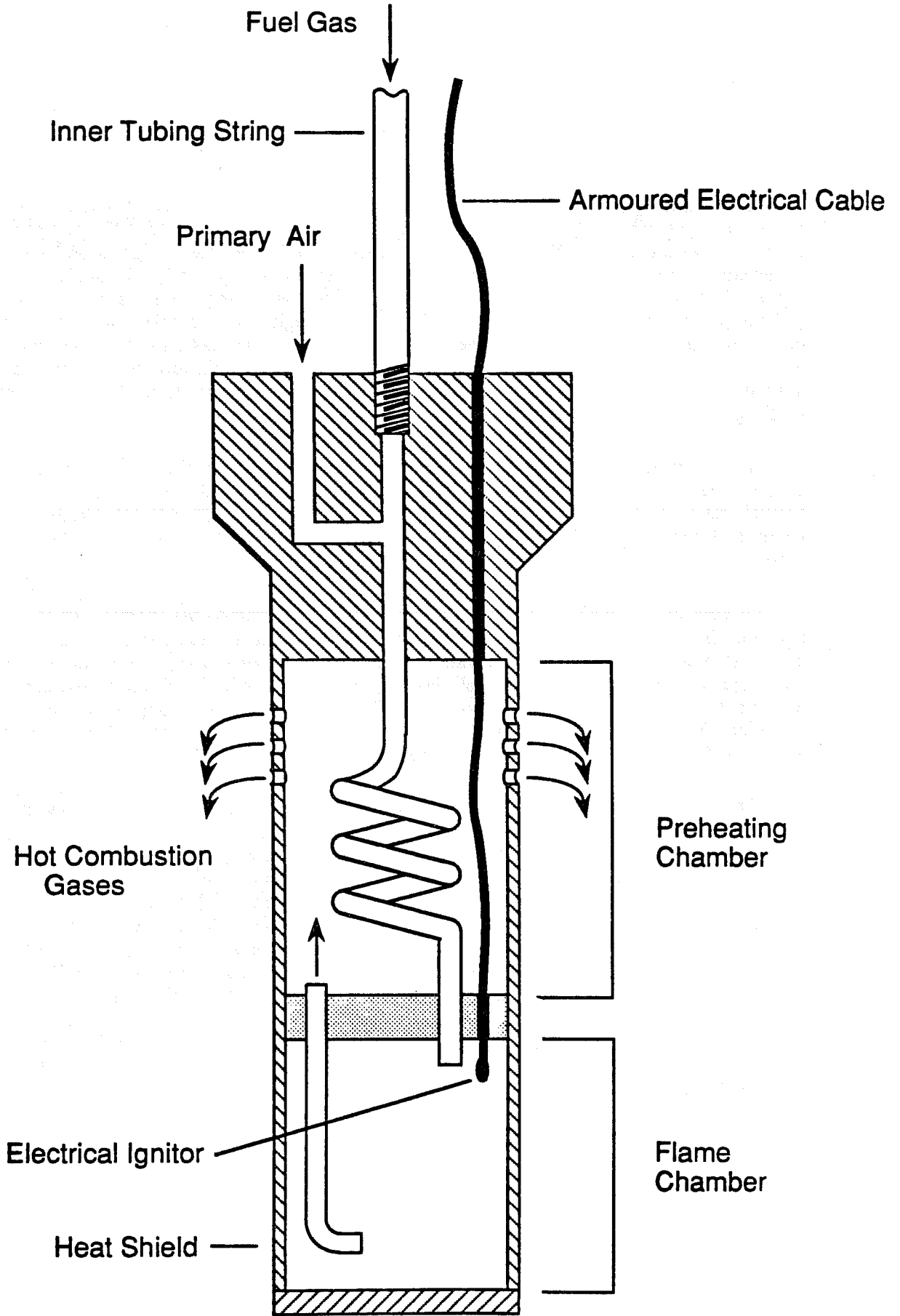


Figure 2.1.6 Dual chamber burner design of Palm (1965).

## 2.2 TUBE RUNS (C. Baena)

### 2.2.1. ABSTRACT

The economics and applicability of an in-situ combustion process for the recovery of crude oil are dictated to a large extent by the nature and the amount of fuel formed during the process. If the amount of fuel deposited is insufficient, as in the case of light oil reservoirs, the combustion front will not be self sustaining (Poettmann *et al.*, 1967). If excessive fuel is deposited, as in the case of very heavy oil reservoirs, the air requirements will be excessive and the process may not be economically viable. Through kinetic studies on crude oil oxidation in porous media, metals have been shown on a qualitative basis to affect the nature and the amount of fuel formed. The aim of this work was to use combustion tube studies to determine on a quantitative basis, how the nature and the amount of fuel formed could be changed by the presence of metallic additives.

These experiments follow from the qualitative observations on the effect of metallic additives on the in-situ combustion of Huntington Beach crude oil made by De los Rios (1987) at SUPRI. He performed kinetic studies on the oxidation of Huntington Beach Crude in porous media and showed that the nature of the fuel formed changed when metallic additives were present.

In this study, combustion tube runs were performed using the metallic additives iron, zinc and tin. Soluble salts of these metals were selected from the results seen in De los Rios' kinetic studies. Unconsolidated core samples were prepared by mixing predetermined amounts of an aqueous solution of the metal salt, Huntington Beach Crude Oil, Ottawa sand and clay in order to achieve the desired fluid saturations. The mixture was then tamped into the combustion tube. Dry air combustion tube runs were performed keeping the conditions of saturation, air flux and injection pressure approximately the same during each run.

The nature of the fuel formed and its impact on the combustion parameters were determined and compared with a control run - an experiment performed in the absence of any metallic additive. It was found that the presence of metallic additives increased the atomic hydrogen to carbon ratio of the fuel from 0.07 for the control run to 0.13 in the presence of iron, 0.61 with zinc present and 0.79 with tin. The H/C ratio of the fuel coupled with the extent to which the oxidation formed CO<sub>2</sub> in preference to CO affected the following combustion parameters: velocity of the burning front, heat of combustion of the deposited fuel, air requirements at 100% combustion efficiency, the air oil ratio and the oil recovery rates. As a result of the increased hydrogen content of fuel, the heat of combustion and the air requirements at 100% combustion efficiency increased as the H/C ratio increased. The presence of a metallic additive increased the burning front velocity and the oil recovery rate. However these were found to be affected by the oxygen utilization efficiency, the nature and the amount of fuel formed

### 2.2.2. LITERATURE SURVEY

The study of the effects of metallic additives on in-situ combustion emerged in the late seventies (Burger and Sahuquet, 1974; Bardon and Gadelle, 1977) as a result of the observations of increased fuel deposition and increased air requirement in reservoirs having minerals with high metallic content in the rock matrix (Earlougher *et al.*, 1970; Hardy *et al.*, 1972).

Researchers (Burger and Sahuquet, 1974; Fassihi, 1981; Sidqi, 1985; Racz, 1985) first attempted to understand the reactions involved in the combustion reaction through determination of the kinetics of crude oil oxidation in porous media in the presence of metallic additives. Their observations of increased fuel deposition in the presence of metallic additives encouraged them (Racz *et al.*, 1985) to test the introduction of selected metallic additives into reservoirs in order to modify the nature of the fuel formed and change the combustion parameters involved in the in-situ combustion reaction. This section will discuss the qualitative observations made during such kinetic studies and the field studies that were performed in the presence of metals and metallic additives.

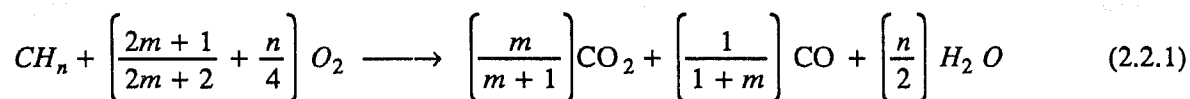
In order to understand the discussion of the effects of metallic additives on in-situ combustion, it is necessary to briefly explain how the oxidation reactions that take place have been modeled as a result of kinetic studies, as several references to these modeled reactions will be made throughout this thesis.

The reaction kinetics have been modeled into three sets of reactions: (1) low temperature oxidation, (2) medium temperature oxidation and (3) high temperature oxidation. A discussion of these reactions and their findings follow.

Low temperature reactions (LTO) result in the formation of chemicals such as peroxides, hydroperoxides, aldehydes, ketones, carboxylic acids and alcohols (Burger and Sahuquet, 1972). Alexander *et al.* (1962) and Al-Saadon (1970) showed that fuel availability was increased when low temperature oxidation of the crude oil took place. Dabbous and Fulton (1974) also found this to be true. They found that LTO causes a substantial decline in recoverable oil from the distillation and cracking zones, an increase in the fuel deposition and marked changes in the fuel characteristics and coked sand properties.

Medium temperature reactions involve distillation, visbreaking and coking of the fuel along with partial oxidation of the products formed (Bardon and Gadelle, 1977; Fassihi, 1981; Sidqi *et al.*, 1985). The amount of coking and the atomic H/C ratio of the fuel were found to decrease with increasing coking temperature (Bousaid, 1968). Increasing pressure was found to increase the amount of hydrocarbon residue formed; but the fuel deposited had a lesser hydrogen content (Sidqi, 1985).

High temperature oxidation (HTO) reactions involve oxidation of the cracked hydrocarbon residue. HTO takes place according to the equation:



where  $m$  is the ratio of carbon dioxide to carbon monoxide formed upon oxidation, and  $n$  is the atomic hydrogen to carbon ratio of the deposited fuel.

The analysis of the reaction rates of the three modeled in-situ combustion reactions has traditionally been expressed in terms of oxygen concentration rather than in terms of carbon oxides formed because oxygen is partially consumed in the low temperature reactions resulting in the formation of oxidized products not found in the exit gas.

The reaction rate  $R_r$  is expressed as:

$$R_r = k P_{O_2}^a C_f^b \quad (2.2.2)$$

where  $a$  is the order of the reaction with respect to the partial pressure of oxygen present,  $P_{O_2}$ ,  $b$  is the order of the reaction with respect to the concentration of the fuel,  $C_f$ ,  $k$  is the rate constant related to the Arrhenius (1889) constant,  $A_r$ , and the energy of activation,  $E$ , given by the expression:

$$k = A_r \exp(-E/RT) \quad (2.2.3)$$

where  $R$  is the universal gas constant.

The Arrhenius rate constant,  $A_r$ , was found to be dependent on the grain size distribution of the porous medium (Burger and Sahuquet, 1971; Bardon and Gabelle, 1977). The energy of activation,  $E$ , was found to be insensitive (Dabbous and Fulton, 1974) to the type of crude and the porous medium.

The reaction rate was found to be first order with respect to the fuel concentration and having an order of 0.5 to 1 (Dabbous and Fulton, 1974) with respect to the oxygen partial pressure. Weijdemer (1968) and Fassihi (1981) found that the order for the LTO reaction in terms of the partial pressure of oxygen was close to unity.

With this brief review of the modeling of the oxidation reactions, the discussion now focusses on the effect of metals and metallic additives on in-situ combustion. Metals have long been known to catalyze hydrocarbon oxidation and cracking reactions and have been extensively used as catalysts in the chemical and petroleum refining industries. Gureyev and Sublina (1965) found that by adding metals such as copper, brass, iron, aluminum, tin, lead or zinc, oxidation of the crude oil was promoted by destroying the antioxidants naturally present in the crude.

The oxidation of hydrocarbons has been found to be catalyzed by metals through a chain reaction mechanism involving initiation, propagation and termination steps. The classical steps are outlined by Racz (1985), and repeated in De los Rios's thesis (1987) and will not be repeated here.

### Kinetic Studies in the Presence of Metals and Metallic Additives

Several kinetic studies have been performed to determine the influence of the presence of metals and metallic additives on the oxidation characteristics of crude oils. A discussion of the work performed and the observations made during these experiments follows.

In two separate experiments, Burger and Sahuquet (1972) studied the influence of 1% nickel oxide and 2000 ppm copper in sand on the oxidation of a 27° API crude. They found that the activation energy of the low temperature reaction was reduced with a corresponding increase in the amount of fuel deposited. This was evident from the occurrence of oxidation at a lower temperature with a high peak for the high temperature reaction.

Fassihi (1981) studied the effect of 2000 ppm copper in sand on the oxidation of a 27° API crude. He found that the activation energy of the low temperature reaction was unaffected, but higher reaction rates were observed in the low temperature reaction as a result of an increased Arrhenius rate constant,  $A_r$ . The activation energy of the medium temperature reaction increased by about fifty percent, but that of the high temperature reaction decreased by fifty percent.

Racz *et al.* (1985) studied the influence of iron pentacarbonyl, and a mixture of manganese, vanadium and other metals. They found through thermogravimetric analysis (TGA) and differential scanning calorimetric (DSC) studies that the influence of iron was the greatest in generating heat at a lower temperature, implying the occurrence of a greater low temperature oxidation reaction and hence increased fuel deposition during the medium temperature reaction. Iron pentacarbonyl was successfully used in a pilot study on the Demjen-Kelet field where recovery was increased from 15% to 60%. A discussion of their field test will be provided later herein.

Drici and Vossoughi (March 1985) studied the influence of vanadium, titanium, nickel, cupric and iron oxides on the oxidation of a 20° API crude using TGA and DSC. Oxidation reactions were first carried out in the presence of increasing amounts of the metal oxides. They observed that the fractional amount of heat released in the low temperature region gradually increased and attained a maximum level and that the high temperature oxidation took place at a lower temperature. They then carried out experiments on mixtures of metal oxide (1% by weight), crude oil (5% by weight) and coarse sand (less than 48 mesh) and found that the heat released during the high temperature oxidation was increased as a result of increased fuel deposition. Finally they studied the oxidation characteristics of the crude oil using mixtures of metal oxide (1% by weight), crude oil (5% by weight) and fine silica powder (90 mesh) and found the effect of the metal oxide to be insignificant primarily because of the large surface area offered by the fine silica powder.

The precursor to the work done in this thesis has been the kinetic studies on Huntington Beach Crude Oil by De los Rios at SUPRI (1987). He performed kinetic studies using 1 and 2% water soluble solutions of salts of iron, tin, magnesium, zinc, potassium, copper, manganese, nickel and cadmium. A discussion of his observations is made later herein.

Observations on the influence of metals and their salts on in-situ combustion were initially made through in-situ combustion studies on reservoirs having a high metallic content in clays and minerals found in the rock matrices of the reservoirs. Results from the Fry Test (Earlougher *et al.*, 1970) showed increased air requirement as the reservoir had a matrix which contained both clays and iron derivatives (pyrite and siderite) that increased the fuel deposition. Similar results were also observed for the field tests performed in May Libby reservoir in the Delhi field (Hardy *et al.*, 1972) which had a 40° API crude.

Such observations have been encouraging. Carcoana (1983) reported that Romania planned to recover 41% of its total EOR recoverable oil by the process of in-situ combustion. Reservoirs in Romania have been found to contain a high concentration of metals such as vanadium, nickel and chromium. These metals were found to act as natural catalysts in laboratory studies run to determine the effect of these naturally occurring minerals. They have not published quantitative results of these studies.

A comprehensive description of a technique tested in the field, which used an initiator to enhance the chain reaction mechanism involved in the metal catalyzed oxidation of hydrocarbons in in-situ combustion, has been published by Racz *et al.* (1985) in Hungary. The next few paragraphs discuss their technology which used tertiary butyl-hydroperoxide (TBH) as initiator in the presence of iron pentacarbonyl catalyst. Oil recovery increased from an estimated primary recovery of 15% to 60% in their test pattern in Demjen-Kelet field when it was subjected to TBH initiated iron pentacarbonyl catalyzed in-situ combustion.

In developing their new technology, they first determined the reaction kinetics through TGA studies for different oil grades in porous media using different air flow rates using a wide range of additives. The object of these experiments was to bring about a decrease in the activation energy of the oxidation process in order to bring about the feasibility of the in-situ combustion oil process for recovering crude oil from the Demjen-Kelet field.

They also studied the influence of the mineral content of the reservoir rocks on the in-situ combustion process. They found that the optimum effect was in the temperature range of 300-400°C. They found that above 600°C the endothermic decomposition of carbonates and bicarbonates present in the rock matrix hindered the feasibility of the in-situ combustion process.

An analysis of the mineral content of the reservoir showed the existence of trace elements of Ba, As, Mn, Ti, V, Cu, Na, Ni, Zr, Co, Sr, K, Fe and Cr. TGA and DSC studies showed iron and iron compounds had a very marked exothermal effect as compared to the other metallic additives.

Using the knowledge that oxidation of hydrocarbons in the presence of metals follows a chain reaction mechanism, they figured that if easily decomposing compounds like peroxides, metal carbonyls and azo-compounds were added to the system, the oxidation reactions would be further enhanced as a result of these initiators. They studied the influence of tertiary-butylhydroperoxide (TBH). Laboratory experiments were performed to determine the amount of oxygen absorption in the presence of 5% TBH at 140 and 160°C at 100 and 400 MPa pressure. The rate of oxidation was found to be significantly increased at atmospheric pressure above 200°C and at a pressure of 400 MPa above 170°C. They concluded that TBH significantly affected LTO and increased fuel deposition between the temperature range of 140-200°C on the pressure.

Dynamic microcalorimetric measurements were performed on the distillation residue having a boiling point above 200°C for the mixture of Demjen-Kelet oil, quartz sand and different metallic additives. The greatest heat generation was observed in systems containing iron. Other metal catalysts were also studied and a mixture of magnesium, vanadium and other metals was found to have similar effects. A shift in the low temperature oxidation peak to lower temperatures in the presence of iron and the metal mixture described above, suggested that the activation energy of the LTO reaction was decreased, implying higher fuel deposition.

To improve the oil displacement and oil recovery by increasing the length of the steam zone and to bring about efficient heat utilization, they decided to carry out the process as a wet combustion process in the field, after testing out and observing good results in the laboratory. They performed wet combustion tube experiments in the absence of the catalyst and found the front temperature to be about 450°C. But when the iron pentacarbonyl catalyst was added (1% solution) to the injected water the combustion front temperature reduced by 120 to 150°C.

The technology developed in the laboratory was finally put to the test in a 50 × 50 m. pilot inverted five spot pattern 280 m. in depth in the Demjen-Kelet field. TBH was injected along with air into the reservoir and its pressure was raised to 2-4 MPa. Once the combustion front was stabilized, water containing the iron pentacarbonyl catalyst (1% solution) was injected at a rate to maintain the temperature in the condensation zone between 200-240°C. This markedly affected the LTO reaction, increasing the fuel deposited in the presence of the iron-pentacarbonyl catalyst and increasing the heat liberated in the high temperature oxidation reactions and bringing about an efficient heat utilization.

The results were good. Ultimate recovery was increased to 60% from the anticipated 15% primary recovery. Because of the success of their pilot study, they are now working towards a full scale operation in the Demjen Kelet field.

This publication has been the only one that has described the development of a technology that injected not only a metal catalyst, but also used an initiator to enhance the chain reactions typical in the oxidation of hydrocarbons in the presence of metallic additives. The literature is sparse with regard to such work.

### 2.2.3. PROBLEM STATEMENT

The economics and applicability of an in-situ combustion process is largely determined by the nature and the amount of fuel formed. The nature of the fuel formed affects:

1. Heat of combustion and hence the extent of visbreaking
2. Front velocity and hence the oil recovery rate
3. Air requirement and hence the economics of the in-situ combustion process.

The nature of the fuel formed and its impact on the combustion parameters can be determined on a quantitative basis by performing combustion tube studies in the presence of metallic salts.

The effect of the metallic additives: stannous chloride, ferrous chloride and zinc chloride on the in-situ combustion characteristics of Huntington Beach crude oil has been determined. Selection of these metallic additives was based on the results of the kinetic studies on Huntington Beach crude oil in the presence of these metallic additives by De los Rios (1987). His observations are summarized in Table 1.

De los Rios (1987) found that Iron, Tin and Aluminum induced similar effect on the oxidation of Huntington Beach Crude Oil (HBO), but to differing extents. Addition of iron or tin produced significant increases in the rates of oxidation. In the case of aluminum, the effects were less pronounced. When ferrous chloride was used by De los Rios, lower activation energies were observed. This resulted in increased oxidation and fuel deposition in the LTO reaction. The medium temperature reaction exhibited greater reaction rates as a result of a larger pre-exponential constant. The activation energy was larger in the medium temperature range, but the pre-exponential constant was very large causing an increase in the reaction rate. The high temperature combustion reaction was found to peak at a lower temperature and it occurred over a narrower temperature range with no significant change in the energy of activation. However the increased fuel deposition at lower temperatures led to larger pre-exponential constants and thus higher reaction rates in the HTO reaction. When stannous chloride was used, effects similar to those of iron were observed. Increased reactivity to oxygen occurred at a lower temperature for all the reactions. Greater reaction rates occurred in the LTO reaction with increased fuel deposition due to reduced activation energy. Larger pre-exponential constants were observed in the medium and high temperature reactions.

Zinc, magnesium, chromium and manganese exhibited similar effects on the oxidation of HBO. Their relative effects varied during the low and medium temperature reactions; but these reactions occurred at a much higher rate. As a result low temperature oxidation and fuel deposition were increased. When zinc chloride was used increased oxygen consumption and carbon oxide production occurred at a lower temperature. However this was not because of a reduction in activation energy, but rather because of an increase in the pre-exponential constant. Higher

activation energy in the medium temperature reaction resulted in a higher, narrower oxidation peak. A reduction in the activation energy was observed in the high temperature reaction. As a result, a broad high temperature peak was observed. Magnesium and chromium exhibited effects similar to zinc; however manganese exhibited a much reduced effect.

Copper, nickel and cadmium produced only a small effect on the effluent gas composition. In the case of copper, De los Rios observed an increase in the activation energy of the low temperature reaction leading to an decrease in the LTO reaction rate for Huntington Beach crude. This observation is different from that observed by Burger and Sahuquet (1972). They reported that the energy of activation decreased in the LTO reaction resulting in increased fuel deposition in their kinetic studies on a 27° API crude. In contrast, Fassihi (1981) observed that there was no change in the energy of activation in the LTO reaction during his kinetic experiments on a 27° API French crude. Such differences in the reactivity of crudes to copper could be explained on the basis that the oxidative reactivity of a crude to a metal may differ based on the crude oil composition. Cadmium exhibited an effect opposite to copper for the LTO reaction. However in the case of both nickel and cadmium, slightly larger activation energies in the HTO reaction resulted in sharper and narrower high temperature peaks.

Of the wide variety of metals studied by De los Rios, salts of the metals of iron, tin, and zinc were used in this study. These salts were chosen after studying their influence on the oxidation reactions as characterized by the exit gas composition and the cell temperature, as observed during the kinetic experiments of De los Rios. Tin and iron were chosen because they exhibited a considerable effect on the LTO reaction increasing the fuel deposited by reducing the activation energy of the LTO reaction. Zinc was chosen as representative of those metals which increased the LTO rate as a result of an increase in the pre-exponential constant and not a result of a decrease of the activation energy in the LTO reaction.

#### 2.2.4. EXPERIMENTAL APPARATUS AND PROCEDURE

The experimental system is similar to those used by a number of researchers at SUPRI (Satman, 1979; Fassihi *et al.*, 1982; Andrade, 1984; Sidqi *et al.*; 1985).

The steps used to carry out the in-situ combustion tube runs are as follows:

1. The sand pack is first prepared by mixing known weights of 20-30 mesh Ottawa sand, clay, oil and water containing the dissolved metal salt in its desired concentration ( none for the control run ) to achieve the desired saturations of the fluids. It is important that this should be done with care to ensure proper mixing as our observations have shown variations in fuel deposition as a result of local and zonal saturation variations.
2. The combustion tube is then prepared by tamping the prepared sand into it, care being take to avoid moving the axial thermowell. Samples are taken at the top, middle and bottom of the pack to check for the desired fluid saturations using the ASTM D-95 extraction technique, similar to Soxhlet extraction. The porosity of the pack is determined on the basis of the weight of the material put into the pack, and on the basis of volume of the pack. The sandpack is tamped to a height of 85 to 90 cms from the bottom of the tube.
3. Three ml. of linseed oil are added to the top of the saturated pack in order to bring about a quick ignition and uniform combustion. The rest of the space above this is filled with clean sand, added to prevent premature coking reactions.

4. The combustion tube is assembled by connecting the flanges and other accessories.
5. The combustion tube is then pressure tested to 150 psig by using nitrogen. The combustion tube is pressurized for over three hours and checked for leaks.
6. The combustion tube is placed inside the pressure cell and the annular space is uniformly filled with Dacotherm insulation to minimize heat losses.
7. The top flange of the pressure cell is secured by bolts and the air supply line is connected to the combustion tube. The separator is connected to the bottom of the combustion tube. The exit line for the gaseous products from the separator is connected to the condenser.
8. After assembly, checks are made for any leaks in the system using nitrogen at 150 psig.
9. Any blockages in the system lines present are detected and rectified.
10. The gas analyzers are checked for calibration in accordance with manufacturers instructions, while other equipment used for data collection are turned on and tested. One should note here that the analyzers should be calibrated at the operating pressure and flow rate, as they were found to be particularly sensitive to pressure.
11. The reservoir is preheated by turning on the external heaters around the pressure shell and leaving it overnight. To maintain an average reservoir temperature between 50 to 75°C, the middle heater is kept at 60°C, the top at 65°C, and the bottom at 82°C as recommended by previous investigators using this system.
12. The next day the analyzers are checked for calibration and the data collection equipment is turned on. The igniter coil is turned on and nitrogen is injected at a flow rate of 3 s.l.p.m. (standard litres per minute), while maintaining the pressure in the combustion cell at 100 psig. The axial thermocouple is raised to a point in the region around the top of the sand pack. When the temperature reaches around 600°F air is injected at 3 s.l.p.m. The pressure drop across the combustion cell, the injection pressure and the outlet gas composition as indicated on the SOLTEC recorder are monitored. The start of combustion is indicated by a jump in the temperature and a drop in the concentration of oxygen in the outlet stream with a corresponding increase in the concentration of carbon dioxide and carbon monoxide. On ignition the air flow rate is maintained at 3 s.l.p.m., and the stop watch and the data acquisition system are started.
13. The igniter is turned off once the burning front is stable. This is indicated by the plots of gas composition on the SOLTEC recorder. This happens when the front has moved approximately 3 to 5 cm. from the point of ignition. Air injection is maintained at 3 s.l.p.m. in order to propagate the front.

14. During the above steps, the exit gas concentration is continuously monitored by the three gas analyzers and recorded on the multi-channel data logger. The data logger is programmed to record data every minute. The inlet and outlet pressures to the combustion cell are monitored continuously and recorded periodically.
15. Every thirty minutes, or when convenient, the entire length of the combustion cell is traversed from top to bottom, by the thermocouple to record the temperature distribution. This usually takes about eight minutes or so depending on the number of points of data taken. The temperature profiles help the determination of the velocity and location of the combustion front and the presence and thickness of the steam plateau.
16. Every three hours the three gas analyzers are checked and recalibrated. The Beckmann Oxygen Analyzer especially had to be checked as the Carbon Monoxide and Carbon Dioxide Analyzers usually maintained their calibration. The Teledyne Oxygen Analyzer was also found to work well provided that the pressure and flow rate through the analyzers was maintained throughout the experiment.
17. The process of air injection and data taking is continued until the burning front sweeps through 90% of the combustion tube. The combustion front is then quenched by injecting nitrogen instead of air.
18. During the runs, the liquid produced is collected in graduated centrifuge bottles. Later these are centrifuged at 3500 rpm for 15 minutes. Water cut and mass of oil produced are determined.
19. After cooling, the equipment is dismantled and the data are analyzed. This includes analyses of the liquid produced and the core left in the combustion tube for determining the carbonaceous residue left behind the combustion front and the oil and water saturations ahead of the front in order to perform a material balance.

### 2.2.5. EXPERIMENTAL PROGRAM

Throughout the study, the objective was to carry out the experiments under as identical conditions as possible of pressure, reservoir temperature, saturations, metal salt concentrations and air flow rates. In all seven runs were performed. The first three were discarded because of problems that arose during the experiments, mostly equipment failure. In the first run the rubber gasket used to seal the combustion tube failed at the high temperature it encountered, resulting in the loss of operating pressure. The second run had problems of failure of the band heaters. Both failed during the ignition period and the burn had to be abandoned. The third run ran fairly well but towards the end of the run the oxygen analyzer began malfunctioning and finally failed. The run was analyzed; however, the variations in the oxygen analysis were significant due to the malfunctioning gas analyzer. Thus these three runs were abandoned. The next four runs were successful and are reported here. The first was the control run, wherein the experiment was performed with no metal salts. The next three runs used tin, iron and zinc chlorides at 1% concentration in the connate water. The operating pressure throughout the runs ranged between 100 and 105 psig. The reservoir temperature was maintained in the range of 50-75°C.

## 2.2.6. OBSERVATIONS AND RESULTS

In this section the observed effects of the different metallic additives: iron, zinc and tin will be examined for the nature of the fuel formed and the combustion parameters. Using the data on the exit gas composition during the runs, computations were performed on the basis of Dew and Martin's model (1964, 1965) to determine the nature of the fuel formed and the combustion parameters.

### Combustion Front Velocity:

Figure 2.2.1 compares the velocity of the combustion fronts for the four experiments. One observes that the velocity of the combustion front is higher in the presence of the metallic additives. The velocity of combustion front is typically a function of the air flux, the oxygen utilization efficiency (Martin *et al.*, 1958; Benham and Poettman, 1958; Moss *et al.*, 1959, Showalter, 1963, Wilson *et al.*, 1963 and Fassihi, 1981), and the nature and amount of fuel formed. For a given amount of oxygen injected, the velocity of the combustion front is dependent upon the amount of oxygen required for combustion which is dependent on the oxygen utilization efficiency and the nature and amount of the fuel formed. In our case, the air injection rate is maintained constant at three standard liters per minute in all the runs. Thus the air flux is dependent on the porosity and gas saturation. The oxygen utilization efficiency and the nature of the fuel formed is discussed later herein.

Of the metals studied, tin exhibited the lowest combustion front velocity: 16.6 cm/hour versus 17 cm/hour for iron and 19.6 cm/hour for zinc. This can be explained from the fact that tin deposits a fuel that is rich in hydrogen (discussed later) which has a greater air requirement at 100% oxygen utilization efficiency. In addition, the run utilizing tin exhibited a greater oxygen utilization efficiency (as seen later), thus the combustion front should have been slower. Zinc which exhibited the lowest oxygen utilization efficiency had the highest combustion front velocity.

### Combustion Front Temperature:

The temperature profiles were taken using the axial thermocouple during the control run, and the runs when iron, tin and zinc were used. A given temperature profile will show distinct regions: a region ahead of the front at the reservoir temperature followed by a region wherein the temperature rises as a result of transfer of heat ahead of the steam plateau, the steam plateau where the temperature is constant over a region followed by a region of increasing temperature until a peak in temperature occurs. This is the combustion front where the high temperature oxidation reaction takes place. The region behind the front shows decreasing temperature as heat is lost to the formation and to the injected air.

The combustion front temperatures lie in the range of 470 to 550°C. The control run had combustion front temperatures lying in the range of 500 to 510°C, with iron run exhibiting slightly lower combustion front temperatures. Zinc exhibited significant variation, but exhibited a combustion front temperature much lower than the control run. Tin exhibited a combustion front temperature higher than the control run. The reason for this is that the combustion front temperature is a function of the amount of heat locally liberated, which in turn is related to the nature and amount of fuel formed and the oxygen utilization efficiency. The greater the H/C ratio of the fuel, the greater would be the amount of air required at 100% efficiency (discussed later) and the greater would be the heat locally liberated as a result of combustion of the fuel, and thus the higher would be the combustion front temperature. The variations that occur in

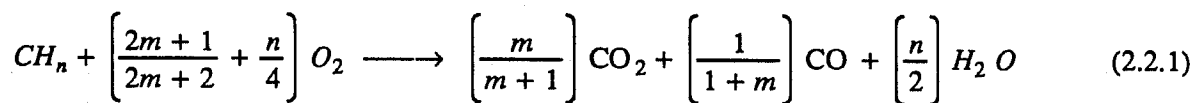
the combustion temperature along the length of the pack are, in addition, a result of the variations in the amount of the fuel deposited. These are a function of the local variations in saturation as a result of packing technique. Variations in saturation as a result of the packing technique will also be discussed later. Figure 2.2.2 shows a plot of front temperatures.

### Exit Gas Composition:

Figures 2.2.3-2.2.6 show the exit gas composition in terms of oxygen, carbon dioxide and carbon monoxide concentration for the four runs in the order: control run, iron, tin and zinc. If we consider Fig. 2.2.3, we can note some features common to all four plots: oxygen peaks are coupled with troughs in the carbon dioxide and carbon monoxide composition plots. This is expected as oxygen is consumed in generating carbon dioxide and carbon monoxide. The concentration of oxygen in the exit gas is an indication of the oxygen utilization efficiency of the run. A comparison the diagrams will show that the oxygen concentration in the exit gas is very low in the case of tin, with increasing oxygen concentration in the exit gas of the iron, zinc and control runs.

In addition, one observes fairly smooth composition curves for the tin and iron runs but larger cyclical variations in the plots for the control run and zinc. The reason for these variations is the differences in the techniques adopted for packing the sand in the tube. In the case of the tin and iron runs, packing of the combustion tube was done by placing a larger volume of sand pack mixture in the combustion tube before squeezing it in with the help of a tamper. In the case of the control and zinc runs, very small amounts of the sand pack mixture were placed in the tube and these were vigorously tamped in. This could have led to saturation and porosity variations in smaller zones in addition to local saturation variations. The differences in the two techniques have been manifested in the variations in the combustion front temperature (Fig. 2.2.2) and in the exit gas concentration (Figs. 2.2.3-2.2.6).

The exit gas composition is the main source of data used to analyze the runs using the Dew and Martin (1964, 1965) model. The HTO combustion reaction is modeled to take place as:



Based on this equation, the data on the exit gas composition is used to determine the atomic hydrogen to carbon ratio, 'n' of the fuel and the ratio of the carbon dioxide to carbon monoxide 'm' in the exit gas. The 'm' and 'n' values are used to determine the combustion parameters as discussed in the following subsections:

### Ratios of H/C of the Fuel and of Carbon Dioxide to Carbon Monoxide Produced:

Figure 2.2.7 shows the m and n values for all the four runs. One observes that the hydrogen to carbon and the carbon dioxide to carbon monoxide ratios for the control run are the lowest. The H/C ratio of the fuel increased from 0.07 in the case of the control run to 0.13 in the presence of iron, 0.61 in the presence of zinc and 0.79 in the presence of tin. This indicates the extent to which the presence of the metallic additives increased the H/C ratio of the fuel. One should note that a decreasing hydrogen to carbon ratio is indicative of a fuel that is increasingly carbon like.

No indications on the nature of the fuel formed can be obtained from the ratio of carbon oxides. The ratio of carbon oxides gives the extent to which the oxidation to carbon dioxide is complete in comparison with the oxidation to carbon monoxide.

### Heat of Combustion:

The  $m$  and  $n$  values are used for the determination of the heat of combustion of the fuel formed. Figure 2.2.8 is a graph of the heat of combustion in terms of the heat generated per pound of fuel deposited. The heat of combustion is a function of the nature of the fuel formed and the ratio of carbon oxides. The observed variations are similar to the variation of the hydrogen to carbon ratios because of the dependence of the heat of combustion on the composition of the fuel burnt. The heat of combustion for the runs ranged from 12,000 to 15,000 Btu/lb of fuel burnt. The control run had the lowest heat of combustion as the fuel formed was essentially carbon.

Increasing values were observed for iron, zinc and tin which deposited fuels having increasing amounts of hydrogen associated with a given carbon atom in the fuel.

### Air Requirement and Combustion Efficiency:

Variations similar to that of the H/C ratios are observed. These air requirements have been determined from the experimental data and are a function of the combustion efficiency of the run. In California, field tests have shown that nearly 100% combustion efficiency can be obtained. Thus it is also useful to determine the air requirements at 100% efficiency. As was indicative from the concentration of oxygen in the exit gas, the oxygen utilization efficiency was the poorest for the control run. Nearly 100% efficiency was observed for the run using tin; with the zinc and iron runs exhibiting efficiencies lying in between. Efficiencies ranged from 80 to 99.7%.

One observes that the air requirements at 100% combustion efficiency ranged from 8 to 9 MMscf/acre-foot. The air requirement for the control run increased as a result of the poorer oxygen utilization efficiency during the run. The zinc and the control runs had more or less the same air requirements, while tin and iron had air requirements close to 8 MMscf/acre-foot; the requirements for tin being slightly lower than that for iron.

### Fuel Consumption:

Figure 2.2.9 shows the fuel consumption per cubic foot of reservoir. Tin and zinc runs exhibited fuel consumption in the range of 1.2 lbs/cu. feet, while iron and the control run exhibited slightly higher values, around 1.3 lbs/cu. feet. The fuel consumption is a function of the fuel availability and the oxygen utilization efficiency. No direct inference can be made from this data as a result of the slight variations in oil saturation, porosity, and oxygen utilization efficiency between runs.

### Ratios:

The air oil ratio is the ratio of the air requirements in scf per barrel of oil displaced. The air requirements were found to be similar in the case of tin and iron, while the control run exhibited higher values; zinc being the highest.

## Recovery Data

All the above computations were made using the Dew and Martin model. Data on the oil recovery and water produced were also collected. Material balances (taking into account the water formed as a result of combustion) were obtained within 0.8%. As implied by the data on the velocity of the burning front, increased oil recovery rates were observed. The oil recovery rate like the combustion front velocities were similarly affected by the oxygen utilization efficiencies, the nature and amount of fuel deposited and the air flux.

Sand was analyzed for unburnt carbeneaceous residue left behind the burning front for the control, iron and zinc run. The amount of carbeneaceous residue remaining unburnt ranged at approximately 0.5% by weight in the reservoir matrix.

### 2.2.7. CONCLUSIONS & RECOMMENDATIONS

In this section the results obtained from the combustion tube studies are summarized and recommendations for future work have been made.

Table 2 summarizes the results obtained for Huntington Beach Crude Oil. The influence of the metallic additives of iron, zinc and tin on the nature of the fuel formed (H/C ratio) and the in-situ combustion characteristics are clearly evident: while the control run was found to deposit a fuel that was essentially carbon, the presence of metallic additives increased the atomic hydrogen to carbon ratio of the fuel from its value of 0.07 in the absence of any metallic chloride to 0.13 in the presence of iron, 0.61 in the presence of zinc and 0.79 in the presence of tin. The H/C ratio coupled with the extent to which oxidation proceeded to the formation of carbon dioxide in comparison to carbon monoxide affected the velocity of the burning front, the heat of combustion, the air requirements at 100% combustion efficiency, the air-oil ratio and the oil recovery rates. As a result of the increased hydrogen content of the fuel, the heat of combustion of the fuel increased. The air requirements at 100% combustion efficiency also increased in the order of increasing atomic H/C ratios of the fuels. The presence of a metallic additive increased the velocity of the burning front. Improved oil recovery rates were also observed.

TABLE 2  
RESULTS OF COMBUSTION TUBE RUNS

Run Designation	Control	Iron	Tin	Zinc
H/C Ratio of Fuel	0.07	0.13	0.79	0.61
Efficiency of O <sub>2</sub> Utilization %	82.3	94.2	98.6	86.9
Heat Of Combustion of Fuel	11942.0	12490.0	14972.0	14481.0
Flame Front Temperature	503.2	503	533.3	492.6
Air Req. for 100% Comb. Eff.(scf/lb)	130.6	135.75	150.4	147.4
Heat Gen./scf air consumed (Btu/scf)	91.3	93.15	99.4	98.0
Front Velocity (cm/hr)	14.8	17.0	16.6	19.6
Fuel Consumption, lbs/cu.ft	1.3	1.32	1.2	1.23
Air Oil Ratio, scf/bbl	9200.0	8450.0	8450.0	9800.0
Air Req., MMscf/acre-ft	8.8	8.3	8.0	9.0
Air Req. for 100% comb. eff. (scf/cu ft res)	-	-	-	-
	169.6	179.4	182.2	180.5

Of the metals studied, tin exhibited the most effects. As its fuel had the highest H/C ratio, the heat of combustion and flame front temperatures were the highest. The air requirements for the tin run at 100% efficiency were also the highest. This had its impact on lowering the combustion front velocity and oil recovery rates. Zinc and iron deposited a fuel with lower H/C ratios and their heat of combustion and air requirements at 100% combustion efficiency were lower.

The above effects that were observed in the presence of metallic additives, as in the case of Huntington Beach Crude Oil have demonstrated that numerical simulations or the designs for field tests in the presence of metallic additives should consider that the reaction kinetics, the nature of the fuel formed and the combustion parameters will be affected by the metallic additives.

In this study, combustion tube experiments were performed using Ottawa sand. Use of actual field cores would be more representative, and future work especially relevant to the reservoir under consideration should use native cores.

The results obtained are specific to the crude oil under consideration, viz. Huntington Beach Crude. Crude oils maybe affected to different extents by the same metallic additive particularly when they are of different composition or API gravity. Future work should study the effect of different metals on different crude oils using combustion tube studies, coupled with differential thermal analysis and thermogravimetric analysis.

The use of metallic additives increases the fuel deposited and is particularly applicable to light oil reservoirs. The presence of metallic salts in heavy oil reservoirs which produce high levels of fuel deposition may render the process uneconomical because of high air requirements.

As observed from the cyclical variations in gas composition and the flame front temperature data, zonal and local saturation variations affect the results. In order to avoid these variations it is recommended that, when studying in-situ combustion in the laboratory, the packing technique should aim at minimizing these saturation variations, both when mixing the constituents of the pack as well as when tamping it into the combustion tube. The results of the tin run indicate that proper packing produces uniform saturation distributions especially if the pack has been properly mixed before its insertion into the tube.

The literature is nearly devoid of field studies on the application of metallic salts on in-situ combustion. The use of metallic salts to solve the problems of fuel deposition especially in light oil reservoirs should be tried in the field after performing combustion tube studies on actual cores in the presence of these salts and the specific crude under consideration at field saturations.

## 2.2.8. REFERENCES

1. Alexander, J.D., Martin, W.L., and Dew, J.N.: "Factors Affecting Fuel Availability and Composition During In Situ Combustion," J. Pet. Tech. (October 1962) 1154-1164.
2. Al-Saadoon, F.T.: "An Experimental and Statistical Study of Residual Oil Saturation After Gas, Water and Steam Drive, and Fuel Availability for the In-Situ Combustion Process," Ph.D. Dissertation, University of Pittsburgh, PA., 1970.

3. Andrade, G.M.: "An Investigation of Pressure Effects on Combustion Tube Runs," M.S. Thesis, Stanford University, CA (1984).
4. Arrhenius, S.: Z. Physik Chem. (1889), Vol. 4, 226.
5. American Society for Testing Materials Standard D-95, published by the AIME.
6. Bardon, C. and Gadelle, C.: "Essai de Laboratoire Pour L'Etude de la Combustion In-Situ," Institute Francais du Petrole, Paris (May 1977).
7. Benham, A.L. and Poettman, F.H.: "The Thermal Recovery Process - An Analysis of Laboratory Combustion Data," J. Pet. Tech. (September 1958) 83-85.
8. Bousaid, J.G.: "Oxidation of Crude Oil in Porous Media", Ph.D. Dissertation, Texas A & M University, TX (1967).
9. Burger, J.G. and Sahuquet, B.C.: "Combustion a Contre-Courant. Interpretation d'Essais par Modele Numerique Unidirectionnel," Rev. Institut Francais De Petrole (1971), Vol. 26, 399-422.
10. Burger, J.G. and Sahuquet, B.C.: "Chemical Aspects of In-Situ Combustion - Heat of Combustion Kinetics," Soc. Pet. Eng. J. (October 1972) 410-420.
12. Carcoana, A.N., Machedon, V.C., Pantazi, I. G., Petcovici, V.C., and Turta, A.T.: "In Situ Combustion - An effective method to enhance oil recovery in Romania", Eleventh World Petroleum Congress, London, 1983.
13. Dabbous, M.K. and Fulton, P.F.: "Low-Temperature-Oxidation Reaction Kinetics and Effects on the In-Situ Combustion Process," Soc. Pet. Eng. J. (June 1974) 253.
14. De los Rios, C.: "The Effect of Metallic Additives on the Kinetics of Oil Oxidation Reactions in in-situ combustion," Engineers Degree thesis, Stanford University, California (October 1987).
15. Dew, J.N. and Martin, W.L.: "Air Requirement for Forward Combustion, " Pet. Eng. (December 1964) 82.; and (January 1965) 82-85.
16. Drici, O. and Vossoughi, S.: "Catalytic Effect of Heavy Metal Oxides on Crude Oil Combustion," paper 63a presented at the 1985 AIChE National Meeting and Petroleum Exposition, Houston, March 24-28.
17. Earlougher, R.C., Galloway, J.R., and Parsons, R.W.: "Performance of the Fry In-Situ Combustion Project," J. Pet. Tech. (May 1970) 551-557.
18. Fassihi, M.R.: "Analysis of Fuel Oxidation in In-Situ Combustion Oil Recovery," Ph.D. Dissertation, Stanford University, CA (1981).
19. Gureyev A.A. and Sablena, Z.A.: "The Role Metals in Oxidation of Hydrocarbon Fuels in the liquid phase," Scientific Research Institute of Fuel and Lubricating Materials, Pergamon Press (1965).

20. Hardy, W.C., Fletcher, P.B., Shepard, J.C., Dittman, E.W., and Zadow, D.W.: "In-Situ Combustion in a Thin Reservoir Containing High-Gravity Oil," J. Pet. Tech. (February 1972) 199-208.
21. Martin, W.L., Alexander, J.D., and Dew, J.N.: "Process Variables of In-Situ Combustion," Trans., AIME (1958) Vol. 213, 28.
22. Moss, J.T., White, P.D. and McNeil, J.S. Jr.: "In-Situ Combustion Process- Results of a Five-Well Field Experiment in Southern Oklahoma", Trans. AIME (1959), Vol. 216, 28-35; J. Pet. Tech. (1959), 55-64.
23. McCarthy, H. Jr., Paiverneker, V.R., and Maycock, J.N.: "Determination of Kinetic Parameters from a Single Thermogram", Proceedings, Third International Conference on Thermal Analysis, Davos, Switzerland (1971), Vol. 1, 355.
24. Poettmann, F.H., Schilson, R.E., and Surkalo, H.: " Philosophy and Technology of In-Situ Combustion in Light Oil Reservoirs," World Oil (1967) Vol. 165, 487-497.
25. Racz.: " Development and Application of a Thermocatalytic In-Situ Combustion Process in Hungary," paper presented at the 1985 European Meeting on Improved Oil Recovery, Rome, Italy, April 16-18.
26. Satman, A.: "In-Situ Combustion Models for The Steam Plateau and for Fieldwide Oil Recovery," PhD Dissertation, Stanford University, CA (1979).
27. Showalter, W.E.: "Combustion-Drive Tests," Soc. Pet. Eng. Journal (March 1963), 53-58.
28. Sidqi, A., Ramey, H.J. Jr., Pettit, P., and Brigham, W.E.: "The Reaction Kinetics of Fuel Formation for In-Situ Combustion," Stanford University Petroleum Research Institute, Stanford, CA, SUPRI TR-46, Report submitted to the U.S. Dept. of Energy, under contract No. DE-AC03-81SF 11564 (May 1985)
29. Weijdem, J.: "Determination of the Oxidation Kinetics of the In-Situ Combustion Process," Report from Koninklijke/Shell Exploratie En Productie Laboratorium, Rijswijk, The Netherlands (1968).
30. Wilson, L.A., Reed, R.L., Clay, R.R. and Harrison, J.H.: "Some Effects on Pressure on Forward and Reverse Combustion," Soc. PEt. Eng. Journal (June 1963), 127-137.

TABLE 1  
SUMMARY OF QUALITATIVE RESULTS OF KINETIC STUDIES  
(De los Rios (1987))

Metallic Additive	Low Temperature	High Temperature
$FeCl_2$	Increased $CO_x$ Production $O_2$ consumption shift to lower T	Increased $CO_x$ Production $O_2$ consumption
$SnCl_2$	Increased $CO_x$ production $O_2$ consumption	Increased $CO_x$ production $O_2$ consumption shift to lower T
$ZnCl_2$	Increased $CO_x$ Production $O_2$ consumption	Decreased $CO_x$ Production $O_2$ consumption shift to lower T
$MgCl_2$	Increased $CO_x$ Production $O_2$ consumption	Decreased $CO_x$ Production $O_2$ consumption shift to lower T
$K_2 Cr_2 O_7$	Inc. $CO_x$ Prod. $O_2$ consumption	Dec. $CO_x$ Prod. $O_2$ consumption shift to lower T
$CuSO_4$	None	None
$AlCl_3$	None	Decreased CO production
$Ni(NO_3)_2$	Inc. $O_2$ Consumption	Dec. $CO_x$ Production $O_2$ consumption
$CdSO_4$	Increased $O_2$ production	Decreased $CO_x$ production $O_2$ consumption
$MnCl_2$	Increased $O_2$ Consumption	Decreased CO Production

TABLE 2  
SUMMARY OF COMBUSTION TUBE RUNS

Operating Pressure: 100-105 psig

Operating temperature: 50-75 deg.C

Air flow rate: 3 standard litres per minute.

Run Designation	HBO	Iron	Tin	Zinc
Length of pack, cm	90.7	83.05	91.15	89.95
Porosity	35.70	34.50	39.98	39.31
Oil Saturation, %	39.86	41.80	34.36	34.24
Water Saturation, %	25.20	28.32	23.2	20.60
Conc.of Metal Salt in water, wt. %	0.00	1.0	1.0	1.0

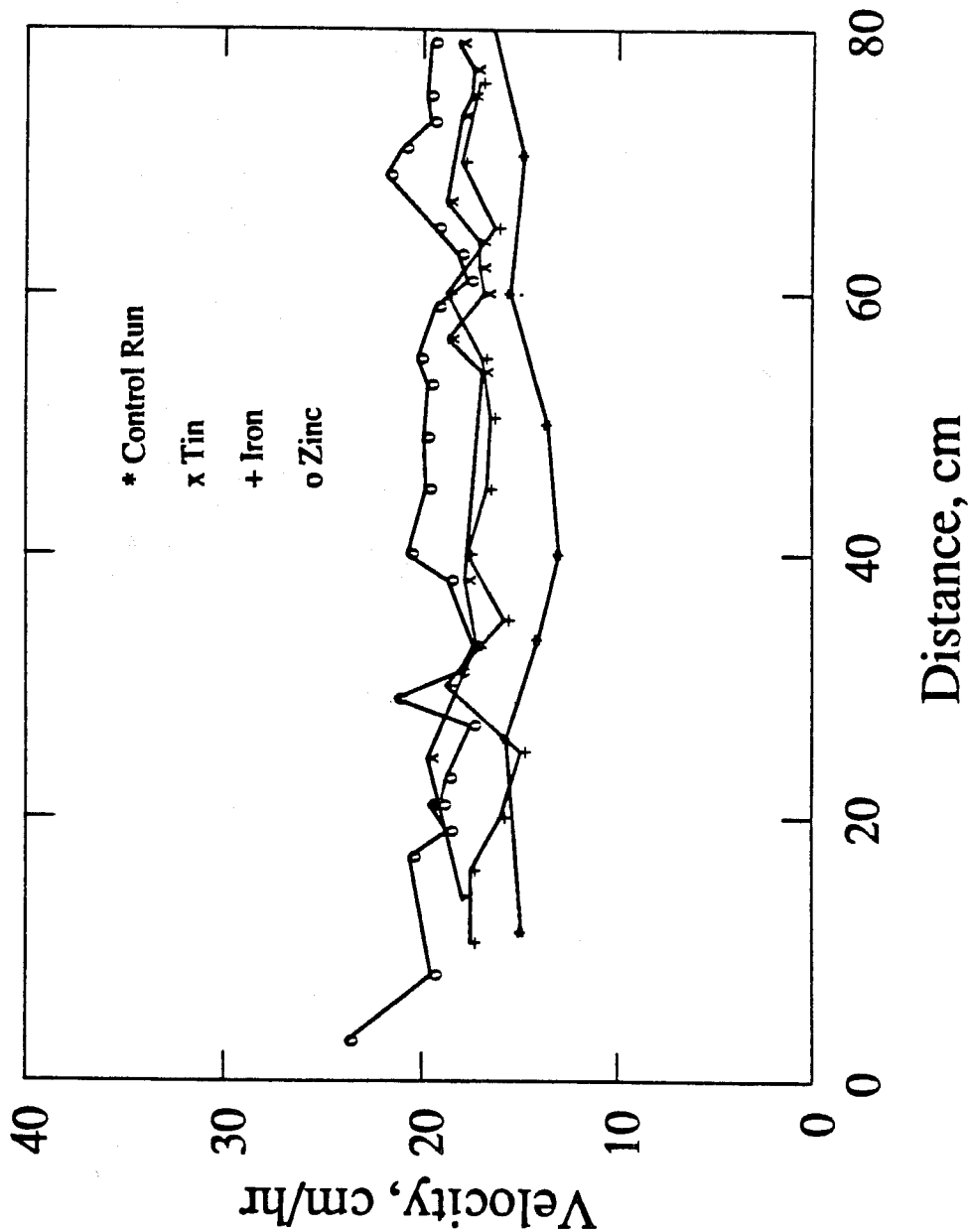


Figure 2.2.1 Velocity of the burning front.

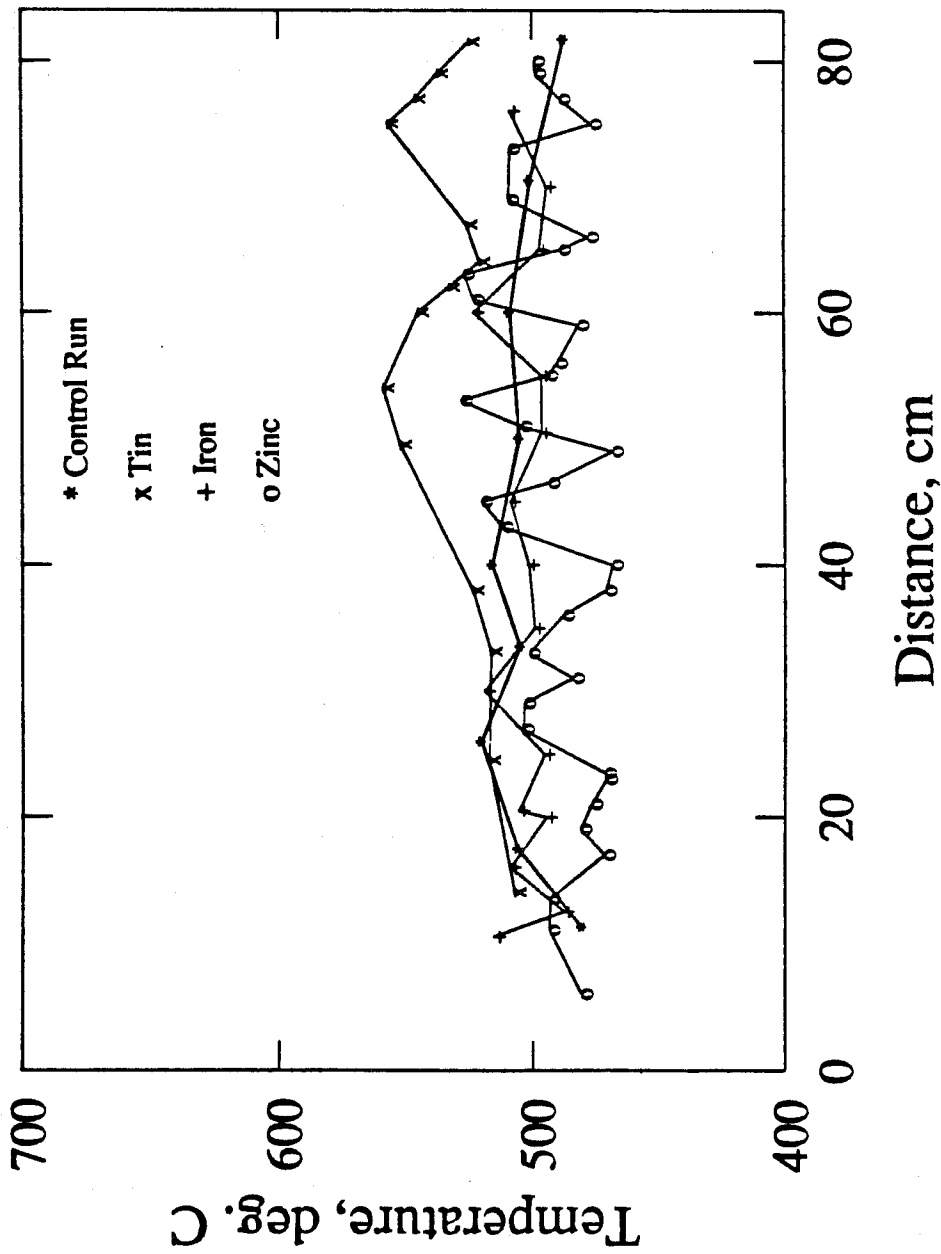


Figure 2.2.2 Temperature profile for control run.

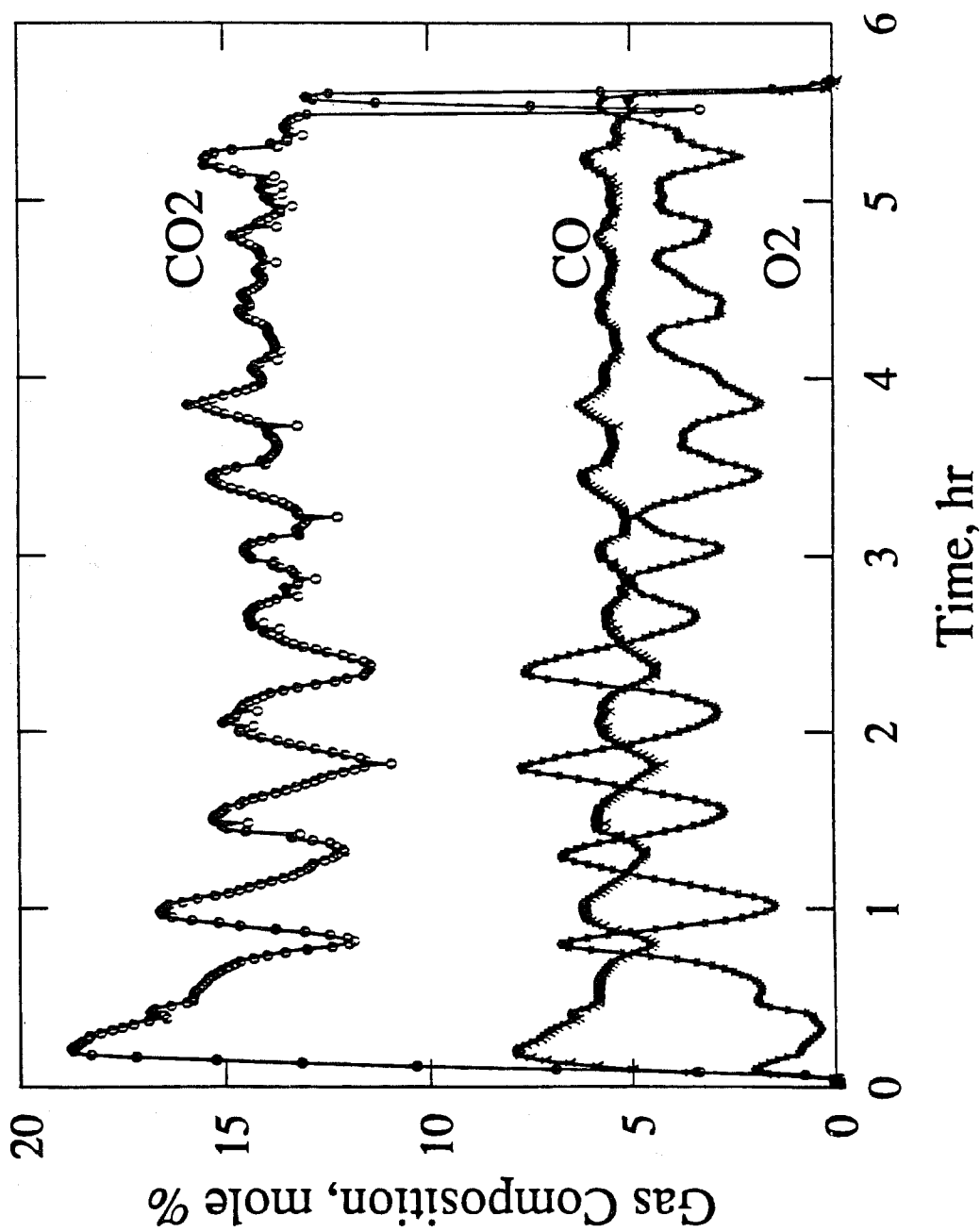


Figure 2.2.3 Exit gas composition for the control run.

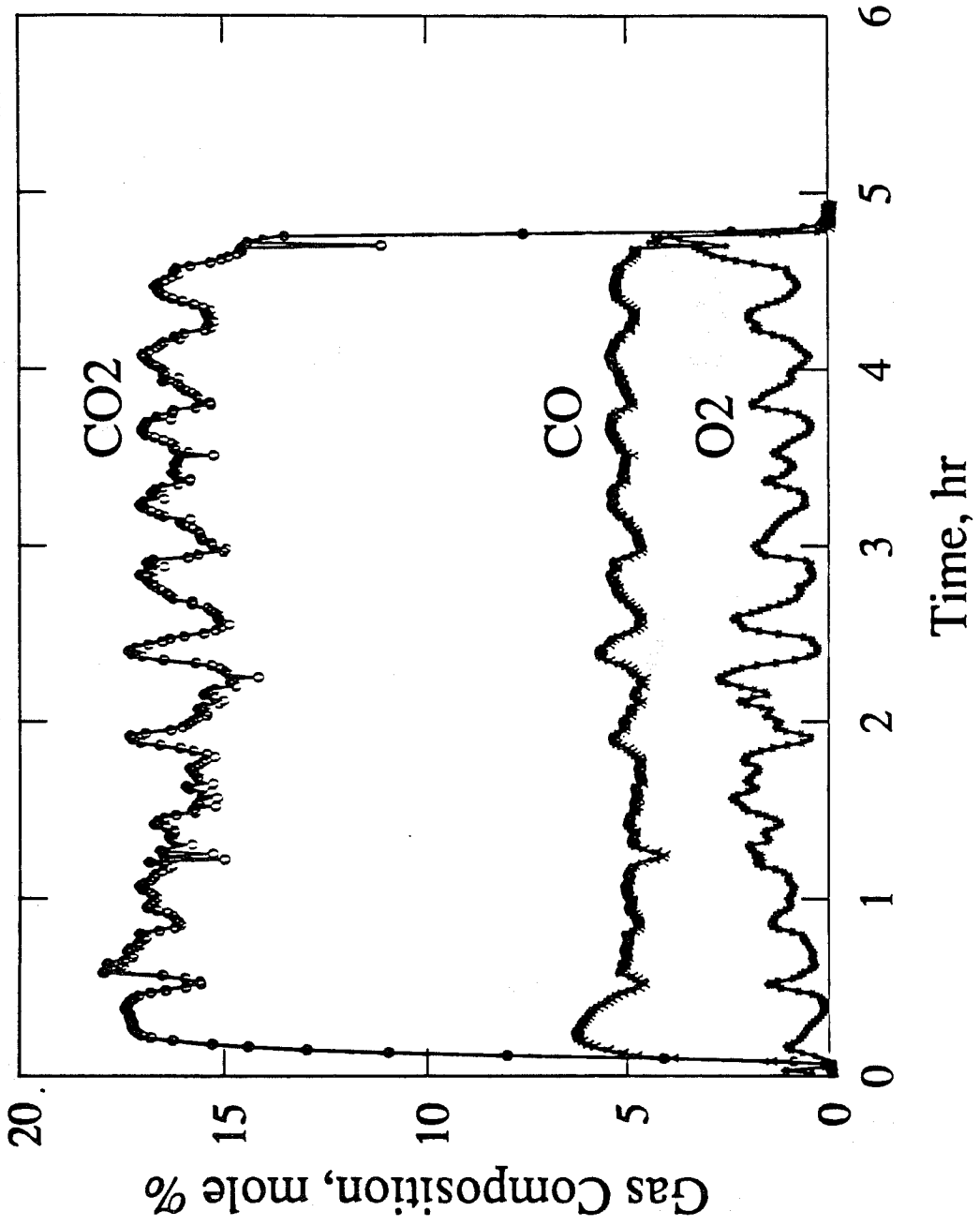
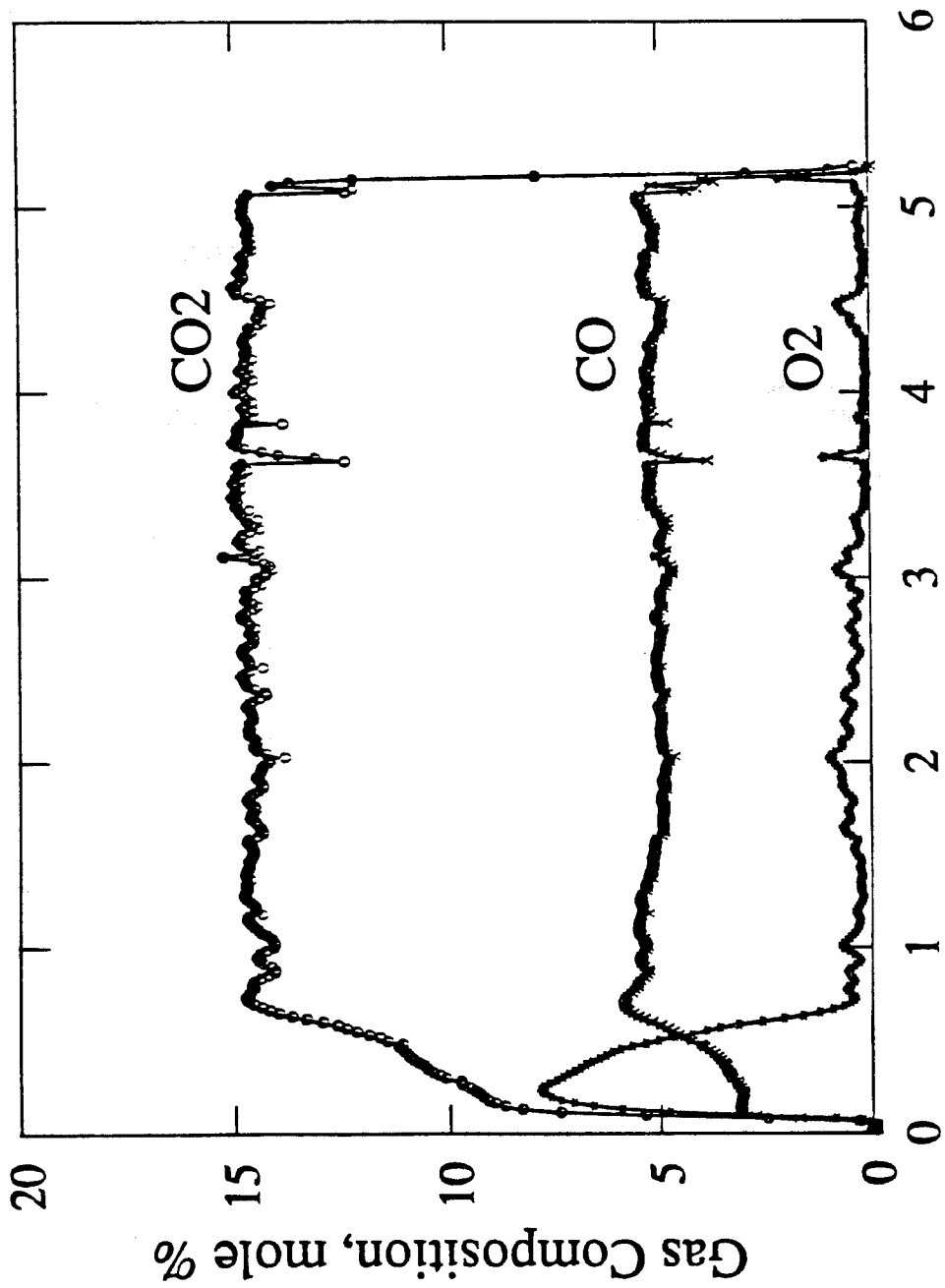


Figure 2.2.4 Exit gas composition for the iron run.



Time, Hours

Figure 2.2.5 Exit gas composition for the tin run.

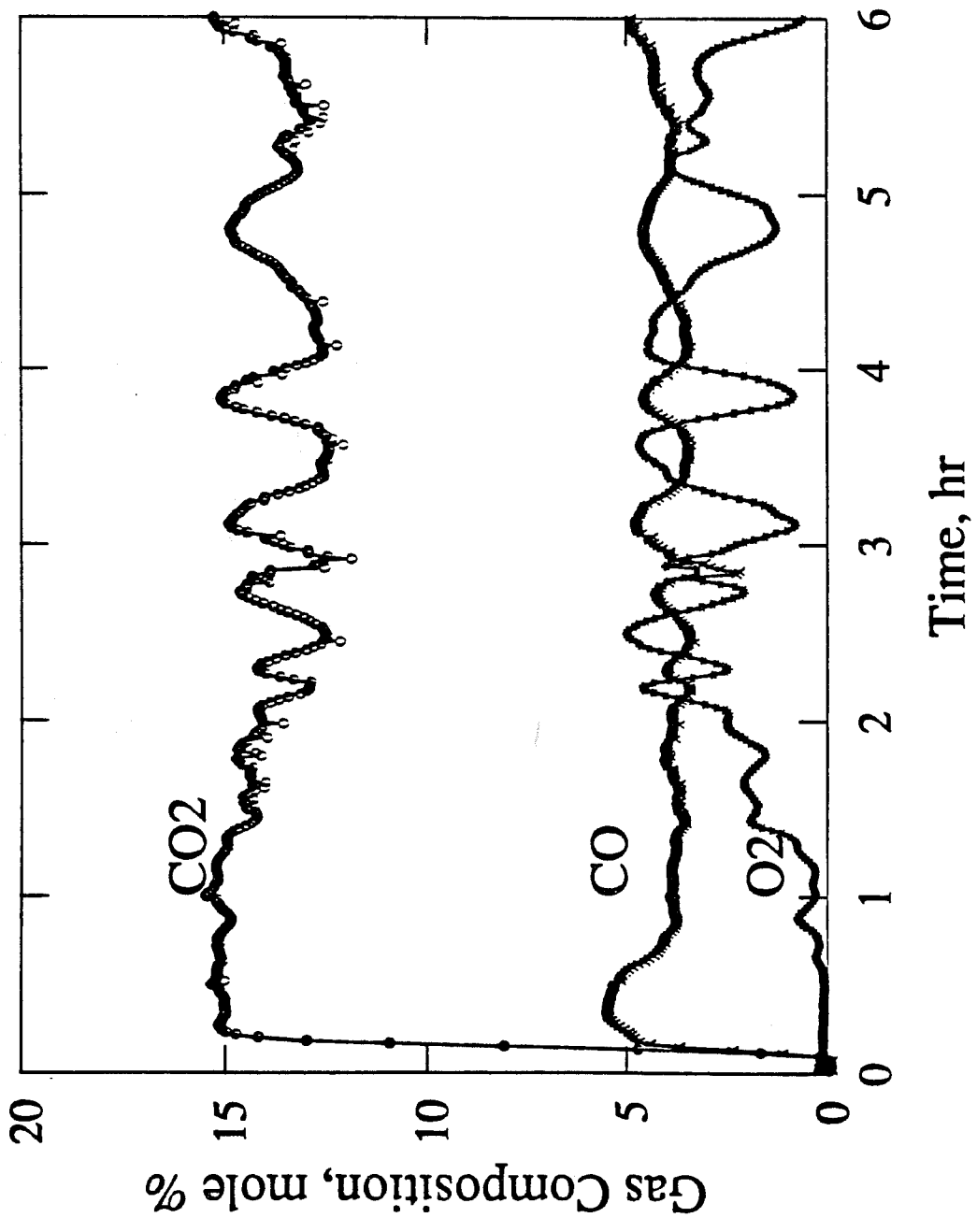


Figure 2.2.6 Exit gas composition for the zinc run.

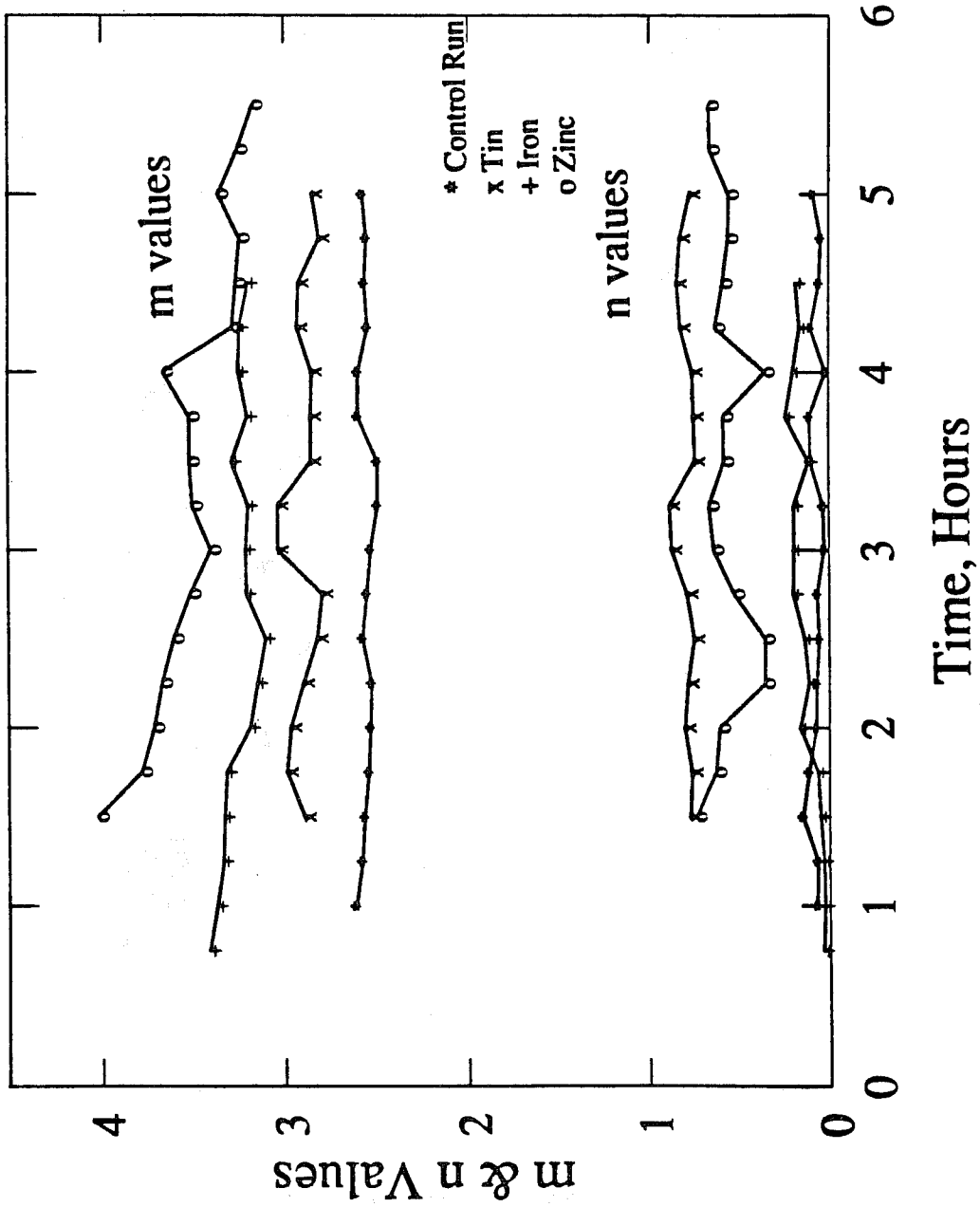


Figure 2.2.7 Plot of  $m$  and  $n$  values.

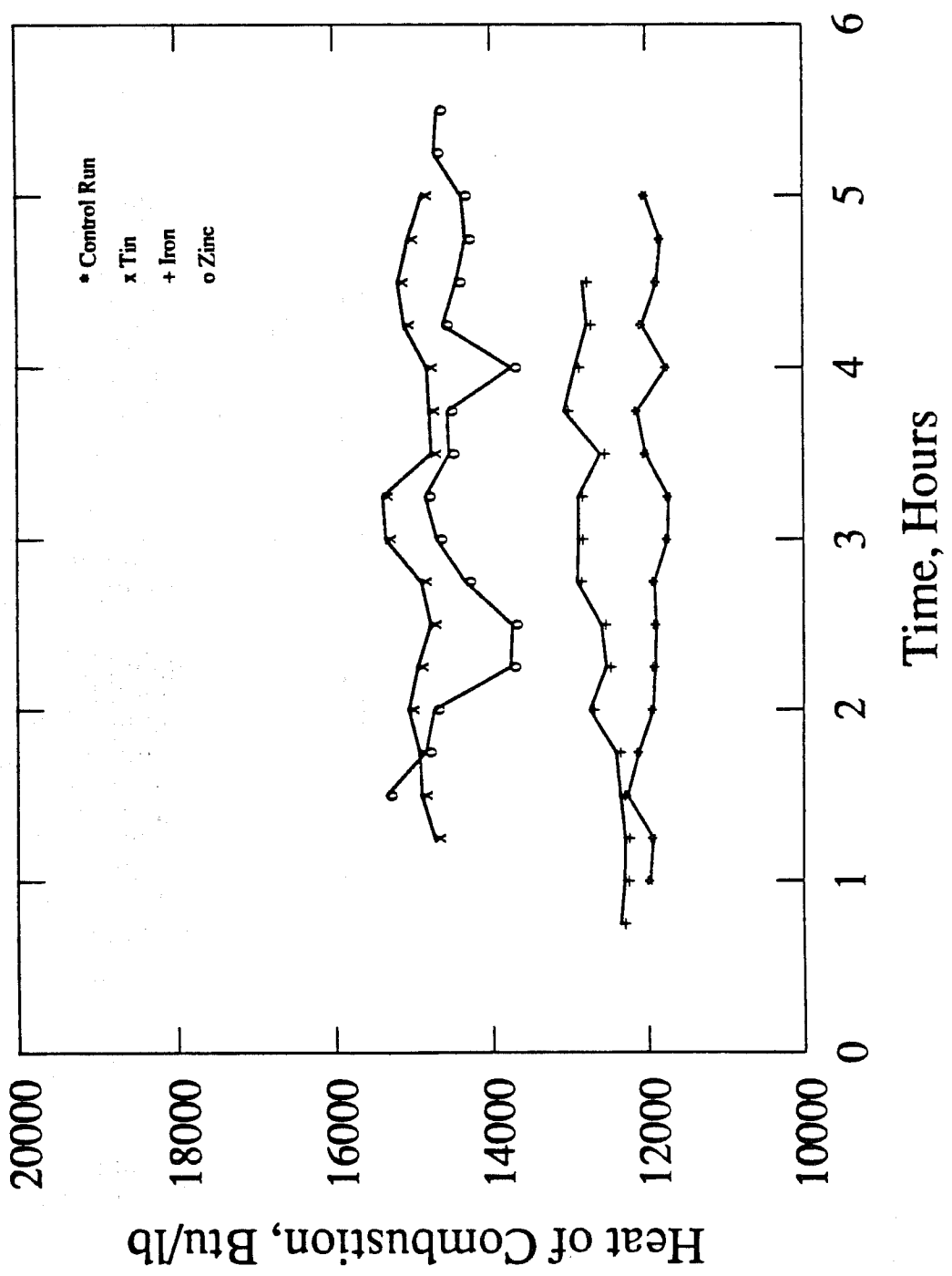


Figure 2.2.8 Heat of Combustion (Btu/lb of Fuel deposited).

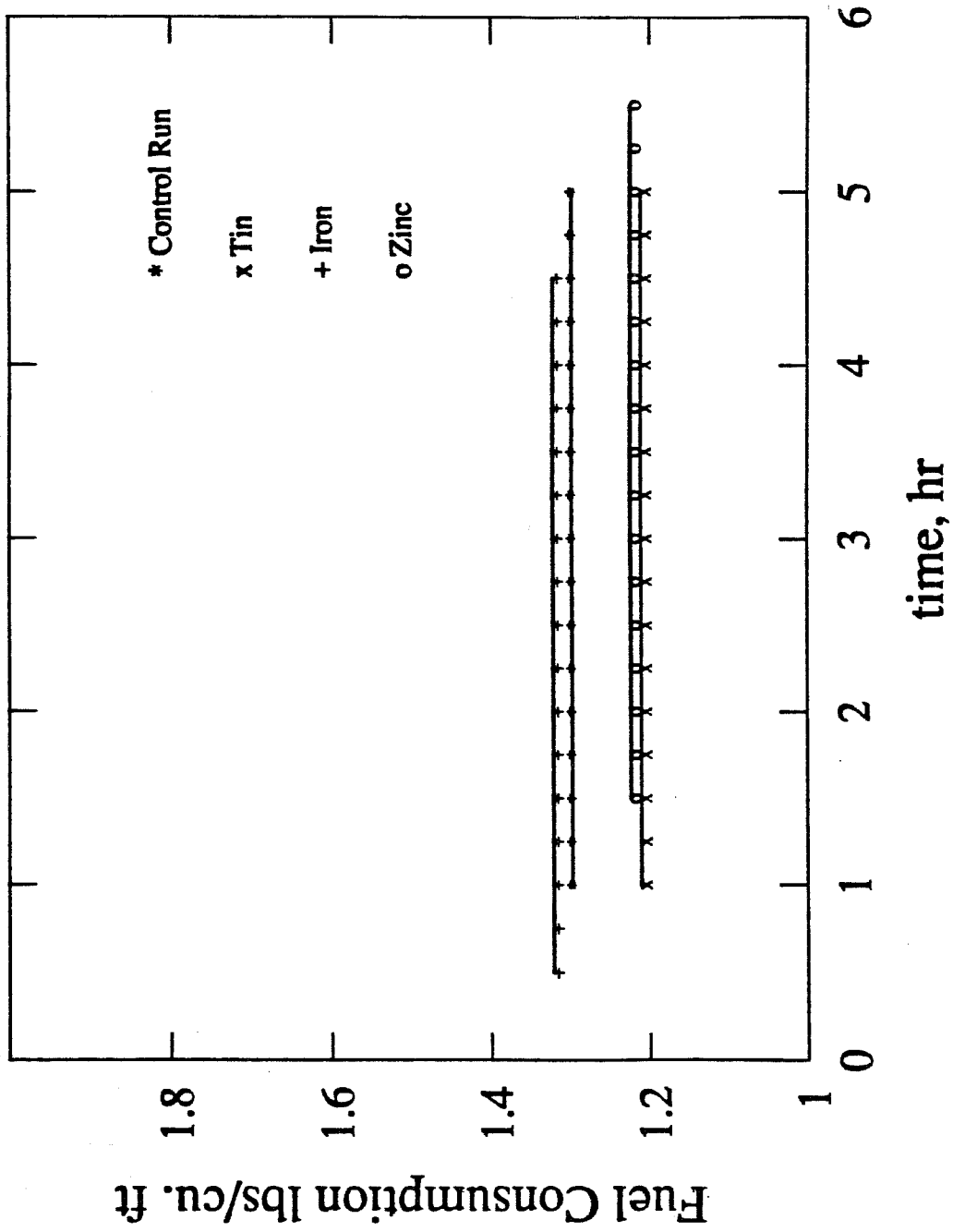


Figure 2.2.9 Fuel consumption per cu. ft. of reservoir.

## **2.3 MULTI-PHASE, MULTI-COMPONENT FLOW MODELING IN POROUS MEDIA WITH TEMPERATURE VARIATIONS (Jeffrey Wingard)**

A technical report on this topic is in the draft stage. The following is a summary of this work.

A solution is presented for the differential equations describing multiphase, multicomponent flow in porous media by the method of characteristics. The model is extended to systems that have variation in temperature. The new model is then applied to a three component system of carbon dioxide, a heavy oil component, and water. The system contains vapor-liquid, liquid-liquid, and vapor-liquid-liquid regions over a wide range of temperatures and pressures. A composition grid for the system at 800°R and 250 psia is shown and the technique is described for tracing the composition path through the phase diagram from injection conditions to initial conditions. Finally, a brief mention of the future plans for the completion of the project concludes the presentation.

### **PROJECT 3: STEAM WITH ADDITIVES**

This project aims at developing an understanding of the mechanisms of the process using commercially available surfactants for reduction of gravity override and channeling of steam. Modeling foam flow in porous media is emphasized because foaming agents have shown promise both in the laboratory and in the field as steam additives.

### **3.1 ANALYSIS OF TRANSIENT FOAM FLOW IN POROUS MEDIUM WITH CATSCAN** (D. Liu)

#### **3.1.1. INTRODUCTION**

Many papers have been published investigating the effects of foam displacement of oil in the porous media. Some field tests have also been carried out to recover oil with foam. While there is little doubt as to the effectiveness of the foam in the recovery of oil, not much is known about the foam flow mechanism in porous media. Furthermore, most of the papers published so far have concentrated on steady state foam behavior.

In fact, in the real world, steady state foam flow is not the usual state. In many of the experiments and field tests, foam flow must be transient in nature most of the time. Hence, it is important to study the transient behavior of foam flow. Few papers have been found, to the author's knowledge, which deal with this kind of aspect experimentally. Data is scarce.

The purpose of this work has been to accumulate experimental data on transient foam flow and with the goal to finally build a semi-empirical mathematical model which will aid in the prediction and simulation of foam field tests.

#### **3.1.2. EQUIPMENT**

As shown in Fig. 3.1.1, nitrogen and surfactant solution are injected simultaneously at constant rates through a foam generator which is essentially another short sandpack. After the foam is generated, it is injected into a sandpack initially saturated with water. Eight (8) pressure taps are located along the sandpack which transfer the pressure to the pressure transducers. The effluent is collected at the outlet. There is a constant backpressure regulator to hold the backpressure at 50 psi for both the outlet and the transducers.

It is seen from Fig. 3.1.2 that the sandpack under investigation was placed in the CAT scanner gantry. CT (Computed Tomography), or CAT-SCAN, has been more and more widely used in the petroleum laboratories as a means to investigate fluid saturations during flow experiments. After the X-rays are produced in the tube, pass through the sandpack, and are received at the detectors, electronic signals are sent to the scanner computer. Then the signals are converted into images which can be analyzed on the post-processing computer. The CAT-SCAN provides information on the density and composition of the medium observed. On the image storage and production side, another computer (a Mac II for the time being) has been hooked up with a laserwriter for hardcopy printing.

#### **3.1.3. PROGRESS REPORT OF 1988**

##### **Calibration Problems**

At the beginning of the year, the main work done was to calibrate the equipment and replace many of the malfunctioning parts.

It was found that no matter how long the equipment was run to reach stability, the pressure readings still drifted dramatically during the experiments. Hence it was suspected that this had to do with the interior working parts of the pressure transducers, demodulators and/or mass flow controller.

After solving the electrical problems of the data acquisition system, the pressure transducers were taken apart for further inspection. Indeed, all the pressure plates were badly eroded. Oxidized deposits were mainly on the high pressure side of the plate due to the contact with the surfactant solution. They were all replaced.

The mass flow controller gave rise to more problems than expected. First it didn't indicate the dial setting. Secondly the gas kept flowing even when the toggle switch was on the closed position or the flow setting was at 0.0. After the controller was replaced by another one which had been used on another experiment, the flow control was still not satisfactory. In the end, a combination of the flow controllers was adopted, which gives relatively good results, at least for the present.

Then in the middle of the year, a piece of new equipment, known as a CAT-SCAN, was added to the project. It is a second generation translate-rotate type, Sodium Iodide ( $N_{aI}$ ) scintillation detector gantry with an EMI scanner computer. The voltage and current used in the experiments were 99 KV and 30 mA, respectively.

Six experimental runs have been made since the addition. A brief summary of the runs is given in Table 1. The foam quality ( gas to liquid volume ratio under experimental conditions) was 90%. The injection rates of foam was kept constant at 1 cc/min. The surfactant concentration varied from 0.1% to 1% for those runs. The sandpack was a transparent acrylic tube of 1 inch (2.54 cm) diameter and 24 inch (61 cm) long. In all these runs, Ottawa sand of 100 to 120 mesh was used. Table 2 presents a summary of the experimental runs.

With the help of the CAT-SCAN, the foam flow in the porous medium was clearly observed and analyzed. The runs were made much easier due to better visualisation. The pressure data recorded along the sand-pack during the experiments were also used for the analysis.

Since each experiment begins with a new sand-pack, one or more cross-sections of the sand-pack were scanned fully saturated with distilled water and analyzed as a basis for future comparisons. Once the experiment started and the foam was flowing into the sand-pack, one cross-section was concentrated upon to be scanned for a period of time to get a CT number-time relationship, which was in turn linearly related to the saturation through the following equation:

$$S_L = \frac{N_{CT} - N_{CTair}}{N_{CTliquid} - N_{CTair}} \quad (3.1.1)$$

where  $S_L$  is the liquid saturation at that cross section of the sandpack.  $N_{CT}$  is the CT number of that cross section at the moment of measurement.  $N_{CTair}$  and  $N_{CTliquid}$  are the CT numbers measured when the sandpack is fully saturated with air (dry sandpack) and water, respectively.

At the end of each experiment, the foam had completely displaced the distilled water from the sand-pack. A CT SCAN at this time gave yet another basis for comparison with other scans for the intermediate stages.

Very good results have been obtained using the CAT-SCAN. For the sake of brevity, only one example will be briefly presented here. The CT Number vs Pore Volumes Injected (also time) is shown in Fig. 3.1.3. This run (RUN 4) was done at the total foam injection rate of 1 cc/min under the experimental conditions of 53 psia and room temperature. The total pore volume of the sandpack was 118 cc. The surfactant (SD1618) concentration was 1.0%. Foam quality in this run was a constant 90%. All the scans for this figure were obtained at the location 1 inch (2.54 cm) from the inlet. It is clearly indicated that it takes many pore volumes to displace all the in-situ fluid. It required about one pore volume at this location, which is equivalent to 24 pore volumes. It was observed that gas breakthrough at the inlet occurred at approximately 0.3 pore volumes. At the beginning of the injection, the CT number drops sharply, as does the liquid saturation (the right ordinant). Then the rate of saturation reduction slows down as the injection progresses.

Figure 3.1.4 shows another CT number vs PV relationship for yet a different location of this same experiment. The error bars on the data points are not actually errors. They are the standard deviations derived from the measurement of the CT numbers in the region of interest. The bigger the error bar is, the more heterogeneous the cross section is. That is, the cross section contains both foam and in-situ fluid. As was observed from the CT pictures, gas fingering was obvious. The main reason was that foam breaks at the displacement front due to the surfactant adsorption on to the sand surface. Obviously this curve shows a similar trend as described above for location 1. The only difference is that it takes a greater volume to displace the in-situ fluid due to its distance from the inlet.

Also from the CT pictures it was seen that the foam passed through the sandpack in a nonuniform way. In other words, foam might first go to the top of the sandpack. Due to its high apparent viscosity, this passage was soon blocked and it would then go to the bottom. However not all the pictures can be presented here. Only one picture is shown in Fig. 3.1.5 for a cross section fully saturated with water just to give the reader an idea what it looks like. This kind of picture can also help check the homogeneity of the sandpack.

In Fig. 3.1.6, the pressure profile is given as a function of pore volumes injected. As expected, the pressure drop is bigger behind the foam front than ahead. However no formula exists to predict this kind of behavior accurately or give an satisfactory explanation. Hence this study confirms the importance of investigating the flow mechanisms of foam and eventually finding a mathematical model based upon experimental data.

### 3.1.4. FUTURE WORK

- A more complete analysis will be made of the runs made so far.
- The effects will be studied on the foam flow behavior varying pore size distribution, surfactant concentration, flow rates, throughput, and foam quality.
- CT software from SHELL will be installed on to the existing computer, a newly purchased Sun 386i workstation.
- A new mathematical model will be proposed.

TABLE 1  
SUMMARY OF THE RUNS TO DATE

Foam quality:	90%
Injection rates:	1 cc/min foam
Surfactant concentration:	0.1 ~ 1%
Permeability:	6.5 ~ 7.0 Darcy
Porosity:	32 ~ 35%
Pore Volume:	120 cc
Backpressure:	50 psi

**2 runs without CT and 6 runs with CT to date**

TABLE 2  
BASIC DATA FOR EACH RUN

data run\	foam quality (%)	Injection Rates (cc/min)	Surfactant Concentration	K (Darcy)	Porosity (%)	P.V. (cc)	CT (Y/N)
1	90	0.1	0.1%	6.5	35	115	N
2	90	0.01	0.1%	7.0	35	120	N
3	90	1.0	0.1%	7.0	33	115	Y
4	90	1.0	1.0%	6.7	32	118	Y
5	90	1.0	1.0%	6.8	33	120	Y
6	90	1.0	0.1%	6.6	32	117	Y
7	90	1.0	0.1%	6.5	33	118	Y
8	90	1.0	0.1%	6.5	32	120	Y
<p>Note: The last four runs also contained some changes in the number of pressure transducers attached.</p>							

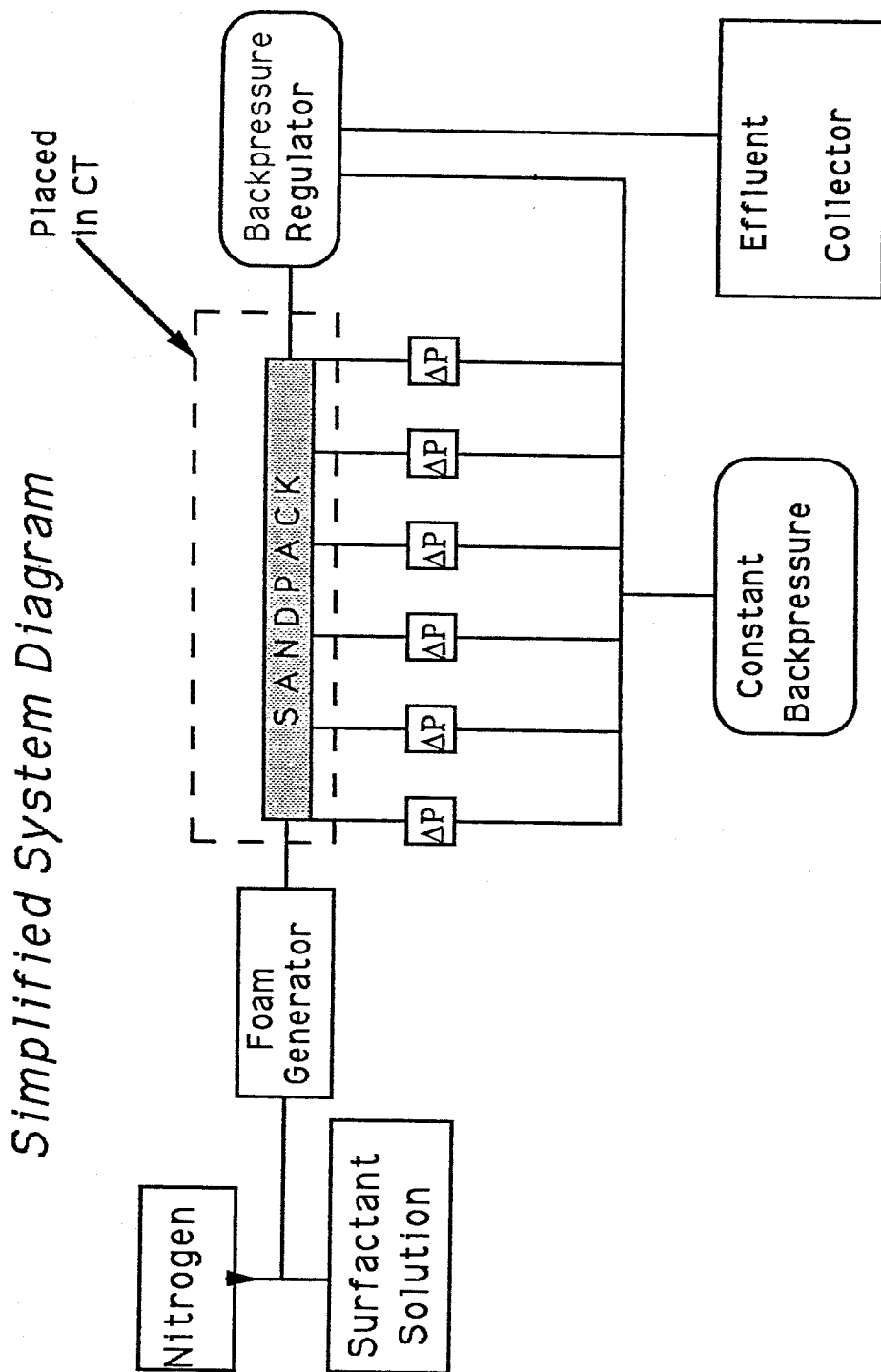


Figure 3.1.1 Schematic diagram of foam flow experiment.

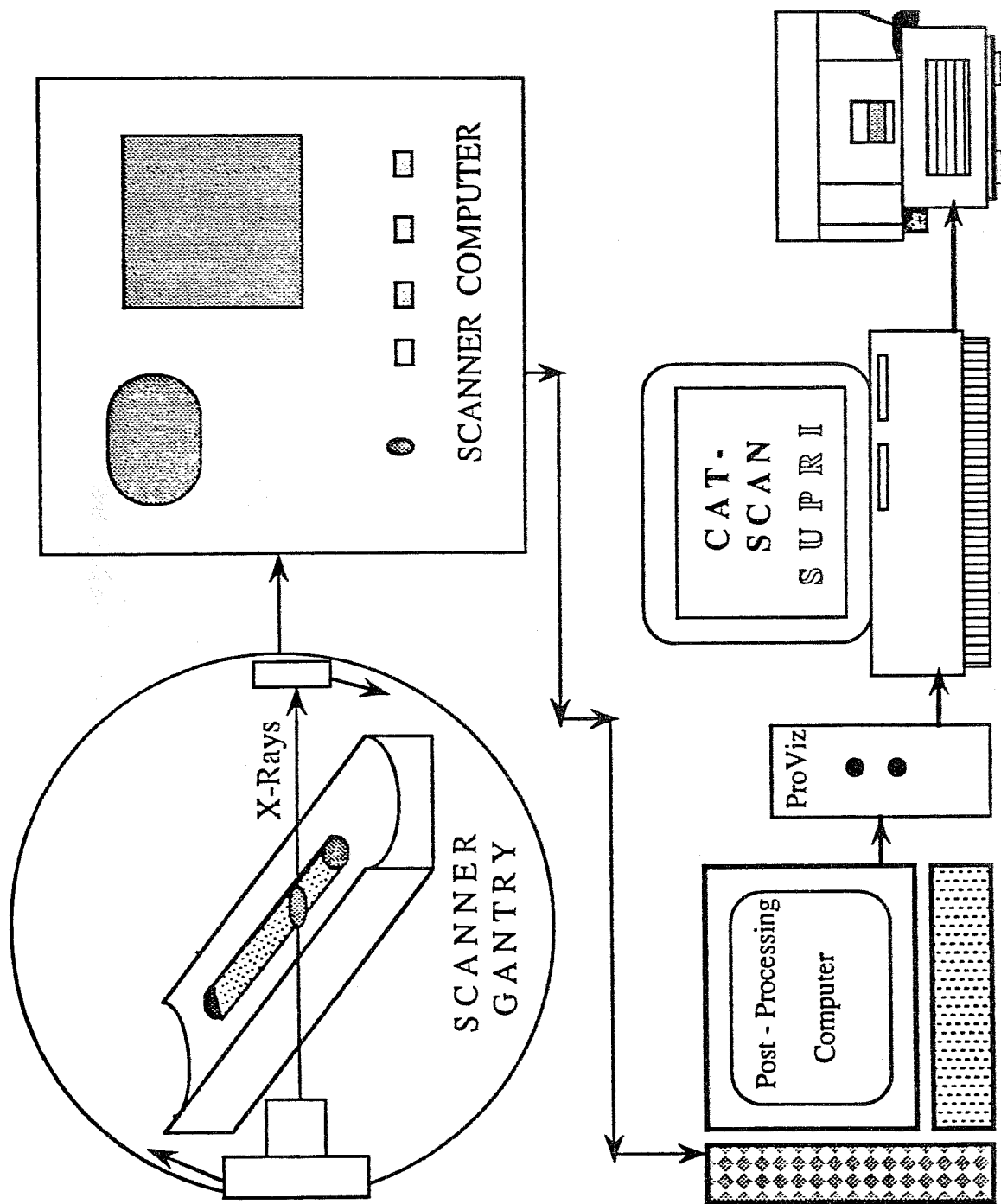


Figure 3.1.2 Schematic diagram of the CT system.

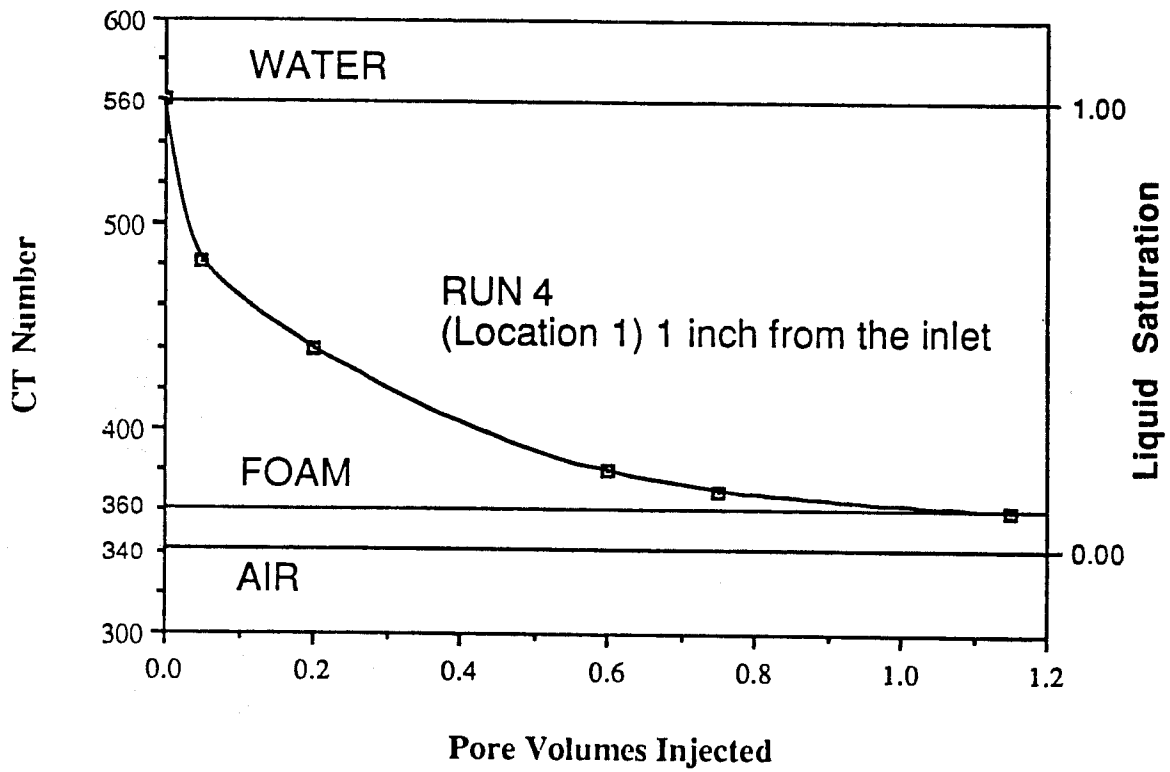


Figure 3.1.3 CT number (liquid saturation) vs. time.

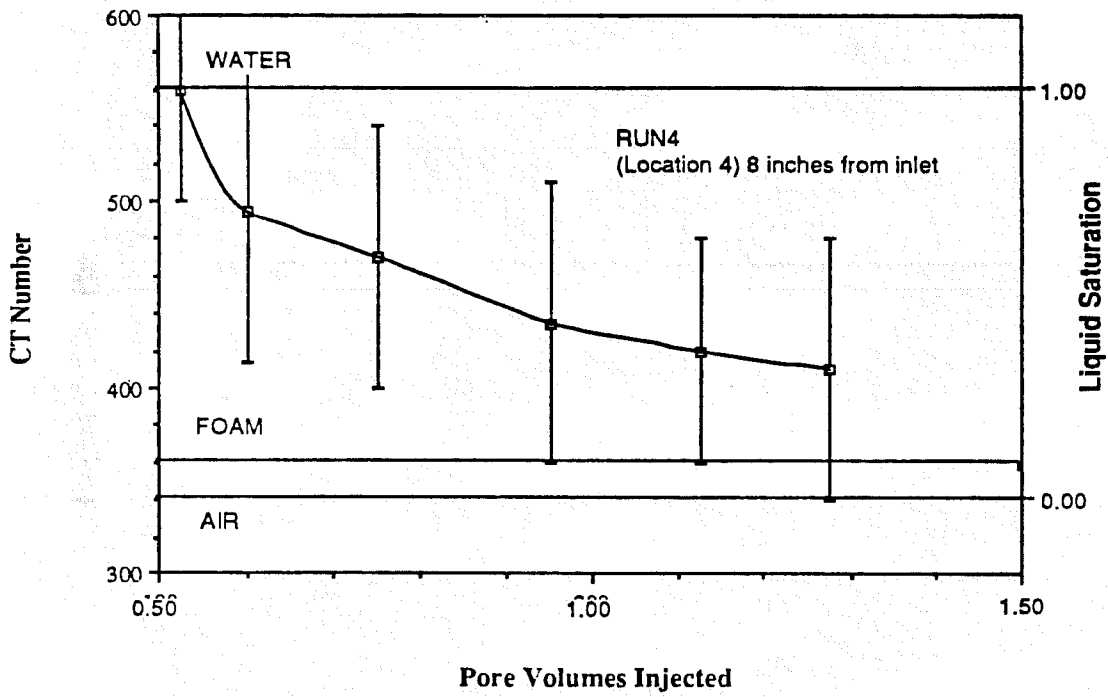


Figure 3.1.4 CT number (liquid saturation) vs. time.

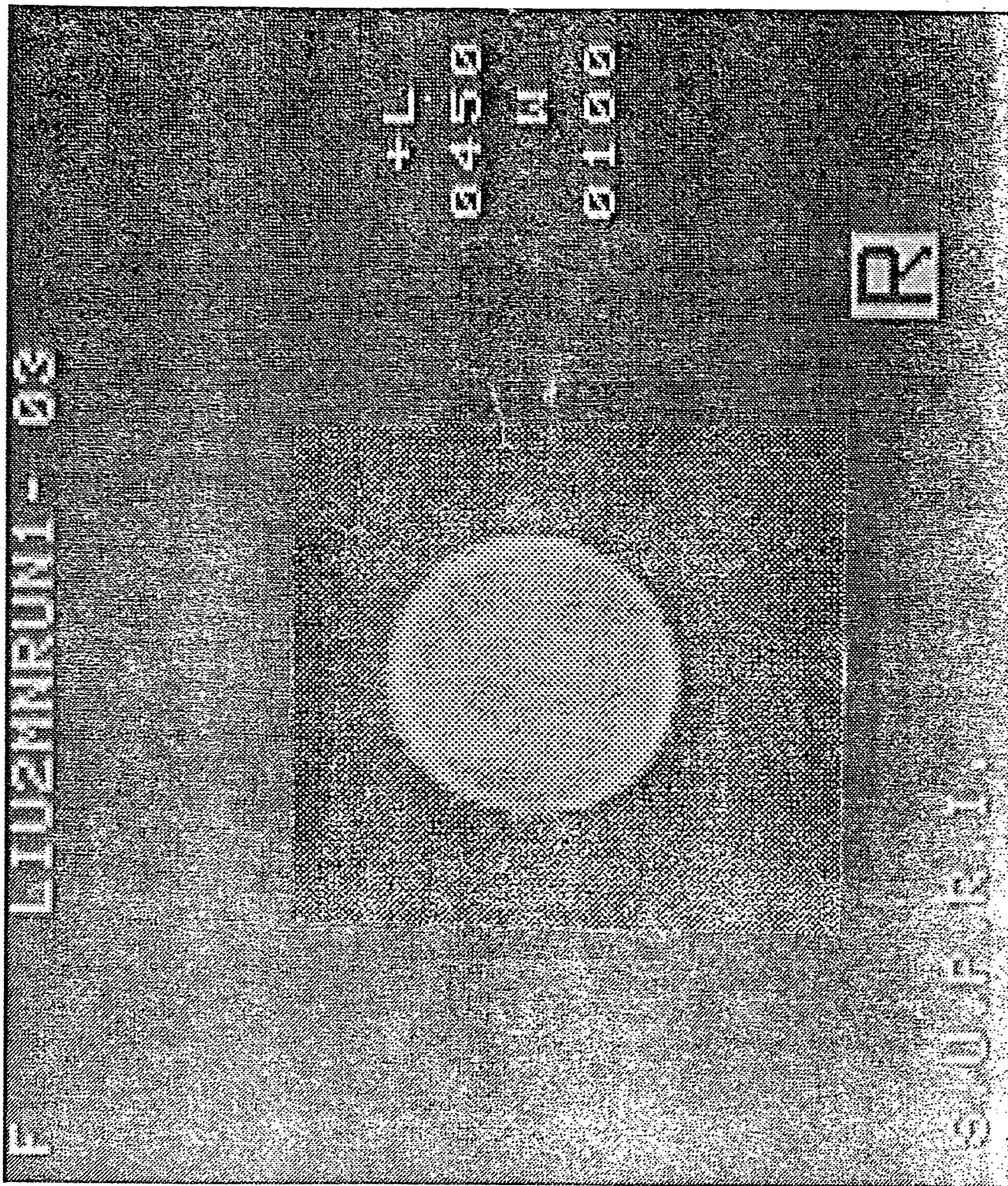


Figure 3.1.5 A sample CT picture.

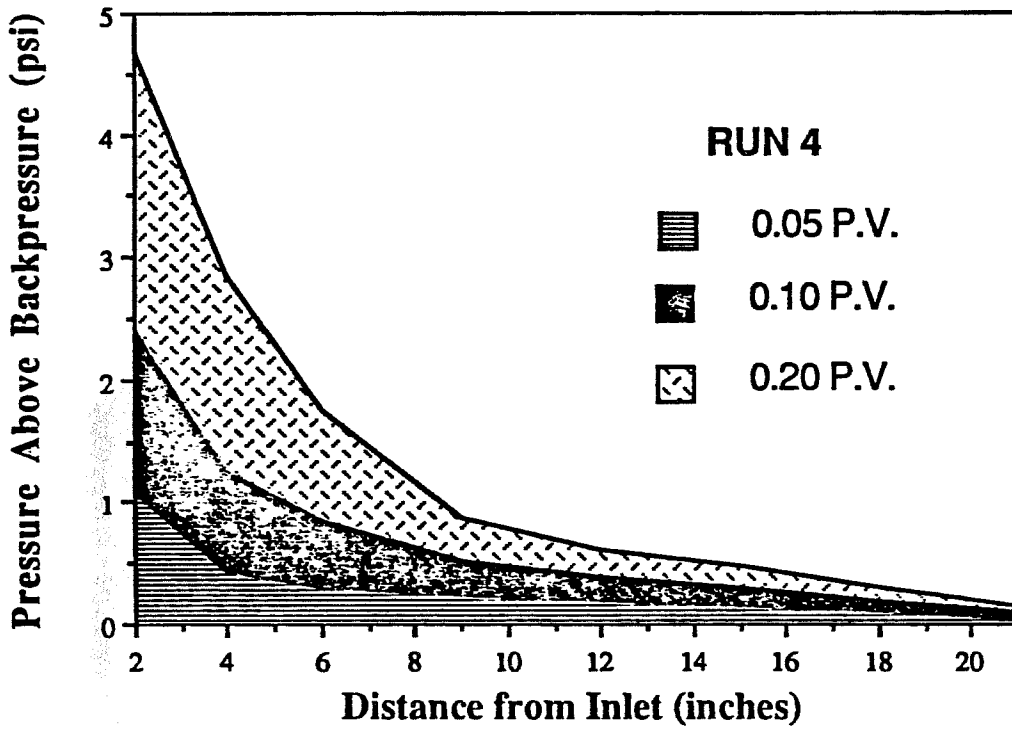


Figure 3.1.6 Pressure as a function of pore volumes.



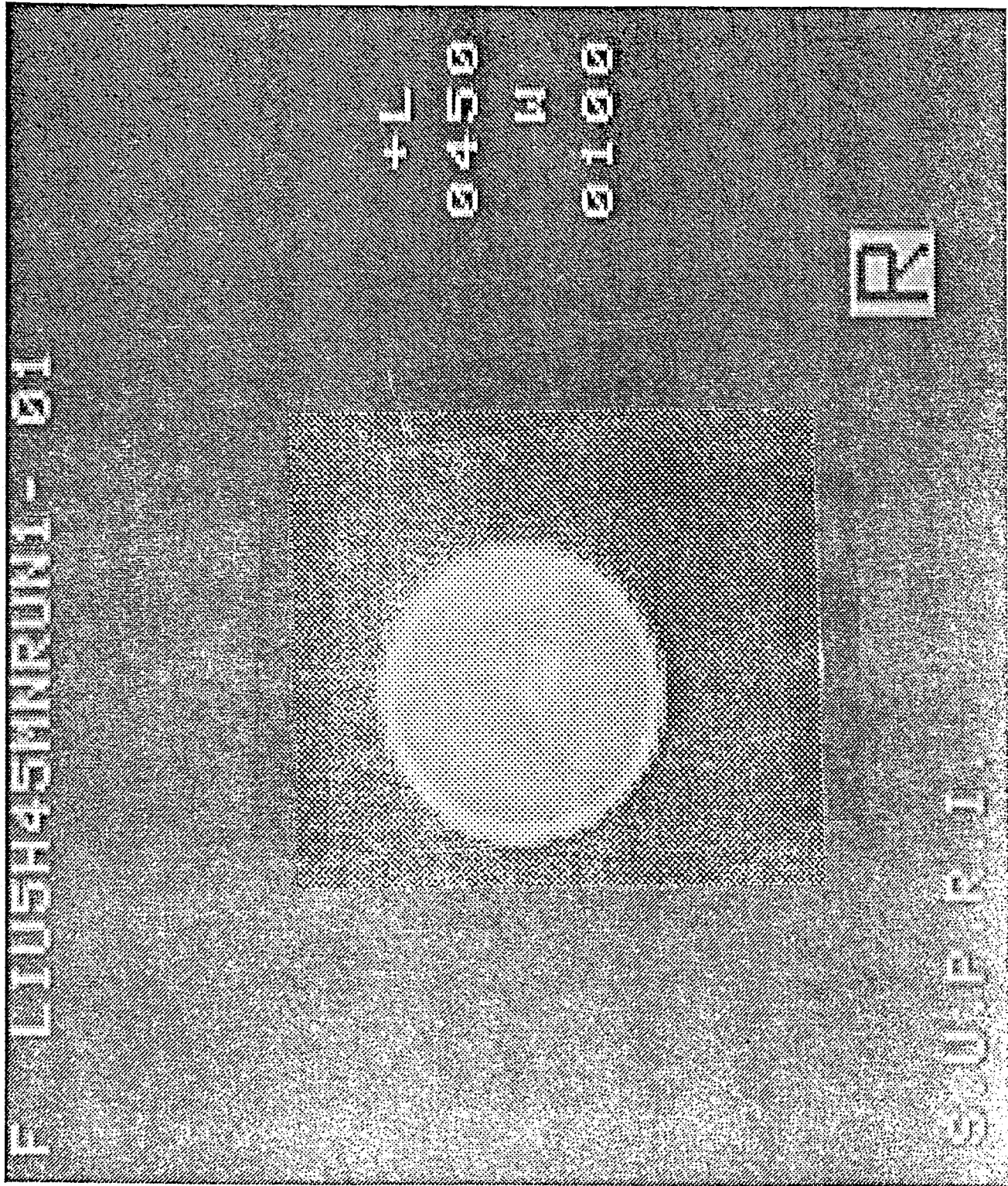


Figure 3.1.7 Foam channeling.

## 3.2 CHARACTERIZATION OF SURFACTANTS AS STEAMFLOOD ADDITIVES (D.C. Shallcross, L.M. Castanier and W.E. Brigham)

### 3.2.1. ABSTRACT

The efficiency of a steamflood can be increased by the use of surfactants that generate steam foam within the oil reservoir. Ideally the foam should preferentially block high permeability streaks and oil-depleted regions of the reservoir through which the steam would otherwise channel. This paper reports the results of an experimental study into the foam-forming characteristics of seventeen different surfactants. Both commercially-available, and experimental surfactants were tested in a one-dimensional sandpack under controlled conditions of pressure and temperature similar to those for steam injection in California oil fields. The surfactant solutions were injected into the sandpack in discrete slugs of a finite duration allowing transient phenomena, such as the persistence of the foam, to be studied. Nitrogen was injected as a noncondensable gas. Four surfactants were found to cause foaming and additional pressure drop within the sandpack at low concentrations.

Another aspect of the study was to link the foamability of surfactants with their chemical structure. Surfactants studied included, alpha olefin sulphonates, internal olefin sulphonates, linear alkyl-xylene sulphonates and linear toluene sulphonates. Under the conditions of the experiment, long chain alpha olefin sulphonates were found to generate the strongest foams. Internal olefin sulphonates, linear toluene sulphonates and linear alkyl-xylene sulphonates generated just as strong foams, but only at successively higher concentrations. In addition, by the novel use of heat flux sensors attached to the outside of the sandpack, heat loss from the one-dimensional model was studied. This allowed a better understanding of the heat transfer mechanisms operating within the tube. Such an understanding is important in correctly interpreting the experimental observations.

### 3.2.2. INTRODUCTION

It is recognized that foam-forming chemical additives may be introduced into a reservoir during a steamflood operation to increase oil recovery. The injected steam and surfactant generate foam within high permeability regions of the reservoir such as the steam-swept regions. The injected steam is partially blocked by this foam and is diverted to sweep across other oil-rich regions of the reservoir. Often noncondensable gas and an electrolytic solution are injected into the reservoir to help stabilize the foam.

Many workers have conducted laboratory and field tests in an effort to identify the most suitable surfactants for use in a steam foam process. The first stage of any screening process for the selection of a suitable surfactant is to test the thermal stability of the surfactants under steam conditions (Castanier and Brigham, 1985; McPhee *et al*, 1988). The foam forming ability and the longevity of any foam formed are then examined. Using such a screening technique McPhee *et al* reduced a field of 109 candidate surfactants down to just eight which were then tested using a laboratory sandpack in which the foam forming ability of the surfactants under reservoir conditions were carefully observed.

In a patent issued in the United States, Dilgren *et al* (1978) found that Siponate DS-10, an alkylaryl sulphonate was the most suitable surfactant of the ones tested. Later, after a more extensive investigation, Dilgren and Owens (1983) concluded that alpha-olefin sulphonates were even more suitable. They suggested that the surfactants used should contain between 14

and 22 carbon atoms in the alkyl chain. They further suggested that of the surfactant molecules, about half should contain between 16 and 18 carbon atoms. In a later patent Muijs and Keijzer (1987) suggested that the alpha olefin sulphonates containing up to 30 carbon atoms in the alkyl chain would also be suitable as a foam-forming surfactant. Muijs *et al* (1988) presented the results of a systematic survey of foam-forming surfactants. They found a relationship between the foam forming ability of a surfactant and its chemical structure. At temperatures around 215°C they found that alpha olefin sulphonates are the most suitable class of surfactant. At higher temperatures alkylaryl sulphonates were found to be better. Duerksen *et al* (1985) concluded after a series of experiments that dimers of the alpha olefin sulphonates might be suitable foam-forming surfactants. They recommended that dimers should be prepared from C<sub>15</sub> - C<sub>20</sub>. Typically olefin sulphonates are obtained by hydrolysis and neutralization of the product formed by reacting sulphur trioxide with olefins.

A recent survey by Castanier and Brigham (1988) shows that alpha olefin sulphonates are now being employed in the field. The field tests reported by Mohammadi and McCollum (1986), and Patzek and Koinis (1988) are examples of tests in which the use of alpha-olefin sulphonates enhanced oil recovery. In particular the use of C<sub>16</sub> - C<sub>18</sub> alpha olefin sulphonates is favoured.

We have studied the foam forming ability of seventeen different surfactants including AOS1618, the most popular alpha olefin sulphonate used in the field. Much of the laboratory work undertaken by Dilgren, Duerksen, Muijs and their respective co-workers was performed using steady state experimental techniques. Steam foam was either injected or allowed to form within an artificial reservoir such as a sandpack. The steam, surfactant, noncondensable gas and electrolyte, if any, were injected continuously. Once steady state was achieved the pressure profiles within the system were observed. These profiles then formed the basis for their studies and observations of the foam forming abilities of the surfactants. The experimental technique employed in our study is, however, of an unsteady-state type. The surfactant solution is not injected continuously but instead as discrete slugs. This allows transient phenomena such as the persistence of the foam and foam decay to be studied.

### 3.2.3. EXPERIMENTAL APPARATUS AND PROCEDURE

The one-dimensional steamflood model consists of a stainless steel tube filled with clean sand. The tube has an average inside diameter of 54.8 mm (2.16 inches) and a length of 1.830 m (72 in. ). The tube is mounted horizontally and wire screens at either end retain the sand within. The sandpack has a porosity of 30.8 percent, and an absolute permeability of about 90D. The sand size distribution is presented in Table 1. To reduce heat losses the entire

TABLE 1  
SAND SIZE DISTRIBUTION

U.S. Mesh Number	Hole Number	Mass Fraction Retained
20	833	0.002
35	495	0.480
40	417	0.286
60	246	0.220
80	180	0.006
pan	--	0.002

length of the tube was wrapped in 7 cm of an insulation material. The brass O-ring used to seal the tube at each end allowed the tube to be pressure tested successfully to 2.5 MPa (350 psig).

Figure 3.2.1 shows a simplified diagram of the experimental apparatus. Distilled water is supplied to the steam generator at a constant rate by a Constametric pump. The generator is operated so as to produce superheated steam which is then injected into the sandpack. A gas controller is used to control the flowrate of nitrogen that is also injected into the sandpack. A second Constametric pump is used to inject the surfactant slugs into the tube. The pressure at the downstream end of the sandpack is maintained at a constant value using a backpressure regulator. During production of foam from the sandpack a manual control system also must be used to maintain the downstream pressure at the desired value.

Temperature within the sandpack is measured using 21 type-J thermocouples distributed along the length of the tube. Pressure gradients within the pack may be determined using the pressures measured at five tapings, that divide the tube into four sections. Tappings are located at each end of the tube, but although provision is made for seven intermediate tapings along the length of the tube, only three are used. These are located 0.406 m (16 in), 0.813 (32 in) and 1.321 m (52 in) downstream from the tube inlet. The five pressure tapings divide the tube into four sections. Transducers whose ranges are 0 - 69 kPa (0 - 10 psi) and 0 - 690 kPa (0 - 100 psi) are connected to each section in parallel to accurately measure the pressure drop across each section. Five thin film heat flux sensors are applied to the outside of the tube beneath the insulation to measure the rate of heat loss from the tube. This allows an estimate to be made of how close to adiabatic the system operates.

Initially the sandpack is saturated with distilled water. A pressure of 580 kPa (70 psig) is maintained at the tube outlet. Slightly superheated steam is then injected into the sandpack at a rate of 4.0 ml/min, cold water equivalent. The progress of the steamflood is monitored using the thermocouples, pressure readings and the heat flux sensors, as the steam front passes along the length of the tube. Steam breaks through at the tube outlet typically about three hours after injection begins. About 30 minutes after steam breakthrough, injection of nitrogen is begun. The nitrogen is injected at a rate of 0.081 l/min, equivalent to a mole fraction of 0.05 in the gas phase.

The injection of the first liquid slug follows at least one hour after the injection of nitrogen begins. The first slug usually contains 0.1 percent by weight of the particular surfactant being studied. All surfactant solutions used during the study were prepared as aqueous solutions containing one percent by weight of sodium chloride. The volume of each slug is ten percent of the total pore volume of the sandpack. At an injection rate of 4.0 ml/min, 35½ minutes are required to inject each slug into the sandpack. The pressure transducers are calibrated before and after each experiment, and between the injection of the surfactant slugs.

Foaming within the sandpack is indicated by an increase in the pressure gradients within the tube. If, one hour after the injection of a surfactant slug has been completed, no response to the slug is observed, a second slug is injected at a higher concentration of 0.25 percent by weight. The concentration of the surfactant is progressively increased to 0.50 and finally 1.00 percent until a response is observed. When a response is observed, the slug producing that response is followed by one or more slugs of the same concentration. Slugs are injected at intervals of at least one hour. During injection of all surfactant slugs, injection of the steam and nitrogen continues.

The same sandpack was used to test all the surfactants. The sandpack was thoroughly cleaned between each experiment to remove all surfactant traces. At the conclusion of an

experiment at least 10 l of distilled water was passed through the sandpack. This was then followed by at least 750 ml (half the total pore volume) of isopropanol to remove all traces of the surfactant. This in turn was followed by the injection of at least 15 l of distilled water. Carbon dioxide was used to remove all nitrogen from the tube. Finally at least 10 l distilled water was used to remove the carbon dioxide. During each cleaning procedure a total of at least 50 l (35 pore volumes) of distilled water was flushed through the sandpack.

### 3.2.4. EXPERIMENTAL OBSERVATIONS

Using the procedure described above seventeen different surfactants were tested in the one-dimensional model. These surfactants included both commercially-available and experimental samples from Chevron, Hoechst and Shell. The chemical structures of the surfactants tested varied between alpha-olefin sulphonates (AOS), internal olefin sulphonates (IOS), linear alkyl-xylene sulphonates (LXS), linear toluene sulphonates (LTS) and others. Within a class of surfactants having the same chemical structure the length of the alkyl chain also varied; e.g. the alpha-olefin sulphonates tested in order of increasing chain length were AOS1416, AOS1618 and AOS2024.

The seventeen surfactants tested are listed in Table 2 in order of decreasing foam-forming ability. The minimum slug concentration which caused a significant increase in the pressure drop is listed for each of the surfactants. Also listed are the magnitude and duration of the pressure drop increase observed in response to the injection of the first slug at that concentration. Of the seventeen surfactants only four generated significant pressure gradients within the sandpack upon injection of a 0.10 percent by weight solution. These surfactants were Shell's Enordet AOS1618, AOS2024 and LTS18, and Chevron's SD1000, a dimerized alpha-olefin sulphonate. Figure 3.2.3 compares the maximum pressure drops generated across the tube in response to the first 0.10 percent concentration slug of each surfactant. The highest pressure drop generated in response to the injection of the first 0.10 percent concentration slug was for the alpha-olefin sulphonate with the longest alkyl chain: AOS2024. Another AOS surfactant having an average five carbon atoms less in the alkyl chain (AOS1618) generated the second highest pressure drop. AOS1618 is the surfactant that was tested by Shell with success in the Kern River Field of California (Patzek and Koinis, 1988). The next surfactant, LTS18, generated a pressure drop less than half that generated by the AOS1618. This surfactant has a similar chain length, but a different chemical structure.

The increases in the total pressure drop across the tube in response to the injection of the single 0.10 percent solutions of AOS1618 and AOS2024 are presented in Fig. 3.2.4. This diagram clearly shows the stronger and long-lasting response to the surfactant of the longer chain length. Not shown in this diagram is the response to the injection of a 0.10 percent slug of AOS1416. This is because AOS1416's minimum foaming concentration was 0.50 percent. These observations suggest that at least for the backpressure of 580 kPa (70 psig) an increase in the alpha-olefin sulphonate's molecular weight leads to the generation of a tougher foam. This observation agrees with the results of Muijs *et al* (1988).

Figures 3.2.5 and 3.2.6 present a comparison between pressure drop responses for the internal olefin sulphonates and the linear alkyl-xylene sulphonates tested. IOS1517, the lightest of the three internal olefin sulphonates to be studied, did not foam at a concentration of 0.25 percent. Both IOS1720 and IOS2024 foamed to a similar extent at a concentration of 0.25 percent, but the response to the heavier IOS2024 lagged behind that of IOS1720 by about 0.3 hours. This suggests that the IOS2024 was adsorbed then desorbed by the sandpack in a process not fully understood by the authors.

The linear alkyl-xylene sulphonate class of surfactant only foamed for the highest surfactant concentration used: 1.0 percent by weight. No foaming was observed for LXS1112 even at this slug concentration, but an increase of two carbon atoms in the average alkyl chain length produced significant foaming. The most aggressive foaming occurred for the surfactant having an average of sixteen carbon atoms in the chain: LXS16. The response to the heaviest surfactant of the class tested, LXS18, lagged behind the others, probably due in part to adsorption and desorption, as mentioned above.

Generally the strength of a foam increases with the concentration of the surfactant injected. This phenomenon is observed when two slugs of the same surfactant concentration are injected successively into the sandpack. Two slugs of a 0.10 percent solution of AOS1618 were injected into the pack (Fig. 3.2.7). In response to the first slug the total pressure drop across the tube peaked at 928 kPa (135 psi). The second slug injected an hour after the foam had collapsed induced a pressure drop that peaked at 1704 kPa (247 psi), nearly twice the previous value. We believe the pressure drop increased because some surfactant remained in the sandpack after the collapse of the foam generated by the first slug. Some surfactant must therefore have been present in the pack prior to injection of the second slug while the first slug was injected into a clean sandpack. Figure 3.2.8 shows a similar increase in the maximum pressure drop responses for four consecutive slugs of 0.10 percent solution of Chevron's Chaser SD 1000. Clearly surfactant injection during each slug builds onto the surfactant present from the preceding slugs to increase the foaming response. The generation of foam within a sandpack is by a complex mechanism that is not fully understood.

### 3.2.5. HEAT TRANSFER MECHANISMS WITHIN THE SANDPACK

Understanding the mechanisms of heat transfer existing within the experimental system significantly improves the ability of the observer to accurately interpret the experimental data. The sandpack tube used in the present study was wrapped in insulation material in order to minimize the heat transfer between the tube and its surroundings. Five thin film heat flux sensors were applied to the outside surface of the tube beneath the insulation in order to measure the rate of heat loss to the surroundings as the foaming process occurred within the tube.

The heat flux sensors that were used are commercially-available sensors manufactured by the RdF Corporation of Hudson, New Hampshire, U.S.A. (Part Number 20457-2). Each sensor essentially consists of forty pairs of thermocouples each pair separated from its mate by a thin plastic film. The thermocouples are connected in series so that a relatively large electrical output is generated from the minute difference in the temperatures on either side of the plastic. As a consequence, a flux of  $500 \text{ W/m}^2$  would typically generate a signal of  $1000 \mu\text{V}$ . The forty thermocouple pairs are arranged in four rows of ten in an area measuring 14 mm by 18 mm. The thermocouples are protected from the environment by additional layers of the plastic film which give the sensor a total thickness of 0.2 mm and an overall dimensions of 19.2 mm by 25.2 mm. At one end of the sensor a type-T thermocouple is sandwiched between the two protective plastic films. This thermocouple allows the temperature of the sensor to be measured.

One of the heat flux sensors was located on the tube's upper surface a distance 0.965 m (38 in) from the inlet, while the other four sensors were distributed about the tube's surface 0.651 m (25½ in) from the inlet (see Fig. 3.2.2). Of these four sensors, one was located at the top of the horizontal tube, another at its base and the other two on one side. Each of the sensors was oriented so that their longer edges were parallel with the tube axis. As a consequence, the flux sensitive area of each sensor subtended an angle of  $14^\circ$  on the tube's surface. The presence of the sensor between the tube surface and the insulation disturbed the flow of heat

through the region in the vicinity of the sensor. Corrections may be made for these disturbances (Shallcross and Wood, 1986) but for the present study any disturbances are insignificant.

The average heat flux at the exterior tube surface during the steamflood and before injection of the first surfactant slug is shown in Fig. 3.2.9. The individual fluxes from the four sensors located 0.651 m from the tube inlet were averaged. Before the steam front reached this location there is virtually no flow of heat from the tube to the surrounding insulation. The tube and insulation are in thermal equilibrium. As the steam front reaches the sensors the rate of heat loss increases to a maximum at about 0.93 hours. At that time the temperature difference between the tube and the insulation is a maximum. As time passes, the insulation temperature gradually increases while the sandpack remains at the steam saturation temperature. As a result, the rate of heat loss decays towards a limit. The injection of nitrogen at 3.7 hours results in a five percent decrease in the rate of heat loss. It is interesting to note that this five percent decrease is observed in the heat flux measured by all four of the sensors located 0.651 m from the inlet. This indicates that the flow of nitrogen is uniformly distributed across the tube.

The two heat flux sensors located at the top and bottom of the tube were used to estimate the angle of inclination of the steam front. Since the average steam front velocity was found to be 1.2 cm/min, and because the average time between the peak fluxes recorded by the top and bottom sensors was 98.6 seconds, the steam front is estimated to be inclined from the vertical by 19°. This indicates that gravity override is present to a small degree.

The twenty-one thermocouples distributed along the length of the sandpack may be used to monitor the heat transfer mechanisms during the foaming process. Figure 3.2.10 presents two views of the same plot of sandpack temperature as a function of both location within the pack and time. The temperature response is shown during the injection of two 0.10 percent slugs of the AOS1618. In the following discussion reference will be made to regions denoted by capital letters on the diagram.

Before injection of the first surfactant slug at 5.0 hours the temperature within the pack is constant at the steam saturation temperature (region A). The exception to this is in the region near the upstream flange where the temperature is slightly elevated (B) due to the presence of a band heater around that flange. Immediately following the beginning of the injection of the slug, the temperature at the upstream end of the tube decreases (C). This is because the steam being injected is no longer superheated, but is at the saturation temperature. As foam is generated near the upstream end, the pressure within the pack in that region begins to increase. This is accompanied by an increase in the steam saturation temperature around the inlet (D). At the same time the downstream sandpack temperature begins to decrease (E). This is because the steam generator delivers a constant level of steam so that an increase in temperature in one region of the reservoir must be accompanied by a decrease in another region. During the life of the foam the upstream temperature (F) is maintained at the steam saturation temperature. An hour after the slug injection the foam collapses rapidly (G and H) and the sandpack temperature returns to its pre-injection value (I). More than an hour later a second slug at the same concentration is injected and foaming occurs (J).

Figure 3.2.11 shows the average heat flux from the four sensors located 0.651 m along the tube as the two 0.10 percent AOS1618 slugs were injected. Figure 3.2.12 shows the average sandpack temperature at the same location. From the heat flux and temperature data it may be seen that the rate of heat loss from the tube varies considerably during the period that foam exists within the sandpack.

Prior to the injection of the surfactant the rate of heat loss from the sandpack is approximately at  $216 \text{ W/m}^2$ . The flux is constant as the system is at steady state with the sandpack at the steam saturation temperature. Immediately upon injection of the surfactant, foam forms at the tube's upstream end. In accordance with the mechanisms described earlier, this results in a decrease in the sandpack temperature downstream. This decrease is shown clearly in Fig. 3.2.12 at  $t = 0.3 \text{ hr}$ . As the temperature of the sandpack decreases, so does the temperature driving force between the sandpack and the surrounding insulation. This results in a decrease in the rate of heat loss at  $t = 0.30 \text{ hr}$  (Fig. 3.2.11). The foam extends deeper into the sandpack passing the vicinity of the sensors at about  $t = 0.45 \text{ hr}$ . An increase in the sandpack temperature accompanies the increase in pressure caused by the foam. This results in a significant increase in the rate of heat loss to  $562 \text{ W/m}^2$ . At about  $t = 1.1 \text{ hr}$ , the foam collapses and the temperature returns to its steady state value. The rate of heat loss drops to  $38 \text{ W/m}^2$  before returning to the steady state level of  $226 \text{ W/m}^2$ . The heat loss rate drops below its steady state value because during the brief period of the high heat flux, the insulation was heated and its temperature elevated. The very low flux reflects the relatively small temperature difference between the insulation and the sandpack. As the insulation cools back to its steady state level, the heat flux gradually increases to its pre-injection level. The phenomena described are repeated when the second slug is injected. The increased pressure gradient within the tube resulted in the higher maximum heat flux of  $661 \text{ W/m}^2$ . So much heat is supplied to the insulation during that time that the insulation's temperature rises above the sandpack's steady state temperature. As a result, as the effects of the slug injection diminish, heat actually flows from the insulation into the sandpack. This is indicated by a negative flux value at  $t = 3.6 \text{ hr}$ . The rate of heat loss eventually returns to the steady state conditions of  $209 \text{ W/m}^2$ .

### 3.2.6. NONCONDENSIBLE GAS

The stability of the steam foam depends upon the rate at which the individual foam bubbles collapse. Because the pressure within the smaller bubbles will be higher than within their larger counterparts, the steam will have a tendency to migrate from the smaller bubbles to neighbouring larger ones. As Janssen-Van Rosmalen *et al* (1985) observed, in order for the steam to migrate from one bubble to another the steam must pass through the liquid film that separates them. If the bubbles contain steam alone then the migration mechanism is simple; the condensation of steam on the lamellae inside the smaller bubble will liberate heat that when passed through the lamellae will vapourize an equal amount of water on its other side, thus generating steam within the larger bubble. The migration rate is therefore controlled by the rate at which heat is transferred through the lamellae. However if a noncondensable gas is present in the bubble then that gas must actually diffuse through the lamellae in order for the smaller bubble to collapse. The addition of the noncondensable gas to a steam foam system therefore tends to stabilize the foam by changing the bubble-collapse rate process from heat transfer control, to diffusion control.

Using an experimental apparatus similar in concept to that used in the present study, Janssen-Van Rosmalen *et al* investigated the importance of noncondensable gas in stabilizing steam foam. The workers injected a 0.5 percent by weight solution of a linear toluene sulphonate surfactant solution into a pack of clean sand. Simultaneously 90 percent quality steam and 1 percent by volume of nitrogen were injected. At a steam saturation temperature of  $150^\circ\text{C}$  the presence of the nitrogen increased the maximum pressure drop observed within the sandpack by 47 percent.

To confirm the above observation an experiment was performed during which nitrogen was not injected. A 10 percent PV slug of a 0.10 percent by weight saline solution of AOS2024 was injected into the sandpack in the absence of nitrogen. In Fig. 3.2.13 the observed total pressure drop across the sandpack is compared with the observations of an experiment

performed under similar conditions but in the presence of nitrogen. The results show that the simultaneous injection of the noncondensable gas significantly increases both the maximum pressure drop attained and the duration of response. In the absence of nitrogen the foam immediately collapsed as soon as injection of the surfactant stopped. Also, the rate of increase in the pressure drop across the pack during the injection of the surfactant slug was halved by the absence of the noncondensable gas. These two observations tend to support the contention of Janssen-Van Rosmalen *et al* that the presence of nitrogen retards the collapse of the foam bubbles.

These results also support Falls *et al* (1986) who suggest that steam foams can be used successfully in the absence of a noncondensable gas to divert the flow of steam within a reservoir. The presence of such a gas, however, increases oil recovery by prolonging the life of the foam.

### 3.2.7. CONCLUSIONS

- Under the experimental conditions alpha olefin sulphonates generate the strongest and most long-lived foams of all the surfactants tested at low concentrations.
- Internal olefin sulphonates and linear alkyl-xylene sulphonates produced just as strong foams but required higher surfactant concentrations. Not enough linear toluene sulphonates were studied to allow similar conclusions to be drawn.
- Generally, under the experimental conditions, within each surfactant class the strength of the foam generated increases with increasing alkyl chain length.
- For any given surfactant, the strength of the foam increases with increasing concentration.
- The use of noncondensable gas both increases the blocking effects and prolongs the life of the foam.
- Despite the presence of the insulation material the sandpack did not operate adiabatically, and heat flux sensors were invaluable in determining the rate of heat loss from the model during operation. The rate of heat lost to the surroundings was influenced by the foaming taking place within the sandpack.

### 3.2.8. ACKNOWLEDGEMENTS

This work was performed at the Stanford University Petroleum Research Institute (SUPRI-A) under U.S. DOE Contract DE-FG19-87BC14126. D.C.Shallcross also gratefully acknowledges the support of the Commonwealth Scientific and Industrial Research Organization, Australia.

### 3.2.9. REFERENCES

1. Castanier, L.M. and Brigham, W.E.: "An Evaluation of Field Projects of Steam with Additives," International Meeting on Petroleum Engineering, Tianjin, People's Republic of China (1988).
2. Castanier, L.M. and Brigham, W.E.: "Selecting Foaming Agents for Steam Injection Improvement," *Chemical Engineering Progress* 61, (6) (1985) 37-40.

3. Dilgren, R.E., Hiraski, G.J., Hill, H.J. and Whitten, D.G.: "Steam-Channel-Expanding Steam Foam Drive," U.S. Patent No. 4,086,964, May 2, 1978.
4. Dilgren, R.E. and Owens, K.B.: "Olefin Sulfonate-Improved Foam Drive," U.S. Patent No. 4,393,937, July 19, 1983.
5. Duerksen, J.H., Wall, R.G. and Knight, J.D.: "Steam Injection Including Alpha-Olefin Sulfonate Dimer surfactant Additives and a Process of Stimulating Hydrocarbon Recovery from a Subterranean Formation," U.S. Patent No. 4,556,107, December 3, 1985.
6. Falls, A.H., Lawson, J.B. and Hirasaki, G.J.: "The Role of Noncondensable Gas in Steam Foams," SPE No. 15053, Paper presented at SPE California Regional Meeting, 55-70, (1986).
7. Janssen-Van Rosmalen, R., DeBoer, R.B. and Keyzer, P.P.M.: "Stability of Steam Foam," Proceedings, Third European Symposium on Enhanced Oil Recovery 1, 329-340 (1985).
8. McPhee, C.A., Tehrani, A.D.H. and Jolly, R.P.S.: "Foam Flooding of Cores under North Sea Reservoir Conditions," SPE No. 17360, Paper presented at SPE/DOE Sixth Symposium on Enhanced Oil Recovery, 433-447 (1988).
9. Mohammadi, S.S. and McCollum, T.J.: "Steam-Foam Pilot in Guadalupe Field, California," SPE No. 15054, 71-82 (1986).
10. Muijs, H.M. and Keijzer, P.P.M.: "Steam Foam process," U.S. Patent No. 4,693,311, September 15, 1987.
11. Muijs, H.M., Keijzer, P.P.M. and Wiersma, R.J.: 1988, "Surfactants for Mobility Control in High-Temperature Steam-Foam Applications," SPE No. 17361, SPE/DOE Symposium on Enhanced Oil Recovery, 905-914 (1988).
12. Patzek, T.W. and Koinis, M.T.: "Kern River steam Foam Pilots", SPE No. 17380, SPE/DOE Sixth Symposium on Enhanced Oil Recovery, 663-676 (1988).
13. Shallcross, D.C. and Wood, D.G.: "The Accurate Measurement of Heat Flux Using a Film Heat Flux Sensor with Application to Axisymmetric Bodies," Proceedings Eighth International Heat Transfer Conference 3, (1986).

TABLE 2  
PRESSURE RESPONSES FOR SEVENTEEN SURFACTANTS

Surfactant	Manufacturer	Minimum Foaming Concentration (wt %)	Maximum Pressure Drop (kPa)	Duration of Pressure Response (min)
AOS2024	Shell	0.10	1611	85
AOS1618	Shell	0.10	928	68
LTS 18	Shell	0.10	396	91
SD 1000	Chevron	0.10	45	19
IOS1720	Shell	0.25	1497	79
IOS2024	Shell	0.25	1438	87
OS fl	Hoechst	0.25	449	45
SAS 60	Hoechst	0.50	1479	80
IOS1517	Shell	0.50	1105	101
AOS1416	Shell	0.50	487	144
LTS1618D	Shell	0.50	290	133
LXS16	Shell	1.00	1583	89
LXS18	Shell	1.00	1464	89
LXS1314	Shell	1.00	1392	112.7
LXS814	Shell	Foaming did not occur for 1.00 wt %		
LSX1112	Shell	Foaming did not occur for 1.00 wt %		
SD 1020	Chevron	Foaming did not occur for 1.00 wt %		

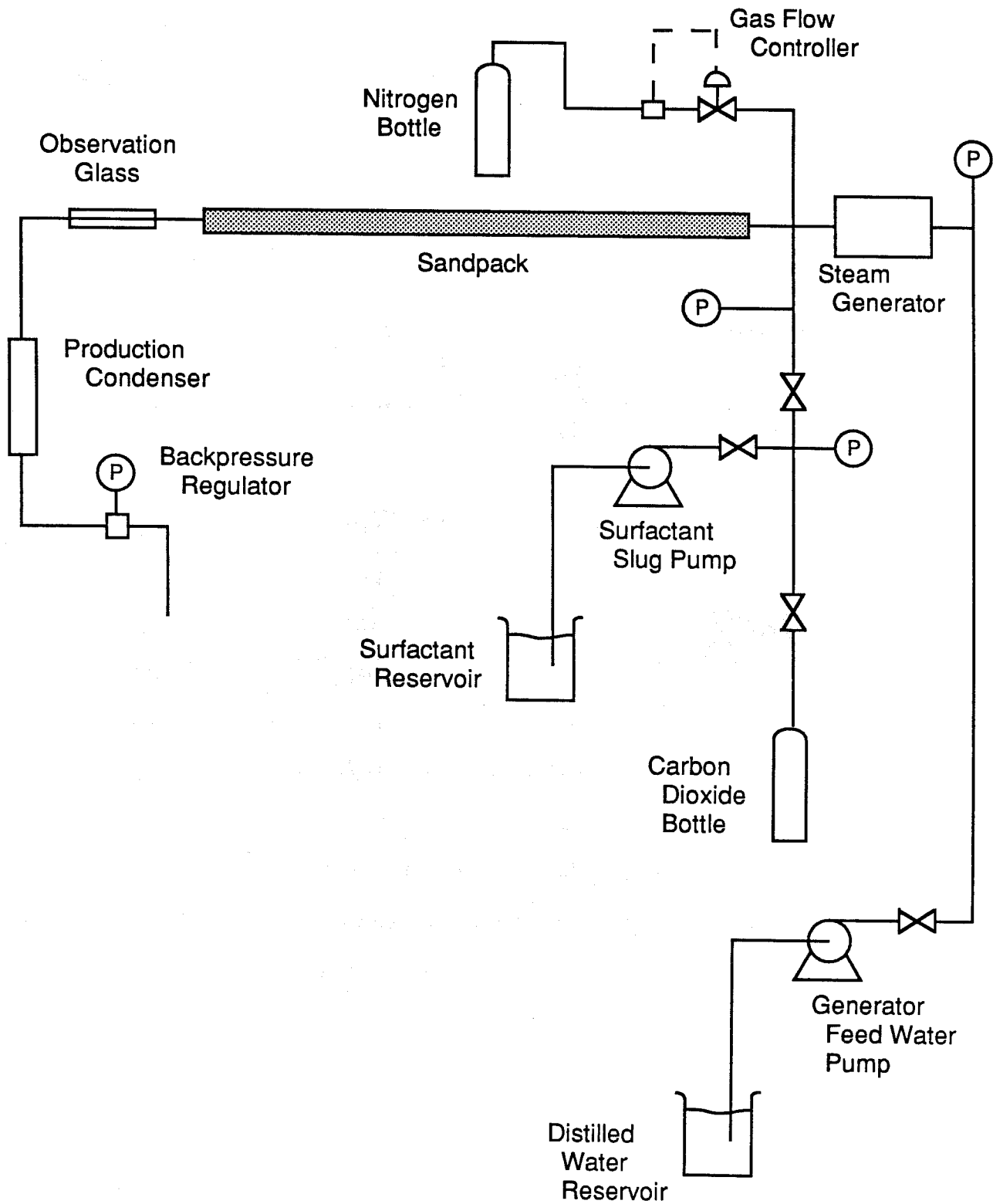


Figure 3.2.1 A simplified representation of the experimental apparatus.



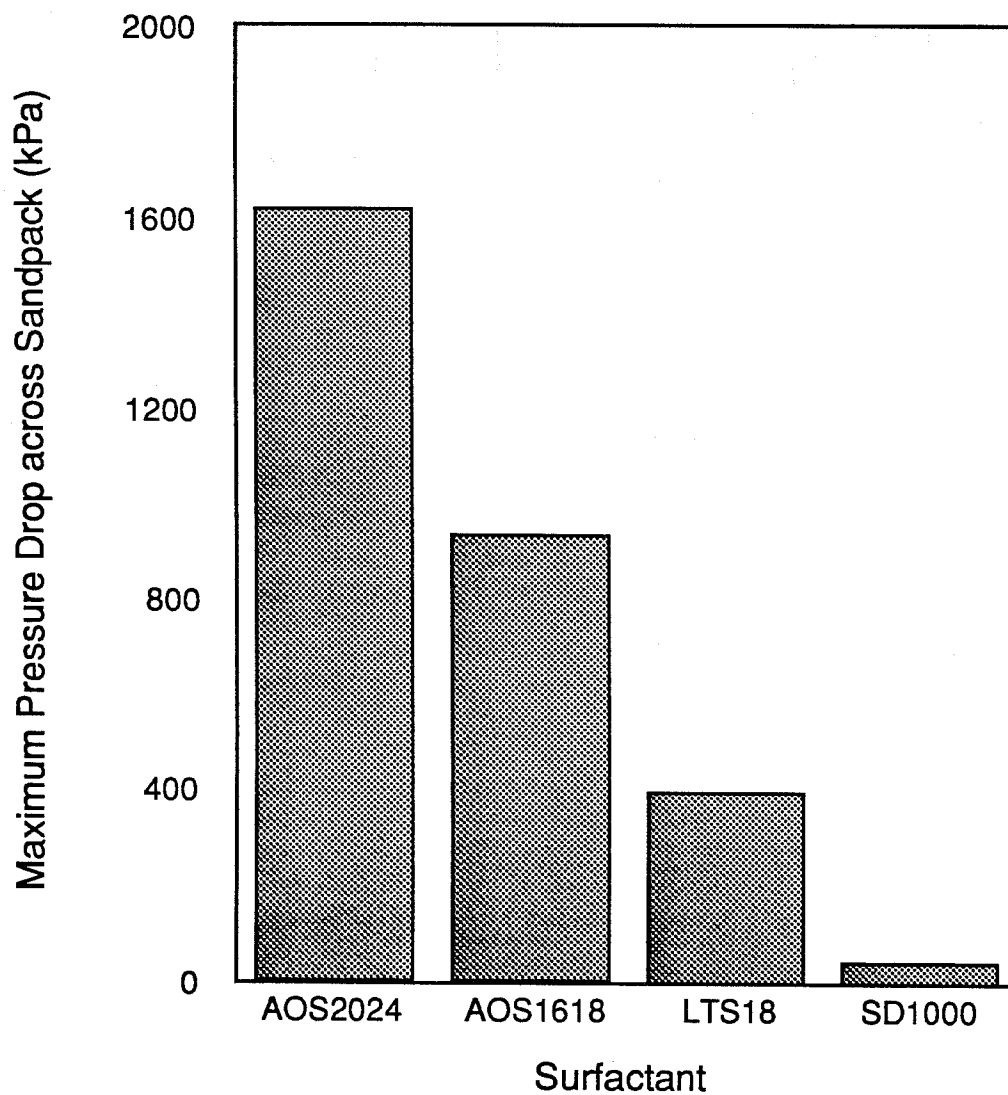


Figure 3.2.3 Maximum pressure drop response to injection of a single slug of 0.10% by weight of the four most active surfactants.

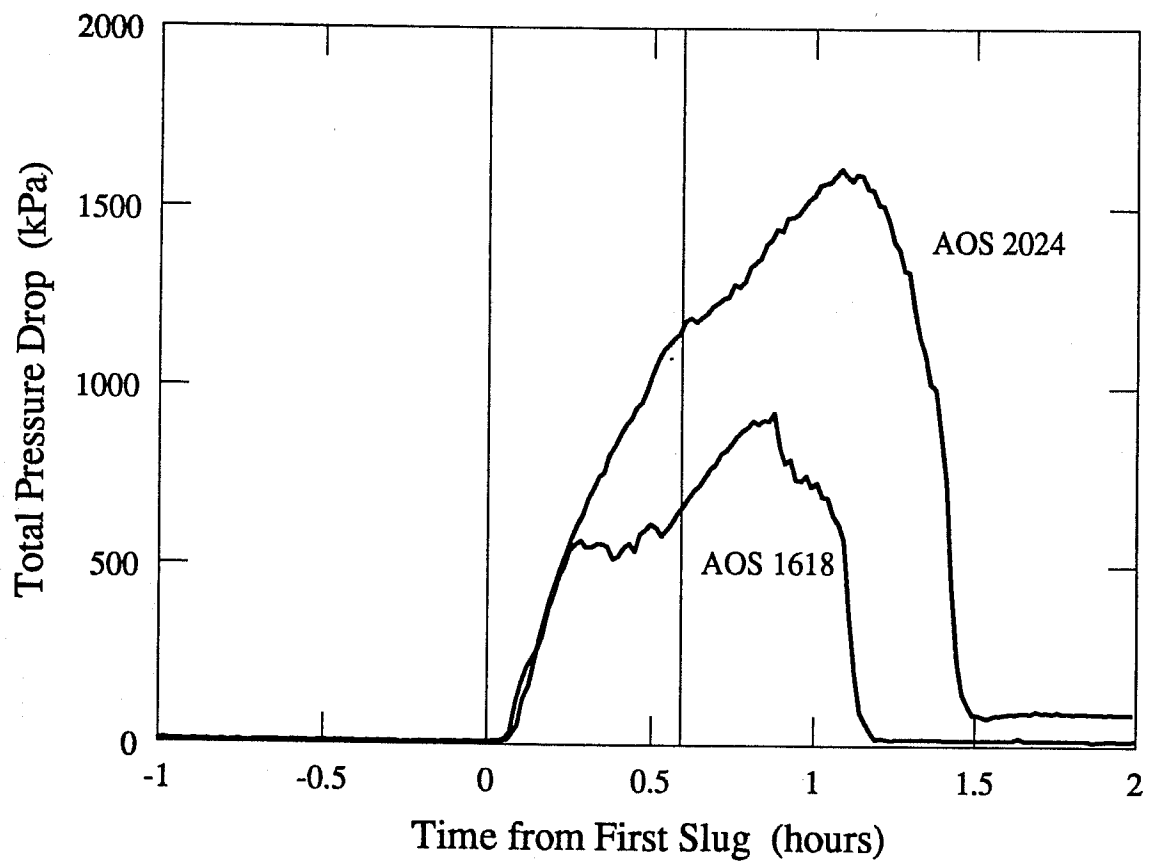


Figure 3.2.4 Total pressure drop responses to injection of single 0.10% slugs of the alpha olefin sulphonates AOS1618 and AOS 2024.

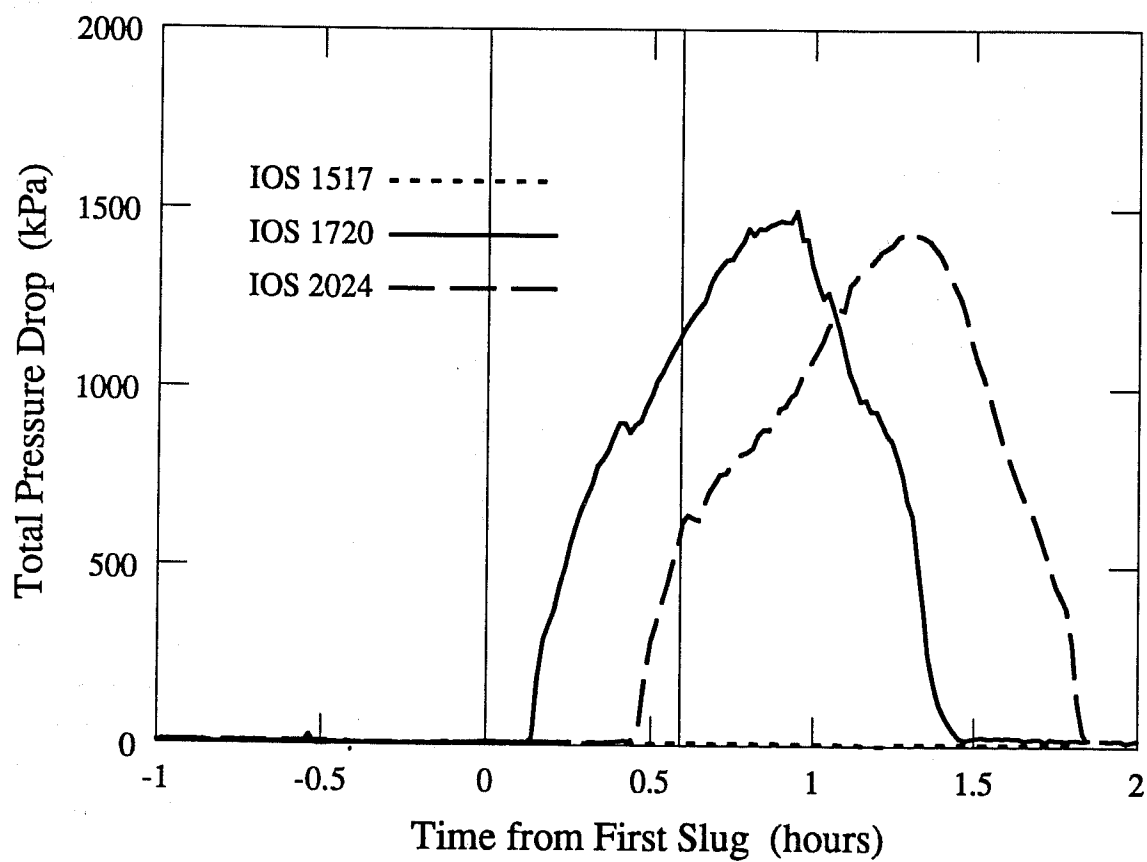


Figure 3.2.5 Total pressure drop responses to injection of single 0.25% slugs of the internal olefin sulphonates.

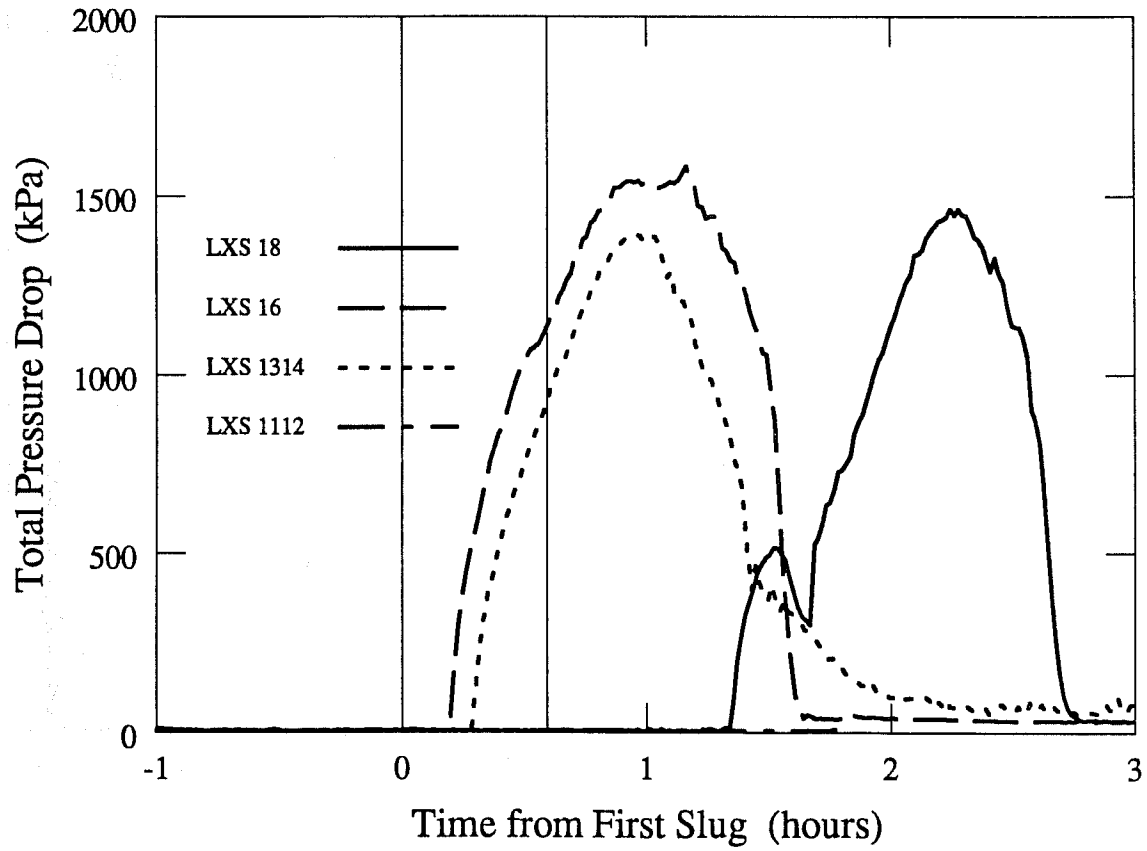


Figure 3.2.6 Total pressure drop responses to injection of single 1.00% slugs of the linear alkyl-xylene sulphonates.

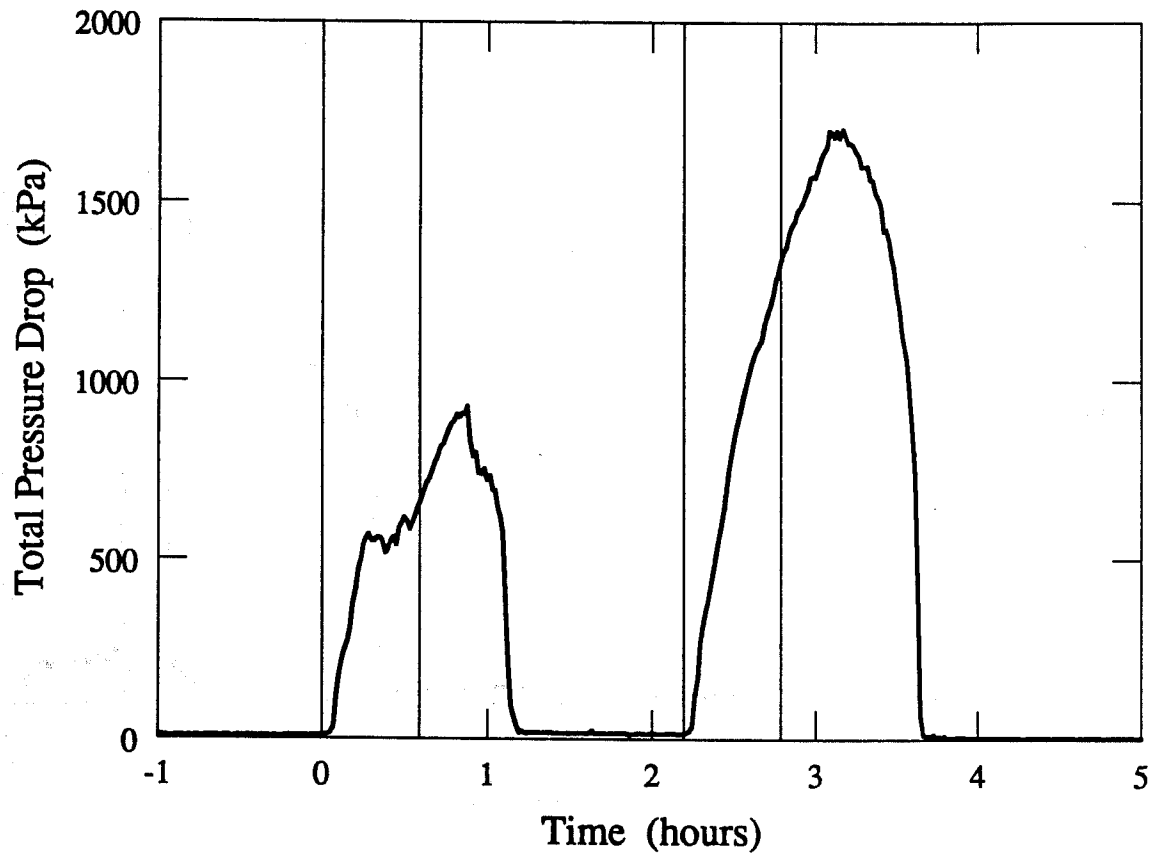


Figure 3.2.7 Total pressure drop response to injection of two consecutive 0.10% slugs of AOS 1618.

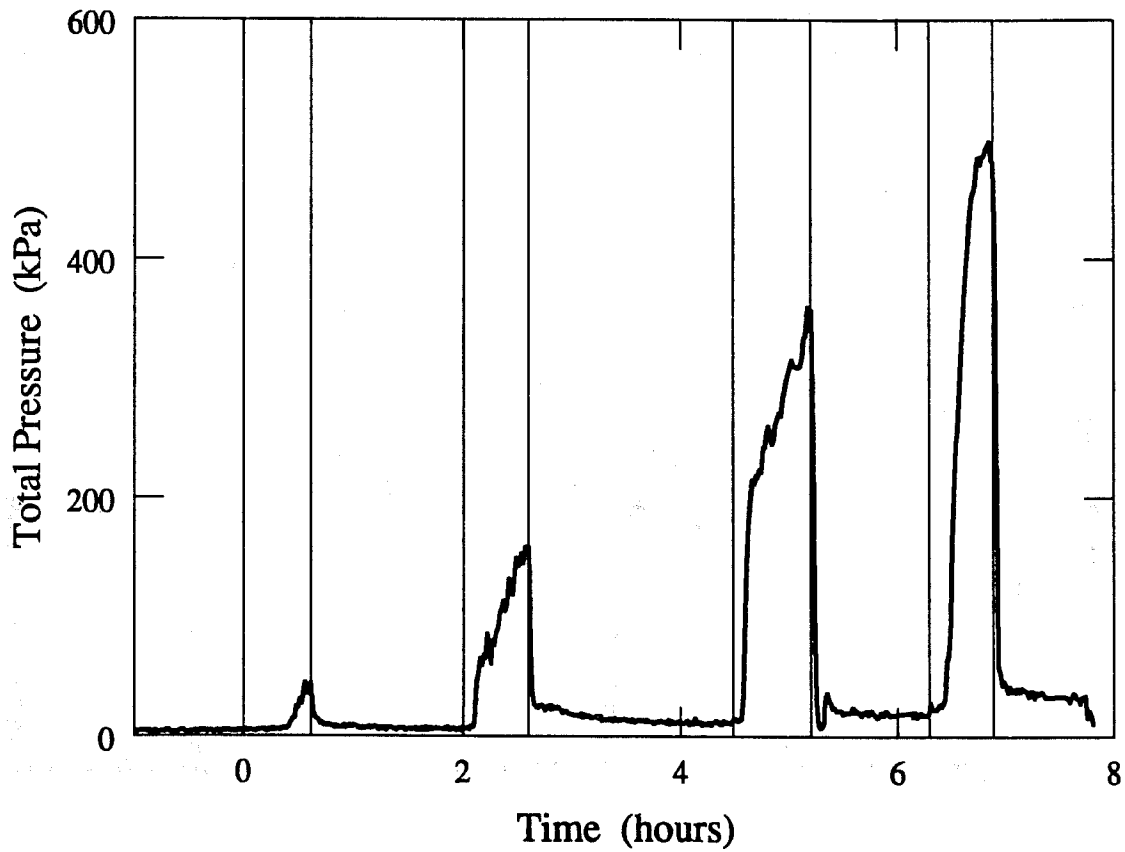


Figure 3.2.8 Total pressure drop response to injection of four consecutive 0.10% slugs of Chevron chaser SD 1000.

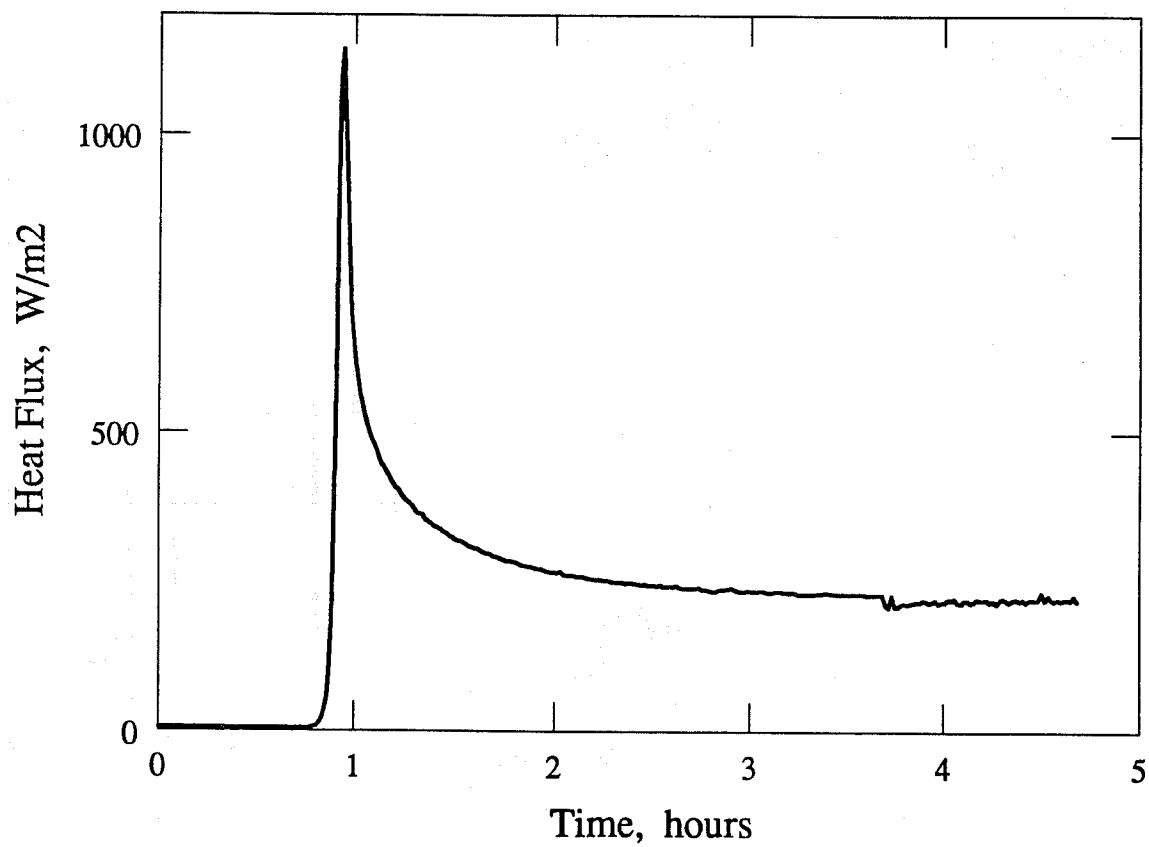


Figure 3.2.9 Average heat flux from sandpack to insulation measured at exterior tube wall at a distance 65.1 cm from tube inlet for typical steamflood.

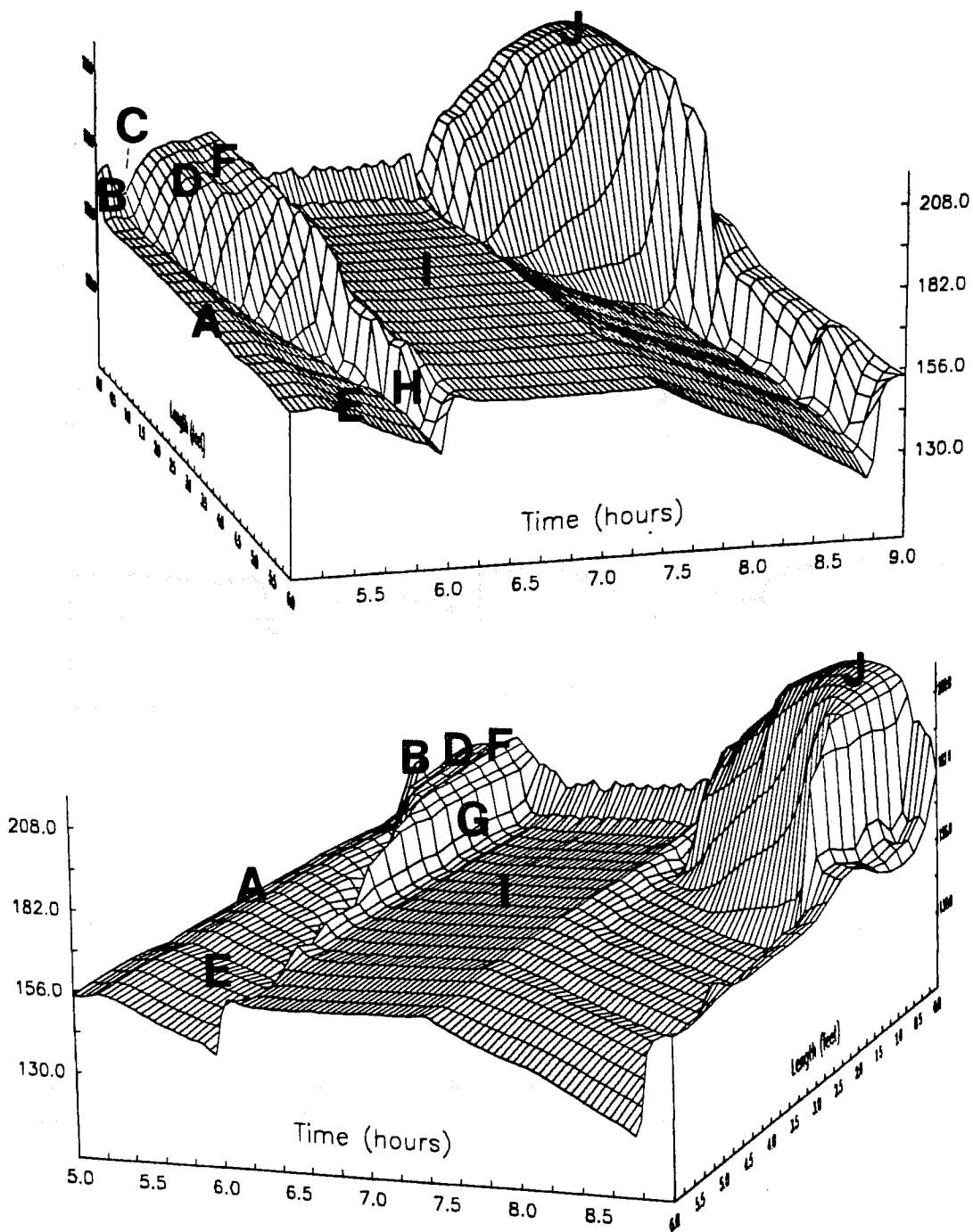


Figure 3.2.10 Two view of the sandpack temperature response to injection of two 0.10% slugs of AOS 1618.

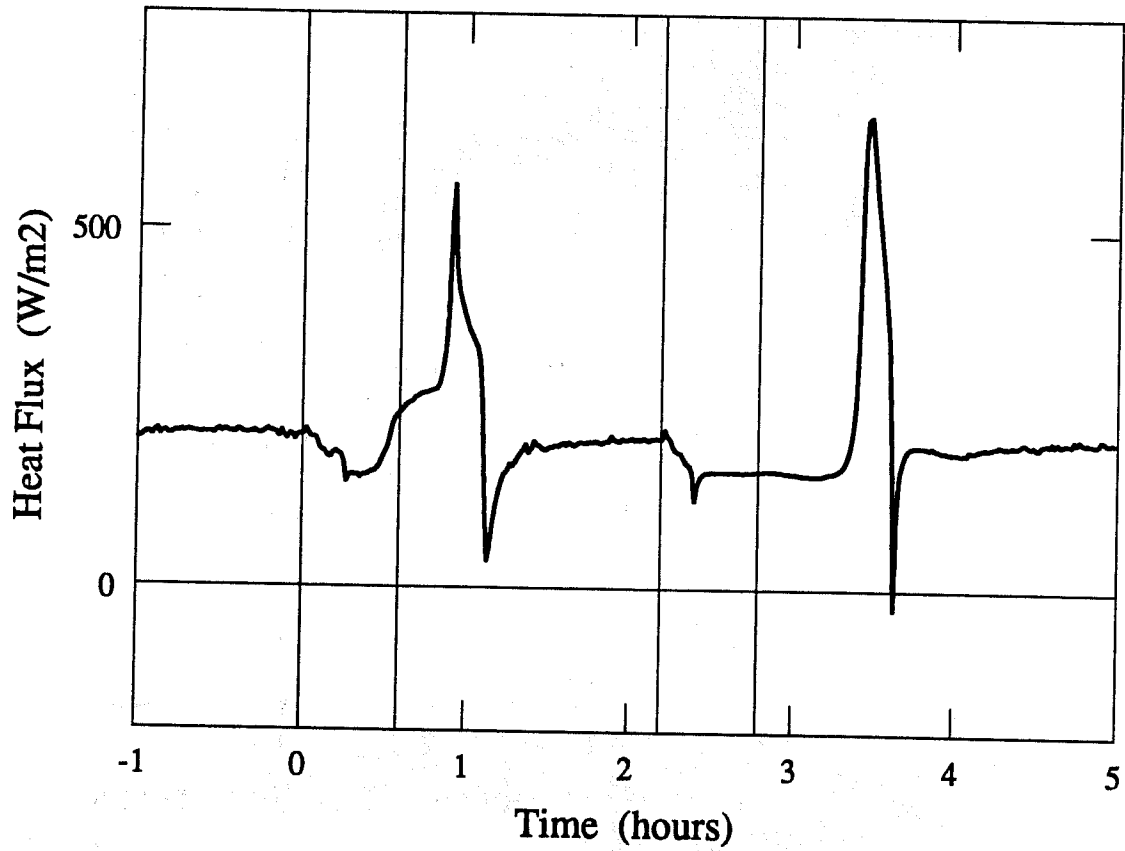


Figure 3.2.11 Average heat flux from sandpack to insulation measured at exterior tube wall at a distance 65.1 cm from tube inlet during injection of two 0.10% slugs of AOS 1618.

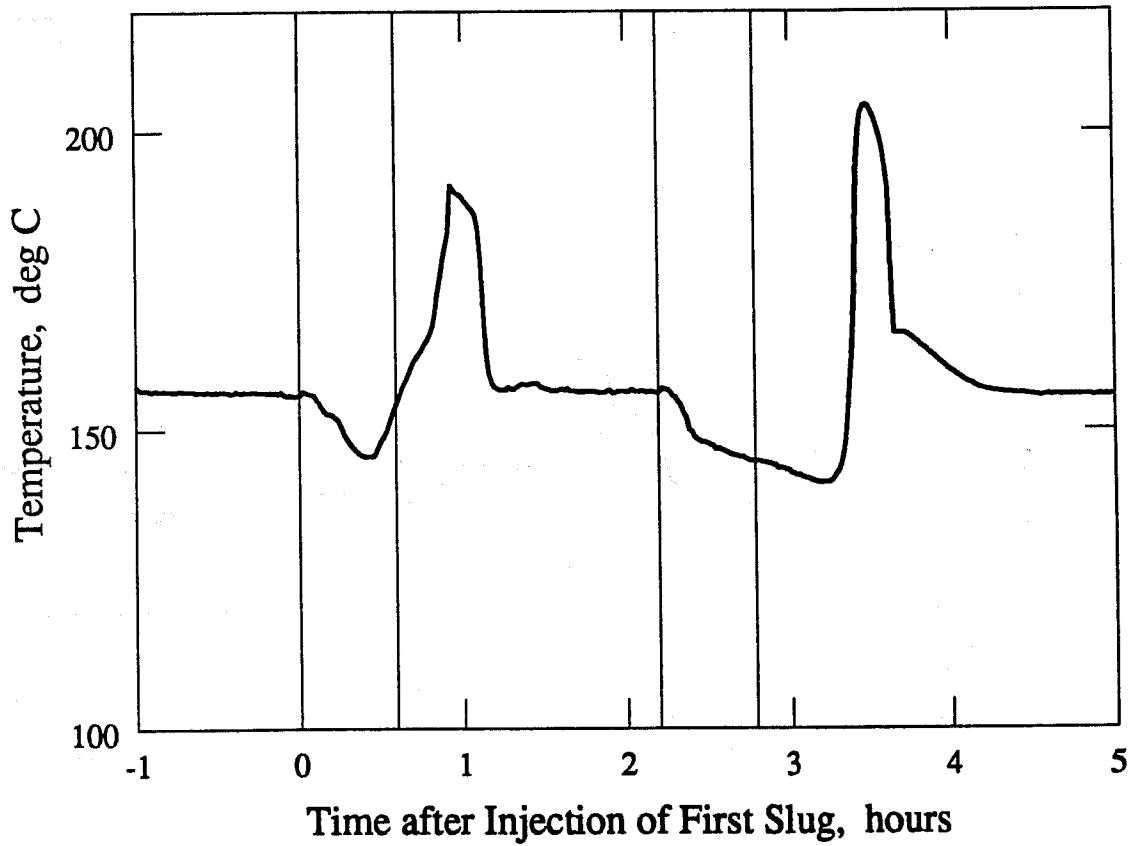


Figure 3.2.12 Sandpack temperature at a distance 65.1 cm from tube inlet during injection of two 0.10% slugs of AOS 1618.

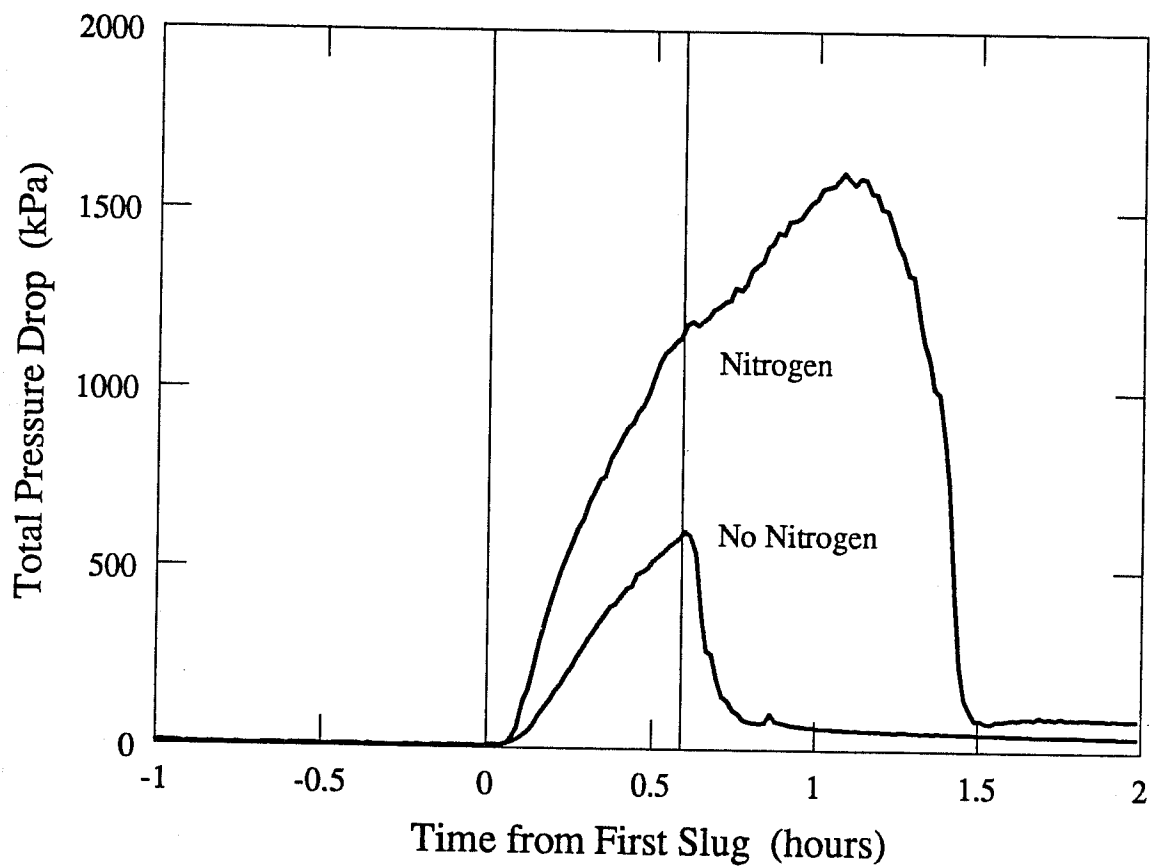


Figure 3.2.13 Total pressure drop response to injection of a 0.10% slug of AOS 2024 in presence and absence of the noncondensable gas.

#### **PROJECT 4: RESERVOIR DEFINITION**

This project involves developing and improving techniques of formation evaluation such as tracer tests and pressure transient tests.

## 4.1 SINGLE WELL TRACER STUDIES (M. Riley)

### 4.1.1. INTRODUCTION

The purpose of the present research is to simplify already existing solutions to the radial Convection-Dispersion (C-D) equation. These solutions are quite complex, even in Laplace space. Since this topic was presented in last year's Annual Report, the introductory material will be omitted for brevity. The reader is referred to the Eleventh Annual Report of the SUPRI Heavy Oil Program, Section 4.2, for more background information.

As indicated in the last annual report, the two methods used to find simplified solutions were changing of variables and perturbation. It was also stated that group theory might give some insights to the nature of the equation. The groups of the radial C-D equation have been calculated and show that the equation has very little symmetry. This shows why attempts at changing variables failed. Since perturbation also failed it was decided to abandon this research topic until other methods of solution can be found.

This report is a review of the effort from January through June 1988. It will consist of two sections; Perturbation and Change of Variables. The first section will complete the tabulation of the Green's functions for the one dimensional C-D equation that were used in the perturbation scheme. The second section will give the groups for the one dimensional C-D and radial C-D equation and show why attempts at changing variables failed.

### 4.1.2. PERTURBATION

The radial C-D equation can be written in dimensionless form as:

$$\frac{\partial^2 C}{\partial r^2} - \frac{\partial C}{\partial r} = \frac{r}{\bar{r}} \frac{\partial C}{\partial \bar{r}}. \quad (4.1.1)$$

Where  $\bar{r}$  is the material balance front position. Rearranging and adding  $\partial C/\partial \bar{r}$  to both sides gives:

$$\frac{\partial^2 C}{\partial r^2} - \frac{\partial C}{\partial r} - \frac{\partial C}{\partial \bar{r}} = \left( \frac{r}{\bar{r}} - 1 \right) \frac{\partial C}{\partial \bar{r}}. \quad (4.1.2)$$

The left side of this equation is essentially the linear C-D equation in dimensionless form. The right side of this equation will be zero when  $r = \bar{r}$ . For this reason it was hoped that a perturbation solution could be found by assuming the right hand side to be zero and solving the left hand side together with the boundary conditions. Each additional term would be found by solving the same equation with the right hand side set equal to the right hand side of Eq. 4.1.2 evaluated using the previous solution.

At each stage the equation being solved is:

$$\frac{\partial^2 C}{\partial r^2} - \frac{\partial C}{\partial r} - \frac{\partial C}{\partial \bar{r}} = F(r, \bar{r}). \quad (4.1.3)$$

Where  $F(r, \bar{r})$  is a known function. Equation 4.1.3 is essentially the inhomogeneous form of the 1-D C-D equation. All of the cases we are interested in have an infinite outer boundary distance. In this case the general solution of Eq. 4.1.3 can be written as:

$$C(r, \bar{r}) = - \int_0^{\infty} \int_0^{\bar{r}} F(\xi, \tau) G(\xi, \tau; r, \bar{r}) d\tau d\xi - \int_0^{\bar{r}} G(0, \tau; r, \bar{r}) \frac{\partial C(0, \tau)}{\partial \xi} - C(0, \tau) \frac{\partial G(0, \tau; r, \bar{r})}{\partial \xi} - G(0, \tau; r, \bar{r}) C(0, \tau) d\tau + \int_0^{\infty} G(\xi, 0; r, \bar{r}) C(\xi, 0) d\xi. \quad (4.1.4)$$

The  $G(\xi, \tau; r, \bar{r})$  in Eq. 4.1.4 is the Green's function for the problem. The form of  $G$  will depend on what kind of inner boundary condition we have.  $G$  is chosen so that the second integral in Eq. 4.1.4 contains only known terms, i.e. if  $C$  is given at  $r = 0$  we want to eliminate the  $\partial C/\partial r$ , so we want  $G(0, \tau; r, \bar{r})$  to equal zero. Similar considerations are used to specify the requirements on  $G$  for other boundary conditions.

The following are the Green's functions for the for most common inner boundary conditions when the outer boundary is at positive infinity.

For a fully infinite system, i.e. the inner boundary at negative infinity, we want  $G$  and its derivative to vanish at negative infinity so that the entire second integral will vanish. This will be called  $G_{FS}$  for the free space Green's function.

$$G(\xi, \tau, r, \bar{r}) = \frac{e^{-\left[\frac{(r-\xi) - (\bar{r}-\tau)}{2\sqrt{\bar{r}-\tau}}\right]^2}}{2\sqrt{\pi(\bar{r}-\tau)}} = G_{FS}. \quad (4.1.5)$$

This is very similar to the free space Green's function for the 1-D diffusivity equation, which is not surprising since the two equations are closely related.

If the inner boundary is at zero and  $C$  is given there, we want  $G$  to vanish at the inner boundary. This solution will be the sum of  $G_{FS}$  and something we will call  $G_I$ , because it is closely related to the image of  $G_{FS}$ , (although it is not simply the image of  $G_{FS}$  in  $\xi = 0$ ).

$$G(\xi, \tau, r, \bar{r}) = \frac{e^{-\left[\frac{(r-\xi) - (\bar{r}-\tau)}{2\sqrt{\bar{r}-\tau}}\right]^2}}{2\sqrt{\pi(\bar{r}-\tau)}} - \frac{e^r e^{-\left[\frac{(r+\xi) + (\bar{r}-\tau)}{2\sqrt{\bar{r}-\tau}}\right]^2}}{2\sqrt{\pi(\bar{r}-\tau)}}. \quad (4.1.6)$$

or

$$G(\xi, \tau, r, \bar{r}) = G_{FS} - G_I. \quad (4.1.7)$$

If the flux is specified at the inner boundary, the so called Danckwerts condition,  $C - (\partial C/\partial r)$  is given. In this case we want  $\partial G/\partial \xi$  to equal zero at  $\xi$  equal zero.

$$G(\xi, \tau, r, \bar{r}) = G_{FS} + G_I - e^r \operatorname{erfc} \left[ \frac{(r+\xi) + (\bar{r}-\tau)}{2\sqrt{\bar{r}-\tau}} \right]. \quad (4.1.8)$$

In Eq. 4.1.8,  $\operatorname{erfc}$  is the complementary error function.

If the  $\partial C/\partial r$  is specified at  $r = 0$ , then we want  $G + \partial G/\partial \xi$  to equal zero. This boundary condition is used for problems where fluid is produced at  $r = 0$ . In this case the inner boundary condition is usually  $\partial C/\partial r = 0$ .

$$G(\xi, \tau, r, \bar{r}) = G_{FS} + G_I + e^{-r} \operatorname{erfc} \left[ \frac{(r+\xi) - (\bar{r}-\tau)}{2\sqrt{\bar{r}-\tau}} \right]. \quad (4.1.9)$$

This completes the tabulation of the Green's functions for the semi-infinite and infinite core. They have been checked for specific cases where known solutions are available, although before they are used they should be rechecked. The author will be happy to provide the derivations and a more detailed discussion on request.

### 4.1.3. CHANGE OF VARIABLES

As discussed in the last Annual Report, the attempts at changing the radial C-D equation into an equation similar to the linear C-D equation failed. In order to find out how closely related the two equations are the Lie groups of the two equations were calculated.

There does not seem to be a simple way to explain what these Lie groups are, but the basic idea is to find all the possible changes of variables that leave the equation invariant, i.e. the equation in the new variables has exactly the same form as the equation in the original variables. The method for doing this is to determine the infinitesimal symmetry groups and from these to calculate the change of variables. This area is a rapidly growing field and the author makes no claim of having full knowledge of the subject. Unfortunately, there do not seem any very good texts on the subject: Bluman and Cole (1974), the standard reference on the subject, is difficult to understand; Seshadri and Na (1985) is much easier to understand and has many examples, but seems to be in error on some important points. A more thorough treatment is given by Olver (1986); his treatment is much too theoretical for the practicing engineer, but he does present an extensive literature review and includes many important points in the exercises.

The symmetry groups for the linear C-D Equation,

$$\frac{\partial^2 C}{\partial x^2} - \frac{\partial C}{\partial x} = \frac{\partial C}{\partial t}, \quad (4.1.10a)$$

are:

$$t \rightarrow 4A_6 t^2 + 4A_4 t + A_2 \quad (4.1.10b)$$

$$x \rightarrow 4A_6 x t + 2A_4 x + 2A_5 t + A_1 \quad (4.1.10c)$$

$$C \rightarrow C[-A_6((x-t)^2 + 2t) + A_4(x-t) - A_5(x-t) + A_3] + C_1(x,t). \quad (4.1.10d)$$

These symmetry groups can now be used to determine the change of variables that leave Eq. 4.1.10a invariant. For example, the parameter  $A_2$  occurs only in the group corresponding to time, this is because changing the time variable to a constant plus time will leave 4.1.10a unchanged. The same is true for the parameter  $A_1$ , although the explanation of the other parameters is more involved. The values of the parameters,  $A_1$  through  $A_6$ , are arbitrary; what is important is that Eq. 4.1.10a possesses six parameter symmetry groups. This is a high degree of symmetry for a second order P.D.E in two independent variables. The more symmetric the equations the more likely they are to have simple closed form solutions. And

comparing symmetry groups can tell how closely related two equations are. For example, the symmetry groups for the linear diffusivity equation,

$$\frac{\partial^2 P}{\partial x^2} = \frac{\partial P}{\partial t}, \quad (4.1.11a)$$

are:

$$t \rightarrow 4A_6 t^2 + 4A_4 t + A_2 \quad (4.1.11b)$$

$$x \rightarrow 4A_6 x t + 2A_4 x + 2A_5 t + A_1 \quad (4.1.11c)$$

$$P \rightarrow P[-A_6(x^2 + 2t) - A_5 x + A_3] + P_1(x, t). \quad (4.1.11d)$$

These symmetry groups are very closely related to those of the linear  $C-D$  equation. The groups for the independent variables are identical and the group for  $C$  has terms  $x-t$  wherever the the group for  $P$  has an  $x$ . This is not a coincidence. The two partial differential equations are closely related and there are at least two ways to transform Eq. 4.1.10a into Eq. 4.1.11a. In fact one way to is to replace  $x$  in Eq. 4.1.10a by  $x-t$ , the distance from the front position.

Now, the groups for the radial  $C-D$  equation,

$$\frac{\partial^2 C}{\partial r^2} - \frac{\partial C}{\partial r} = r \frac{\partial C}{\partial t}, \quad (4.1.12a)$$

are:

$$t \rightarrow A_2 \quad (4.1.12b)$$

$$r \rightarrow 0 \quad (4.1.12c)$$

$$C \rightarrow CA_1 + C_1(r, t). \quad (4.1.12d)$$

This is very disappointing. The only change of variables that leave the radial  $C-D$  equation invariant are those that can be found by inspection: adding a constant to time, multiplying  $C$  by a constant or adding to  $C$  any solution of 4.1.12a. These symmetry groups indicate that Eq. 4.1.12a possesses very little symmetry and that although it looks very much like Eq. 4.1.10a, these two equations are not closely related. The lack of symmetry also indicates that simple solutions to the equation probably do not exist. It was at this point that the decision was made to abandon the project.

#### 4.1.4. REFERENCES

1. Bluman, G.W. and Cole J.D.,: "Similarity Methods for Differential Equations", Appl. Math. Sci., No. 13, Springer Verlag, New York, 1974.
2. Seshadri, R. and Na, T.Y.,: "Group Invariance in Engineering Boundary Value Problems", Springer Verlag, New York, 1985.
3. Olver, P.J.,: "Applications of Lie Groups to Differential Equations", Springer Verlag, New York, 1986.

## 4.2 THERMAL RECOVERY WELL TEST DESIGN AND INTERPRETATION (A. Ambastha)

A technical report on this topic is in the draft stage. The following is an abstract of this work.

A composite reservoir model is used to analyze well-tests from a variety of enhanced oil recovery projects, geothermal reservoirs, and acidization projects. A composite reservoir is made up of two or more regions. Each region has its own rock and fluid properties. Transient pressure behavior of a well in a two-region composite reservoir has been considered extensively in the literature, and several methods have been proposed to estimate front (or discontinuity) radius, or swept volume. This study considers transient pressure derivative behavior of a well in a two-region composite reservoir to establish the applicability and the limitations of different methods to estimate front radius or swept volume. A finite-radius well with wellbore storage and skin is assumed to produce (or inject) at a constant rate. Three outer boundary conditions are considered: infinite, closed, and constant-pressure. A study of drawdown and buildup responses has resulted in a set of correlating parameters for the pressure derivative responses, and new design and interpretation relations for well-tests in composite reservoirs. Guidelines have been presented for the applicability of different methods to estimate front radius. Producing time effects on buildup responses show that analyzing a well-test after short producing (or injection) time may be difficult.

Dynamic phenomena, such as phase changes and multi-phase flow effects in a region near the front, can cause a sharp pressure drop at the front. Such a sharp pressure drop is modeled as a thin skin at the front in this study. An analytical solution for the transient pressure behavior of a well in a two-region composite reservoir with a skin at the front is obtained using the Laplace transformation. A thin skin at the front can explain a short duration pseudosteady state even for small mobility and storativity contrasts. The effects of a skin at the front are similar to the effects of storativity ratio. Thus, neglecting a thin skin at the front can cause large errors in parameter estimation using a type-curve matching method.

Pressure derivative behavior of a well in a homogeneous, or a three-region composite reservoir is also discussed. Several well tests from composite reservoirs are analyzed to establish the applicability and the limitations of the deviation time method to estimate front radius.

### 4.3 FLOW THROUGH PERFORATIONS (G. Ahmed)

For the background of this work, please refer to SUPRI Eleventh Annual report.

#### 4.3.1. SOLUTION BY GREEN'S FUNCTION

This approach follows developments in potential theory. A solution is first developed for a point source of known strength. The point source is then integrated to form a line source of uniform strength. The line source simulates the perforation with a uniform flux. Two alternative solutions are developed, the first involves Bessel's functions in the solution with the eigenvalues derived from an algebraic equation of Bessel's functions. For the second solution, eigenvalues are simply written down from a trigonometric identity and the solution contains expressions of Modified Bessel's functions.

#### 4.3.2. BESSEL'S FUNCTION SOLUTIONS

A point source solution is developed for a hollow cylindrical box with no flow at the internal boundary (the cased well) and with a choice of condition at the external boundary. The point source solution is then integrated to a line source solution which approximates the solution to a perforation with uniform flux.

##### Point Source Solution

Potential ( $V$ ) at any point  $(r, \phi, z)$  for a point source of steady strength  $q$  located at  $(r_0, \phi_0, z_0)$  in a cylindrical box of inner radius  $r_w$  and outer radius  $r_e$  and thickness  $h$  for no flow at  $r = r_w, z = 0, z = h$ , and constant potential (zero) at  $r = r_e$ , is given by:

For  $z < z_0$

$$V(r, \phi, z) = \frac{q\mu}{2\pi\kappa} \sum_{n=0}^{\infty} \sum_{r=1}^{\infty} k_r (2 - \delta_n^0) \frac{2 \cosh(k_r z) \cosh(k_r (h - z_0))}{\sinh(k_r h)} \frac{\hat{R}_n(k_r r_0) R_n(k_r r)}{b^2 \hat{R}_{n+1}(b) R_{n+1}(b) - (a^2 - n^2) \hat{R}_n(a) R_n(a)} \cos(n(\phi - \phi_0)) \quad (4.3.1)$$

where

$$a = k_r r_w$$

$$b = k_r r_e$$

$n$  and  $r$  are integers

and,

$$R_n = J_n(k_r r) - \frac{J'_n(a)}{Y'_n(a)} Y_n(k_r r) \quad (4.3.2)$$

$$\hat{R}_n = J_n(k_r r) + \frac{J'_n(a)}{Y'_n(a)} Y_n(k_r r) \quad (4.3.3)$$

$$\delta_n^0 = \begin{cases} 1 & \text{if } n = 0 \\ 0 & \text{if } n \neq 0 \end{cases} \quad (4.3.4)$$

The eigenvalues ( $k_r$ ) for  $r$  varying from 1 to  $\infty$  are obtained from the following equation:

$$J_n(k_r r_e) Y'_n(k_r r_w) - J'_n(k_r r_w) Y_n(k_r r_e) = 0 \quad (4.3.5)$$

For  $z > z_0$ ,  $z$  and  $z_0$  are interchanged in the right-hand side of Eq. 4.3.1.

### Line Source Solution

Potential ( $V$ ) at any point ( $r, \phi, z$ ) for a line source of steady strength  $q$  (uniform along the length), located at  $z_0$  and  $\phi_0$  and length  $l_p$  is obtained by integrating the point source solution given by Eq. 4.3.1, with respect to  $r_0$  from  $r_0 = r_w$  to  $r_0 = r_w + l_p$ . Potential at a radial distance  $\alpha$  from the line source will be assumed to be the potential at the perforation surface.  $\alpha$  is the radius of the actual perforation.

$$V(r, \phi, z) = \frac{q' \mu}{2\pi\kappa} \sum_{n=0}^{\infty} \sum_{r=1}^{\infty} \int_{r_0=r_w+\epsilon}^{r_w+l_p} k_r (2 - \delta_n^0) \frac{2 \cosh(k_r z) \cosh(k_r (h-z_0))}{\sinh(k_r h)} \frac{\hat{R}_n(k_r r_0) R_n(k_r r)}{b^2 \hat{R}_{n+1}(b) R_{n+1}(b) - (a^2 - n^2) \hat{R}_n(a) R_n(a)} \cos[n(\phi - \phi_0)] dr_0 \quad (4.3.6)$$

where,  $q'$  is source strength per unit length of the perforation.

### 4.3.3. MODIFIED BESSEL'S FUNCTION SOLUTION

As in the solution with Bessel's function, a point source solution is developed for a hollow cylindrical box with no flow at the internal boundary but a choice of condition at the external boundary. The point source solution is then integrated to a line source solution which approximates the solution to a perforation with uniform flux.

### Point Source Solution

Potential ( $V$ ) at any point ( $r, \phi, z$ ) for a point source of steady strength  $q$  located at  $(r_0, \phi_0, z_0)$  in a cylindrical box of inner radius  $r_w$  and outer radius  $r_e$  and thickness  $h$  for no

flow at  $r = r_w$ ,  $z = 0$ ,  $z = h$  and constant potential (zero) at  $r = r_e$ , is given by:

$$r_w \leq r < r_0$$

$$V(r, \phi, z) = \frac{q\mu}{\pi\kappa h} \sum_{n=0}^{\infty} \sum_{m=1}^{\infty} \frac{(2 - \delta_n^0)}{\hat{R}_n \left[ \frac{m\pi}{h}, r_w, r_e \right]} \cos \left[ \frac{m\pi}{h} z_0 \right] \cos \left[ \frac{m\pi}{h} z \right] \\ R_n \left[ \frac{m\pi}{h}, r_0, r_e \right] R_n \left[ \frac{m\pi}{h}, r_w, r \right] \cos \left[ n(\phi - \phi_0) \right] \quad (4.3.7a)$$

$$r_0 < r \leq r_e$$

$$V(r, \phi, z) = \frac{q\mu}{\pi\kappa h} \sum_{n=0}^{\infty} \sum_{m=1}^{\infty} \frac{(2 - \delta_n^0)}{\hat{R}_n \left[ \frac{m\pi}{h}, r_w, r_e \right]} \cos \left[ \frac{m\pi}{h} z_0 \right] \cos \left[ \frac{m\pi}{h} z \right] \\ R_n \left[ \frac{m\pi}{h}, r_w, r_0 \right] R_n \left[ \frac{m\pi}{h}, r, r_w \right] \cos \left[ n(\phi - \phi_0) \right] \quad (4.3.7b)$$

where  $n$  and  $m$  are integers,  $\delta_n^0$  is defined at (4.3.11) and,  $\hat{R}_n$  and  $R_n$  are expressions containing the Modified Bessel's functions of the first and second kinds. These expressions are defined in the following:

$$\hat{R}_n \left[ \frac{m\pi}{h}, r_w, r_e \right] = K_n \left[ \frac{m\pi}{h} r_e \right] I'_n \left[ \frac{m\pi}{h} r_w \right] - I_n \left[ \frac{m\pi}{h} r_e \right] K'_n \left[ \frac{m\pi}{h} r_w \right] \quad (4.3.8)$$

The following expressions are applicable if the point of observation lies between the inner boundary  $r = r_w$  and the location of the point source  $r = r_0$  which is a singularity.

$$R_n \left[ \frac{m\pi}{h}, r_0, r_e \right] = I_n \left[ \frac{m\pi}{h} r_0 \right] K_n \left[ \frac{m\pi}{h} r_e \right] - I_n \left[ \frac{m\pi}{h} r_e \right] K_n \left[ \frac{m\pi}{h} r_0 \right] \quad (4.3.9)$$

$$R_n \left[ \frac{m\pi}{h}, r_w, r \right] = I_n \left[ \frac{m\pi}{h} r \right] K'_n \left[ \frac{m\pi}{h} r_w \right] - I'_n \left[ \frac{m\pi}{h} r_w \right] K_n \left[ \frac{m\pi}{h} r \right] \quad (4.3.10)$$

The following expressions are applicable if the point of observation lies between the location of the point source  $r = r_0$  and the outer boundary  $r = r_e$ .

$$R_n \left[ \frac{m\pi}{h}, r_w, r_0 \right] = I_n \left[ \frac{m\pi}{h} r_0 \right] K'_n \left[ \frac{m\pi}{h} r_w \right] - I'_n \left[ \frac{m\pi}{h} r_w \right] K_n \left[ \frac{m\pi}{h} r \right] \quad (4.3.11)$$

$$R_n \left[ \frac{m\pi}{h}, r, r_e \right] = I_n \left[ \frac{m\pi}{h} r \right] K_n \left[ \frac{m\pi}{h} r_e \right] - I_n \left[ \frac{m\pi}{h} r_e \right] K_n \left[ \frac{m\pi}{h} r \right] \quad (4.3.12)$$

### Line Source Solution

Potential ( $V$ ) at any point ( $r, \phi, z$ ) for a line source of steady strength  $q$  (uniform over the length), is obtained by integrating the point source solution given by Eq. 4.3.7.

$$V(r, \phi, z) = \frac{q'\mu}{\pi\kappa h} \sum_{n=0}^{\infty} \sum_{m=1}^{\infty} \frac{(2 - \delta_n^0)}{\hat{R}_n \left[ \frac{m\pi}{h}, r_w, r_e \right]} \cos [n(\phi - \phi_0)] \cos \left[ \frac{m\pi}{h} z \right] R_n \left[ \frac{m\pi}{h}, r, r_e \right] \cos \left[ \frac{m\pi}{h} z_0 \right] \int_{r_0=r_w+\epsilon}^{r_w+l_p} R_n \left[ \frac{m\pi}{h}, r_w, r_0 \right] dr_0 \quad (4.3.13)$$

### Cylindrical Source Solution

Potential ( $V$ ) at any point ( $r, \phi, z$ ) for a cylindrical source of steady strength  $q$  (uniform over the length), is obtained by generating the surface of a cylinder using a number of coordinate transformations:

$$V(r, \phi, z) = 2 a \cos^2 \theta \int_{r_0=r_w+\epsilon}^{r_w+l_p} r_0 dr_0 \int_{\frac{-a}{r_0}}^{\frac{a}{r_0}} \phi_0 d\phi_0 \int_{-\sqrt{(a^2-r_0^2\phi_0^2)}}^{\sqrt{(a^2-r_0^2\phi_0^2)}} S(r_0, \phi_0, z_0) G(r, \phi, z; r_0, \phi_0, z_0) dz_0 \quad (4.3.14)$$

where

$$S(r_0, \phi_0, z_0) = \frac{r_0^2 (-\cos\phi_0 \sin\theta + \sin\phi_0 \cos\theta)^2 - z_0^2}{(r_0^2 (-\cos\phi_0 \sin\theta + \sin\phi_0 \cos\theta)^2 + z_0^2)^2} \quad (4.3.15)$$

$G(r, \phi, z; r_0, \phi_0, z_0)$  is given by Eq. 4.3.7

$a$  is the radius of perforation

$\theta$  is the horizontal angle of the axis of the perforation

### 4.3.4. COMPUTATION

Complete cylindrical source solution given by Eq. 4.3.14 involves double infinite summation and triple integration. This would be very difficult to compute. The approximation of taking the perforation as a line source is considered adequate for use. Even the point source

solution given by Eq. 4.3.7. is difficult to compute, particularly when the point of observation is close to the source. The solution involves complex expressions of modified Bessel functions and their derivatives. The double infinite summation is over the order and the argument of these functions. It involves operations on extremely small and extremely large values of these functions resulting in over and under flow of the computer capacity. This makes the solution difficult to converge.

The zero length perforation solution has been computed and compared with an electrolytic analog study reported by McDowel and Musket. The results show fairly good agreement, which confirms the accuracy of the solution.

## **PROJECT 5: FIELD SUPPORT SERVICES**

This project aims at providing technical support for design, such as the use of numerical thermal simulators to study practical field problems, monitoring of DOE sponsored or industry initiated field projects, and economic evaluation procedures.

## 5.1 A COMPARISON OF NEWTON AND QUASI-NEWTON METHODS FOR PARALLEL RESERVOIR SIMULATORS (J. Barua and R. Horne)

### 5.1.1. ABSTRACT

Parallel computers hold much promise for scientific computation. So a great deal of effort has been devoted to finding ways to parallelize linear equation solvers.

However in fully implicit reservoir simulators the original problem is the solution of nonlinear equations. These nonlinear equations are usually solved using Newton's method. This report explores the use of Quasi-Newton methods to solve the nonlinear equations in parallel.

The Quasi-Newton method turns out to have certain advantages and disadvantages. For example, using QN one can take the highly parallel *iterative* Jacobi matrix solution techniques, which are poorly convergent, and still get good serial performance. However the Quasi-Newton method does not do as well as Newton's method when using a preconditioned conjugate-gradient scheme - unless the cost of factorizing the preconditioner is high.

Experiments on a parallel computer show that even with a highly parallel method, problem sizes need to be quite large to get good efficiency.

The Quasi-Newton method can also be used to speed up serial programs if the cost of factorizing the preconditioner is high or if a simple iterative scheme is used.

### 5.1.2. INTRODUCTION

There is great current interest in parallel computing in all scientific fields. It is easy to see why. The fastest supercomputers today use cycle times of a few nanoseconds. Considering that light itself can only travel 11.78 inches in one nanosecond (electricity travels even less) supercomputers seem to be approaching the point of diminishing returns.

Parallel computers capable of similar absolute performance can be made at a much lower total cost. It is likely that parallel computers will eventually greatly exceed the performance of conventional supercomputers, so they represent an important new factor for reservoir simulation.

The form of parallel computers has not yet been standardized. Different approaches to solve the hardware issues have resulted in different types of parallel computers, e.g. message-passing, shared-memory, data-flow, systolic arrays and connectionist machines. Of these the first two types seem to be the most promising for general purpose use.

Writing parallel software has proved to be a problem though. It is relatively simple to make good use of 3-4 processors working in parallel. In some cases this can be done automatically on existing serial code by the compiler and/or the hardware. But it is difficult to make effective use of say 100 processors working in parallel. It is this latter type of machine that holds the most promise and our interest is in programs for these machines.

Usually one is forced to use an algorithm that is less than optimal for a serial computer in order to make best use of the parallel computer. Furthermore, one cannot rely on the compiler/hardware to automatically detect and take advantage of concurrency; rather the code will have to be explicitly written to run in parallel.

The remainder of this report discusses some of the issues involved in writing such a reservoir simulator. We begin by showing why it is so difficult to get good speedup on parallel machines. We then describe Quasi-Newton methods and indicate how they apply to this problem. Next we describe some of the details of parallel machines and programs for them, followed by results of our parallel simulator. Finally we compare the Quasi-Newton method with existing methods.

### 5.1.3. AMDAHL'S LAW AND MATRIX SOLUTION

It is widely known that the matrix solution step in a simulator is the most difficult part to parallelize. Since matrix problems are common to virtually all scientific fields, much research is currently being devoted to parallelizing the problem.

Amdahl's law (1967) shows why this is so difficult to parallelize. It basically states that the time for a given computation  $T$ , is the sum of two components: a serial component  $S$  that must be performed in serial, and a parallel component  $P$  that can be performed in parallel. Therefore, on a single-processor machine the total time is:

$$T_1 = S + P \tag{5.1.1}$$

Now supposing that we lose no time for synchronization/communication etc. when running in parallel on  $p$  processors, the time for same process will then be:

$$T_p = S + P/p \tag{5.1.2}$$

where the subscript  $p$  indicates time on the  $p$  processor parallel machine. The achieved speedup is then:

$$\frac{T_1}{T_p} = \frac{S + P}{S + P/p} \tag{5.1.3}$$

Consider a triangular matrix, trivially solvable on a serial computer, it is a major challenge for a parallel computer. Such matrices arise during back-substitution in direct solvers and also in the more powerful iterative solvers. Since one element of the solution can only be obtained after the previous element has been obtained, there is an unavoidable serial component in solving this matrix.

Some degree of parallelism is possible in that once the  $i$ th element is known, the entire  $i$ th column can be subtracted from the right-hand side in parallel. However, this requires synchronization/communication between processors because all must wait until the element is determined before proceeding. In the case of a sparse matrix, each processor might only be able to perform the subtraction on just one element of the right-hand side. The time wasted in synchronization/communication might outweigh what is saved by performing in parallel.

For the sake of a specific illustration, let us assume that 20% of the time is spent in serial only code and 80% in parallelizable code. Then substituting in Eq. 5.1.3 we find that speedup is,

$$\frac{T_1}{T_p} = \frac{1.0}{0.2 + 0.8/p} \quad (5.1.4)$$

Using Eq. 5.1.4 we find that with 100 processors the speedup would be just 4.8. The speedup with an infinite number of processors is 5. Actual speedup will be even less because of time lost in synchronization or communication.

Similar loss of parallelism also occurs (to a lesser degree) when factorizing a sparse matrix. A sparse matrix limits the gain obtained by eliminating rows or columns in parallel.

The simple illustration above shows how even a small serial component costs dearly when trying to get the maximum speedup on a parallel computer. Because of this effect, it has been widely believed that there was an upper limit of about 200 on the speed-up possible in useful scientific computation.

Recently, Gustafson *et al.* (1988) debunked this belief (and became very famous) by showing speedups of 1000 on 1024 processors. This result was based on a modified form of Amdahl's law. They also report the speedup by Amdahl's law as shown here to be around 500. This means that only 0.1% of the time was spent on the serial component and in communication - a remarkable feat indeed.

Only one of their test cases had a matrix solution step, the others being explicit methods. They used a point-Jacobi Preconditioned Conjugate Gradient method to solve the matrix. This method is almost ideally suited for parallel computation, since the only serial component arises in the dot-products.

Interestingly, by using point-Jacobi, they were able to handle much larger problems than usual by storing only the main diagonal of the matrix. Instead of doing the matrix-vector product that occurs in each PCG iteration they used an additional function evaluation to obtain the result.

Their parallel speedup has been so spectacular that all other results (including those presented here) pale in comparison. However it remains to be seen whether such speedup will be possible with a more powerful matrix solution scheme, so there still is some room for other researchers.

Parallel matrix solvers have also appeared in petroleum applications. Scott *et al.* (1987) tried various parallel SOR methods. They concluded that the submatrix method showed the best potential speedup. This method had various parts of the reservoir at different iteration levels. A new iteration was begun before the previous one had completed the entire reservoir.

Killough and Wheeler (1987) tried domain decomposition as a preconditioner for an Orthomin (1976) accelerated iterative method. They have shown that a preconditioner consisting of block Gauss-Sidel (each block corresponding to a domain) combined with Watts (1971) line corrections results in a powerful method. This method compares favorably with current serial methods. Efrat and Tismenetsky (1986) proposed a Bi-Conjugate Gradient algorithm that also compares favorably with current serial methods.

Our objective is not to develop parallel matrix solution methods but to apply these techniques to solving the *nonlinear equations* in parallel. In principle, whichever matrix solution method eventually emerges as most parallel can be used - although it turns out that not all solution methods will benefit from using a Quasi-Newton approach.

#### 5.1.4. PARALLEL SOLUTION OF NONLINEAR EQUATIONS

A great deal of the time spent in reservoir simulation is on the matrix solutions. So any serial component in this step has a significant effect on the overall speedup achieved. The aim therefore is to find ways to minimize the serial component while obtaining times comparable to conventional serial methods when run on a single processor.

Algorithms that have the best potential parallel speedup, e.g. Jacobi-PCG or Jacobi-Orthomin, will usually converge slowly. Algorithms that do converge rapidly, (see Behie (1985) for a comparison of the more powerful ones) have significant serial component and so will fare badly under Amdahl's law. Domain decomposition is powerful but not as parallelizable as Jacobi methods - principally because of the need to transfer the results of the solutions in each domain.

While linear matrix solution in reservoir simulation is the most time-consuming, it is a step in the solution of a nonlinear system of equations:

$$\mathbf{f}(\mathbf{x}) = 0 \tag{5.1.5}$$

where  $\mathbf{f}$  is the system of equations that result (in the fully implicit black-oil case) after applying a finite-difference method on the oil, water and gas equations for each block and moving all the terms to the left hand side. Here  $\mathbf{x}$  is the vector of unknowns, i.e.  $P_o$ ,  $S_w$ , and  $S_g$  or  $R_s$ . It is common to linearize Eq. 5.1.5 by applying *Newton's* method and solving instead:

$$\mathbf{J}_k \mathbf{s}_k = -\mathbf{f}(\mathbf{x}_k) \tag{5.1.6}$$

where  $\mathbf{J}$  is the Jacobian of  $\mathbf{f}$  and  $\mathbf{s}_k$  is the correction added to  $\mathbf{x}_k$  in the  $k$ th Newton iteration. Most research is focused on methods to solve Eq. 5.1.6 in parallel. We looked at an alternative method of solving the non-linear problem, Eq. 5.1.5.

A class of such algorithms is based on building up secant information of  $f(\mathbf{x})$  as the non-linear iterations proceed. These are called *Quasi-Newton* methods.

### 5.1.5. QUASI-NEWTON METHODS

Quasi-Newton methods are the multi-dimensional analogue of the traditional 1-d secant method. These methods have been used successfully in the finite-element and ODE fields to improve the convergence of *modified-Newton* methods, i.e. methods where the Jacobian is factored once and subsequent Newton iterations only involve back-substitution.

Mattheis and Strang (1979) showed how a Quasi-Newton method could succeed where the modified-Newton method failed. A good reference work for Quasi-Newton methods is Dennis and Schnabel (1983). We briefly describe the method below using their nomenclature.

Suppose at the  $k$ th nonlinear iteration the method takes a step  $\mathbf{s}_k = \mathbf{x}_{k+1} - \mathbf{x}_k$ , causing a change  $\mathbf{y}_k = \mathbf{f}(\mathbf{x}_{k+1}) - \mathbf{f}(\mathbf{x}_k)$  to the nonlinear system of equations. Then the next Jacobian approximation, denoted by  $\mathbf{A}_{k+1}$ , must satisfy the secant passing through these two iterates, i.e.

$$\mathbf{A}_{k+1}\mathbf{s}_k = \mathbf{y}_k \quad (5.1.7)$$

This equation is termed the Quasi-Newton equation. Equation 5.1.7 has two known vectors i.e.  $\mathbf{s}_k$  and  $\mathbf{y}_k$  and an unknown matrix  $\mathbf{A}_{k+1}$ . It is impossible to uniquely solve Eq. 5.1.7 for the unknown matrix except in the 1- $d$  case, when we simply obtain a single number equal to the slope of the secant.

Because of the large number of matrices which satisfy Eq. 5.1.7, several different Quasi-Newton methods have been proposed, all of which attempt to update the current Jacobian approximation  $\mathbf{A}_k$  rather than obtain a new approximation  $\mathbf{A}_{k+1}$  from scratch. We have tried two of these methods namely the BFGS (Broyden, 1970) update and Broyden's (1965) first update. The BFGS (Broyden, 1970) update has certain desirable properties like maintaining the symmetry and positive definiteness of the Jacobian. Our testing, admittedly not exhaustive, showed that Broyden's (1965) update generally works better for the nonsymmetric Jacobians that arise in petroleum reservoir simulation.

Two significant differences occur when using a Quasi-Newton method to solve Eq. 5.1.5 instead of Newton's method. First, the convergence *is no longer quadratic, it is only super-linear* (i.e. faster than linear but possibly either much faster or only a little bit faster than linear).

The second significant difference is that  $\mathbf{s}_k$  is now the solution to the equation:

$$\mathbf{A}_k \mathbf{s}_k = -\mathbf{f}(\mathbf{x}_k) \quad (5.1.8)$$

in other words it is the solution of an *approximate* Jacobian.

We initially chose the approximate Jacobian so that it is easily solved by a highly parallelizable algorithm and tried to see if the secants improve it enough for us to solve Eq. 5.1.5. For instance for a point-Jacobi iteration the approximate Jacobian is  $A = \text{diagonal}(J)$ . We can, in principle, use any linear method that is applicable to a Newton scheme. However because of the various tradeoffs involved not all linear methods will benefit from the Quasi-Newton approach.

The inverse form of Broyden's (1965) update is particularly convenient for parallel processing. This is given as:

$$A_{k+1}^{-1} = A_k^{-1} + \frac{(s_k - A_k y_k) s_k^T A_k^{-1}}{s_k^T A_k^{-1} y_k} \quad (5.1.9)$$

Since this is a recurrence relation one could simply obtain  $A_0^{-1}$  once and then use Eq. 5.1.9 to convert it into  $A_1^{-1}$  and so on without any further inversions. Since matrix-vector products are highly parallelizable, having an inverse appears to be an attractive solution.

However, applying Eq. 5.1.9 directly is inadvisable for several reasons. Obtaining an inverse of a matrix is a costly and numerically undesirable process. Then the inverse of a sparse matrix may be dense therefore requiring substantial storage, finally the matrix-vector products are relatively expensive.

It is instead better to store  $A_0$  or its factors and a series of update vectors, and this is how the update is usually applied (Mattheis and Strong, 1979). While detailed steps are provided in the appendix, suffice it to say here that at the  $k$ th iteration we have to solve:

$$A_0 d_k = f(x_k) \quad (5.1.10)$$

for  $d_k$ , which subsequently undergoes some simple corrections, which all highly parallel, to give  $s_k$ . Now notice that this is a solution to the initial approximate Jacobian. We do not construct an approximate Jacobian though. Rather we simply set  $A_0 = J_0$  and solve Eq. 5.1.10 approximately.

We might try to spend less effort on Eq. 5.1.10 than in solving Eq. 5.1.6 since  $A_0$  is supposed to be only an approximation to the true Jacobian. We also save considerable effort if we store the factors of  $A_0$  during the first iteration. Thus if we use line-Jacobi we store the factors of the tri-diagonal system along each line, similarly we can store the factors for the domains in domain decomposition or we can store the LU factors of  $A_0$  when doing LU decomposition. Each subsequent iteration then only needs forward/back-substitution making it faster than the factor & forward/back-substitution needed for a Newton iteration.

The non-linear convergence rate of this algorithm is given by a theorem (Dennis and Schrabel, 1983) that states the following. If the conditions for quadratic convergence of Newton's method are met and, if  $\|A_0 - J(x_*)\|_2$  is less than some positive constant  $\delta$ , then Broyden's method converges  $q$ -superlinearly to the solution  $x_*$ . Otherwise if the approximate Jacobian satisfies an even simpler condition we can expect linear convergence.

The exact values for  $\delta$  and the  $q$ -superlinear convergence rate are not specified by the theorem (i.e. unlike the 1-D secant case, we cannot directly obtain a number giving the precise convergence rate). However as expected, we have found from experiment that an approximation closer to the true Jacobian converges faster than a poor approximation. A close approximation requires more work - so there is a tradeoff between what we gain by cutting short the matrix solution and what we lose in slower convergence to the zero of the nonlinear equations.

### 5.1.6. QUASI-NEWTON EXPERIMENTS

Tests on single phase problems gave very good results. A single point-Jacobi iteration on Eq. 5.1.10 was enough for *QN* to converge in 5-6 iterations even when pressures were changing by up to a 1000 psi in one time step. Changing from square grid blocks to 300 to 1 aspect ratio blocks did not need more than 12-13 iterations. Newton's method *could not converge at all* with a single point-Jacobi iteration on Eq. 5.1.6. These first experiments showed us that the *QN* method could indeed make good use of the secant information.

For two-phases it turns out that the initial Jacobian must be at least a block-Jacobi on the  $2 \times 2$  oil-water system. This is probably because of a move from diagonal dominance to block-diagonal dominance.

This change proved to be adequate to simulate waterfloods. We chose a 2-phase quarter 5-spot water flood simulation that had been earlier solved using Newton's method. While Newton's method averaged 3 iterations/time step (using a direct solver), Quasi-Newton took an average of 24 iterations/time step. However since the cost of each iteration was so low there was no need to try anything fancier to solve Eq. 5.1.10.

Figure 5.1.1 shows the total time taken as a function of number of grid blocks on a serial machine. There are two obvious ways to increase the number of grid blocks. We can keep the size of grid blocks constant and increase their number. This makes the problem easier to solve since the wells move further apart. The corresponding curve is labeled "Easy" in this figure.

Alternatively we can keep the overall size of the model constant and put more blocks into the same area. The size of blocks now decreases. This makes the problem harder to solve since transients are more severe in smaller blocks. This curve is labeled "Hard".

Figure 5.1.1 shows the expected difference in total times. It also shows how the Quasi-Newton method behaves with increasing problem size. One might wonder that since we are building up secants, do the number of secants needed increase as the dimensions of the problem increase? From Fig. 5.1.1 it is apparent that they do not.

Also shown is the linear increase line - with constant degree of difficulty, the simulation times would be expected to follow this. The  $kN^2$  curve shows how an algorithm scaling with the square of number of grid blocks would fare. The spectacular performance of *QN* in comparison is, of course, due to the point-Jacobi approximation we are using. Even if we use a better approximation, as long as the approximation involves  $O(N)$  work the overall algorithm will also scale linearly for constant degree of difficulty.

Figure 5.1.2 shows that a move from 2-D to 3-D also makes the problem more difficult. However each curve is itself near linear.

We now briefly describe the some of the issues that were involved in parallelizing the code.

### 5.1.7. SHARED-MEMORY AND MESSAGE PASSING ARCHITECTURES

These two are emerging as the most successful general purpose parallel architectures. Both usually operate as MIMD (Multiple Instruction Multiple Data) machines, i.e. each processor runs its own code on its own data. The difference between the two is basically in how they handle global data. While the detailed architecture of individual machines vary they exhibit certain broad characteristics mentioned below.

Message-passing machines handle global data by passing messages between processors. The processors are connected by a network, usually the hypercube topology is used. Such machines can have a very large number of processors.

Programs for these machines are quite a bit different from ordinary serial code, since messages must be passed to access global data. Messages move relatively slowly so one also has to spend effort on minimizing communication. On the other hand software written for this type of machine can be made to run on a network of *computers*, not just a network of *processors*.

Shared-memory machines have a globally shared memory that can be accessed by all processors. Each processor usually operates out of a cache, but here the caches have to be more sophisticated than is usual in uniprocessor machines (parallel computers are also termed multiprocessors).

If a change is made to global memory by one processor all caches must sense this, determine if they hold the memory location in cache and either invalidate the data or read it in. These machines suffer from the high bus traffic that results from multiple processors working with one shared memory. This architecture is therefore not suitable for a very large number of processors.

On the software side a shared-memory machine is much easier to program and communication between processors is very fast.

### 5.1.8. PROGRAMMING A SHARED-MEMORY MACHINE

Runs were made on a 16 processor shared-memory MIMD machine, the Encore Multimax. The machine uses National Semiconductor NS32032 32 bit CPUs and NS32081 floating point co-processors. The operating system is similar to Unix. Each processor has its own local memory as well as access to a global shared memory. Encore has recently come out with a 256 processor machine using more powerful chips.

The shared-memory method made it relatively easy to port the simulator to the machine, the resulting code could even run almost unchanged on a conventional serial machine. The only problem was that the environment available to us was most conducive to the C language so the simulator was written in C.

Argonne National Laboratory's parallel processing package of process control, synchronization and communication primitives (described in Lusk, *et al*, 1987) provides the necessary parallel extensions to what is otherwise standard C language. The important primitives for shared-memory machines are named CREATE, LOCK/UNLOCK and BARRIER and we briefly describe them below.

### CREATE

This primitive simply copies the entire program to a specified number of processors, starting them up at a specified subroutine. Each processor then runs its own copy of the program, using local memory for all variables except those explicitly allocated in global memory.

All operations done in serial like printouts, summing partial dot products etc. are done by the copy on processor 0. Each copy tests to see if it is on processor 0, only the desired one passes and then proceeds to perform the serial code.

### LOCK AND UNLOCK

These primitives are used to control access to global variables. To show why this is sometimes needed, consider the case of two processors incrementing a global variable. Suppose that the global variable is set at 21. Now if processors A and B each do an increment we expect it should become 23. But suppose processor A reads in 21 and before it can write it out, processor B also reads in 21. Then A will write out 22 and so will B, giving an incorrect answer. To ensure correctness, A must be able to exclude B until it is done.

LOCK lets A make sure that B cannot access the variable until it has done its job and performed an UNLOCK. If two processors simultaneously try to get the LOCK only one will succeed (it shouldn't matter which one it is). The unsuccessful one must then wait until the first processor does an UNLOCK. A typical application for these primitives is self-scheduling where a processor determines what it should work on dynamically e.g.

```
LOCK();           /* obtain the lock */
my_index = global_index; /* get index to work on */
global_index++;   /* increment index */
UNLOCK();        /* let the lock go */
```

This sequence can be used in a simulator when doing table look-ups for example. Each processor gets a grid block to work on and returns for another until all are done.

Note that if one processor has the lock, all other processors trying to get the lock must wait, so there is some overhead.

In simulation the problem can be easily partitioned so we do not use this primitive at all. Instead we simply pre-schedule by assigning different parts of the reservoir (and corresponding parts of arrays and vectors) to each processor.

## BARRIER

This primitive is used to synchronize the processors. Upon encountering a BARRIER statement a processor temporarily halts execution of the program. When all processors have halted at the BARRIER, it "opens" and they all resume work.

The BARRIER primitive is useful in ensuring the consistency of data across all the processors. For example, suppose processors A and B are assigned grid blocks 1-22 and 23-44 respectively of a 1-D reservoir. Let's assume that the processors first go through their assigned blocks performing table look-ups and store the results. On a second pass they use these stored values and calculate the flow equation at each block.

Now say that B finishes all its table lookups first (because the table searches ran faster on its pattern of grid block pressures, for example). Meanwhile A is doing the lookup for block 19. B now does the flow equation for block 23 while A does lookup for block 20. The flow equation for block 23 will now be incorrect since it includes flow in from block 22 on which A has not yet done the lookup.

The solution, as shown in Fig. 5.1.3, is to put a BARRIER after the table lookups to ensure that they are all done before work begins on the flow equations. It is also possible for each processor to maintain copies of the grid blocks surrounding its region and thus make sure of its own data by itself. This leads to redundant calculations and introduces some complexity in the code so we simply used BARRIERS to make sure things were consistent. However the extra copies will be the preferred method on a message-passing machine.

Due to different times for table look-up, different outcomes of *if then* statements, and presence/absence of reservoir edges and wells, each processor will be doing varying amounts of work even if all have the same number of grid blocks to deal with. This means that the load will *never be perfectly balanced*. Some processor will take longer than the others to complete a given stage of the computation. So there is a slowdown at BARRIERS since all the processors must wait there until the slowest one catches up. Also some time is needed for the system to actually execute the BARRIER statement itself.

In spite of this, we initially chose to err on the safe side by liberally using BARRIERS in the code. It is possible to fine tune the BARRIERS to reduce their number by figuring out which routines will be guaranteed consistent data even without them - usually this is any routine that works only on the grid blocks/data assigned to that processor. Some of this fine tuning was done before making final runs.

If each processor is able to do lots of useful work between BARRIERS the ratio of time lost at the BARRIER to time spent on useful work will be small. This effect is illustrated in the final results discussed below.

### 5.1.9. FORMING THE JACOBIAN AND THE FUNCTION

Apart from the matrix solution there are few subtleties involved in porting a simulator to a parallel machine. The only one we came across occurs when forming the Jacobian or evaluating the function. It is natural to take advantage of the structure of the equations to speed up the code as follows.

In the two-dimensional case for example, the flow equation at a block includes the flow rate into the block from its North, South, East and West neighbors. At each block we need only calculate the flow rate and its derivative for flow to *two* neighbors, say South and East.

These calculations can be stored at the current block and also added to the neighboring blocks to the South and East as contributions from North and West respectively. Thus by the time a block's turn comes up, its flow rates from North and West are *already available*, thus saving almost half the effort.

This method is easy to implement in a serial computer but there is a little subtlety needed when doing it on a parallel computer. Because the flow rates/derivatives are *summed* on the main diagonal of the Jacobian and in *f* there is chance for error during the summation.

For example, let block 44 be on processor A and block 88 be on processor B. Let block 88 be the South neighbor of block 44. Now suppose that just when processor B is working on block 88, processor A is at block 44 and is about to add in block 88's flow rate from the North. Both processors might then try to add to the same memory location on block 88 at the same time. This will produce an uncertain result.

Because these contributions occur very frequently (though most are not risky) using a LOCK/UNLOCK method would be too expensive. Maintaining extra copies of neighboring blocks will solve the problem but lead to redundant calculations. We chose to store (not sum) these contributions in the space reserved for vectors used by the Quasi-Newton method. This method tends to work very nicely, because when the maximum storage space is needed (when forming the Jacobian) the QN method has no need for its space. When *f* is being made, the QN method can spare only a little space but that space is enough to solve the problem.

Constructing the Jacobian or *f* is then a two-pass process. In the first pass we go through each block storing rates and derivatives at the block and at its neighbors to South and East. A BARRIER at the end makes sure that all are done. Finally in the second pass we run down each block adding on the previously stored entries (with the appropriate change in sign), add accumulation terms and wells to complete the Jacobian or *f*.

### 5.1.10. PARALLELIZING DOT-PRODUCTS

Dot-products turns out to have a significant serial component. Each processor can, in parallel, perform dot-products on part of the vectors. The partial results then must be summed to give the final dot-product. This leads to the following code example:

```
BARRIER(); /* wait for consistent arguments */  
MakePartialDotProducts();  
BARRIER(); /* wait for all to finish */  
if (ProcessorID == 0)  
    SumUpResults(); /* sum in serial */  
BARRIER(); /* wait for serial sum to finish */
```

So this simple task requires 3 BARRIERS and a serial step. It is possible to save some time through careful coding. For example, by checking the places the routine is *called* from we can remove the first BARRIER from this routine and place it before the *call* only where needed.

It is also possible to save time on the serial step by making use of more than one processor. Suppose the partial results are stored in a vector. We can recursively add the bottom half of the vector to the top half in parallel, halve the vector length and repeat until this length is one.

With a large number of processors this saving can be useful. It reduces the floating-point time to  $\log_2(p)$  instead of  $p$ .

With 16 processors the serial sum involves at most 16 floating point add/accumulates. The faster method reduces this to 4 floating point add/accumulates but requires integer comparison, decision making and BARRIERS after each add/accumulate. Total time thus would probably not be reduced so we did not implement the logarithmic method.

Because of the limited size of the problems we could run, even this small serial number of instructions had quite an effect. For example, on a 400 grid block problem, there are 800 elements on each vector. On 12 processors,  $800 / 12$  or 67 floating point instructions are enough for an ideally parallel solution. Instead we need  $67 + 12$  dot-products appear very frequently in the QN method (and also in CG type methods) this is a significant cause of slowdown. The slowdown becomes less severe as the vector size increases.

This dot-product problem can also be solved using the LOCK/UNLOCK primitives. When each processor is done with its partial result it can simply get the lock on a global sum variable, add on its result and release the lock. Speedup is not improved since 16 sums still have to be done, one after the other but this time with the added overhead of a LOCK/UNLOCK pair surrounding each sum.

### 5.1.11. PARALLEL EXPERIMENTS

During the parallel simulator experiments reservoir block sizes were kept constant, while their numbers were changed to present different sizes of problems. As shown in Fig. 5.1.1 this tends to slightly reduce the total time but work still is close to linear.

For simplicity we used global memory to store all the data structures and this limited the problem size to 400 blocks. A production simulator could of course use global memory much more sparingly and not face this limit.

Timing were made using the CLOCK (described in Lusk, 1987) macro. The clock was started after input data had been read in and global arrays allocated. So the timing results are for actual run time in microseconds on 10 time steps of the 2-D waterflood studied earlier.

The number of processors used could be specified on the command line. Serial runs were made by using one processor. Although 16 processors are available, it was unwise to use that many. Since this is a multitasking machine, there was a chance that somebody could, for example, logon to processor 15. Then at BARRIERS all processors would be stuck waiting for 15 to get free. Runs were made during reserved time slots to prevent this happening but we still left a few processors idle to allow some room for the system's own housekeeping programs.

Figure 5.1.4 shows clearly the benefit of moving from a serial computer to a parallel computer. It compares the times on 1 processor with the times on 12 processors. We see how the total time needed for a problem increases much more gradually on a parallel machine.

Figure 5.1.5 compares the speedup at various problem sizes to the ideal speedup. We see that for a  $5 \times 5$  problem there is a *decrease* in speedup as the number of processors increases. This is because with such a small problem each processor is doing very little work before coming up against slowdowns at BARRIERS.

On the whole we see that as the problem size increases (i.e. as granularity gets coarser), the closer we get to ideal speed-up. Figure 5.1.6 shows the speedup on 4 processors with various problem sizes. >From 100 grid blocks onwards we are close to ideal speedup. The slope of the curve is still positive at 400 grid blocks so it is likely that speedup would be slightly higher at larger grid sizes.

Figure 5.1.7 shows the speedup on 12 processors with various problem sizes. At small sizes we can see the detrimental effect of BARRIERS - we get a speedup of only 2.5 on the 5x5 problem. This effect has not been overcome at 400 grid blocks as the positive slope shows. It appears that the problem size would have to be 2-3 thousand blocks before we could approach ideal speed-up. As the number of processors go up this threshold will also rise. In general, problem sizes have to be very large in order to get good speedup - for example Gustafson *et al.* (1988) got their best results with 2 million finite elements (2048 elements on each of 1024 processors) - a problem that would have taken 20 years to solve on a single processor!

#### 5.1.12. QUASI-NEWTON EXPERIMENTS (contd.).

One of the reasons why we were limited in problem size was that we allocated space for 30 pairs of update vectors. This provided enough space to converge to the zero of Eq. 5.1.5. To reduce memory demands we changed the program so that it would only store a limited number of update vectors. If this space was used up before solving Eq. 5.1.5, the QN method would then restart with a fresh Jacobian. This led to a slight increase in the total number of iterations because by restarting we lost all the accumulated secant information. Total time was however reduced because we avoided the long update sequences needed to get to say,  $A_{20}^{-1}$  from  $A_0^{-1}$ .

We next included a third phase i.e. gas. We chose the data for the first SPE comparative solution project (described by Odeh, 1981) to work on and we used various numbers of grid blocks in our tests. Once again we found that the addition of a new phase required a better approximation. We found that we could no longer get away with a single block-Jacobi iteration. Instead we would have to perform at least 3-4 block-Jacobi iterations to approximately solve Eq. 5.1.10, in order to make any progress at all.

The variable substitution scheme (see for example Aziz and Settari, 1979) needed for gas introduced a new problem for the Quasi-Newton method. The update vectors that store the secant information relate to one set of variables. If any of these variables change we must terminate the Quasi-Newton iterations and restart with the new set of variables. Thus we lose the secant information that has accumulated.

This is painful regardless of type of Jacobian approximation we use. With a poor approximate Jacobian we are relying on the secants to improve it greatly. With a better approximation, we are forced to re-factor a Jacobian - if LU decomposition were being used on a serial machine, this cost can be very high.

We tried at length to avoid the variable substitution by using *total gas* as a variable. Thus our third variable became:

$$\tilde{S}_g = \frac{S_g}{B_g} + \frac{R_s S_o}{B_o}$$

Given  $\tilde{S}_g$  it is relatively straightforward to find  $S_g$  and  $R_s$  using a simple 1-d Newton method. There doesn't seem to be any theoretical reason why this should not work. However at the time of writing this report we have not been able to get it to work properly when free gas goes into solution. So we continue to use variable-substitution to handle gas.

### 5.1.13. NEWTON OR QUASI-NEWTON?

>From our experiments we have found that the Quasi-Newton method may sometimes do better than Newton's method *even on serial machines*. We can compare the methods on a standard test case. The first SPE comparison project (Odeh, 1981) is a moderately difficult test case. It is a  $10 \times 10 \times 3$  black oil problem with a high gas injection rate and oil production rate. Researchers have sometimes used this problem to test the efficacy of matrix solution methods.

For this case due to the high transmissibility in the vertical direction and the high mobility of gas, a point-Jacobi method converged very slowly to the solution of Eq. 5.1.10. When talking about different Jacobi methods we will mean the number of grid blocks involved. Within each grid block we always simultaneously solve all three flow equations.

So while point-Jacobi was adequate for the 2-D case we needed a better method for 3-D. The simplest change was to move to z-line-Jacobi and so solve for all unknowns in each vertical line of blocks simultaneously. This method is also highly parallel since we can assign grid blocks by vertical lines to each processor and each can then independently solve their own

lines. The convergence can, of course, be improved by using red-black Gauss-Sidel/SOR (with each *line* colored red or black).

We first tried both z-line-Jacobi and a direct solver on this problem on the serial machine. To improve the efficiency of direct solution we used a band LU solver with ZXY ordering. Table 1 shows a comparison of the two nonlinear methods in simulating the first 100 days of this simulation. Time steps started at 1 day and increased by a factor of 1.5 thereafter. No time step cuts were necessary.

All cases used the same nonlinear convergence test which worked as follows. Convergence was deemed to have been reached only if either (a)  $|x(i)| < 1.0$  and  $|s(i)| < 2 \times 10^{-5}$ , or (b)  $|\frac{s(i)}{x(i)}| < 2 \times 10^{-5}$ , for all  $i = 1, \dots, N$ . Here  $x$  is the vector of unknowns, i.e. pressure etc. and  $s$  is the step vector calculated by the nonlinear method.

The (a) test appears lax but it does not work out that way. Usually pressure converges slower than saturations so the (b) test will prevent premature acceptance. The (a) test protects us from the situation of a tiny gas saturation appearing in the denominator of test (b), magnifying an acceptable step, and not allowing the iterations to complete. The actual numbers used are *ad-hoc* but seem to be adequate for good material balance.

The code used single-precision except in a few places like summing oil in place etc. The Quasi-Newton method was restarted if it failed to converge in 7 iterations.

In cases A through D the z-line-Jacobi was used with various convergence tolerances. Jacobi iterations continued until either the  $l_2$  norm of the residual had dropped below a specified fraction of the  $l_2$  norm of initial residual (i.e. of  $f$ ), or a maximum number of Jacobi iterations had been done. In case E, the ZXY band solver was used. Time reported is the total time for 100 days of this simulation.

Case E shows how QN saves work with direct solvers because in most iterations it can get away with just a back-substitution. However for this problem the modified-Newton method also works and gives virtually the *same speed-up* as QN. This may be because the problem is only weakly nonlinear, i.e. the Jacobian does not change much during a time step. QN methods are usually used in this form, namely to speed up modified-Newton methods. Unfortunately the speedup may not be realized unless the problem is highly nonlinear, e.g. an elastic body turning plastic in finite-element simulation.

Cases A through D represent *iterative* solutions, and show the advantage of Quasi-Newton methods with iterative solutions. It is clear that Newton's method is *also speeded up* by use of approximations. But, case D shows that as the approximation gets worse the QN method *performs better*.

Newton's method not only takes 44% longer - it produces a less accurate answer. For example it calculates the final pressure at block (10, 10, 3) to be 3835.8 psi while QN gave the same answer obtained by LU, namely 3838.3 psi. Material balance error was several orders of magnitude better in the QN method.

Case A shows a case where QN did worse than Newton's method. Here the linear convergence tolerance was tight resulting in a very good solution - Newton's method takes the same number of iterations as with the direct solver. This case shows another important factor for QN methods - if we are going to spend a great deal of effort in solving a matrix accurately, then we might as well solve the most up-to-date matrix and use Newton's method.

However in case D, we are able to get the same solution as a direct method while running 14 times faster even though we are using a poorly convergent linear scheme. The basic reason for this good performance of QN is the following - Newtons' method has approximate (new) tangents while QN has approximate (old) tangents but exact secants so eventually it converges to the non-linear root faster.

The picture changes when we use a PCG type linear scheme like ORTHOMIN. Even though it is applied iteratively ORTHOMIN is *directly* solving in the directions it looks at. By forcing it to work on an old Jacobian, the QN method will, in general, adversely affect the non-linear convergence. However QN still retains the advantage of saving factors.

Table 2 shows a comparison using a Red-Black z-Line Gauss-Sidel ORTHOMIN(7) linear algorithm with the various non-linear algorithms. We have also compared QN with the modified-Newton scheme since that also saves factors. This test is more difficult than that in Table 1 because the oil and gas rates have been doubled. Except for the very first case where the QN method had to undergo a time step cut (TSC) we see that it can successfully simulate this test while saving factors (nFAC). Since we are using a tri-diagonal pre-conditioner the cost of factorization is low so the QN method does not get the overall best speed. But it does seem to be more reliable than the modified-Newton which in 3 cases has failed to converge.

Table 3 compares the methods on a easier problem - the same test as in Table 2 but with the gas injector nearly shut-in. Here we see that the modified-Newton method works better than the QN method and is almost as fast as Newton's method even though the cost of factorization is low.

This type of behavior has appeared in several other tests - QN can save factors and is generally more robust than a modified Newton method - but it may not always be fastest.

#### 5.1.14. CONCLUSIONS

We have investigated the use of a combination of linear and nonlinear techniques to speedup the solution of the nonlinear equations arising in simulation.

We have found that with purely iterative schemes, a Quasi-Newton method may have an absolute speed advantage - i.e. reduced number of non-linear iterations than a Newton method with the same scheme.

With conjugate-gradient type schemes the number of non-linear iterations will generally be more using a QN scheme. However if the cost of factorization is high then the QN method may be faster since it can solve the problem with fewer factors. It tends to be more robust than modified-Newton schemes.

Experiments on a parallel machine show that even with a highly parallel matrix solution method, the achieved speedup is dependent on problem size. Problem size needs to be quite large in order to get good speedup. The method itself is highly parallel, slowdown occurs mainly due to time lost at synchronization points.

### 5.1.15. NOMENCLATURE

- A Approximate Jacobian matrix.
- $B_o$  Oil formation vol. factor, res. bbl/STB.
- $B_g$  Gas formation vol. factor, res. bbl/SCF.
- $c$  work vector.
- $d$  work vector.
- $f$  system of flow equations written in residual form.
- J Jacobian matrix.
- $p$  Number of parallel processors.
- $P$  Time spent on parallel code on uniprocessor, frac.
- $P_o$  Oil Pressure.
- $R_s$  Solution gas oil ratio, SCF/STB.
- $s$  step vector.  $x_{k+1} = x_k + s_k$ .
- $S$  Time spent on serial code on uniprocessor, frac.
- $S_g$  Gas saturation, frac.
- $S_o$  Oil saturation, frac.
- $S_w$  Water saturation, frac.
- $T_i$  Time to complete on  $i$  processors.
- $x$  Vector of unknowns, i.e. pressure etc.
- $y$  Yield of step,  $y = f(x + s)$

### 5.1.16. REFERENCES

1. Amdahl, G., "Validity of the single-processor approach to achieving large-scale computer capabilities", AFIPS Conf. Proc., **30**, 483-485 (1967).
2. Aziz, K. and Settari, A., *Petroleum Reservoir Simulation*, Applied Science, London (1979).
3. Behie, A., "Comparison of Nested Factorization, Constrained Pressure Residual, and Incomplete Factorization Preconditionings" paper SPE 13531, presented at the 8th SPE Symposium on Reservoir Simulation, Dallas, Texas, Feb 10-13, 1985.
4. Broyden, C. G., "A class of methods for solving nonlinear simultaneous equations", *Math. Comp.*, **19**, 577-593 (1965).
5. Broyden, C. G., "The convergence of a class of double rank minimization algorithms. 2. The new algorithm", *J. Inst. Math. Appl.* **6**, 221-231 (1970).
6. Dennis, J. E. and Schnabel, R. B., *Numerical Methods for Unconstrained Optimization and Nonlinear Equations*, Prentice-Hall, Englewood Cliffs, New Jersey (1983).

7. Efrat, I. and Tismenetsky, M. "Parallel Iterative Linear Solvers for Oil Reservoir Models", *IBM J. Res. Develop.*, 184-192, (March 1986).
8. Gustafson, J. L., Montry, G. R. and Benner, R. E., "Development of parallel methods for a 1024-processor hypercube", *SIAM J. Sci. Stat. Comp.*, Vol. 9, No. 4, July 1988.
9. Killough, J. E. and Wheeler, M. F., "Parallel Iterative Linear Equation Solvers: An Investigation of Domain Decomposition Algorithms for Reservoir Simulation", paper SPE 16021, presented at the 9th SPE Symposium on Reservoir Simulation, San Antonio, Texas, Feb 1-4, 1987.
10. Lusk, E. et al., *Portable Programs for Parallel Processors*, Holt, Rinehart, Winston, Inc. New York (1987).
11. Mattheis, H. and Strang, G., "The solution of nonlinear finite element equations", *Int. J. Num. Meth. Engg.*, 14, 1613-1626 (1979).
12. Odeh, A., "Comparison of Solutions to a Three-Dimensional Black-Oil Reservoir Simulation Problem", *J. Pet. Tech.*, 33, 13-25 (1981).
13. Scott, S. L., Wainwright, R. L., Raghavan, R. and Demuth, H., "Application of Parallel (MIMD) Computers to Reservoir Simulation", paper SPE 16020, presented at the 9th SPE Symposium on Reservoir Simulation, San Antonio, Texas, Feb 1-4, 1987.
14. Vinsome, P. K. W., "Orthomin, an Iterative Method for Solving Sparse Banded Sets of Simultaneous Linear Equations", paper SPE 5729, presented at the 4th SPE-AIME Symposium on Reservoir Simulation, Los Angeles, California, Feb, 1976.
6. Watts, J. W., "A Method of Improving Line Successive Overrelaxation in Anisotropic Problems - A Theoretical Analysis", *SPEJ*, 105-118, (March 1971).

### 5.1.17. APPENDIX IMPLEMENTING THE QUASI-NEWTON METHOD

We give below the steps needed to implement the QN method using update vectors. The steps include the tests used to deal with gas.

We write this in a pseudo-code which we hope will be clear. Vectors are written in bold type, greek letters are scalars. As in programming languages the equality sign is meant to be an assignment statement. The dot product is written as  $( \cdot )$ . The superscript  $i$  indicates the  $i$ th vector of a series.

We make use of the same vectors/matrices used for Newton's method, i.e.  $\mathbf{J}$  is the Jacobian,  $\mathbf{x}$  the vector of unknowns,  $\mathbf{s}$  the step vector and two other vectors  $\mathbf{c}$  and  $\mathbf{d}$ . In addition if  $MaxIts$  updates are to be performed, we require storage for update vectors,  $\mathbf{u}^1, \mathbf{u}^2, \dots, \mathbf{u}^{MaxIts}$  and  $\mathbf{v}^1, \mathbf{v}^2, \dots, \mathbf{v}^{MaxIts}$ . As pointed out by Mattheis and Strang (1979) the update vectors can be stored on disk if space is at a premium.

At the start of the simulation set a status flag on all blocks to indicate whether they contain free gas or not. Decide on convergence tolerance for the linear iterations,  $\epsilon$ , and the maximum number of linear iterations *MaxL*. Proceed as follows.

At each time step call the following routine repeatedly until the flag *converged* is *TRUE*.

1. Set *converged* = *FALSE*. Form the function  $f(x)$  and its Jacobian  $J(x)$ . Iteratively solve  $J_s = -f$  until  $\|J_s + f\|_2 < \epsilon \|f\|_2$ , or *MaxL* iterations have been done. Set iteration counter  $k = 0$ .
2. Add step, i.e. set  $x = x + s$ . Make convergence test described in the text, if satisfied then set *converged* = *TRUE*, and return to caller. If  $k > \text{MaxIts}$  return to caller.
3. Form  $f(x)$ , checking blocks for changes from saturated to unsaturated. Update status of all blocks. If any changes have occurred return to caller.
4. Iteratively solve  $Jd = f$  until  $\|Jd - f\|_2 < \epsilon \|f\|_2$ , or *MaxL* iterations have been done. Perform a loop as follows:  
    for  $i = 1, k$   
         $\alpha = (u^i, d)$   
         $d = d + \alpha v^i$   
    endfor
5. Obtain  $\alpha = \frac{-1.0}{(d + s, s)}$ . Set  $c = \alpha d$
6. Increment  $k$ .
7. If  $k \leq \text{MaxIts}$  then store update vectors, i.e. set  $u^k = s$ , and  $v^k = c$ .
8. Obtain  $\alpha = (s, d)$ . Set  $s = -(d + \alpha c)$ . Go to step 2.

TABLE 1  
 COMPARISON USING ITERATIVE/DIRECT METHODS  
 SPE Comp. Sol. Project 1, 10x10x3 (100d) zLineJac

Case	Method	Residual Tol.	Maximum of Jacobi Itns.	Number of Nonl'nr Itns.	Number of Jacobi Itns.	Time sec
A	Newton	0.001	100	43	2408	251.1
	QN	0.001	100	60	3249	331.8
B	Newton	0.01	50	51	1680	182.7
	QN	0.01	50	70	1623	174.9
C	Newton	0.1	20	78	1133	139.1
	QN	0.1	20	81	774	94.1
D	Newton	0.2	15	92	946	126.1
	QN	0.2	15	81	708	87.4
E	Newton	ZXY band solver		43		1225.5
	QN	" "		58		545.6

TABLE 2  
 COMPARISON USING PCG-TYPE METHOD  
 SPE Comp Sol Project 1, 200 MMSCFD, 40,000 BD

Method	Tol	Time	Oil Mat Bal	nIT	nFAC	nSOL
Newton	.2	38.4	0.000506	48	48	132
QN(4)		62.3	TSCut	90	47	208
MN(4)		40.5	0.002628	56	30	135
Newton	.1	41.4	0.000612	42	42	153
QN(4)		51.0	0.000024	59	27	189
MN(4)		45.4	TSCut	62	26	171
Newton	.01	58.2	0.000025	35	35	237
QN(4)		61.2	0.000016	42	19	263
MN(4)			Stuck at 10 days after TSCut			
Newton	.001	88.1	0.000003	32	32	373
QN(4)		94.7	0.000014	42	19	415
MN(4)			Stuck at 10 days after TSCut			
Newton	2,4,8	68.1	0.000001	36	36	281
QN(4)	to	58.6	0.000024	37	23	240
MN(4)	.001		Stuck at 10 days after TSCut			

Linear method: Red-Black z-Line Gauss-Sidel ORTHOMIN(7)

TABLE 3  
 COMPARISON USING PCG-TYPE METHOD  
 SPE Comp Sol Project 1, 40,000 BD, 1 MMSCFD

Method	Tol	Time	Oil Mat Bal	nIT	nFAC	nSOL
Newton	.2	28.6	0.002341	33	33	102
QN(4)		36.1	0.001810	43	22	137
MN(4)		27.4	0.003172	36	18	101
Newton	.1	27.5	0.000951	27	27	103
QN(4)		31.7	0.000889	33	17	123
MN(4)		27.8	0.000951	31	17	105
Newton	.01	42.8	0.000091	24	24	174
QN(4)		44.2	0.000071	28	13	188
MN(4)		41.6	0.000087	27	13	175
Newton	2,4,8 to 0.001	38.7	0.000000	26	26	154
QN(4)		51.8	0.000011	32	16	219
MN(4)		44.7	0.000007	30	16	186

Linear Method: Red-Black z-Line Gauss-Sidel ORTHOMIN(7)

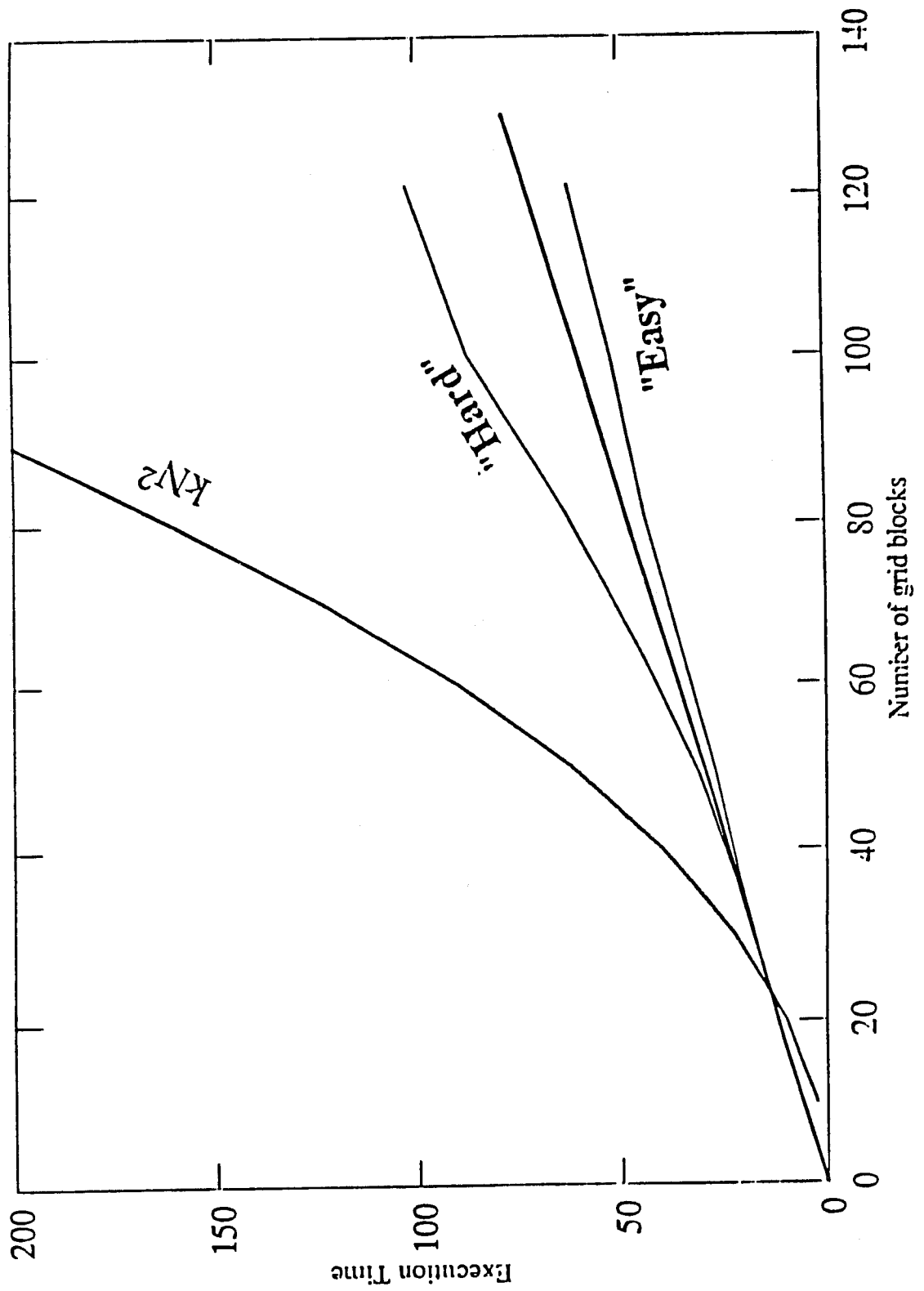


Figure 5.1.1.1 Quasi-Newton method on 2-D oil-water systems.

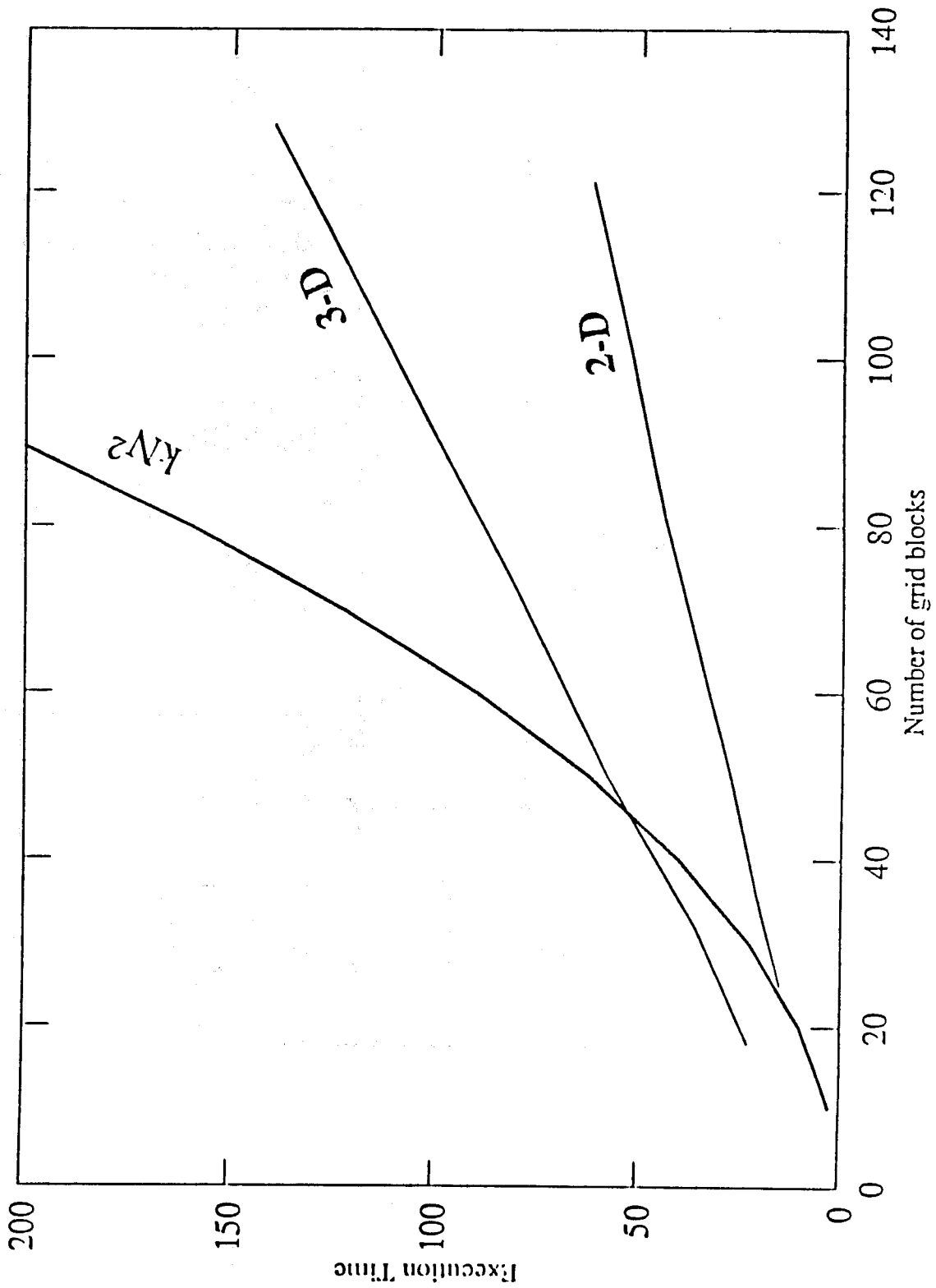


Figure 5.1.2 Quasi-Newton method on oil-water systems.

### Processor A

Look up krO, krW, bO  
etc. for blocks  
1-22

BARRIER(n);

Evaluate Eqn. for  
blocks  
1-22

### Processor B

Look up krO, krW, bO  
etc. for blocks  
23-44

BARRIER(n);

Evaluate Eqn. for  
blocks  
23-44

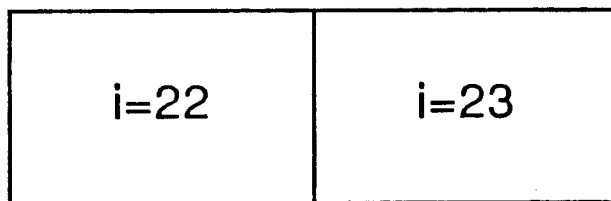


Figure 5.1.3 Using BARRIERS.

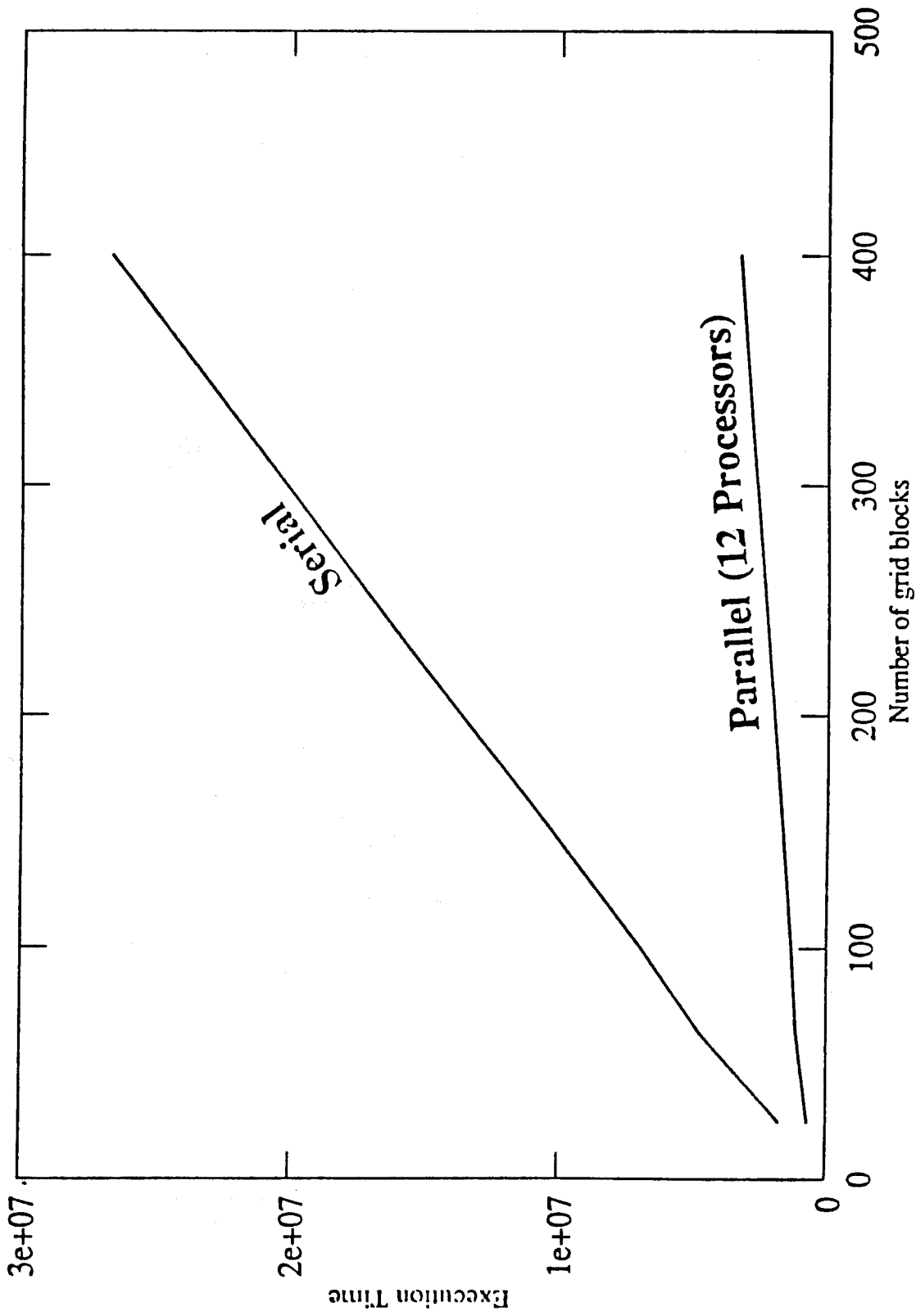


Figure 5.1.4 Serial vs. parallel.

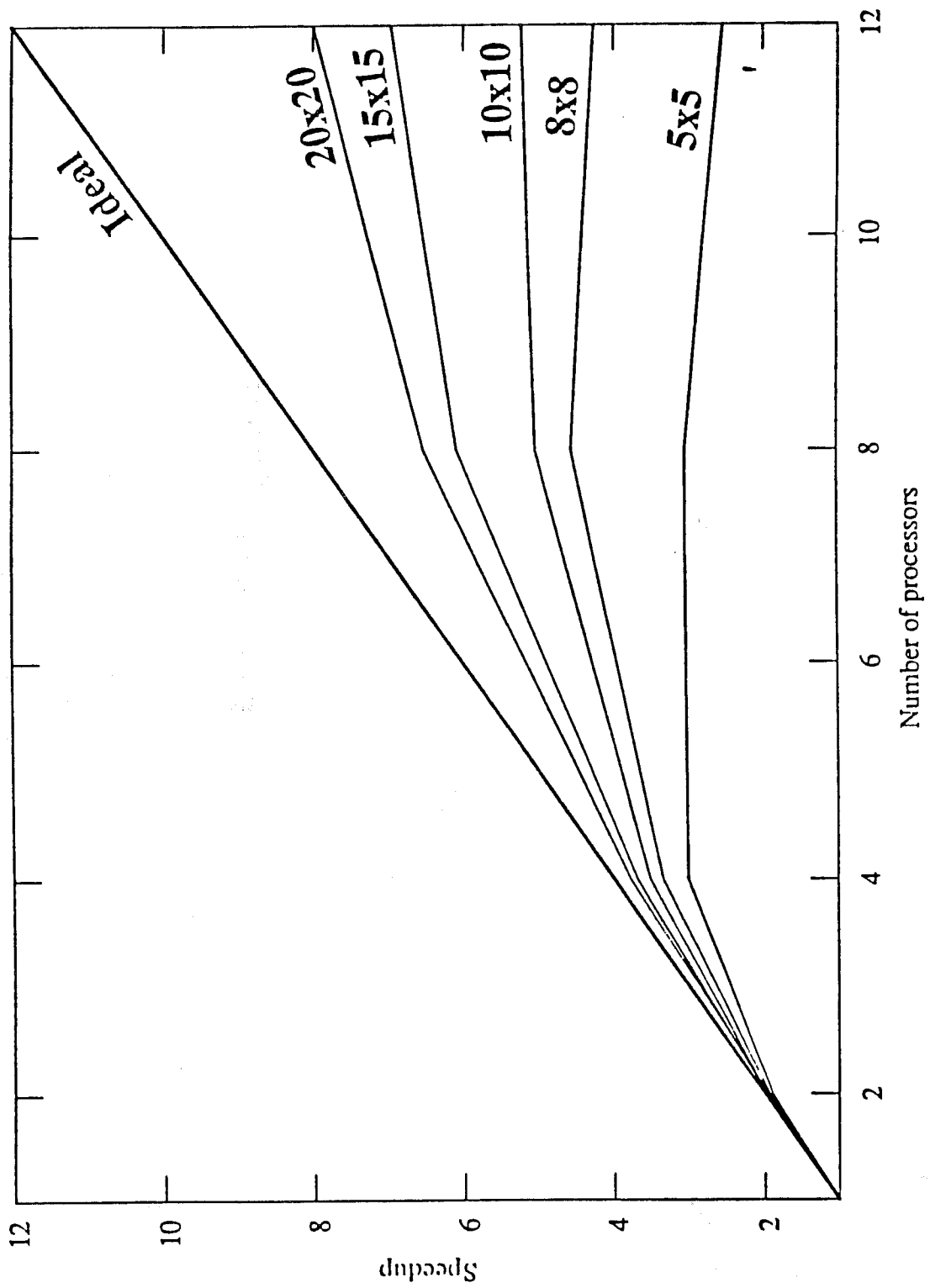


Figure 5.1.5 Speed-up vs. problem size.

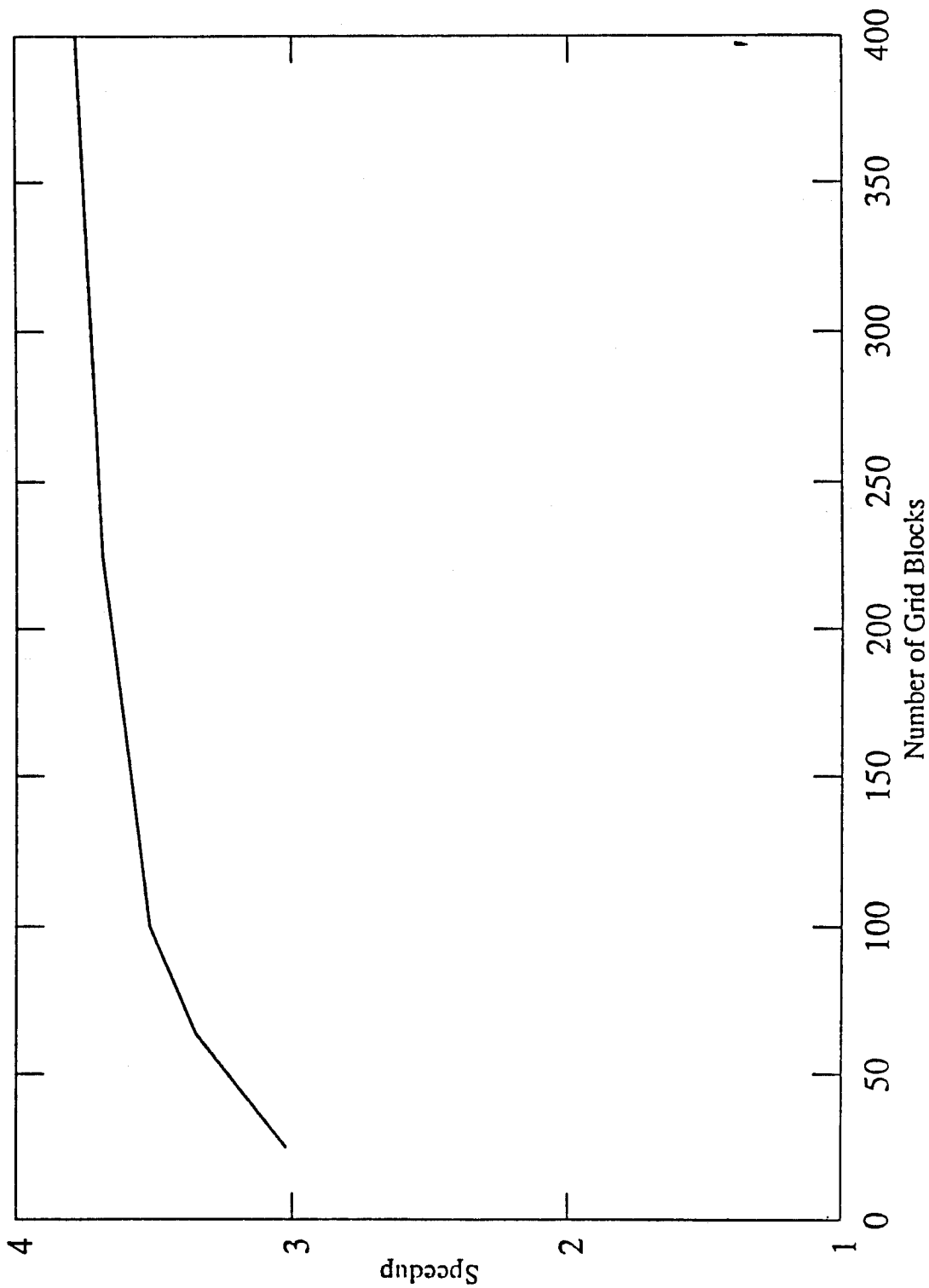


Figure 5.1.6 Speed-up on four processors.

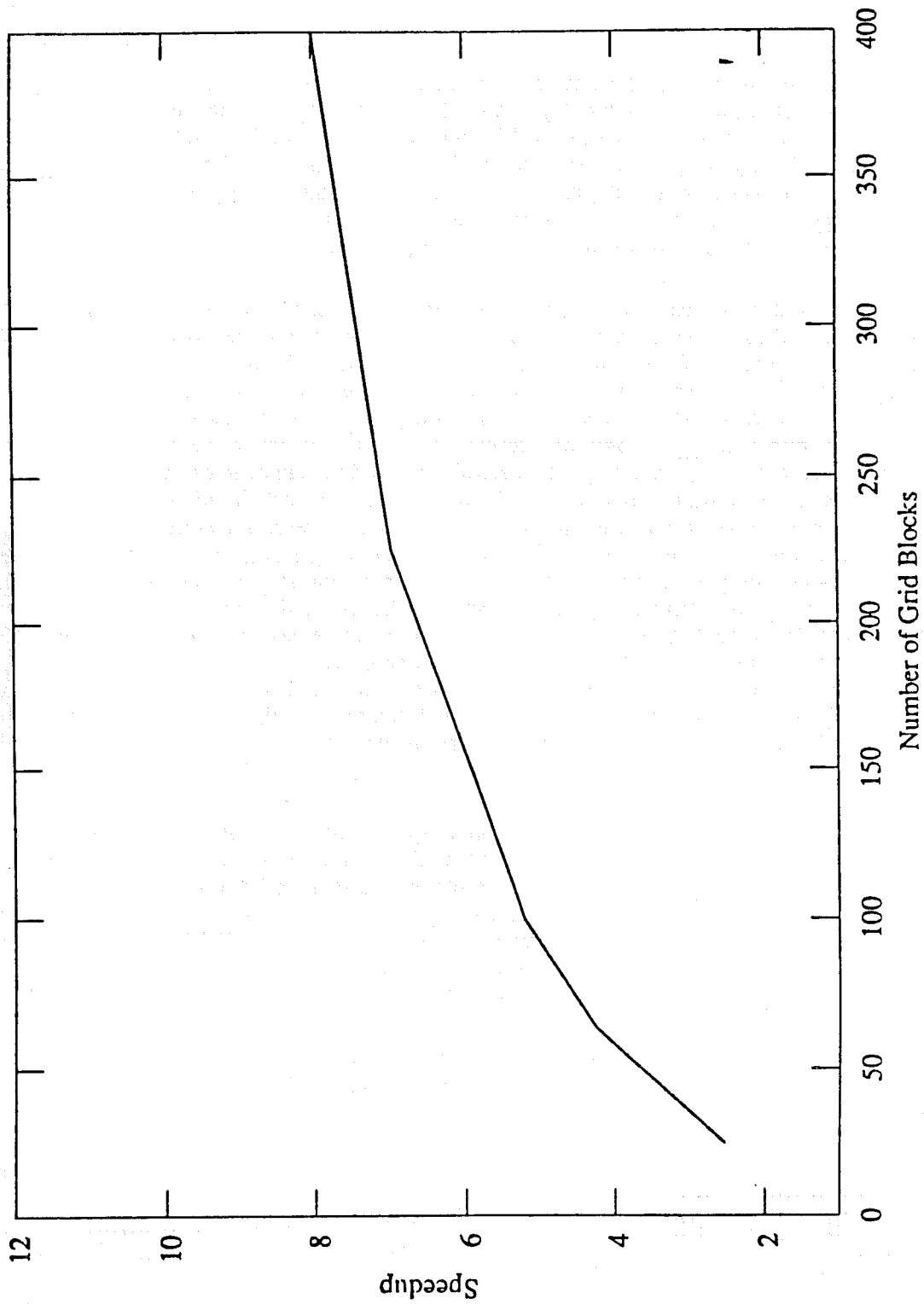


Figure 5.1.7 Speed-up on twelve processors.

## 5.2 STEAM DRIVE SEMI-ANALYTICAL MODEL (R. Gajdica)

### 5.2.1. EMPHASIS OF THIS RESEARCH

I am conducting my research in the area of enhanced oil recovery by thermal methods, with emphasis on downhole steam injection. The absence of significant new domestic oil discoveries coupled with the uncertainty of international oil supplies makes any process that increases the recovery of oil from existing fields an important one. The potential for thermal recovery in North America is great, and thermal recovery could play an important role in meeting the energy needs of this nation. During the past 25 years, steam-injection processes have become an important means of exploiting heavy oil reserves.

Thermal recovery projects are generally not implemented unless there is potential for economic gain. Risk is generally low because the projects are initiated on heavy oil reservoirs that have already been located. The primary unknown is how the reservoir will respond to the application of heat. Thermal reservoir simulators are used to predict this response. Many good finite difference thermal models are in use today (1-12) providing engineers with a prediction of reservoir behavior. However, thermal simulators are expensive to run, require large computers, and often consume a great deal of time before satisfactory results are obtained. There is a need for empirical and semi-analytical models that will accurately predict reservoir behavior without incurring the time and expense of thermal reservoir simulation. Many such models have been published over the last three decades (13-30), with varying degrees of assumptions and accuracy. A model has value if the assumptions involved are not too restrictive and the results obtained are reasonably accurate. These models range from simple to complex, but all of the models reported in the petroleum literature have the common assumption of a horizontal reservoir. This assumption is fine in some cases, but most oil reservoirs have dip, and in many reservoirs the dip is quite severe. It stands to reason that the existing analytical models would not give the correct results if the formation is dipping. Part of the research work is to investigate the effect of formation dip on the recovery of oil from heavy oil reservoirs.

The goal of this research is to develop a semi-analytical model that will predict the response of a reservoir to steam injection. The model should predict thermal reservoir simulator results without actually running the simulator. Effects of formation, water, and oil compressibility and thermal expansion should be accounted for. This contribution would allow quick, extensive analysis of thermal systems without the cost of simulation. Optimum reservoir operating conditions would be obtained and oil recovery maximized. The Computer Modelling Group general purpose thermal simulator ISCOM will be used to check results.

A one-dimensional, three phase model that meets all of the above criteria has been completed. The model matches the thermal simulator pressure distributions, fluid saturation distributions, oil flow rates, water flow rates, breakthrough times, and cumulative productions quite well. I am currently working on modifying the program into a two-dimensional cross-sectional system. Although gravity effects are accounted for in the one-dimensional model, there is no tendency toward phase segregation because there is only one grid block in the z direction. A two-dimensional model will have to account for the effects of gravity override of the steam and underrun of the water. Existing work dealing with the shapes of steam fronts will be used or modified to determine front shapes. This shape will be integrated into the one-dimensional model to form a two-dimensional model.

### 5.2.2. MAJOR ASSUMPTIONS

The Cartesian coordinate system is used. The model is a two-dimensional system with an injection well at one end and a production well at the other. The reservoir is considered to be homogeneous, but may be anisotropic with respect to permeability. The thermal properties of the overburden and underburden are assumed to be identical. Capillary pressure is assumed to be negligible at all times. This assumption is a good one in the high permeability reservoirs typically associated with heavy oil. The fluid system used in this work consists of two components which exist in three phases. The two components are oil and water. The three phases are the oil, water, and gas phases. The assumption is made that the oil component may exist only in the oil phase, and the oil phase consists of only oil component. No distillation of the oil takes place. No water component may enter the oil phase, and no solution gas exists in the oil phase. The water component may exist in both the water and gas phases. The water and gas phases consist of only water component. The component-phase relationships are summarized in the table below.

<u>Phase</u>	<u>Component</u>	
	Oil	Water
Oil	X	
Water		X
Gas		X

### 5.2.3. INITIAL CONDITIONS

Initially, there is no gas phase in the reservoir. The gas phase exists only after steam has been introduced. The initial water phase saturation is the irreducible water saturation. Thus, at initial conditions, the water phase is immobile. The initial oil phase saturation is unity minus the irreducible water saturation. The initial pressure at the top of the reservoir at the injection well and at the top of the reservoir at the production well is defined by the input data file. If the reservoir is horizontal, the two pressure values should be the same. The pressure at other points in the reservoir is determined by a hydrostatic head calculation. The initial temperature is also read from the input data file.

### 5.2.4. BOUNDARY CONDITIONS

The reservoir length, width, and height are designated as the  $x$ ,  $y$ , and  $z$  directions, respectively. Wells drilled in the  $z$ -direction penetrate the reservoir at either end. An injection well is completed at  $x = 0$  and a production well is completed at  $x = L$ . The injection well is a constant rate steam injector with a constant quality. The production well produces at constant pressure. At all the boundaries of the reservoir, there is a no flow boundary with respect to mass. The boundaries are also no flow with respect to heat except for the top and bottom of the reservoir. At these two faces, heat transfer is allowed to the overburden and underburden.

### 5.2.5. PROGRAM STRUCTURE

The program begins with some item tasks that need to be performed only once. The necessary input and output files are opened and initialized. The data file is read. Many variables are initialized. Initial oil and water in place is calculated. Fractional flow curves are constructed and analyzed.

The first global time loop is then entered. This time loop is for times prior to water breakthrough at the production well. The time is incremented, and an estimate is made for  $p_0$ , the pressure at the injection well. A few other variables are initialized. This is the beginning of the pressure loop. The gas fractional flow curve is reconstructed using the newest pressure estimate. The first estimate of average gas saturation behind the steam front is made. The heat balance calculations are made to determine overburden heat losses and amount of steam condensed. The volume of the steam zone and the distance to the steam front is calculated. The average gas saturation behind the front is revised to account for the condensation effect. The distance to the water front is then calculated. At this point in the program, the location of the two fronts and the average phase saturations in each zone have been calculated.

Pressure drop calculations are then made. Starting with the pressure estimate at the injection well, the pressure at the injection sand face, steam front, water front, production sand face, and finally the production well is calculated. This calculated production well pressure is compared to the specified bottomhole pressure. If the difference between these two pressures is less than a specified convergence tolerance, then convergence is achieved and the pressure loop is exited. If convergence is not achieved, the pressure estimate at the injection well is revised and the pressure loop is repeated until convergence is achieved. After convergence is achieved, the oil and water flow rates for the time step are calculated, and that is the end of the time step. The program then increments time and starts the time loop over again. This procedure is repeated until water breakthrough at the production well or maximum time is reached.

After water breakthrough, the second time loop is entered. Instead of incrementing time, the fractional flow of water,  $f_w$ , is incremented. This variable is incremented from the fractional flow of water at the front at breakthrough up to the maximum fractional flow of water. This maximum value is unity for horizontal reservoirs, but may be greater than or less than unity for dipping reservoirs, depending on the location of injection. For each fractional flow increment, the corresponding fractional flow tangent slope and thus pore volume injected is calculated. The injected pore volume is multiplied by the current pore volume of the reservoir to get volume injected, and the volume injected is divided by the injection rate to get time. Once time is determined, the pressure guess and convergence scheme is the same as the first time loop. This time loop is repeated until steam breakthrough or maximum time is reached.

## 5.2.6. DATA ORGANIZATION

The data set used by this model is very much like the data used by a thermal reservoir simulator. The general control data is the number of grid blocks in the x, y, and z directions. The number of grid blocks in the y direction is always one. Time step size and maximum time are also required. The reservoir description data consists of grid block size in the x, y, and z directions, angle of formation dip, porosity, and permeability in the x and z directions. The initial condition data includes initial pressure and temperature at either end of the reservoir, and the initial oil and water saturation. The PVT data section has data that is used to calculate fluid volumes with changes in pressure and temperature. A reference pressure and temperature for porosity and oil and water densities is required. Surface pressure and temperature are also needed. Oil and water densities at the reference conditions are then read. Compressibility and thermal expansion coefficients for both oil and water are used to calculate volume changes. Two coefficients that define the steam viscosity are also used. Finally, the number of entries in the tables for fluid viscosity, oil-water relative permeability, and liquid-gas relative permeability are specified.

Three tables of data are required. The first is a table of oil and water viscosity as a function of temperature. The second is water and oil relative permeabilities for a water-oil system. The last is gas and liquid relative permeabilities for a gas-liquid system. The thermal data section includes compressibility and thermal expansion of the formation, density and specific heat of the reservoir rock, and thermal conductivity and thermal diffusivity of the overburden.

Finally, the injection rate, steam quality, temperature, maximum pressure, and injectivity index at the injection well are specified. Production well data includes the constant bottomhole pressure, maximum liquid rate, wellbore radius, shape factor, and skin factor.

### 5.2.7. FRACTIONAL FLOW CALCULATIONS

Fractional flow curves with tangent constructions are used to determine average phase saturations behind fronts. The relative permeability for the oil-water system is used along with the oil and water phase viscosities at initial conditions to determine the average water saturation behind the water front. Since this calculation is not pressure dependent and the temperature does not change much, this calculation is done once instead of every iteration.

$$f_w = \frac{1 + \frac{7.827 \cdot 10^{-6} k_x k_{ro} A (\rho_w - \rho_o) \sin\theta}{\mu_o q B}}{1 + \frac{\mu_w}{\mu_o} \frac{k_{row}}{k_{rw}}} \quad (5.2.1)$$

The relative permeability for the gas-liquid system in conjunction with the steam and water viscosities are used to determine the average gas saturation behind the steam front. This calculation is quite pressure and temperature dependent so it must be repeated every iteration. The average gas saturation is an approximation assuming no heat losses and must be corrected for condensation.

$$f_g = \frac{1 - \frac{7.827 \cdot 10^{-6} k_x k_{rw} A (\rho_w - \rho_g) \sin\theta}{\mu_w q B}}{1 + \frac{\mu_g}{\mu_w} \frac{k_{rog}}{k_{rg}}} \quad (5.2.2)$$

After water breakthrough has occurred, the slope of the water fractional flow curve is used to determine time. Thus, it is necessary that the curve have no inflection points or negative time steps would be calculated. To ensure that the curve is smooth, the relative permeability data used to calculate the fractional flow curve is smoothed. The method of Corey is used to accomplish this. For the water-oil system,

$$S_w^* = \frac{S_w - S_{w,irr}}{1 - S_{w,irr} - S_{or}} \quad (5.2.3)$$

$$k_{rw} = k_{rw,end} (S_w^*)^{n_w} \quad (5.2.4)$$

$$k_{row} = (1 - S_w^*)^{n_o} \quad (5.2.5)$$

For the liquid-gas system

$$S_l^* = \frac{S_l - S_{l,irr}}{1 - S_{l,irr} - S_{gr}} \quad (5.2.6)$$

$$k_{rg} = k_{rg,end} (1 - S_l^*)^{n_s} \quad (5.2.7)$$

$$k_{rog} = (S_l^*)^{n_i} \quad (5.2.8)$$

### 5.2.8. DETERMINATION OF FRONT LOCATIONS

The reservoir is divided into three zones. Moving from injector to producer, the zones are the steam, water, and oil zones. The steam zone is the portion of the reservoir where a gas phase exists. The temperature in this zone is the steam temperature. The water zone is the portion of the reservoir swept by the water front but all the steam has condensed into the water phase. This zone is nearly all at the initial reservoir temperature. The last zone is the oil zone. This zone is at the initial reservoir conditions both in terms of fluid saturations and temperature. The two interfaces between these three zones are the steam front and the water front. The locations of these two fronts must be determined for each time step in order to forecast recovery.

The length to the steam front is calculated using the method presented by Marx and Langenheim (15). The area of the steam zone is

$$A = \frac{q_{inj} M_R H}{4 (T_{inj} - T_i) \alpha_{ob} M_{ob}^2} \left[ e^{x^2} \operatorname{erfc}(x) + \frac{2x}{\sqrt{\pi}} - 1 \right] \quad (5.2.9)$$

where

$$x = \frac{2 \lambda_{ob} \sqrt{t}}{M_R H \sqrt{\alpha_{ob}}} \quad (5.2.10)$$

$$M_R = (1 - \phi) \rho_r C_r + \phi [ S_w \rho_w C_w + S_o \rho_o C_o + S_g \rho_s \left( \frac{L_v}{\Delta T} + C_w \right) ] \quad (5.2.11)$$

$$M_{ob} = \frac{\lambda_{ob}}{\alpha_{ob}} \quad (5.2.12)$$

and heat injection rate

$$q_{inj} = q_w \rho_{st} (h_w + f_s L_v) \quad (5.2.13)$$

Heat losses to the adjacent formations are also calculated as

$$Q_{ob} = q_{inj} t - \frac{q_{inj} M_R^2 H^2}{4 M_f^2 \alpha_{ob}} \left[ e^{x^2} \operatorname{erfc}(x) + \frac{2x}{\sqrt{\pi}} - 1 \right] \quad (5.2.14)$$

The average gas saturation behind the steam zone is corrected using the results of the Marx and Langenheim calculation. Saturated steam properties are calculated from accurate correlations (32). Overburden heat losses and reservoir thermal properties are used in a latent heat balance to determine how much steam has condensed. The remaining steam constitutes the gas saturation behind the steam front.

The location of the water front is calculated using a Buckley-Leverett (31) frontal advance calculation. The pore volume injected is the sum of the volume of the steam and water in the reservoir. The pore volume is the volume of the reservoir with formation compressibility taken into account. Thus, the number of pore volumes injected and the length to the water front can be calculated.

$$PVI = \frac{5.6146 q_w t \frac{\rho_{w,st}}{\rho_{w,wz}} + L_{sz} W H \phi_{sz} S_{g,sz} \left(1 - \frac{\rho_{g,sz}}{\rho_{w,sz}}\right)}{L W H \bar{\phi}} \quad (5.2.15)$$

$$L_{sz+wz} = \frac{PVI L}{\bar{S}_w - S_{wi}} \quad (5.2.16)$$

Both of these calculation are pressure dependent so they must be repeated every iteration.

## 5.2.9. PRESSURE DROP THROUGH INJECTION WELL

The pressure drop through the injection well is determined by an injectivity index. The constant flow rate is corrected to reservoir flow rate, and the pressure drop is simply the flow rate divided by the injectivity index.

$$\Delta p = \frac{q_w \rho_{w,st}}{I_w \rho_{w0}} \quad (5.2.17)$$

## 5.2.10. PRESSURE DROP THROUGH STEAM ZONE

The pressure drop through all three zones is calculated using Darcy's law for multiphase flow. The volume of the steam and therefore the total flow rate is known. The oil phase has been reduced to the residual oil saturation so it is not mobile. Thus, only the gas and water phases contribute to the conductive path. The gas phase saturation is determined from the gas fractional flow curve and then adjusted for condensation. The three phase relative permeabilities in all zones are calculated using Stones (32) second model. The length of the zone is known, so the pressure drop can be easily calculated.

$$\Delta p = \frac{q_t B_w L_{sz}}{1.127 \cdot 10^{-3} k_x A \left( \frac{k_{rw}}{\mu_w} + \frac{k_{rg}}{\mu_g} \right)} \quad (5.2.18)$$

### 5.2.11. PRESSURE DROP THROUGH WATER ZONE

All of the steam has condensed into water so there are only two phases flowing in this zone. The total flow rate is the sum of the water and oil rates adjusted for reservoir conditions. The length of the water zone is the length to the water front minus the length of the steam zone. The water saturation in the water zone is determined from the water fractional flow curve. The pressure drop is calculated just as in the steam zone.

$$\Delta p = \frac{q_t B_t L_{wz}}{1.127 \cdot 10^{-3} k_x A \left( \frac{k_{rw}}{\mu_w} + \frac{k_{ro}}{\mu_o} \right)} \quad (5.2.19)$$

### 5.2.12. PRESSURE DROP THROUGH OIL ZONE

In the oil zone, the oil phase is mobile, and the water phase could possibly be mobile. The change in pore volume associated with pressure changes, coupled with the changes in fluid volumes, could increase the water saturation above irreducible water saturation. The flow rate is the total rate of the two phases. The length of the oil zone is the total length of the system minus the length to the water front. The pressure drop is then calculated using Darcy's law.

$$\Delta p = \frac{q_t B_t L_{oz}}{1.127 \cdot 10^{-3} k_x A \left( \frac{k_{rw}}{\mu_w} + \frac{k_{ro}}{\mu_o} \right)} \quad (5.2.20)$$

### 5.2.13. PRESSURE DROP THROUGH PRODUCTION WELL

The shape factor of the well is used in a formula to calculate the pressure drop through the well.

$$\Delta p = \frac{q_t B_t \left[ \ln \left( \frac{cc}{r_w} \sqrt{\frac{\Delta x^2 + \Delta y^2}{\pi}} \right) + s \right]}{7.081 \cdot 10^{-3} H k_x \left( \frac{k_{ro}}{\mu_o} + \frac{k_{rw}}{\mu_w} \right)} \quad (5.2.21)$$

### 5.2.14. CALCULATION OF FLOW RATES

The oil and water components in place are calculated at initial conditions and at the end of each time step. This calculation is done for each of the three zones using average phase saturations and phase densities for each zone.

$$OIP_{sz} = \frac{L_{sz} A \phi_{sz} S_{o,sz}}{5.6146} \frac{\rho_{o,sz}}{\rho_{o,st}} \quad (5.2.22)$$

$$WIP_{sz} = \frac{L_{sz} A \phi_{sz} S_{w,sz}}{5.6146} \frac{\rho_{w,sz}}{\rho_{w,st}} \quad (5.2.23)$$

$$GIP_{sz} = \frac{L_{sz} A \phi_{sz} S_{g,sz}}{5.6146} \frac{\rho_{g,sz}}{\rho_{w,st}} \quad (5.2.24)$$

$$OIP_{wz} = \frac{L_{wz} A \phi_{wz} S_{o,wz}}{5.6146} \frac{\rho_{o,wz}}{\rho_{o,st}} \quad (5.2.25)$$

$$WIP_{wz} = \frac{L_{wz} A \phi_{wz} S_{w,wz}}{5.6146} \frac{\rho_{w,wz}}{\rho_{w,st}} \quad (5.2.26)$$

$$OIP_{oz} = \frac{L_{oz} A \phi_{oz} S_{o,oz}}{5.6146} \frac{\rho_{o,oz}}{\rho_{o,st}} \quad (5.2.27)$$

$$WIP_{oz} = \frac{L_{oz} A \phi_{oz} S_{w,oz}}{5.6146} \frac{\rho_{w,oz}}{\rho_{w,st}} \quad (5.2.28)$$

$$OIP = OIP_{sz} + OIP_{wz} + OIP_{oz} \quad (5.2.29)$$

$$WIP = WIP_{sz} + GIP_{sz} + WIP_{wz} + WIP_{oz} \quad (5.2.30)$$

The difference in the volumes of each phase is what has been produced over the time step. Volume divided by time gives the oil and water rates for that time step. Cumulative volumes produced are also calculated.

$$q_o = \frac{OIP^{n+1} - OIP^n}{\Delta t} \quad (5.2.31)$$

$$q_w = \frac{WIP^{n+1} - WIP^n}{\Delta t} \quad (5.2.32)$$

### 5.2.15. NOMENCLATURE

- A* - cross-sectional area to flow, sq.ft
- B* - formation volume factor, rcf/scf
- cc* - shape factor for production well
- C* - specific heat, btu/lbm-F

- $f_g$  - fractional flow of gas
- $f_s$  - quality of steam, fraction
- $f_w$  - fractional flow of water
- $GIP$  - gas in place, scf
- $h$  - enthalpy, btu/lbm
- $H$  - height of reservoir, ft
- $I$  - injectivity index, scf/day/psi
- $k$  - permeability, md
- $L$  - length of reservoir, ft
- $L_v$  - latent heat of vaporization, btu/lbm
- $M$  - volumetric heat capacity, btu/cu.ft-F
- $n$  - Corey exponent
- $OIP$  - oil in place, scf
- $p$  - pressure, psia
- $q$  - rate, scf/day or btu/day
- $Q$  - cumulative, scf or btu
- $r$  - radius, ft
- $s$  - skin factor, dimensionless
- $S$  - saturation, fraction
- $t$  - time, days
- $T$  - temperature, F
- $W$  - width of reservoir, ft
- $WIP$  - water in place, scf
- $x$  - coordinate direction along length of reservoir
- $y$  - coordinate direction along width of reservoir
- $z$  - coordinate direction along height of reservoir
- $\alpha$  - thermal diffusivity, sq.ft/day
- $\theta$  - angle of formation dip, degrees
- $\Delta t$  - time step
- $\Delta x$  - grid block length in  $x$ -direction
- $\Delta y$  - grid block length in  $y$ -direction
- $\phi$  - porosity, fraction
- $\rho$  - density, lbm/cu.ft
- $\mu$  - viscosity, cp

## SUBSCRIPTS 0

- $g$  - gas
- $end$  - endpoint
- $i$  - initial
- $irr$  - irreducible
- $l$  - liquid

- o* - oil
- ob* - overburden
- or* - oil residual
- oz* - oil zone
- r* - rock
- rg* - gas relative
- ro* - oil relative
- rog* - oil relative in oil-gas system
- row* - oil relative in oil-water system
- rw* - water relative
- R* - fluid filled reservoir
- s* - steam
- st* - standard
- sz* - steam zone
- t* - total
- w* - water, or well
- wz* - water zone
- x* - *x* direction
- y* - *y* direction
- z* - *z* direction
- 0 - at injection well
- 1 - at injection sandface
- 2 - at steam front
- 3 - at water front
- 4 - at production sandface
- 5 - at production well

#### **SUPERSCRIPTS 0**

- \* - normalized
- - average

#### **5.2.16. REFERENCES**

1. Spillette, A. G. and Nielsen, R. L.: "Two-Dimensional Method for Predicting Hot Waterflood Recovery Behavior," J. Pet. Tech. (June 1968) 627-638; Trans., AIME, Vol. 243.
2. Shutler, N. D.: "Numerical, Three-Phase Simulation of Linear Steamflood Process," Soc. Pet. Eng. J. (June 1969) 232-246; Trans., AIME, Vol. 246.
3. Shutler, N. D.: "Numerical, Three-Phase Model of the Two-Dimensional Steamflood Process," Soc. Pet. Eng. J. (Dec. 1970) 405-417; Trans., AIME, Vol. 249.

4. Abdalla, A. and Coats, K. H.: "A Three-Phase Experimental and Numerical Simulation Study of the Steamflood Process," paper SPE 3600 presented at the SPE-AIME 46th Annual Fall Meeting, New Orleans (Oct. 3-6, 1971).
5. Vinsome, P. K. W.: "A Numerical Description of the Steam Injection Process by a Stabilized IMPES Method," paper SPE 5248 presented at the SPE-AIME 49th Annual Fall Meeting (Oct. 6-9, 1974).
6. Coats, K. H., George, W. D., Chu, C., and Marcum, B. E.: "Three-Dimensional Simulation of Steamflooding," Soc. Pet. Eng. J. (Dec. 1974) 573-592; Trans., AIME, Vol.257.
7. Coats, K. H.: "Simulation of Steamflooding with Distillation and Solution Gas," Soc. Pet. Eng. J. (Oct. 1976) 235-247.
8. Ferrer, J. and Farouq-Ali, S. M.: "A Three-Phase, Two-Dimensional Compositional Thermal Simulator for Steam Injection Processes," J. Cdn. Pet. Tech. (Jan.-March 1977) 78-90.
9. Weinstein, H. G., Wheeler, J. A., and Woods, E. G.: "Numerical Model for Thermal Processes," Soc. Pet. Eng. J. (Feb. 1977) 65-78; Trans., AIME, Vol. 263.
10. Coats, K. H.: "A Highly Implicit Steamflood Model," Soc. Pet. Eng. J. (Oct. 1978) 369-383.
11. Crookston, R. B., Culham, W. E., and Chen, W. H.: "A Numerical Simulation Model for Thermal Recovery Processes," Soc. Pet. Eng. J. (Feb. 1979) 37-58.
12. Rubin, B. and Buchanan, W. L.: "A General Purpose Thermal Model," Soc. Pet. Eng. J. (April 1985) 202-214.
13. Lauwerier, H. A.: "The Transport of Heat in an Oil Layer Caused by the Injection of Hot Fluid," Appl. Sci. Res. (1955) Vol. 5, 145.
14. Jordan, J. K., Rayne, J. R., and Marshall, S. W. III: "A Calculation Procedure for Estimating the Production History During Hot Water Injection in Linear Reservoirs," paper presented at the 20th Technical Conference on Petroleum Production, Pennsylvania State U., University Park, Pa. (May 9-10, 1957).
15. Marx, J. W. and Langenheim, R. H.: "Reservoir Heating by Hot Fluid Injection," Trans., AIME Vol. 216 (1959) 312-315.
16. Landrum, B. L., Smith, J. E. and Crawford, P. B.: "Calculation of Crude Oil Recoveries by Steam Injection," Proc., Texas Petroleum Research Committee, Oil Recovery Conference (Oct. 29-31, 1959).
17. Dougherty, E. L. and Sheldon, J. W.: "The Use of Fluid-Fluid Interfaces to Predict Behavior of Oil Recovery Processes," Soc. Pet. Eng. J. (June 1964) 171-182; Trans., AIME, Vol. 231.
18. Fayers, F. J.: "Some Theoretical Results concerning the Displacement of a Viscous Oil by a Hot Fluid in a Porous Medium," J. Fluid Mech. Vol. 13 (1965) 65.
19. Boberg, T. C. and Lantz, R. B.: "Calculation of the Production Rate of a Thermally Stimulated Well," J. Pet. Tech. (Dec. 1966) 1613-1623; Trans., AIME, Vol. 237.
20. Martin, J. C.: "A Theoretical Analysis of Steam Stimulation," J. Pet. Tech. (March 1967) 411-418.; Trans., AIME, Vol. 240.
21. Davidson, L. B., Miller, F. G., and Mueller, T. D.: "A Mathematical Model of Reservoir Response During the Cyclic Injection of Steam," Soc. Pet. Eng. J. (June 1967) 174-188; Trans., AIME, Vol. 240.
22. Davies, L. G., Silberg, I. H., and Caudle, B. H.: "A Method of Predicting Oil Recovery in a Five-Spot Steamflood," J. Pet. Tech. (Sep. 1968) 1050-1058.
23. Seba, R. D. and Perry, G. E.: "A Mathematical Model of Repeated Steam Soaks of Thick Gravity Drainage Reservoirs," J. Pet. Tech. (Jan. 1969) 87-94.

24. Mandl, G. and Volek, C. W.: "Heat and Mass Transport in Steam-drive Processes," Soc. Pet. Eng. J. (March 1969); Trans., AIME, Vol. 246.
25. Kuo, C. H., Shain, S. A., and Phocas, D. M.: "A Gravity Drainage Model for the Steam-Soak Process," Soc. Pet. Eng. J. (June 1970) 119-126; Trans., AIME, Vol. 249.
26. Clossman, P. J., Ratliff, N. W., and Truitt, N. E.: "A Steam-Soak Model for Depletion-Type Reservoirs," J. Pet. Tech. (June 1970) 757-770; Trans., AIME, Vol. 249.
27. Rincon, A. Diaz-Munoz, J., and Farouq-Ali, S. M.: "Sweep Efficiency in Steamflooding," J. Cdn. Pet. Tech. (July-Sep. 1970).
28. Farouq-Ali, S. M.: Oil Recovery by Steam Injection, Producers Publishing Company, Bradford, Pa. (1970).
29. Satter, A. and Parrish, D. R.: "A Two-Dimensional Analysis of Reservoir Heating by Steam Injection," Soc. Pet. Eng. J. (June 1971) 185-197; Trans., AIME, Vol. 251.
30. Shutler, N. D. and Boberg, T. C.: "A One-Dimensional, Analytical Technique for Predicting Oil Recovery by Steamflooding," Soc. Pet. Eng. J. (Dec. 1972) 489-498.
31. Buckley, S. E. and Leverett, M. C.: "Mechanism of Fluid Displacement in Sands," Trans., AIME (1941) Vol 146, 107.
32. Stone, H. L.: "Estimation of Three-Phase Relative Permeability and Residual Oil Data," J. Can. Pet. Tech., Vol. 12, No. 4 (1973) pp. 53-61.
33. Tortike, W. S. and Farouq Ali, S. M.: "Saturated Steam Property Functional Correlations for Fully Implicit Thermal Reservoir Simulation" SPE paper 17094.

## **5.3 COMPUTERIZED AXIAL TOMOGRAPHY (L. Castanier)**

### **5.3.1. SUMMARY**

A second generation CAT system was purchased and installed in the SUPRI laboratories. Calibration was performed on Ottawa sandpacks, Salem limestone and various sandstones. Measurement of liquid saturation in gas/water systems is possible within 0.5% saturation. An experiment aiming at the study of foam flow through porous media is now in progress.

### **5.3.2. OBJECTIVES**

Computerized Axial Tomography (CAT-SCAN) is a non-destructive measurement technique using determination of X-ray adsorption coefficients to determine the density and/or the composition of a sample section. It has been used extensively in medical applications for the past 15 years. Recently, attempts have been made to apply this technique to petroleum related problems. Some of the possible benefits are:

- Indepth examination of core heterogeneities
- Identification of specific minerals
- Density, porosity and multiphase saturation determinations
- Experimental simulation of EOR processes

SUPRI's objective is to have a reliable laboratory tool for all of the above goals. It will be operated on a routine basis to complement existing laboratory facilities and techniques.

### **5.3.3. CHOICE OF A SCANNER**

As part of a university with limited resources both in manpower and money we opted for a simple and economical program of computerized tomography.

An extensive review of existing systems in the oil industry and in other universities was performed. Visits with Shell and Mobil personnel and with the universities of Houston and Texas at Austin as well as a study of existing medical and petroleum literature on the topic showed that a second generation CAT scan system would be adequate for our purpose.

References 1 and 2 give details of this review process. Consultations with the medical community at Stanford and Choppe Memorial Hospital in San Mateo (California) led us to purchase an EMI 5005 scanner. As the computers associated with this scanner are obsolete it was decided to network it with a Macintosh II Apple computer for post-processing.

### **5.3.4. INSTALLATION AND MAINTENANCE**

The scanner was purchased in November 1987 and installation was completed in January 1988. Safety considerations required lead shielding of the scan room as well as surveys from Health Physics personnel. Medical Systems Inc. of San Francisco was awarded the

maintenance contract and performed the CAT-scan installation. Except for minor problems mostly caused by the inexperience of the operators, the system has performed very well since March 1988. The only major modification to the medical system was the fabrication of an accurate positioning setup for repeatable measurements. Positioning on the axis of the scanner is now done using two laser beams (Uniphase Inc.) and the longitudinal accuracy is obtained by the use of a Daedal metering table. These modifications increased the accuracy of the positioning from about  $\pm 1$  cm to  $\pm 0.001$  cms. Table 1 gives additional information on the system.

### 5.3.5. PROGRESS TO DATE

A study was performed in collaboration with Victor Mossoti of the United States Geological Survey on the effect of acid rain on the Salem limestone. References 4 and 5 describe this study and its results in detail. The one-dimensional experiment used by Treinen (Ref. 5) to study foam flow through a sandpack was placed in the scanner and calibrated. The results to date are described in Section 3 of this report. In both cases the liquid saturation in a gas/water system was successfully determined. The liquid saturation can be calculated within 0.5% saturation unit in both sandpacks and limestone.

Experiments are in progress aiming at designing a three-dimensional steam model that could be scanned. Tests have been conducted on various geometries and materials ranging from aluminium to sand in order to investigate the proper design for the model. The preliminary results show that the realization of such a model is feasible and that determination of oil, water and gas saturations is theoretically feasible.

### 5.3.6. FUTURE WORK

Shell development has offered to provide SUPRI with access to the software developed by their personnel (Ref. 2). A SUN 386 workstation has been purchased and will be installed and networked to be able to use this software. Long term testing of the system will continue. The reference library of phantoms will be expanded to cover most of the fluids and materials used in our research. Simultaneously, adaptation of the software to analysis of our laboratory data will continue. Flow experiments for EOR process will be modified for use in the CAT scan and calibrated.

TABLE 1  
SUPRI'S CT SYSTEM

#### Scanner

EMI 5005 (second generation)	
Price	\$25,000
Installation	\$15,000
Maintenance	\$17,000 /yr.
2D 200 Eclipse computers	(32K each)
320 x 320 image with 256 gray levels	
Scan field between 24 and 40 cms	
Imaging	185 to 705 (high accuracy)
Intensity	0 to 40 ma
Energy	80 to 140 keV
Fixed-anode oil-cooled X-ray tube	

